

Magennis, Eugene Peter (2013) Bacterial auto-nemesis: templating polymers for cell sequestration. PhD thesis, University of Nottingham.

Access from the University of Nottingham repository:
<http://eprints.nottingham.ac.uk/14503/16/602962.pdf.pdf>

Copyright and reuse:

The Nottingham ePrints service makes this work by researchers of the University of Nottingham available open access under the following conditions.

- Copyright and all moral rights to the version of the paper presented here belong to the individual author(s) and/or other copyright owners.
- To the extent reasonable and practicable the material made available in Nottingham ePrints has been checked for eligibility before being made available.
- Copies of full items can be used for personal research or study, educational, or not-for-profit purposes without prior permission or charge provided that the authors, title and full bibliographic details are credited, a hyperlink and/or URL is given for the original metadata page and the content is not changed in any way.
- Quotations or similar reproductions must be sufficiently acknowledged.

Please see our full end user licence at:
http://eprints.nottingham.ac.uk/end_user_agreement.pdf

A note on versions:

The version presented here may differ from the published version or from the version of record. If you wish to cite this item you are advised to consult the publisher's version. Please see the repository url above for details on accessing the published version and note that access may require a subscription.

For more information, please contact eprints@nottingham.ac.uk

Bacterial Auto-nemesis - Templating polymers for cell sequestration

by Eugene Peter Magennis MPharm.

Thesis submitted to The University of Nottingham
for the degree of Doctor of Philosophy, January 2013



Contents

| | |
|--|-----------|
| List of Figures | 9 |
| List of Schemes | 19 |
| List of Abbreviations | 21 |
| Abstract | 27 |
| Acknowledgements | 29 |
| 1 Introduction | 30 |
| 1.1 Background | 30 |
| 1.2 Introduction to bacterial cell wall and surface structures | 30 |
| 1.2.1 The bacterial cell | 31 |
| Gram-positive bacteria | 31 |
| Gram-negative bacteria | 31 |
| Bacterial surface charge | 33 |
| Bacterial surface sugars | 33 |
| Bacterial sugar binding proteins | 34 |
| 1.2.2 Oral disease and microbial pathogens | 35 |
| 1.3 Bacterial detection, neutralisation and capture | 38 |
| 1.3.1 Bacterial recognition through saccharides | 41 |
| Tunable bacterial binding using saccharides | 44 |

| | | |
|----------|--|-----------|
| 1.3.2 | Bacterial capture and elimination through cell charge | 48 |
| 1.3.3 | Bacterial detection and capture via specific cell wall constituents and surface shape | 50 |
| | Tunable binding of bacteria by antibiotic displaying polymers | 52 |
| | Cell shape-dependent recognition and capture | 52 |
| 1.3.4 | Inactivation of bacteria through cell signal interference | 55 |
| 1.3.5 | Optical detection methods | 60 |
| | Gold nanoparticles | 61 |
| | Conjugated polymer systems | 64 |
| 1.3.6 | Summary of bacterial recognition | 69 |
| 1.4 | Introduction to materials of cell recognition polymerisation methods | 69 |
| 1.4.1 | Atom transfer radical polymerisation (ATRP) | 71 |
| | ATRP in water | 71 |
| 1.4.2 | ATRP as a route to bacteria binding polymers | 74 |
| 2 | Aims of the Thesis | 75 |
| 2.1 | Investigation into Functionality | 75 |
| 2.2 | Investigation into Toxicity | 76 |
| 2.3 | Templating | 76 |
| 2.4 | Rebinding Studies | 76 |
| 2.5 | Bacterial mediated chemistry | 76 |
| 3 | Materials and Methods | 78 |
| 3.1 | Materials | 78 |
| 3.1.1 | Chemicals | 78 |
| 3.1.2 | Bacterial Strains | 79 |
| 3.1.3 | Equipment | 81 |

| | | |
|----------|--|------------|
| 3.2 | Methods | 83 |
| 3.2.1 | Microscopy binding Experiments | 83 |
| 3.2.2 | Aggregation Assay | 84 |
| 3.2.3 | Fluorescent <i>E. coli</i> generation | 84 |
| 4 | Selection of Functionalities A: Charge | 85 |
| 4.1 | Introduction | 85 |
| 4.2 | Methods | 86 |
| 4.2.1 | Synthesis of Benzyl-2-bromo-2-methylpropanoate (1) | 86 |
| 4.2.2 | Polymerisation of 2-(dimethylamino)ethyl methacrylate (DMAEMA) (2) . . | 87 |
| 4.2.3 | Synthesis of Coumarin 343 alkyl bromide (3) | 88 |
| 4.2.4 | Fluorescent labeling of poly(2-(dimethylamino)ethyl methacrylate) (4) . . . | 89 |
| 4.2.5 | Quaternisation of Fluorescent poly(2-(dimethylamino)ethyl methacrylate) (5) | 90 |
| 4.2.6 | Sulfobetainisation of Fluorescent poly(2-(dimethylamino)ethyl methacrylate) | |
| | (6) | 92 |
| 4.2.7 | Binding experiments and aggregation assay | 93 |
| 4.3 | Results and discussion | 93 |
| 4.4 | Conclusions | 110 |
| 5 | Selection of Functionalities B: Carbohydrates | 111 |
| 5.1 | Introduction | 111 |
| 5.1.1 | Boronic acids to bind bacterial surface sugars | 112 |
| 5.1.2 | Glycopolymers to bind to bacterial lectins | 113 |
| 5.2 | Methods | 114 |
| 5.2.1 | Synthesis of <i>tert</i> -butyl (2-aminoethyl)carbamate (1) | 114 |
| 5.2.2 | Synthesis of <i>tert</i> -butyl (2-methacrylamidoethyl)carbamate (2) | 115 |
| 5.2.3 | Synthesis of 2-methacrylamidoethanaminium chloride (3) | 116 |

| | | |
|--------|--|-----|
| 5.2.4 | Synthesis of 2-((2-methacrylamidoethylamino)methyl) phenylboronic acid (4) | 117 |
| 5.2.5 | Polymerisation of 2-((2-methacrylamidoethylamino)methyl) phenylboronic acid (5) | 118 |
| 5.2.6 | Polymerisation of 2-((2-methacrylamidoethylamino)methyl) phenylboronic acid and <i>N</i> -(3-(dimethylamino)propyl) methacrylamide (6) | 119 |
| 5.2.7 | Polymerisation of <i>N</i> -(3-(dimethylamino)propyl)methacrylamide (7) | 120 |
| 5.2.8 | Synthesis of 2-iodoethyl 11-oxo-2,3,5,6,7,11-hexahydro-1 <i>H</i> -pyrano[2,3- <i>f</i>] pyrido[3,2,1- <i>ij</i>]quinoline-10-carboxylate (8) | 121 |
| 5.2.9 | Fluorescent tagging of poly(2-((2-methacrylamidoethylamino)methyl)phenyl- boronic acid-co- <i>N</i> -(3-(dimethylamino) propyl)methacrylamide) (9) | 123 |
| 5.2.10 | Fluorescent tagging of poly(<i>N</i> -(3-(dimethylamino)propyl)methacrylamide) (10) | 124 |
| 5.2.11 | Determination of the association constant (K_{eq1}) of Alizarin Red S-2-((2- methacrylamidoethylamino)methyl) phenylboronic acid complex | 125 |
| 5.2.12 | Determination of the association constant (K_{eq}) of glucose-2-((2-methacryl- amidoethylamino)methyl)phenylboronic acid complex | 127 |
| 5.2.13 | Synthesis of fluorescent glycopolymers | 128 |
| 5.3 | Results and Discussion | 129 |
| 5.3.1 | Sugar binding polymers | 129 |
| 5.3.2 | Sugar displaying polymers | 141 |
| 5.4 | Conclusions | 146 |

6 Polymer Toxicity Testing

147

| | | |
|----------|--|------------|
| 6.1 | Introduction | 147 |
| 6.1.1 | Actions against bacteria | 148 |
| 6.1.2 | Actions against human cells | 149 |
| 6.2 | Methods | 150 |
| 6.2.1 | Antibacterial Activity - Minimum inhibitory concentration | 150 |
| 6.2.2 | Cytotoxicity testing: 3-(4,5-Dimethylthiazol-2-yl)- 2,5-diphenyltetrazolium bromide (MTT) assay | 153 |
| 6.3 | Results and Discussion | 155 |
| 6.3.1 | Minimum inhibitory concentration | 155 |
| 6.3.2 | MTT Assay | 158 |
| 6.4 | Conclusions | 162 |
| 7 | Auto-nemesis | 164 |
| 7.1 | Introduction | 164 |
| 7.2 | Methods | 167 |
| 7.2.1 | Synthesis of 2-(N-Morpholino)ethyl-2-bromobutyrate (1) | 167 |
| 7.2.2 | Bacterial Growth | 168 |
| 7.2.3 | Measurement of redox potential | 168 |
| 7.2.4 | Polymerisation of [2-(methacryloyloxy)ethyl]trimethylammonium chloride and [2-(methacryloyloxy)ethyl]dimethyl-(3-sulfopropyl) ammonium hydroxide via. ATRP in water (P1) | 169 |
| 7.2.5 | Polymerisation of [2-(methacryloyloxy)ethyl]trimethylammonium chloride and 2,3-dihydroxypropyl methacrylate by ATRP in water (P2) | 170 |
| 7.2.6 | Polymerisation of [2-(methacryloyloxy)ethyl]dimethyl- (3-sulfopropyl)ammonium hydroxide and 2,3-dihydroxypropyl methacrylate by ATRP in water (P3) | 171 |
| 7.2.7 | Optimisation of bacterial ATRP (b-ATRP) | 172 |

| | |
|--|------------|
| System A: Ratio of initiator to copper to ligand: 1.0 : 2.5 : 2.5 (P4) | 172 |
| System B: Ratio of initiator to copper to ligand: 1.0 : 5.0 : 2.5 (P5) | 173 |
| Reducing catalyst concentration - System C: Ratio of initiator to copper to ligand: 1.0 : 10 : 5.0 (P6) | 173 |
| Reducing catalyst concentration - System D: Ratio of initiator to copper to ligand: 1.0 : 0.025 : 0.025 (P7) | 174 |
| 7.2.8 Investigation into system components | 175 |
| 7.2.9 Polymerisation of [2-(methacryloyloxy)ethyl]trimethylammonium chloride and 2,3-dihydroxypropyl methacrylate using bacterial activated ATRP (b-ATRP) (P8) | 177 |
| 7.2.10 Polymerisation of [2-(methacryloyloxy)ethyl]dimethyl-(3-sulfopropyl) ammonium hydroxide and 2,3-dihydroxypropyl methacrylate using bacterial activated ATRP (b-ATRP) (P9) | 179 |
| 7.2.11 Bacterial aggregation measured using the Coulter counter | 181 |
| 7.2.12 Bacterial aggregation measured using changes in optical density (OD ₆₀₀) . . | 181 |
| 7.3 Results and Discussion | 181 |
| 7.4 Conclusions | 197 |
| 8 "Click" Chemistry applications | 198 |
| 8.1 Introduction | 198 |
| 8.1.1 Applications of "click" chemistry | 199 |
| 8.2 Methods | 200 |
| 8.2.1 Synthesis of 3-acetamido-2-oxo-2 <i>H</i> -chromen-7-yl acetate (1) | 200 |
| 8.2.2 Synthesis of 3-azo-7-hydroxycoumarin (2) | 201 |
| 8.2.3 Synthesis of 3-(trimethylsilyl)prop-2-yn-1-yl methacrylate (3) | 202 |
| 8.2.4 Polymerisation of 2-(dimethylamino)ethyl methacrylate (DMAEMA) and 3-(trimethylsilyl)prop-2-yn-1-yl methacrylate (4) | 203 |

| | | |
|----------|--|------------|
| 8.2.5 | Quaternisation of poly((DMAEMA)-co-(TMSPMA)) (5) | 204 |
| 8.2.6 | Deprotection of poly((TMAEMA)-co-(TMSPMA)) (6) | 204 |
| 8.2.7 | Bacterial mediated "click" reaction | 205 |
| 8.3 | Results and Discussion | 206 |
| 8.4 | Conclusions | 214 |
| 9 | Discussion and Conclusions | 216 |
| A | Supporting Microscopy Images | 224 |
| A.1 | Microscopy images - Boronic investigations | 224 |
| A.1.1 | Boronic co-polymer and controls | 224 |
| A.1.2 | Microscopy image - Glycopolymers | 226 |
| A.2 | Click chemistry supporting images | 228 |
| B | Supporting Spectra | 235 |
| B.1 | Benzyl-2-bromo-2-methylpropanoate | 235 |
| B.2 | Coumarin 343 alkyl bromide | 237 |
| B.3 | <i>tert</i> -butyl (2-aminoethyl)carbamate | 239 |
| B.4 | <i>tert</i> -butyl (2-methacrylamidoethyl)carbamate | 240 |
| B.5 | 2-methacrylamidoethanaminium chloride | 241 |
| B.6 | 2-((2-methacrylamidoethylamino)methyl)phenylboronic acid | 243 |
| B.7 | Coumarin 343 iodide | 244 |
| B.8 | 2-(N-Morpholino)ethyl-2-bromobutyrate | 245 |
| B.9 | 3-(trimethylsilyl)prop-2-yn-1-yl methacrylate | 247 |
| B.10 | 3-acetamido-2-oxo-2 <i>H</i> -chromen-7-yl acetate | 249 |
| B.11 | 3-azo-7-hydroxycoumarin | 251 |
| B.12 | Zwitterionic and Quaternary Templated Polymers | 253 |
| B.13 | Zwitterionic and Glycerol Templated Polymers | 256 |

| | |
|---|------------|
| B.14 Quaternary and Glycerol Templated Polymers | 259 |
| C Additional Supporting Information | 262 |
| D Analysis of bacterial clutering with templated polymers | 264 |
| D.1 Introduction | 264 |
| D.2 Method | 264 |
| D.3 Results and discussion | 265 |
| D.3.1 Control Polymers | 266 |
| D.3.2 <i>E. coli</i> water washed polymers (P7-WE) | 267 |
| D.3.3 <i>E. coli</i> salt washed polymers (P7-SE) | 268 |
| D.3.4 <i>P. aeruginosa</i> water washed polymers (P7-WP) | 269 |
| D.3.5 <i>P. aeruginosa</i> salt washed polymers (P7-SP) | 270 |
| E Estimation of monomer reactivity ratios | 271 |
| E.1 Introduction | 271 |
| E.2 Methods | 271 |
| E.2.1 METAC:MEDSA ratio of 85:15 R1 | 272 |
| E.2.2 METAC:MEDSA ratio of 90:10 R2 | 272 |
| E.2.3 METAC:MEDSA ratio of 94:6 R3 | 272 |
| E.2.4 METAC:MEDSA ratio of 94:6 R4 | 273 |
| E.2.5 Calculation of reactivity ratios | 273 |
| E.2.6 Results and Discussion | 273 |
| Bibliography | 224 |

List of Figures

| | | |
|------|---|----|
| 1.1 | Example of the cellular structure of a Gram-positive bacterium: <i>Staphylococcus aureus</i> . ^[1] | 32 |
| 1.2 | Example of the cellular structure of a Gram-negative bacterium: <i>Escherichia coli</i> . ^[2] | 32 |
| 1.3 | Scheme showing the difference between monovalent interactions and polyvalent interactions. | 39 |
| 1.4 | Overview of various bacterial targets | 41 |
| 1.5 | Figure showing carbohydrate binding involved in cell recognition. | 42 |
| 1.6 | General structure of neoglycopolymer generated via. ROMP. R = O- or C-glycoside derivatives | 42 |
| 1.7 | a) Structures of glycopolymers displaying glucose with glucose competition assay between polymers and oscillating temperature bacterial aggregation assay <i>E. coli</i> MG1655 expressing green fluorescent protein. | 46 |
| 1.8 | Structures of glycopolymers and the interaction between their vesicles with <i>E. coli</i> | 47 |
| 1.9 | Representation of polymer-antibody-complex to facilitate phagocytosis | 51 |
| 1.10 | Schematic outline for the preparation of imprinted polymer beads | 53 |
| 1.11 | Structures of AI-2 of <i>V. harveyi</i> complex with and without borate and AI-2 of <i>S. typhimurium</i> | 55 |
| 1.12 | Structure of DPD-analogues, the C1 modifications occurred at position R | 56 |

| | |
|---|----|
| 1.13 Schematic diagram illustrating the CD-C4 complex as found with ^1H NMR and ROSEY NMR experiment | 56 |
| 1.14 Schematic representation of boronate ion forming a stable complex with a diol compound. | 57 |
| 1.15 Structure of N-(β -ketocapryloyl)-DL-homoserine lactone (3-oxo-C6-AHL) | 58 |
| 1.16 Structure of fluorescent gold bacterial nano-sensor consisting of: a) the three nanoparticle sensors indicated by the varying R groups and b) the conjugated fluorescent transducer | 63 |
| 1.17 Schematic representation of bacterial nano-sensor where a) the bacteria displaces the conjugated polymer from the nanoparticle surface inducing fluorescence and b) the sensor array where varying the bacteria influences the level of fluorescence produced. | 64 |
| 1.18 General structure of an unsubstituted polythiophene | 64 |
| 1.19 General structure of carbohydrate polythiophene. R = CH_2 or CHCH, R' = various amide spacers | 65 |
| 1.20 Interaction between glyco-polythiophenes and their respective receptor protein. Left-right: Sialic acid polythiophene (SPT), SPT and influenza A virus, SPT and influenza B virus, blank, mannose-polythiophene (MPT), MPT and <i>E. coli</i> HB101 | 66 |
| 1.21 Structure of a single layer of photopolymerised glycofunctionalized PDA liposome | 67 |
| 1.22 Structure of Surfactin, a peptidolipid[3] | 68 |
| 1.23 Scanned images of (A) Agar plate prior to bacterial inoculation (B) 18 hours after inoculation and incubation at 26°C with 3 colonies of <i>Bacillus cereus</i> (C) 18 hours after inoculation and incubation at 26°C with 3 colonies of <i>E. coli</i> BL | 68 |
| 1.24 General mechanism of CRP | 70 |
| 3.1 Growth curve of <i>E. coli</i> MG1655 | 80 |
| 3.2 Typical phase contrast image of <i>S. mutans</i> | 81 |

| | | |
|------|---|-----|
| 4.1 | Fluorescently labelled of pDMAEMA | 90 |
| 4.2 | Quaternised Fluorescent pDMAEMA | 91 |
| 4.3 | Sulfobetainated Fluorescent pDMAEMA | 93 |
| 4.4 | Charge investigation strategy | 94 |
| 4.5 | Kinetic plot for the polymerisation of DMAEMA in Toluene | 95 |
| 4.6 | a) Assigned ^1H NMR spectra of modified polymer 5a b) ^1H NMR spectra of quaternised poly(DMAEMA) 5 highlighting the decrease in the proportion of protons adjacent to the tertiary amine. Purple (5a), turquoise (5b), green (5c), red (5d). . | 98 |
| 4.7 | Phase contrast and fluorescent microscopy images of polymer 5a (a & b), 5b (c & d), 5c (e & f) and 5d (g & h) with <i>E. coli</i> MG1655 after undergoing procedure described in 3.2.1. The binding of the polymers to the bacteria remains strong however the size of the aggregates decreases. | 100 |
| 4.8 | Phase contrast and fluorescent microscopy images of polymer 5a (a & b), 5b (c & d), 5c (e & f) and 5d (g & h) with <i>S. mutans</i> NCTC 10449 after undergoing procedure described in 3.2.1. Binding to <i>S. mutans</i> remains as the level of quaternisation increases on the polymer chain. | 101 |
| 4.9 | Phase contrast and fluorescent microscopy images of polymer 6a (a & b), 6b (c & d), 6c (e & f) and 6d (g & h) with <i>E. coli</i> MG1655 after undergoing procedure described in 3.2.1. It can be seen that as the level of betaine functionality increases the binding of the polymer to the bacteria decreases. | 103 |
| 4.10 | Phase contrast and fluorescent microscopy images of polymer 6a (a & b), 6b (c & d), 6c (e & f) and 6d (g & h) with <i>S. mutans</i> NCTC 10449 after undergoing procedure described in 3.2.1. As the levels of betaine functionality is increased the binding to the bacterium remains strong. | 104 |
| 4.11 | Aggregation assay of <i>E. coli</i> and fully modified polymers | 105 |
| 4.12 | Schematic for mixed culture binding experiment | 106 |

| | | |
|------|---|-----|
| 4.13 | (a) Overlapped images from mixed binding experiment utilising the fluorescent betaine polymer 6d with <i>E. coli</i> MG1655 mCherry and <i>S. mutans</i> after undergoing procedure described in 3.2.1. Images were recorded using phase contrast microscopy | |
| | (b) then separate fluorescent channels (d)-(e) and combined for analysis (c). | 107 |
| 4.14 | (a) Overlapped images from mixed binding experiment utilising the fluorescent betaine polymer 6d with <i>E. coli</i> MG1655 mCherry and <i>S. mutans</i> after undergoing procedure described in 3.2.1. Images were recorded using phase contrast microscopy | |
| | (b) then separate fluorescent channels (d)-(e) and combined for analysis (c). | 108 |
| 5.1 | Figure showing carbohydrate binding involved in cell recognition. | 112 |
| 5.2 | Structure of glycopolymers employed in this study. | 128 |
| 5.3 | Comparison between fluorescent glucose sensor and 2-((2-methacrylamidoethylamino)-methyl)phenylboronic acid | 130 |
| 5.4 | Schematic overview of the Alizarin Red assay | 131 |
| 5.5 | Emission spectra of AR-S complex with increasing concentrations of boronic acid (4) | 132 |
| 5.6 | Benesi-Hildebrand plot for change in emission at 572 nm as a result of increasing AR-S with increasing concentrations of AR-S-boronic acid complex. | 133 |
| 5.7 | Change in emission at 472 nm as a result of increasing AR-S with increasing concentrations of AR-S-boronic acid complex. | 134 |
| 5.8 | Emission spectra of AR-S-boronic acid complex with increasing concentrations of glucose. | 135 |
| 5.9 | Polymerisation kinetics of the amine homopolymer and the boronic co-polymer using RAFT. | 136 |
| 5.10 | GPC traces of a) non-fluorescent boronic co-polymer 6 and b) non-boronic polymer 7 | 137 |
| 5.11 | Phase contrast and fluorescent microscopy images of polymer 9 with <i>E. coli</i> MG1655 (a & b) and <i>S. mutans</i> NCTC 10449 (c & d) after undergoing procedure described in 3.2.1 | 139 |

| | | |
|------|---|-----|
| 5.12 | Microscopy images of <i>E. coli</i> MG1655 with a) Non-fluorescent boronic co-polymer 6 and b) Non-fluorescent, non-boronic polymer 7 after undergoing procedure described in 3.2.1. | 140 |
| 5.13 | Aggregation assay of <i>E. coli</i> with boronic and amine polymers. | 140 |
| 5.14 | Sample GPC trace of Galactose furnished glycopolymer 12 | 142 |
| 5.15 | Phase contrast and fluorescent microscopy images of <i>E. coli</i> MG1655 with mannose glycopolymer 11 (a & b) and galactose glycopolymer 12 (c & d) after undergoing procedure described in 3.2.1 | 143 |
| 5.16 | Phase contrast and fluorescent microscopy images of <i>S. mutans</i> NCTC 10449 with mannose glycopolymer 11 (a & b) and galactose glycopolymer 12 (c & d) after undergoing procedure described in 3.2.1 | 145 |
| 6.1 | Schematic representation of the potential mechanism for cytotoxic action of cationic polymers at membranes. Electrostatic attraction of polycations to anionic membrane headgroups is followed by insertion into the membrane and disruption of bilayers. | 148 |
| 6.2 | Modified a) Cationic pDMAEMA polymer (Cat-P1) and b) Betaine pDMAEMA polymer (Bet-P1) tested against <i>E. coli</i> MG1655 | 151 |
| 6.3 | 96 Well plate layout for MIC assay | 152 |
| 6.4 | Modified polymers tested in the MTT assay | 154 |
| 6.5 | MIC Results for betaine polymer. | 156 |
| 6.6 | MIC Results for Quaternized polymer. | 157 |
| 6.7 | MTT metabolism to fomazan. | 159 |
| 6.8 | MTT results of cationic polymers | 160 |
| 6.9 | MTT results of betaine polymers | 161 |
| 7.1 | Plot of change in OD ₆₀₀ and change in redox potential against time | 182 |

| | | |
|------|--|-----|
| 7.2 | Polymerisation kinetics of the different bacterial ATRP systems | 183 |
| 7.3 | Representative example of co-polymer composition calculation of METAC and MEDSA for polymer P1 | 185 |
| 7.4 | Representative example of co-polymer composition calculation of METAC and DHPMA for polymer P2 | 187 |
| 7.5 | Representative example of co-polymer composition calculation of MEDSA and DHPMA for polymer P3 | 189 |
| 7.6 | Bacteria population sizes with no polymer. | 191 |
| 7.7 | Aggregation behaviours of <i>E. coli</i> MG1655 mCherry and <i>P. aeruginosa</i> PAO1 pmE6032 GFP with P1 | 191 |
| 7.8 | Aggregation behaviours of <i>E. coli</i> MG1655 mCherry and <i>P. aeruginosa</i> PAO1 pmE6032 GFP with P7-WE | 192 |
| 7.9 | Aggregation behaviours of <i>E. coli</i> MG1655 mCherry and <i>P. aeruginosa</i> PAO1 pmE6032 GFP with P7-SE | 193 |
| 7.10 | Aggregation behaviours of <i>E. coli</i> MG1655 mCherry and <i>P. aeruginosa</i> PAO1 pmE6032 GFP with P7-WP | 194 |
| 7.11 | Aggregation behaviours of <i>E. coli</i> MG1655 mCherry and <i>P. aeruginosa</i> PAO1 pmE6032 GFP with P7-SP | 194 |
| 7.12 | Plot of change in OD ₆₀₀ against time for <i>E. coli</i> bacteria with its templated poly- mers, non-templated polymers and water. | 196 |
| 7.13 | Plot of change in OD ₆₀₀ against time for <i>P. aeruginosa</i> bacteria with its templated polymers, non-templated polymers and water. | 196 |
| 8.1 | General "click" reaction scheme | 207 |
| 8.2 | Schematic overview for bacterial mediated fluorescent bacterial tagging. R = methacry- late based polymer. | 208 |

| | | |
|-----|--|-----|
| 8.3 | removal of the TMS protecting group from the polymer was monitored using ^1H NMR tracking the removal of the methyls | 209 |
| 8.4 | Ultraviolet transilluminator image of bacteria after "click" | 210 |
| 8.5 | Phase contrast (a) and fluorescent (b) microscopy images of <i>E. coli</i> MG1655 with no polymer or azide present. | 210 |
| 8.6 | Phase contrast and fluorescent microscopy images of <i>E. coli</i> MG1655 with either alkyne polymer polymer (6) (a & b) or 3-azo-7-hydroxycoumarin (2) (c & d). . . . | 211 |
| 8.7 | Microscopy images of <i>E. coli</i> MG1655 mixed with 3-azo-7-hydroxycoumarin (2) and alkyne polymer 6 | 212 |
| 8.8 | Ultraviolet image of TLC plate of the polymer after "click" and coumarin azide . . | 214 |
| 9.1 | Chemical bacterial binding spectrum | 217 |
| 9.2 | Bacterial auto-nemesis | 218 |
| 9.3 | Bacterial ATRP summary | 219 |
| 9.4 | Bacterial templating summary | 220 |
| 9.5 | Antibiotic pro-drug concept | 222 |
| A.1 | Microscopy images of boronic co-polymer 9 with <i>E. coli</i> MG1655 | 225 |
| A.2 | Microscopy images of boronic co-polymer 9 with <i>S. mutans</i> NCTC10449 | 226 |
| A.3 | Microscopy images of mannose displaying glycopolymer 11 with <i>E. coli</i> MG1655 . | 227 |
| A.4 | Microscopy images of mannose displaying glycopolymer 12 with <i>E. coli</i> MG1655 . | 229 |
| A.5 | Microscopy images of mannose displaying glycopolymer with <i>S. mutans</i> NCTC 10449 | 230 |
| A.6 | Microscopy images of galactose displaying glycopolymer 12 with <i>S. mutans</i> NCTC 10449 | 231 |
| A.7 | Microscopy images of <i>E. coli</i> MG1655 with no polymer or azide present. | 232 |
| A.8 | Microscopy images of <i>E. coli</i> MG1655 with polymer 6 but no azide. | 233 |

| | | |
|------|---|-----|
| A.9 | Microscopy images of <i>E. coli</i> MG1655 with 3-azo-7-hydroxycoumarin (2) but no alkyne polymer. | 234 |
| B.1 | ¹ HNMR spectra of Benzyl-2-bromo-2-methylpropanoate. | 235 |
| B.2 | ¹³ CNMR spectra of Benzyl-2-bromo-2-methylpropanoate. | 236 |
| B.3 | FT-IR spectra of Benzyl-2-bromo-2-methylpropanoate. | 236 |
| B.4 | ¹ HNMR spectra of Coumarin 343 alkyl bromide. | 237 |
| B.5 | FT-IR spectra of Coumarin 343 alkyl bromide. | 238 |
| B.6 | FT-IR spectra of <i>tert</i> -butyl (2-aminoethyl)carbamate | 239 |
| B.7 | ¹ HNMR spectra of <i>tert</i> -butyl (2-methacrylamidoethyl)carbamate | 240 |
| B.8 | FT-IR spectra of <i>tert</i> -butyl (2-methacrylamidoethyl)carbamate. | 240 |
| B.9 | ¹ HNMR spectra of 2-methacrylamidoethanaminium chloride. | 241 |
| B.10 | ¹³ CNMR spectra of 2-methacrylamidoethanaminium chloride. | 242 |
| B.11 | ¹ HNMR spectra of 2-((2-methacrylamidoethylamino)methyl)phenylboronic acid. | 243 |
| B.12 | ¹ HNMR spectra of iodide terminated coumarin dye. | 244 |
| B.13 | ¹ HNMR spectra of 2-(N-Morpholino)ethyl-2-bromobutyrate. | 245 |
| B.14 | ¹³ CNMR spectra of 2-(N-Morpholino)ethyl-2-bromobutyrate. | 246 |
| B.15 | ¹ HNMR spectra of 3-(trimethylsilyl)prop-2-yn-1-yl methacrylate. | 247 |
| B.16 | ¹³ CNMR spectra of 3-(trimethylsilyl)prop-2-yn-1-yl methacrylate. | 248 |
| B.17 | FT-IR spectra of 3-(trimethylsilyl)prop-2-yn-1-yl methacrylate. | 248 |
| B.18 | ¹ HNMR spectra of 3-acetamido-2-oxo-2 <i>H</i> -chromen-7-yl acetate. | 249 |
| B.19 | ¹³ CNMR spectra of 3-acetamido-2-oxo-2 <i>H</i> -chromen-7-yl acetate. | 250 |
| B.20 | FT-IR spectra of 3-acetamido-2-oxo-2 <i>H</i> -chromen-7-yl acetate. | 250 |
| B.21 | ¹ HNMR spectra of 3-azo-7-hydroxycoumarin. | 251 |
| B.22 | ¹³ CNMR spectra of 3-azo-7-hydroxycoumarin. | 252 |
| B.23 | FT-IR spectra of 3-azo-7-hydroxycoumarin. | 252 |
| B.24 | ¹ HNMR spectra of non-templated polymer of MEDSA AND METAC. | 253 |

| | |
|--|-----|
| B.25 ^1H NMR spectra of water wash <i>E. coli</i> templated polymer of MEDSA AND METAC. | 253 |
| B.26 ^1H NMR spectra of salt wash <i>E. coli</i> templated polymer of MEDSA AND METAC. | 254 |
| B.27 ^1H NMR spectra of water wash <i>P. aeruginosa</i> templated polymer of MEDSA AND METAC. | 254 |
| B.28 ^1H NMR spectra of salt wash <i>P. aeruginosa</i> templated polymer of MEDSA AND METAC. | 255 |
| B.29 ^1H NMR spectra of non-templated polymer of MEDSA AND DHPMA. | 256 |
| B.30 ^1H NMR spectra of water wash <i>E. coli</i> templated polymer of MEDSA AND DHPMA. | 256 |
| B.31 ^1H NMR spectra of salt wash <i>E. coli</i> templated polymer of MEDSA AND DHPMA. | 257 |
| B.32 ^1H NMR spectra of water wash <i>P. aeruginosa</i> templated polymer of MEDSA AND DHPMA. | 257 |
| B.33 ^1H NMR spectra of salt wash <i>P. aeruginosa</i> templated polymer of MEDSA AND DHPMA. | 258 |
| B.34 ^1H NMR spectra of non-templated polymer of METAC AND DHPMA. | 259 |
| B.35 ^1H NMR spectra of water wash <i>E. coli</i> templated polymer of METAC AND DHPMA. | 259 |
| B.36 ^1H NMR spectra of salt wash <i>E. coli</i> templated polymer of METAC AND DHPMA. | 260 |
| B.37 ^1H NMR spectra of water wash <i>P. aeruginosa</i> templated polymer of METAC AND DHPMA. | 260 |
| B.38 ^1H NMR spectra of salt wash <i>P. aeruginosa</i> templated polymer of METAC AND DHPMA. | 261 |
| C.1 GPC data for the polymerisation of 2-(dimethylamino)ethyl methacrylate by ATRP in the charge chapter. | 262 |
| C.2 GPC data for poly(2-(dimethylamino)ethyl methacrylate) by ATRP in the charge chapter. | 263 |

| | | |
|------|---|-----|
| D.1 | Change in <i>E. coli</i> MG1655 mCherry cluster sizes with time in suspension with the non-templated control polymer P1 | 266 |
| D.2 | Change in <i>P. aeruginosa</i> PA01 GFP cluster sizes with time in suspension with the non-templated control polymer P1 | 266 |
| D.3 | Change in <i>E. coli</i> MG1655 mCherry cluster sizes with time in suspension with the water washed <i>E. coli</i> templated polymer P7-WE | 267 |
| D.4 | Change in <i>P. aeruginosa</i> PA01 GFP cluster sizes with time in suspension with the water washed <i>E. coli</i> templated polymer P7-WE | 267 |
| D.5 | Change in <i>E. coli</i> MG1655 mCherry cluster sizes with time in suspension with the salt washed <i>E. coli</i> templated polymer P7-SE | 268 |
| D.6 | Change in <i>P. aeruginosa</i> PA01 GFP cluster sizes with time in suspension with the salt washed <i>E. coli</i> templated polymer P7-SE | 268 |
| D.7 | Change in <i>E. coli</i> MG1655 mCherry cluster sizes with time in suspension with the water washed <i>P. aeruginosa</i> templated polymer P7-WP | 269 |
| D.8 | Change in <i>P. aeruginosa</i> PA01 GFP cluster sizes with time in suspension with the water washed <i>P. aeruginosa</i> templated polymer P7-WP | 269 |
| D.9 | Change in <i>E. coli</i> MG1655 mCherry cluster sizes with time in suspension with the salt washed <i>P. aeruginosa</i> templated polymer P7-SP | 270 |
| D.10 | Change in <i>P. aeruginosa</i> PA01 GFP cluster sizes with time in suspension with the salt washed <i>P. aeruginosa</i> templated polymer P7-SP | 270 |
| E.1 | Graph of the 95% confidence intervals for the estimation of METAC AND DHPMA reactivity ratios. | 275 |

List of Schemes

| | | |
|-----|---|-----|
| 1.1 | Co-polymerization of poly(<i>p</i> -phenylene ethenylene) followed by subsequent conjugation to sugar amine. | 44 |
| 1.2 | Schematic for generation of thiol terminated mannose-acrylamide-co-acrylamide copolymer and binding to gold nanoparticles followed by incubation with bacteria. . | 62 |
| 1.3 | General mechanism of ATRP | 71 |
| 1.4 | Copper mediated ATRP | 73 |
| 4.1 | Synthesis of Benzyl-2-bromo-2-methylpropanoate | 86 |
| 4.2 | Polymerisation of 2-(dimethylamino)ethyl methacrylate | 87 |
| 4.3 | Synthesis of Coumarin 343 alkyl bromide | 88 |
| 4.4 | Fluorescent labeling of pDMAEMA | 89 |
| 4.5 | Quaternisation of fluorescent pDMAEMA | 90 |
| 4.6 | Sulfobetainisation of fluorescent pDMAEMA | 92 |
| 5.1 | Synthesis of <i>tert</i> -butyl (2-aminoethyl)carbamate | 114 |
| 5.2 | Synthesis of <i>tert</i> -butyl (2-methacrylamidoethyl)carbamate | 115 |
| 5.3 | Synthesis of 2-methacrylamidoethanaminium chloride | 116 |
| 5.4 | Synthesis of <i>tert</i> -butyl (2-aminoethyl)carbamate | 117 |
| 5.5 | Polymerisation of 2-((2-methacrylamidoethylamino)methyl)phenylboronic acid . . | 118 |

| | | |
|------|---|-----|
| 5.6 | Polymerisation of 2-((2-methacrylamidoethylamino)methyl)phenylboronic acid and <i>N</i> -(3-(dimethylamino)propyl)methacrylamide | 119 |
| 5.7 | Polymerisation of <i>N</i> -(3-(dimethylamino)propyl)methacrylamide | 120 |
| 5.8 | Synthesis of 2-iodoethyl 11-oxo-2,3,5,6,7,11-hexahydro -1 <i>H</i> -pyrano(2,3- <i>f</i>)pyrido(3,2,1- <i>ij</i>)quinoline-10-carboxylate | 121 |
| 5.9 | Fluorescent tagging of poly(2-((2-methacrylamidoethylamino)methyl)phenylboronic acid-co- <i>N</i> -(3-(dimethylamino)propyl)methacrylamide | 123 |
| 5.10 | Fluorescent tagging of poly(<i>N</i> -(3-(dimethylamino)propyl)methacrylamide) | 124 |
| 7.1 | Mechanism of AGET ATRP | 166 |
| 7.2 | Synthesis of 2-(<i>N</i> -Morpholino)ethyl-2-bromobutyrate | 167 |
| 7.3 | Polymerisation of MEDSA and METAC by ATRP in water | 169 |
| 7.4 | Polymerisation of DHPMA and METACT by ATRP in water | 170 |
| 7.5 | Polymerisation of DHPMA and MEDSA by ATRP in water | 171 |
| 7.6 | Polymerisation of METAC and 2,3-dihydroxypropyl methacrylate by bacterial acti- vated ATRP | 177 |
| 7.7 | Polymerisation of MEDSA and DHPMA by bacterial activated ATRP | 179 |
| 8.1 | Synthesis of 3-acetamido-2-oxo-2 <i>H</i> -chromen-7-yl acetate (1). | 200 |
| 8.2 | Synthesis of 3-azo-7-hydroxycoumarin (2). | 201 |
| 8.3 | Synthesis of 3-(trimethylsilyl)prop-2-yn-1-yl methacrylate (3) | 202 |
| 8.4 | Polymerisation of 2-(dimethylamino)ethyl methacrylate | 203 |
| 8.5 | Quaternisation of polymer (4) using methyl iodide | 204 |
| 8.6 | Removal of TMS protecting groups from dual functional polymer | 205 |

Abbreviations

| Abbreviation | Explanation |
|----------------------|---|
| ^1H NMR | Proton nuclear magnetic resonance spectroscopy |
| ^{13}C NMR | Carbon 13 nuclear magnetic resonance spectroscopy |
| ATRP | Atom transfer radical polymerisation |
| <i>E. coli</i> | <i>Escherichia coli</i> |
| <i>P. aeruginosa</i> | <i>Pseudomonas aeruginosa</i> |
| <i>S. mutans</i> | <i>Streptococcus mutans</i> |
| 3-oxo-C12-AHL | <i>N</i> -(3-oxododecanoyl)-L-homoserine lactone |
| 3-oxo-C6-AHL | <i>N</i> -(β -ketocapryloyl)-DL-homoserine lactone |
| AA | Acrylamide |
| AFM | Atomic force microscopy |
| AGET | Activators generated by electron transfer |
| AHL | <i>N</i> -acyl-L-homoserine lactone |
| AI-2 | Autoinducer 2 |
| AR-S | Alizarin Red S |
| ARGET | Activator regenerated by electron transfer |

| Abbreviation | Explanation |
|--------------|--|
| ATRP | Atom transfer radical polymerisation |
| b-ATRP | Bacterial activated atom transfer radical polymerisation |
| BiPy | Bipyridine |
| CC | Column chromatography |
| CFU | Colony forming units |
| ConA | Concavalin A |
| CRP | Controlled radical polymerisation |
| Cu | Copper |
| D-Ala D-Ala | D-Alanine, D-Alanine |
| DCM | Dichloromethane |
| DEAEM | <i>N,N</i> -diethylaminoethyl methacrylate |
| DHPMA | 2,3-dihydroxypropyl methacrylate |
| DLS | Dynamic light scattering |
| DMAEMA | 2-(dimethylamino)ethyl methacrylate |
| DMF | Dimethylformamide |
| DMSO | Dimethyl Sulfoxide |
| DNA | Deoxyribonucleic acid |
| DP | Degree of polymerisation |
| DPD | (S)-4,5-dihydroxy-2,3-pentanedione |
| ECM | Extra-cellular matrix |

| Abbreviation | Explanation |
|--------------------|---|
| EDAC | 1-ethyl-3-(3-dimethylaminopropyl)-carbodiimide |
| EGMP | Ethylene glycol methacrylate phosphate |
| <i>E. coli</i> | <i>Escherichia coli</i> |
| FBS | Foetal bovine serum |
| FimH | Fimbriae adhesin responsible for binding to D-Mannose |
| FRET | Förster resonance energy transfer |
| FT-IR | Fourier transform infrared spectroscopy |
| GBP | Glucan binding protein |
| GFP | Green fluorescent protein |
| GPC | Gel permeation chromatography |
| HMTETA | 1,1,4,7,10,10-hexamethyltriethylenetetramine |
| I | Initiator |
| IA | Itaconic acid |
| IgG | Immunoglobulin G |
| k_{act} | pseudo first order activation rate constant |
| k_{deact} | pseudo first order deactivation rate constant |
| K_{eq} | Association constant for diol and boronic species |
| K_{eq1} | Association constant for alizarin red-s and boronic species |
| k_{p} | polymerisation rate constant |
| k_{t} | Termination rate constant |

| Abbreviation | Explanation |
|--------------|--|
| L | Ligand |
| LB | Luria Broth |
| LCST | Lower critical solution temperature |
| LPS | Lipopolysaccharides |
| M | Monomer |
| M_n | Number average molecular weight |
| M_w | Weight average molecular weight |
| MA | Methacrylic acid |
| MBAA | <i>N, N'</i> -methylene bisacrylamide |
| MEDSA | [2-(methacryloyloxy)ethyl]dimethyl-(3-sulfopropyl)ammonium hydroxide |
| METAC | [2-(methacryloyloxy)ethyl]trimethyl ammonium chloride |
| MIC | Minimum inhibitory concentration |
| MIP | Molecularly imprinted polymer |
| MPT | mannose-polythiophene |
| Mt | Transition metal |
| MTT | 3-(4,5-Dimethylthiazol-2-yl)-2,5-diphenyltetrazolium bromide |
| NHS | <i>N</i> -hydroxysuccinimide |
| NIPAM | <i>N</i> -isopropylacrylamide |

| Abbreviation | Explanation |
|-----------------------------|---|
| NMR | Nuclear magnetic resonance |
| OD | Optical density |
| OD ₆₀₀ | Optical density measured at 600 nm |
| p(DMAEMA) | poly[2-(dimethylamino)ethyl methacrylate] |
| p(NIPAM) | poly[N-isopropylacrylamide] |
| P _n -X | Dormant polymer |
| P _n [*] | Growing polymer radical |
| <i>P. aeruginosa</i> | <i>Pseudomonas aeruginosa</i> |
| PBS | Phosphate buffered saline (pH 7.4) |
| PDA | 10,12-Pentacosdioic acid |
| PCR | Polymerase chain reaction |
| PDI | Poly dispersity index |
| PEO | poly(Ethylene oxide) |
| <i>P. gingivalis</i> | <i>Porphyromonas gingivalis</i> |
| PPE | Poly(<i>p</i> -phenylene ethynylene) |
| ppm | parts per million |
| <i>Pseudomonas</i> | <i>Pseudomonas aeruginosa</i> |
| PVP | poly(4-vinylpyridine) |
| QS | Quorum sensing |

| Abbreviation | Explanation |
|--------------|---|
| RAFT | Reversible addition-fragmentation chain transfer polymerisation |
| RI | Differential refractometer |
| ROMP | Ring opening metathesis polymerisation |
| RP | Radical polymerisation |
| SAMs | Self-assembled monolayers |
| siRNA | small interfering ribonucleic acid |
| SPR | Surface plasmon resonance |
| SPT | Sialic acid polythiophene |
| SR & NI | Simultaneous reverse and normal initiation |
| TEM | Transmission electron microscopy |
| TLC | Thin layer chromatography |
| TMS | Tetramethylsilane |
| TMSPMA | 3-(trimethylsilyl)prop-2-yn-1-yl methacrylate |
| V501 | 4, 4'-Azobis (4-Cyanovaleric Acid) |
| X | Halogen |

Abstract

The detection and control of microorganisms such as bacteria is important in a wide range of industries and clinical settings. Detection, binding and removal of such pathogenic contaminants can be achieved through judicious consideration of the targets which are available at or in the bacterial cell. Polymers have the ability to present a number of binding ligands for cell targeting on one macromolecule and so avidity of interaction can be greatly increased.

The goal of the project was to test whether polymers generated with bacteria *in situ* would have their composition significantly altered to determine if a templating process was occurring. It was also anticipated that the templated polymers would have better re-binding properties than those produced in the absence of bacteria.

A series of chemical functionalities were analysed for their binding properties to bacteria. The functionalities were chosen with consideration to the cell surface characteristics. Further to identification of the most binding and least binding functionalities the polymers were tested for their cytotoxicity against bacteria and human epithelial cells. Concentration ranges were determined which could facilitate bacterial binding and templating yet minimise the lethality of the processes.

Templated polymers of the bacteria were generated using a novel method of atom transfer radical

polymerisation (ATRP) which we have termed *bacterial activated atom transfer radical polymerisation* (b-ATRP). This polymerisation method has maximised the potential for templating processes to occur during the polymerisation. Templated polymers differed in both their composition and their binding behaviour to non-templated polymers.

The bacterial organic reduction process has also been demonstrated to have greater scope for use within the organic chemistry field as demonstrated by the use of this system to enable in "click-chemistry" *via* the reduction of copper.

Acknowledgements

I would like to thank my supervisors Cameron Alexander, Beppe Mantovani, Klaus Winzer and also Francisco Fernandez Trillo without whose help this wouldn't have been possible. I would like to thank my friends and colleagues that I have met during my time in Nottingham for not only the academic support but also for their friendship. Finally I would like to thank GlaxoSmithKline Consumer Healthcare for funding.

Chapter 1

Introduction

1.1 Background

Bacteria are a cause of significant acute and also chronic disease and their infections can have a serious and detrimental impact on quality of life and mortality.[4, 5] Socio-economic factors associated with infectious diseases have large societal impacts.[6] Bacteria are utilised by a wide range of industries from food to biotechnological. The latter of these require highly specific methods of bacterial labelling and detection. Currently expensive monoclonal antibodies provide excellent results but excluding price, can be otherwise technically difficult due cold-chain necessity and immunogenicity. The detection and capture of microorganisms using chemical and polymeric methods is accordingly an expanding and developing field.[7]

1.2 Introduction to bacterial cell wall and surface structures

In order to understand the interactions between bacteria and exogenous monomeric ligands it is necessary for one to be aware of chemical functionalities present at the surface of bacterial cells.

1.2.1 The bacterial cell

Historically bacteria have been divided into two classes or groupings based upon their interactions with iodine and crystal violet dye (the so called "Gram stain").[8]

Those bacteria which were stained dark were denoted as Gram-positive or if they stained a lighter pink colour the bacteria were classed as Gram-negative. The difference in the staining of these bacteria reflects a substantial difference between the structures of their cell walls.[9] The thick cell wall of the Gram-positives are responsible for their differences in Gram staining.

Gram-positive bacteria

Gram-positive bacteria such as *Streptococcus mutans* have a thick outer cell wall made up of mainly peptidoglycan (Figure 1.1). In the Gram-positive bacteria peptidoglycan can account for 30-70% of the total cell mass.[10] As the name suggests peptidoglycan consists of s glycan chains cross-linked by peptide units. The structure of peptidoglycan can vary significantly between species of Gram-positive bacteria while it remains constant for Gram-negatives.

The Gram-positive bacteria have the characteristic inclusion of cell wall glycopolymers for example teicholic acid.[1] Although the outer structure of the cell for most Gram-positive bacteria is largely similar, the composition of the glycopolymers is highly variable which is a key surface feature.

Gram-negative bacteria

This structure contrasts with Gram-negative bacteria such as *Porphyromonas gingivalis* that have a plasma membrane, surrounded by a thin peptidoglycan sacculus all contained within an outer membrane (Figure 1.2).[2]

The Gram-negative bacteria, as shown in Figure 1.2, have a much smaller proportion of peptidoglycan than Gram-positive bacteria (Figure 1.1). Their surfaces are characterised by the presence of the lipopolysaccharides (LPS) and lipoprotein.

The bacterial lipopolysaccharides (LPSs) consist of three parts; Lipid A (endotoxin), a core non-

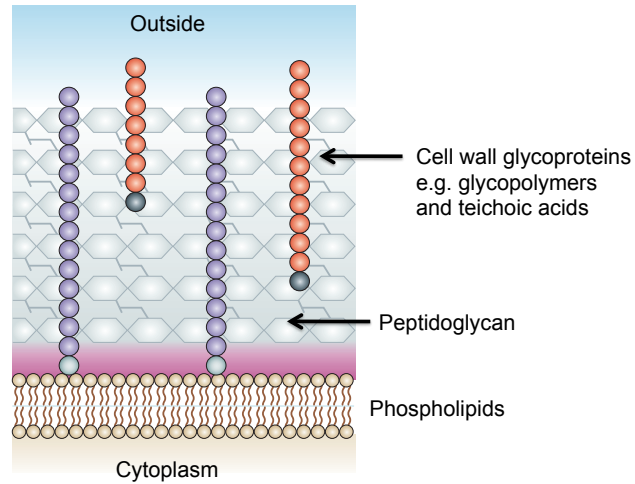


Figure 1.1: Example of the cellular structure of a Gram-positive bacterium: *Staphylococcus aureus*.^[1]

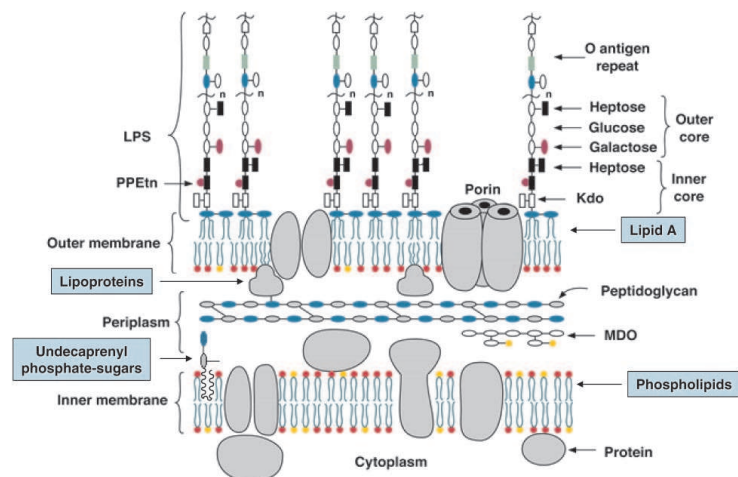


Figure 1.2: Example of the simplified cellular structure of a Gram-negative bacterium: *Escherichia coli* (*E. coli*).^[2]

repeating oligosaccharide and the final polysaccharide of repeating units known as the O-antigen.[2] From Figure 1.2 it can be seen that *lipid A* is an essential component of the cell's outer membrane. It is also responsible for the activation of the innate immunity cascade. The outer most component of the LPS is the so-called O-antigen and this unit has high variability. It is made of various saccharides and non-saccharide components. This variability can be illustrated with the above example of *Escherichia coli* (*E. coli*) where the species displays 170 O-serotypes.[2]

Bacterial surface charge

It is known that microorganisms are largely negatively charged,[11] whilst most healthy animal cells have asymmetric charge distribution and have an external containment membrane comprising of zwitterions. The Gram-negative bacteria, as discussed, contains lipopolysaccharides whereas the Gram-positive bacteria have cell wall glycopolymers e.g. teichoic acid.[1] Both features on the surface of the bacterial cell serve to impart a negative charge.[12] Bacterial cells also contain phospholipid stabilised membranes. These are found on the inner membrane of the Gram-negative bacteria or are the single membrane of Gram-positive bacteria. The phospholipid membrane of bacteria are highly negatively charged which further results in the cells holding a net negative charge.[11]

Bacterial surface sugars

In addition, the bacterial surface contains other polysaccharide based structures.[10, 13, 2] They can be found in different forms and different levels of abundance depending on the type and strain of bacteria.[14]

Glycan, as previously discussed is a variable hexose and a constituent of all cell walls, it contains an amino sugar which is only found in bacteria. The chain length can vary greatly within a particular cell but there is a correlation between average chain length and cell shape.[10]

Polysaccharides may also be found in constituents of cell walls such as lipopolysaccharides, which are found on the Gram-negative bacterial surface, as discussed earlier.

Bacterial sugar binding proteins

Lectins are important carbohydrate specific recognition proteins relevant for most living processes. They enable the communication between cells and are involved with both normal cell and tissue function and also the development of disease.[15]

Lectins are utilised by a variety of pathogens to enable attachment and infection of the host. One such characterised example is that of the mannose specific fimbriae (fimH) of the *E. coli*. [16] This lectin varies in its propensity to bind to mannose containing molecules. This variation reflects the ability of the bacteria phenotypes to infect different host tissues. For example those which bind with a low affinity are more likely to infect the oral and gastrointestinal mucosa. As stated these lectins are not restricted to one bacterial strain.

The galactose-binding adhesin on *Fusobacterium nucleatum* (FN-2) is capable of detecting subtle differences in galactosyl residues as confirmed through agglutination inhibition assays.[17] It induces binding to soluble sugars and also enables attachment of the *F. nucleatum* to other oral bacteria[18] such as *Prophyromonas gingivalis* and *Actinobacillus actinomycetemcomitans* as well as a variety of eukaryotic cells including human buccal epithelial cells, gingival and periodontal ligament fibroblasts.

Fusobacterium nucleatum are not the only bacteria in the mouth to contain protein receptors for sugar recognition. *Streptococcus mutans* is a species which produces and recognises glucan - an α 1-6 linked linear polymer of glucose with an α 1-3 linked glycosidic bridges which is produced as a result of sucrose metabolism with the other metabolite being lactic acid.[14] Postulations as to the precise function of the glucan binding protein (GBP) range from; to aid bacterial attachment and retention to surfaces, to its role as an essential surface enzyme[19] and also for maintaining biofilm structure.[20]

After reviewing key bacterial surface structures a rational design approach can be taken to consider how polymers with key functionalities can aid in cellular capture.

1.2.2 Oral disease and microbial pathogens

Many diseases of the oral mucosa are known to have a bacterial aetiology[21, 22, 14] and although preventable with good oral hygiene, still affect many adults and children in the developed world where access to preventative treatments are readily available. It is therefore an area where an improvement in the treatment is needed and knowledge of the key bacteria involved and their key surface structures may help.

Current measures aimed at preserving oral health involve mechanical abrasion to remove food debris and biological matter i.e. brushing teeth, or chemical obliteration of bacterial populations i.e. mouthwash. These measures are largely effective but non-specific. Most bacteria in the mouth exist in a balance with the host, serving to protect the mucosa from harmful invaders.

The effects of removing the native oral bacterial population and its subsequent re-colonisation may be illustrated with the example of prolonged antibiotic usage. It is well documented in the literature that use of broad spectrum antibiotics can lead to infection with opportunistic pathogens such as fungi due to ablation of the natural flora.[23] Although the effects of the current dental hygiene measures are not as extreme they could play a similar role in those patients with a weakened immune response.

Further highlighting a need for an advancement to current dental hygiene measures is that of infective endocarditis and bacteraemia as a result of brushing teeth or dental care measures.[5] It has been demonstrated that when comparing bacteraemia with species known to cause infective endocarditis resulting from teeth brushing, dental extraction and dental extraction with co-administration with amoxicillin there can be the introduction of bacteria into the blood stream. Subjects were randomly assigned to groups by a computer and blood samples taken at specified intervals. The levels of bacteria in the blood were all found to be short lived but without the

antibiotic could persist for up to 60 minutes. Blood bacterial levels were lower in the brushing group compared with the extraction group but it should be highlighted the relative frequency of this hygiene procedure.

The preservation of oral health is widely documented and advocated by all healthcare professionals. Its benefits extend beyond the mouth and aesthetics and can help prevent a variety of conditions such as stroke[24] and other fatal cardiovascular health problems[25, 26].

It is beyond the scope of this work to explain in detail all diseases of the oral mucosa therefore only the aetiology of dental caries and periodontitis shall be described.

Dental caries have been extensively reviewed in the lancet where information from systematic reviews, peer reviewed journals among others were used.[27] These studies proposed that all the various types of caries share the same formation key steps. Endogenous bacteria within the biofilm of the tooth produce acids as a result of carbohydrate metabolism, leading to a local drop in pH and demineralisation of the tooth. The cariogenic bacteria attributed to this process are *Streptococcus mutans* (*S. mutans*), *Streptococcus sobrinus* and *Lactobacillus sp.*,[28, 27] it is however *Streptococcus mutans* which is more significantly implicated.[14]

Much work has been published in this field and the association is clear that there is a link with significance figures of up to $P > 0.0001$ quoted between the presence of dental caries and *S. mutans*. [29]

Periodontal disease is similar to formation of dental caries in that there is an imbalance between the host and bacterial factors. The disease involves a group of infections whereby the gum and connective tissues of the mouth are attacked. It exists as a spectrum from mild inflammation of the gums known as gingivitis to complete loss of the gum tissue and eventually the tooth: periodontitis. Many species of bacteria isolated from humans have been implicated in the progression of this disease with the Gram-negative anaerobic bacterium *Porphyromonas gingivalis* (*P. gingivalis*)

being implicated in the severe adult forms.[30]

Although this bacterium has one of the most prominent and significant roles in the development of this disease state it is not alone in that there are a multitude of putative pathogens, which have been implicated and subject to analysis.

An early study involved 24 male subjects and 1 female subject with initially healthy gums and good oral hygiene. They were to allow the accumulation of dental plaque and subsequent development of mild gingivitis. Samples of the plaques were collected at one week intervals and anaerobically cultivated. Gram-positive *Actinomyces* particularly *A. viscosus* and *A. israelii* levels were found to increase the most significantly in both number and mass.[22]

Of the Gram-positive cocci *Streptococci sanguis* and *Streptococci mitis* levels had initially risen but then dropped over the 3 week period. This was in line with the fact that these bacteria are known to be initial colonisers of the tooth. Gram-negative species were largely represented by *Veillonella* sp. although there had been an increase in several other varieties including *Fusobacterium nucleatum* (*F. nucleatum*), *Campylobacter* and *Bacteroides melaninogenicus*. The study highlighted the connection between plaque age and gingivitis scoring, but no correlation between bacteria count/DNA content of plaque and gingivitis i.e. gingivitis continued to worsen once bacterial levels had plateaued.[22]

This correlates well with later work which highlights that *F. nucleatum*, *Campylobacter* sp., *P. gingivalis* and *Treponema* sp. amongst others, as only being present in diseased sites and rarely those of healthy individuals.[21, 31]

In 1998 work by Socransky *et al.* was carried out to categorise common bacterial communities using community ordination.[32] 185 subjects were selected, mostly with a history of periodontal disease but not in the preceding 3 months, producing a total of 13,261 plaque samples. An ordination group designated the "red complex" was associated with the deepest periodontal pockets and the most bleeding upon probing. This complex was constituted of *Bacteriodes forsythus*, *P. gingivalis*

and *Treponema denticola*. The authors were unable to state the reason for the association between the organisms but noted their aggregation occurred *in vitro*. Interestingly they also noted that sites containing *P. ginigivalis* were associated with the deepest pockets, either alone or with the others of the complex, supporting current evidence of its involvement with this disease.

The red complex is highly associated with an "*orange complex*" which is made up of several other bacterial forms including *Fusobacterium nucleatum*. This serves to display the complex picture of periodontal disease. The "*orange complex*" was also associated with an influence upon pocket depth although its connection to the clinical situation was less clear than that of the "*red complex*".

The authors postulated that better knowledge of these complex ecosystems may aid in strategies to control them, as; **influencing one member of such an interdependent community may affect the colonisation by all members.**

1.3 Bacterial detection, neutralisation and capture

The benefits of the successful detection and capture of bacteria, range from healthcare and beyond into industry. Many types of established detection techniques have already been employed for a variety of pathogens, utilising a number of analytical techniques.[33] These systems can offer sensitive detection but may require large capital investment in analytical equipment e.g. flow-cytometers which can cost in excess of 30,000 (pounds sterling) or require the prior knowledge of putative pathogens e.g. immunoassays. Whilst techniques such as polymerase chain reaction (PCR) are cheap they are unable to retrieve the bacterial pathogen/contamination.

It is from the limitations of current technologies that the investigation of polymeric systems for cell detection is continuing to grow. Polymers offer a versatile scaffold onto which a number of chemistries can be applied to tailor the system to the desired functionality. The aim of this project is to introduce methods that utilise polymer-bacteria interactions to generate specific recognition

devices. The benefits from the capture of micro-organisms in a selective manner range from food hygiene to biological warfare counter-measures. The selective removal of specific key pathogens in diseases, such as those affecting the mouth, have benefits due the complex and often inter-dependent microbial ecosystems which exist in the human body.[32]

Polymeric materials have the potential to present ligands to receptors in a multivalent manner where macromolecular entities displaying multiple copies of one or more recognition elements can bind multi-centre receptors (Figure 1.3).

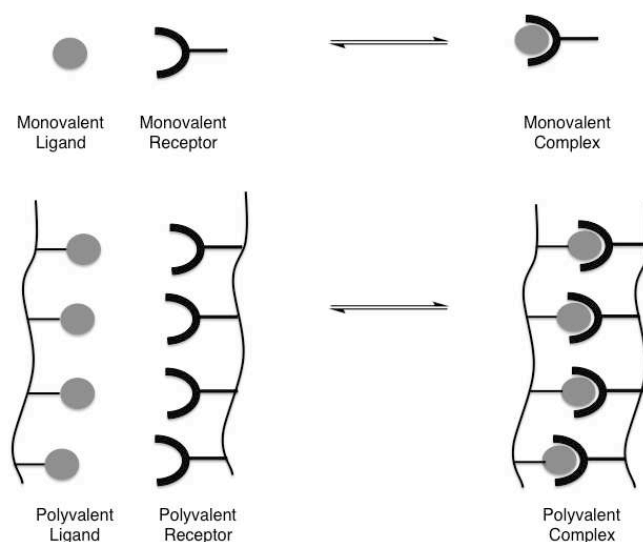


Figure 1.3: Scheme showing the difference between monovalent interactions and polyvalent interactions which differ in characteristics including magnitude. Polyvalent interactions increase strength of binding through cooperation. Adapted from Mammen, Choi and Whitesides.[34]

This has the benefit of replicating closely the types of interactions that occur in living systems[34] for example when viruses and bacteria encounter their hosts. In a key review, Mammen, Choi and Whitesides described how these multivalent interactions can be exploited to provide benefits to pharmaceuticals and diagnostics. Polymeric ligands have already been demonstrated to inhibit virus interactions with human cells.[35]

Polymer scientists are accordingly well placed to utilise the multivalent characteristics of living systems for treatment and prevention of disease. Polymers are also synthetically useful for scaling up production; generating quantities sufficient to enable a move from lab bench to patient bedside. A variety of chemical groups have been identified already for their propensity to bind bacteria, viruses and yeasts. Many of these have been employed in polymers to induce attachment for capture,[36] inhibition,[37] detection[38] and toxicity.[39]

Polymers are useful, as different functionalities can be incorporated per chain to enable highly tuneable behaviour. These various chemical groups and functionalities may be useful for targeting various micro-organisms when one considers the biological target at hand (Figure 1.4). As such in this introduction chapter, four sections shall explore the current state of the art of polymer-bacterial binding based upon microbiological target features:

Bacterial recognition through saccharides

Cell surface charge

Cell wall and shape

Intercell communication molecules

These are followed by an introduction to chemistries that may be included to enable visual bacterial detection.

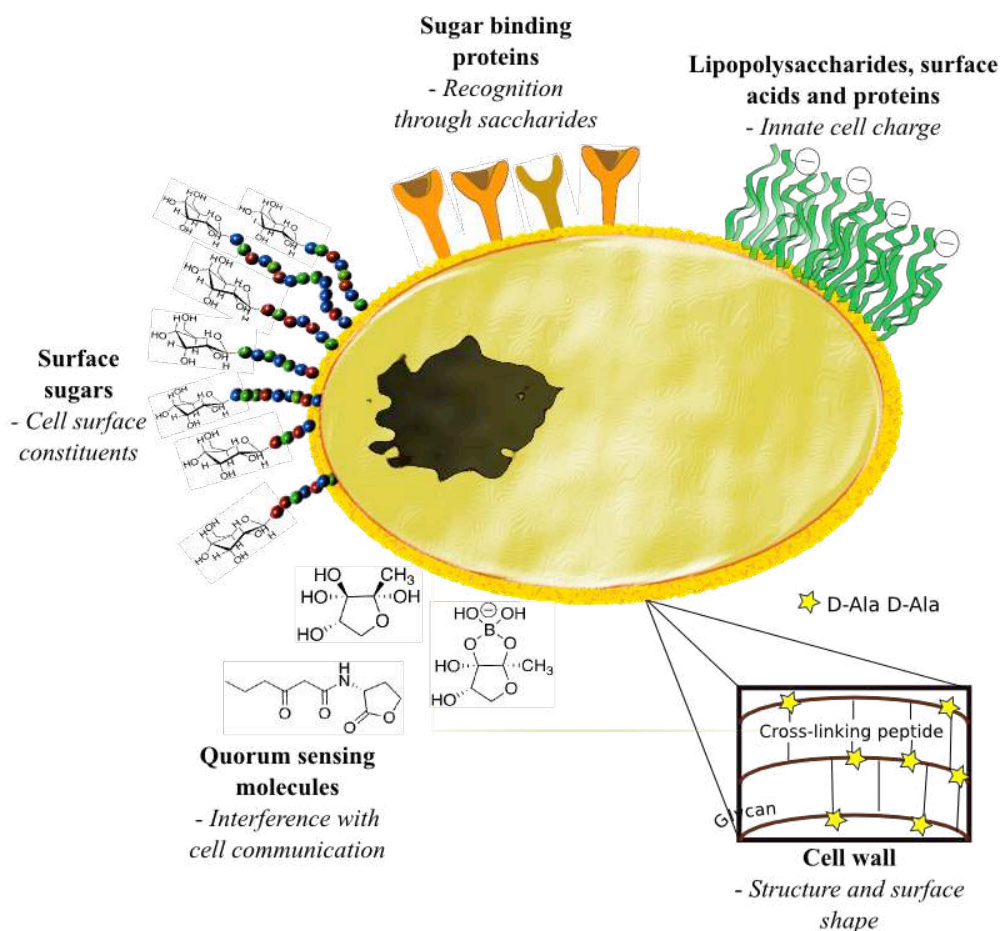


Figure 1.4: Overview of various bacterial targets.

1.3.1 Bacterial recognition through saccharides

The presence of carbohydrate recognition sites is well documented for many bacterial strains. Not only are sugars on eukaryotic cells important binding sites for micro-organisms such as bacteria but they are also found on the surface of bacteria to aid intercellular binding and identification.[40] Organisms can bind to each other's surface sugars in a homotypic (cells of the same type) and a heterotypic (cells of a different type) manner (Figure 1.5). Specific carbohydrate recognition proteins, termed lectins, are important for these binding processes.

Saccharide recognition and binding presents an ideal means to manipulate and influence cell recog-

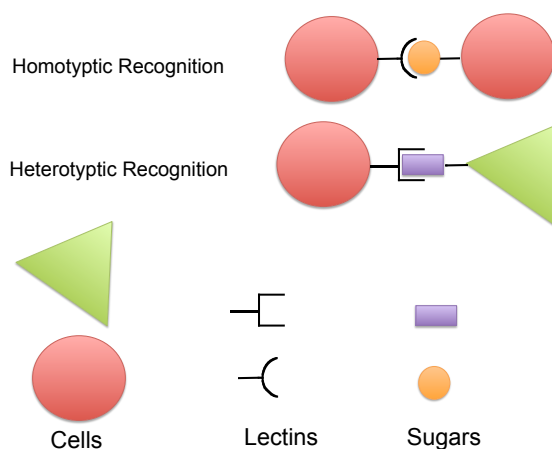


Figure 1.5: Figure showing carbohydrate binding involved in cell recognition. This can be either homotypic i.e. cells of the same type or heterotypic where different types of cells associate.

nition and disease processes in a specific yet tuneable manner.

Kiessling's group has contributed to the understanding of how polymeric systems may utilise the polyvalent nature of some lectins. Ring Opening Metathesis Polymerisation (ROMP) has been used to generate neoglycopolymers (Figure 1.6) which can bind avidly to a range of cell types.[41, 42, 43, 44, 45] The specific sequence and structure of sugars is important for cell recognition and the multivalent systems prepared by ROMP displayed significantly greater binding affinities than their monomeric counterparts.[43]

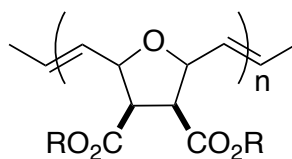


Figure 1.6: General structure of neoglycopolymer generated via. ROMP. R = O- or C-glycoside derivatives based upon glucose or mannose.

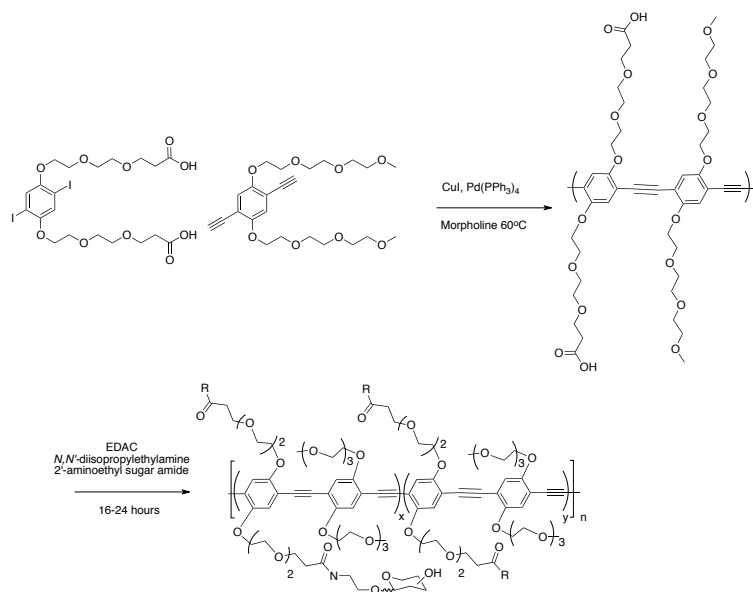
Similar ROMP polymers were used to show that binding to the lectin concanavalin A is increased by increasing the polymer chain length and thereby increasing the number of binding functionalities.[44] More importantly this relationship between polymer size and binding is non-

linear showing first exponential increases followed by an eventual plateau in binding. Apart from chain length, the structural order by which the sugars are presented can have a significant influence over its interaction with binding lectins.[42] Increasing the polymer chain length, or rather increasing the number of binding units, has also been demonstrated to result in a greater chemotactic response in variety of bacteria relative to the monomeric sugar.[41] This further shows the relevance of polymer therapeutics within the bacterial binding field.

The sugars both displayed and recognised by cells are known to impact greatly upon pathogenicity and virulence.[46] Many bacteria display specific proteins to aid adhesion to the host. For example *E. coli* FimH can bind oligomannose moieties to similar degrees between strains however the strains of *E. coli* vary in the propensity for their FimH to bind monomannose and so the bacteria may be classified according to this. The strength of this binding imparts specific colonisation modalities. A high affinity is associated with uropathogenic strains and a low affinity is associated with gut and intestinal strains.[16] Accordingly, carbohydrate-displaying polymers could potentially be tuned for specific cell recognition through mimicry or binding to FimH and associated variants.

The specific binding of *E. coli* to mannose has been utilised in the generation of fluorescent polymeric bacterial recognition systems.[47] Disney *et al.* demonstrated binding of polymeric mannose to *E. coli*. Poly(*p*-phenylene ethynylene) (PPE) was generated using Palladium-catalysed polymerisation (Scheme 1.1).

The resultant polymers were modified to display mannose and galactose moieties through 1-ethyl-3-(3-dimethylaminopropyl)-carbodiimide (EDAC) and *N, N'*-diisopropylethylamine mediated coupling to 2'-aminoethyl mannoside and galactoside. A Förster resonance energy transfer (FRET) experiment with the fluorescent glycopolymers and fluorescent sugar binding concavalin A (ConA) demonstrated that the polymer exhibited the ability to bind ConA and that this was not attributed to non-specific binding between ConA and the polymer. The polymers were then incubated with



Scheme 1.1: Co-polymerisation of poly(*p*-phenylene ethenylene) followed by subsequent conjugation to sugar azide. Polymers used: 1) $R = OH$ $x : y = 0 : 1$, 2a) $R = OH$ or $NH(CH_2)_2OH$ $x : y = 1 : 1$ sugar = mannose, 2b) $R = OH$ or $NH(CH_2)_2OH$ $x : y = 1 : 1$ sugar = galactose.

E. coli and an *E. coli* mutant that could not express the mannose-binding FimH. Only fluorescence and aggregation was seen with the mannose-functionalised polymers and the mannose-binding bacteria. The fluorescence observed from the bacterial clusters exhibited a redshift due to π -stacking as the bacteria brought the polymer chains closer together. This binding was attributed to the mannose binding FimH of the *E. coli*. Moreover, the binding of the polymeric mannose was greater than the sum of individual mannose recognition elements which the authors attributed to polyvalency.

Tunable bacterial binding using saccharides

Tunable bacterial capture involves the capture and release of bacteria when an external stimulus is applied, for example heat. This may be seen as advantageous whilst generating materials for bacterial capture and detection as it can enable a system to become reusable in a controlled manner. If stimuli such as heat is used where changes in the polymer conformation enables the attachment

and release of bacteria this negates the need for harsh or complex washes like strong acids, bases, multistep wash and re-purification steps and maximises the usefulness of the material.[48] Such systems may employ sugar binding mechanisms previously discussed, but preferably weak enough to allow release of the target and also the inclusion of other monomers or functionality to effect a tunable binding.

Thermoresponsive glycopolymers have been generated for bacterial capture and release.[48] Pasparakis *et al.* combined the polyvalency effects obtained from glycopolymers and the lower critical solution temperature (LCST) of poly(isopropylacrylamide) polymers to generate a reversible recognition system. Polymers of *N*-isopropylacrylamide (NIPAM) and *N*-hydroxyethylmethacrylamide or acrylamido *N*-hexanoic acid were generated via free radical polymerisation. Sugar functionalities were attached using beta-D-glucose pentaacetate followed by its deprotection (P1) or *N*-hydroxysuccinimide (NHS) mediated coupling to D-(+)-glucosamine HCl (P2) (Figure 1.7a).

The polymers had sharp LCSTs of 41°C and 44°C respectively. Above this temperature the polymers were in chain collapsed conformation and carbohydrate moieties were unavailable for binding with bacteria (*E. coli* MG1655pGFP). However, when the temperature was lowered the chains opened and bacterial aggregation was possible. Upon increasing the temperature again the bacteria dispersed as the carbohydrate functionalities became once again hidden. This was possible after three temperature cycles and was demonstrated to involve sugar binding proteins on the bacteria by using a glucose competition binding assay (Figure 1.7b).

The involvement of *E. coli* FimH was confirmed through a similar competitive assay with sucrose to which FimH has a lower affinity. As expected no loss in bacterial aggregation was observed. This offers an attractive method to generate a reusable material for bacterial detection and to control biofilm formation and its subsequent release.

The binding of sugar containing polymers to bacteria has been proposed to replicate the mecha-

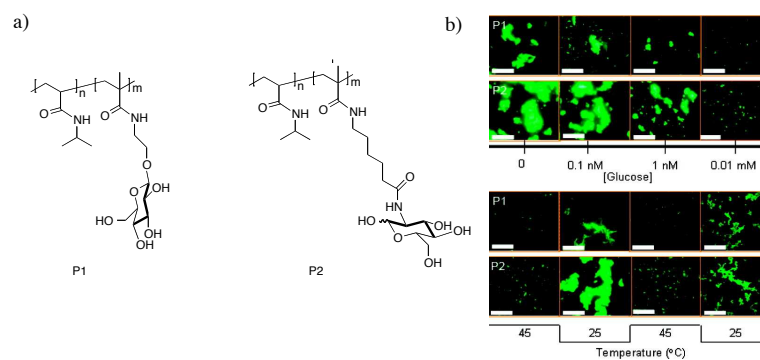


Figure 1.7: a) Structures of glycopolymers displaying glucose (P1) or glucosamine (P2) moieties b) (top). Glucose competition assay between polymers P1 and P2. b) (bottom) Oscillating temperature bacterial aggregation assay with polymers P1 and P2. P1 is a glucose-displaying polymer with the sugar attached at the anomeric carbon. P2 is a glucosamine displaying polymer with the sugar attached at the 2-amino position. Bacteria are *E. coli* MG1655 expressing green fluorescent protein.[48]

nisms by which inter-bacterial communication takes place. The size of vesicles formed by glycopolymers has been demonstrated to influence how bacterial aggregation takes place.[49] Pasparakis and Alexander generated a sugar displaying polymer vesicle system to enable the first insights into communication to bacteria by utilising sugar binding sites on the bacterium *E. coli* MG1655. Hydrophilic polymers, displaying glucose functionality were generated by either ATRP (P3) or Reversible Addition-Fragmentation chain Transfer (RAFT) polymerisation (P4) (Figure 1.8a) in methanol before being polymerised with the less soluble diethyleneglycol methacrylate in methanol or ethanol. Vesicles formed in solution however the size of the vesicles for P3 were smaller than those for P4 (around 300nm compared to 450 nm when below the lower critical solution temperature of 28°C).

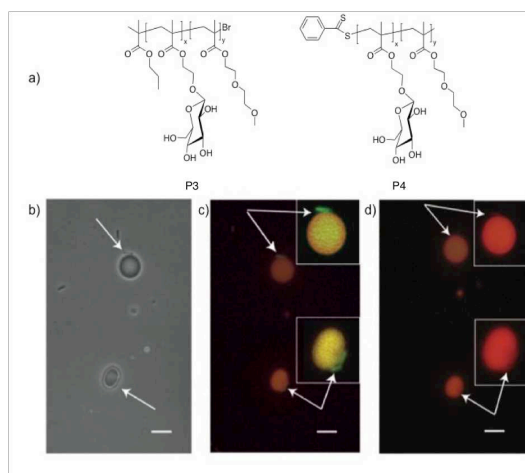


Figure 1.8: a) Structures of P3 produced by ATRP and P4 produced by RAFT. b) Interaction between vesicles of P4 with bacteria using phase contrast microscopy. c) Fluorescent microscopy image of the red, ethidium bromide encapsulated vesicles of P4 with the fluorescent green *E. coli*. d) Fluorescent microscopy image showing the transfer of the cationic ethidium bromide to the *E. coli* resulting in its colour change.

It was observed that the vesicles were able to release the fluorescent ethidium bromide dye which entered the bacteria and changed their fluorescence from green to red-orange. This gave an insight into the potential use of polymeric vesicles, displaying sugars to induce different types of bacterial

aggregates and engage in the delivery of dyes or communication molecules to bacteria.

Bacterial recognition and binding is demonstrable using saccharide functionalised polymers. These closely replicate binding events observed in nature, as such they present a method by which the polymer chemist may induce targeted capture.

1.3.2 Bacterial capture and elimination through cell charge

Almost all bacteria have an innate negative charge at physiological pH which has facilitated the use of various cationic antimicrobials through initial charge-charge binding followed by disruption of surface structures or insertion into the membrane.[12, 50] Interactions with cationic polymers can enable non-specific but highly avid bacterial binding. There has been a significant amount of work focused around the propensity for these materials to effectively bind and kill bacteria.

Rawlinson *et al.* have shown polycations to not only bind and effectively kill bacteria but increase the cytotoxicity of antibiotics against bacteria.[51] Poly[2-(dimethylamino)ethyl methacrylate] was modified with iodomethane on the tertiary amine to create polycations. These polycations exhibited their own antimicrobial action with minimum inhibitory concentrations (MIC); which are the concentrations of a compound required to inhibit bacterial growth. These ranged between 0.1-1 mg/mL for Gram-negative bacteria and 0.1- >18 mg/mL for Gram-positive bacteria. The polymers were not internalised by the bacteria and when used in concentrations four to ten times below their own MIC caused a decrease in the MIC of erythromycin against the Gram-negative bacteria used in this study and had a similar effect against Gram-positive bacteria. This was attributed to increasing cell permeability, as the site of action for erythromycin is within the cell.[52, 53]

The killing effect of these polymers has also been shown to be increased when combined with a hydrophobic component.[37] Lenoir *et al.* reported polycationic surfactants which can kill all *E.*

coli with concentrations as low as 150 $\mu\text{g/mL}$ with a contact time of two hours. This was a higher concentration than for their comparator benzalkonium chloride but the authors note that their relative concentration of quaternary ammonium component was lower in the polymer compared with the monomeric antimicrobial.

Klibanov *et al.* demonstrated polycations can be used to generate surfaces which can kill a variety of bacteria upon contact.[54] Cationic surfaces based upon poly(4-vinylpyridine) (PVP) were generated using two different methods following lamination of the glass. One method involved growing the polymers off the glass surface and for the other method, polymer was grafted to the glass. In both methods a permanent charge was subsequently added by reaction with an alkylbromide in nitromethane. They were assessed for their ability to kill bacteria when the bacteria were presented in an aerosol, to replicate an action similar to sneezing or coughing. Both the laminated glass surface and the unmodified polymer surfaces displayed poor inhibition of bacterial growth. Following modification of the polymer bacterial kill effectiveness increased. The effectiveness of this killing action was influenced not only by length of the PVP chain but also the hydrophobic alkyl group used to introduce a permanent positive charge. Longer PVP chains were more effective than shorter alkyl chains.

Matyjaszewski's group generated surfaces based upon poly[2-(dimethylamino)ethyl methacrylate] (PDMAEMA), which underwent post polymerisation modification with iodoethane to introduce a permanent positive charge.[39] These surfaces were extremely effective at killing bacteria and this was related to the charge density as extrapolated from initiator density and polymer thickness.

1.3.3 Bacterial detection and capture via specific cell wall constituents and surface shape

The cell wall of Gram-positive bacteria has features which make it susceptible to the action of antibiotics such as betalactams and glycopeptides. As such these molecules can be used as targeting ligands for polymeric systems. As well as searching for targets on the cell surface, one may also utilise the shape of the bacterial cells to aid in specific detection.

The recognition of cells using cell shape or techniques which generate a three dimensional structures to bind microorganisms shall be referred to as lithography, imprinting or soft-lithography. In the experimental chapters of this thesis the term "*templating*" shall be used to refer to sequence templated polymers, whereby the monomer sequence in a linear polymer shall be dictated by the desired target.

The Whitesides group developed a vancomycin displaying polymer which has the ability to bind to the cell wall of Gram-positive bacteria to promote subsequent opsonisation.[55, 56, 57]

The first study involved the synthesis of a bifunctional polymer displaying vancomycin as the targeting group and fluorescein groups as the antigen for recognition by immunoglobulins targeted at it. This was followed by its interaction with self-assembled monolayers (SAMs) displaying the terminal D-Alanine, D-Alanine (D-Ala D-Ala) necessary for replicating the binding between vancomycin and Gram-positive bacteria.[56] Specific interaction was confirmed using surface plasmon resonance (SPR). It was confirmed that after 30 minutes the quantity of polymer attached had plateaued. Utilising SPR it was shown the polymeric film could not be detached with washes of buffer nor with sodium dodecyl sulphate in sufficient concentrations to remove proteins from sensor chips. The polymer could however be removed using soluble ligands displaying the dipeptide D-Ala D-Ala. This demonstrates the strength of the polyvalent system used and also the contribution of vancomycin binding.[57] The polymer was able to form a molecular bridge between SAMs and an

anti-fluorescein antibody (IgG^{F}) as confirmed using immunofluorescence.

The biological relevance was also shown via successful binding to the bacterium *Enterococcus faecalis*. The advantage to this approach is that it is a general strategy against Gram-positive bacteria. In an alternative approach Bertozzi and Bednarski utilised the mannose receptor of *E. coli* to induce antibody binding to bacteria using a modified monomeric mannose. This latter strategy may be more restrictive to specific bacterial strains although the binding site is likely to be highly conserved and resistance unlikely.[58]

Whitesides *et al.* extended the concept and demonstrated the ability for the system to promote an immune response through phagocytosis.[55] The bacteria-polymer-antibody complex (Figure 1.9) was shown to cause a statistically significant increase in phagocytosis of *Staphylococcus aureus*, compared to antibody independent mechanisms for bacteria internalisation.

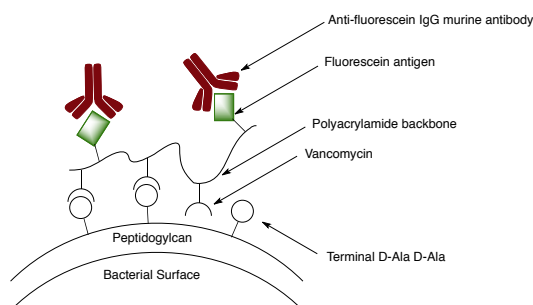


Figure 1.9: Schematic representation of interaction between vancomycin-fluorescein polymers and bacteria with IgG^{F} antibodies. The vancomycin component of the polymer binds to peptidoglycan on the cell wall of the bacterium. The fluorescein component is recognised by anti-fluorescein IgG antibodies and directed phagocytes to the bacterium

A combination of flow cytometry and optical microscopy was used to confirm the interaction between the bacteria and macrophages involved complete internalisation and not surface association. This was the first example where a bifunctional polymer was used to promote antibody-mediated immunity.

Tunable binding of bacteria by antibiotic displaying polymers

The generation of tunable binding systems as previously discussed is not only possible with gly-copolymers but also antibiotic based polymers and so have been used in this way.[59] The group of Stephen Rimmer applied a similar concept, this time employing vancomycin as the binding functionality and hyperbranched p(NIPAM) as the temperature sensitive polymer backbone to cause the change in the polymer conformation. The hyperbranched p(NIPAM) was first generated with carboxylic acid end groups and it was then subjected to post-polymerisation modifications; amidation at pH 9.5 to attach vancomycin and attachment of aminoanthracene to aid in the visualisation of the polymer with the bacteria. The unmodified and modified polymers were compared in this study to investigate the influence of vancomycin as well as the LCST on bacterial binding.

Interestingly in this paper the authors discovered that the binding of the polymers to the bacteria induced a change in the polymer LCST from their original of over 37°C to 26°C or 4°C. This was observed as a need to lower the temperature far below the native unbound polymer's LCST in order to release the bacteria from their bound aggregated state. The authors attributed this observation to a signification alteration in the degree of solvation of the polymer chains after binding to the bacteria as the chains were no longer interacting with the solvent in the same way once bound to bacteria.

Cell shape-dependent recognition and capture

While considering the cell structure one can also factor in the different shapes micro-organisms may present. Examples of where these may be taken advantage of involve the use of imprinting or lithography. The origins of this technique date back in the 1930s[60] and in brief, it involves a polymerisation in the presence of a template using a combination of functional monomers to interact with the target and also cross-linking monomers to generate a three dimensional structure around the target. This approach of cell lithography or imprinting is similar to molecular imprinting where small molecules are used as the templates. After the polymerisation the template is

removed and the material is used for specific recognition of the imprinted target through rebinding. Interactions between the target and the functional monomers used are usually of weak individual but high multiple affinity further supported through the spacial arrangements.

Using bacterial charge as well as shape has lead to one of the first examples of the principles of imprinting applied to microorganisms. This involved lithography of *Listeria monocytogenes* (rod-shaped) and *Staphylococcus aureus* (cocccoidal) under mild conditions and neutral pH to ensure compatibility with the bacteria.[61] An aqueous-organic/bacterial suspension was used, this took advantage of bacteria partitioning along the aqueous-organic interface to generate imprinted polymer beads. The schematic representation of the technique as applied by Harvey *et al.* for spore imprinting can be seen in Figure 1.10.

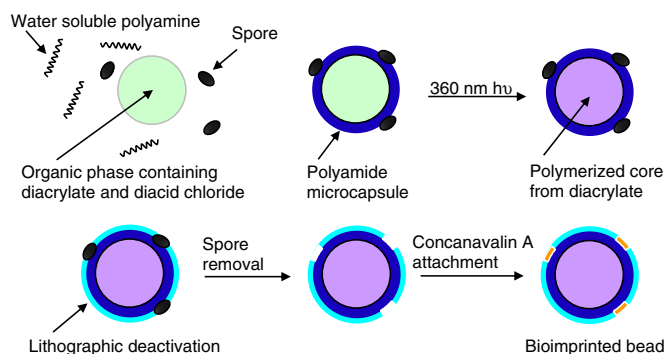


Figure 1.10: Schematic outline for the preparation of imprinted polymer beads.[62]

A diacid chloride reacted to form covalent bonds between the bacterial surface and poly(amines) in the organic droplets to generate a poly(amide) shell around the organic component dispersed with fixed bacteria. The organic component also contained diacrylate which was then photopolymerised to solidify the core of the beads. Residual amines which were unreacted on the surface were able to adsorb bacteria through charge-charge interaction so non-imprinted areas on the beads were treated with diisocyanato-terminated perfluoroether to block these potential binding sites. This ensured that only where the bacteria were in place, the amines would be retained to support bacte-

rial rebinding. Bacteria were removed via acid reflux to yield pockets matching the size and shape of the bacteria templated and also displaying amines to aid retention of bacteria. This process, in effect, generated lithographic prints of bacteria. The beads demonstrated increased specificity for their target organism when binding experiments were performed with bacteria used to form imprints compared to the other bacteria strains. The technique was modified slightly by Havey *et al.* and it was then applied to bacterial spores of *Bacillus thuringiensis kurstaki*. Relative numbers of cells captured using the templated beads were 39% compared to only 13% for the non-imprinted beads. The authors noted the spore capture they obtained was equivalent to polyclonal antibody covered beads.[62] This looks promising however these studies used only 200 bacterial spores, suspended in 0.4 mL of buffer and required 10 mg of beads.

A number of groups have focused upon soft-lithography for bacterial and macromolecular detection. Polymers organise around the molecular stamp, for example yeast cells as shown by Dickert and Hayden, under constant pressure.[63]

Schirhagel *et al.* generated imprinted polymer coatings for bacterial separation.[64] The chips were based upon poly(dimethylsiloxane) and were able to distinguish between *Synechococcus* OS-B', *Synechococcus elongates* PCC 7942 and *Synechocytis* PCC 6803. The structural differences in the prints were detected with atomic force microscopy (AFM) and then they were compared for their propensity to bind their target bacterium against the non-imprinted bacteria. In all cases binding, as determined by an automated counting procedure, was found to be greater for the imprinted surface. The devices were also reusable after washing with 0.01% polylysine to disrupt bacterial adherence. This procedure enabled separation efficiencies to reach as high as 90% when employing successive binding and washing steps of the same sample, depending on the number of repetitions. This flexibility of soft-lithographic imprinting techniques has enabled the detection of yeast,[63] viruses,[65] pollen[66] and human erythrocytes.[67]

The variable cell shape and its cell wall are useful in detection and binding bacteria. Bacteria have a highly diverse spectrum of shapes and sizes. Utilisation of this alone combined with other chemistries may generate materials for specific bacterial detection and binding.

1.3.4 Inactivation of bacteria through cell signal interference

Many bacteria use molecular signals called autoinducers to regulate behaviour at a population level.[68] This system is known as quorum sensing (QS) and has been extensively researched and reviewed.[69] The molecules involved vary greatly across bacterial species.[70] As quorum sensing signals are involved with bacterial growth and biofilm formation,[71] control of the signals may impart an ability to manipulate bacterial infections while bypassing the ability of micro-organisms to become resistant.[72]

The quorum sensing molecules of *Vibrio harveyi* and *Salmonella typhimurium* (*S. typhimurium*) (*Salmonella enteric* Serovar Typhimurium) are coded as AI-2 (autoinducer 2). The signals are structurally different from each other (Figure 1.11) yet they are both derived from the precursor (*S*)-4,5-dihydroxy-2,3-pentanedione (DPD).

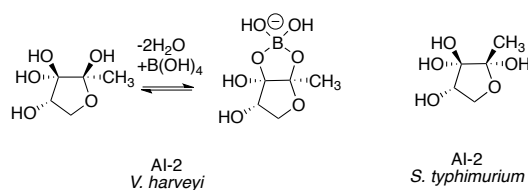


Figure 1.11: Structures of AI-2 of *V. harveyi* complex with and without borate and AI-2 of *S. typhimurium*

The enzyme through which DPD is converted to AI-2, LuxS has been identified in numerous species but not their quorum sensing molecules. Modulation of quorum sensing may be beneficial as these molecules are often involved in expression of genes involved with bacterial virulence. Towards this

end structural analogues of DPD have been obtained through C1 substitution (Figure 1.12) and their antagonistic and agonist properties investigated, demonstrating the structural specificity of autoinducer receptors some of which remain unknown.[73]

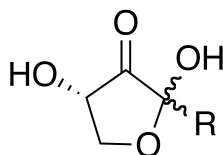


Figure 1.12: Structure of DPD-analogues, the C1 modifications occurred at position R.

One such analogue substituted with an azobutyl functionality which was found to inhibit quorum sensing was conjugated, using copper (I) catalysed azide-alkyne cycloaddition. Commercial polyamidoamine dendrimer (0.0 generation) was coupled with 5-hexynoic acid followed by DPD-azide-alkyne cycloaddition. It was then labelled with rhodamine. The fluorescent functionalised dendrimer was then able to label both Gram-positive and Gram-negative bacteria as a probe for the QS AI-2 Lsr receptors. Such labelling with the bacteria was not possible when presented as a fluorescently labelled DPD molecule, highlighting the need for the multivalent scaffold.[74]

Control of quorum sensing molecules, such as *N*-acetylhomoserine lactones which are autoinducers (AI) of *Pseudomonas aeruginosa* (C4) and other Gram-negative bacteria has been shown via binding to cyclodextrins (CDs).[75] The hydrophobic tail of C4-AI complexed with α and β but not γ -cyclodextrins (Figure 1.13). This was due to the physical size of the cavity of the γ -cyclodextrins being too small.

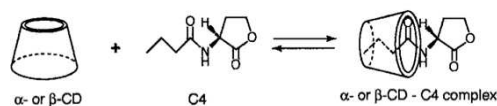


Figure 1.13: Schematic diagram illustrating the CD-C4 complex as found with ^1H NMR and ROSEY NMR experiment.[75]

These experiments took place in rather simple environments with minimal competition from other organic molecules. Kato *et al.* also noted that very large quantities of cyclodextrins would be required to affect autoinducer activity. The cyclodextrins were then fixed on cellulose gels to act as absorbents of quorum sensing signals.[76] The influence of these materials upon the growth of *Serratia marcescens* was investigated, utilising the bacteria's production of prodigiosin a red pigment whose production is modulated by the quorum sense system. It was shown that the absorbant cyclodextrin-cellulose gels did not affect the growth of the bacteria but caused a decrease in prodigiosin production. Interestingly the decrease was greatest when the gel was anionic in nature. The authors attributed this to the charge stabilising the complex formed between the autoinducer and the cyclodextrins. This could be likely due to the presence of the secondary amine present in the *N*-aceylhomoserine lactone forming a cationic charge in solution.

The same principle was extended to the *Pseudomonas aeruginosa rhl* and *las* *N*-acyl-L-homoserinelactone (AHL) quorum sense systems, the former of which was monitored through detection of pyocyanin and β -Galactosidase respectively.[77] The authors found that β -CD cyclodextrin could control both quorum pathways independently.

An alternative route to encasing quorum sensing molecules has been to inactivate them with compounds which may form covalent bonding with the autoinducers and render them biologically inert. The ability for boronic acids to form linking complexes with diol containing molecules, including sugars is well established (Figure 1.14).[78]

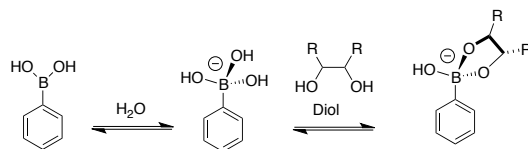


Figure 1.14: Schematic representation of boronate ion forming a stable complex with a diol compound.

The structure of AI-2 in *Vibrio harveyi* and *Salmonella typhmuri*um is very similar and both con-

tain diols (Figure 1.11). Unsurprisingly there has been research into the influence that boronic acid compounds can have upon these molecules. Ni *et al.* highlighted some of the structural modifications which phenylboronic acid may undergo to increase its activity with quorum sensing molecules.[79]

As a variety of boronic acid containing molecules may influence quorum sensing to a greater or lesser extent it seems hardly surprising that polymeric materials displaying such functionality has been employed to influence this intercellular bacterial communication system.

Xue *et al.* generated dual functionality polymeric systems comprising monomers which were capable of binding bacteria and also boronic acid groups which affect quorum sensing. Glycopolymers were also utilised for their binding capacity and effects on quorum sensing.

The materials were investigated against *Vibrio harveyi* as this marine bacterium exhibits luminescence in response to quorum sensing molecules. With low polymer concentrations autoluminescence was decreased initially (five hours) but increased by the seventh hour. The authors attribute the observed oscillation to the reversible nature of the boronic-autoinducer complex, compounded by its concentration dependent nature. As the binding functionality increased bacterial clustering, microenvironments of higher concentrations of AI may develop. This did not however, occur with higher concentrations of the AI binding polymer probably owing to saturation of the media with boronic binding functionalities.[80]

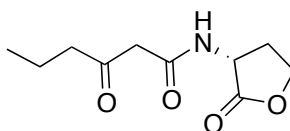


Figure 1.15: Structure of N-(β -ketocapryloyl)-DL-homoserine lactone (3-oxo-C6-AHL).

Piletska *et al.* using computer modelling to predict polymer binding candidates for binding to N-(β -ketocapryloyl)-DL-homoserine lactone (3-oxo-C6-AHL), a quorum sensing molecule of *Vibrio fischeri* (Figure 1.15).[81]

From their model they predicted six monomers that would be useful for their functionality; *N, N'*-methylene bisacrylamide (MBAA), *N, N*-diethylaminoethyl methacrylate (DEAEM), itaconic acid (IA), methacrylic acid (MA), ethylene glycol methacrylate phosphate (EGMP) and acrylamide (AA). These monomers were thermally polymerised with a non-binding cross-linking monomer (ethyleneglycol dimethacrylate) to generate a polymer library. The polymers varied in their content of functional monomers, in that they were either high (20-30%), low (5%) or absent of functional monomers.

The polymers containing AA, MBAA, MAA and IA proved to be the most potent binding polymers for 3-oxo-C6-AHL (79-88%). None of the polymers tested inhibited bacterial growth and growth of the bacteria was comparable to the control specimen. This demonstrated the polymers were non-toxic, they did however significantly decrease the bioluminescence observed indicating decreased quorum sensing by the bacteria. The effect this could play on biofilm formation was also explored with the polymer containing 5% itaconic acid. The addition of 3-oxo-C6-AHL to *V. fischeri* cultures caused an increase by 40% in biofilm formation demonstrating that this molecule plays a role in switching the bacteria into this phenotropic role. However when incubated in the presence of the polymer it decreased biofilm formation by 56% suggesting all exogenous 3-oxo-C6-AHL had been bound by the itaconic acid containing polymer.

The group of Piletska extended their work on the binding of quorum sensing molecules by generating molecularly imprinted polymers (MIPs) based upon the same functional monomers in their earlier papers however this time it was focused upon a quorum sensing molecule of *Pseudomonas aeruginosa*.^[82] The structure of its quorum sensing molecule *N*-(3-oxododecanoyl)-L-homoserine lactone (3-oxo-C12-AHL) is very similar to that of *V. fischeri* but with the extension of the alkyl side chain and a structural analogue (N-butyryl-homoserine lactone) that is also secreted by *Pseudomonas aeruginosa*.

The polymers were tested for their binding affinities for the target molecule within concentration ranges typically observed in biofilms as well as *N*-butyryl-homoserine lactone. The MIP was

found to have not only a higher binding affinity and binding capacity but also was specific for the target molecule as the binding to the analogue was below the detectable limits compared to the non-templated polymer. Finally the polymers were studied for their effect upon biofilm formation using the static biofilm assay. The biofilms were visualised with wheat germ agglutinin-Alexa Fluor 488 conjugate. This stain binds to *N*-acetylglucosaminy and sialic acid residues which are found in the exopolysaccharide of *Pseudomonas aeruginosa* biofilms. The authors found that the presence of MIP at a concentration of 20 mg/mL completely inhibited biofilm formation while at 10 mg/mL there was a decrease of 75% and at 5 mg/mL it was decreased by 70%. This compared to the non-imprinted polymer which at 20 mg/mL did decrease biofilm formation by 40%. For the lower concentrations tested the inhibition was less than for MIP. This work highlighted that functional monomers are important for binding to the target but that also imprinting can increase the specificity of the system even further.

Quorum sensing may prove one of the most useful mechanisms through which to manipulate bacteria. Control of these signals can influence virulence and significantly influence the progression of an infectious disease.[83, 84]

Polymer materials capable of inactivating these signals may be able to aid in the manipulation of bacterial pathogenesis through utilisation of multivalent scaffolds which have added benefits beyond small molecules.

1.3.5 Optical detection methods

The binding strategies can be applied readily in the detection of bacteria and micro-organisms. Spectroscopic techniques or other chemistries can enable detection once binding has occurred. Advances in polymer science have now allowed the development of point of care novel bacterial detection sensors.

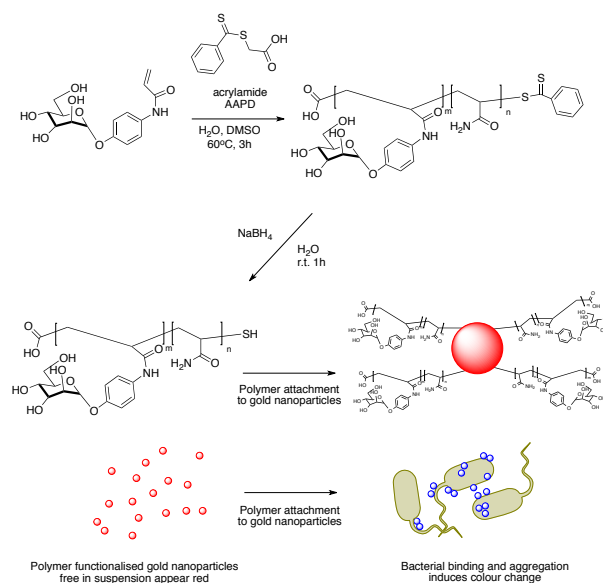
Simple visualisation of bacterial contamination would be an attractive characteristic of such a recognition system. It would offer the user a simple method to detect the presence of bacterial contamination without the need for complex and often expensive laboratory equipment for near user testing. These systems often employ methods previously described as targeting ligands but also have an additional capability to identify the presence of microorganisms by eye. Such systems include gold nanoparticles and conjugated polymer systems.

Gold nanoparticles

Gold nanoparticles absorb visible light at wavelengths that depend upon their particle size and aggregation state. For example the aggregation of gold nanoparticles from the dispersed state will cause a colour change from red to blue. They present an ideal platform onto which multivalent systems like polymers can be displayed as they can utilise the cluster glycoside effect, where binding is dependent upon multiple carbohydrates of the correct type and orientation.[85] Spain *et al.* demonstrated reversible addition-fragmentation chain transfer polymerisation (RAFT) polymerisations are useful towards this end as they produce material of a defined architecture and the aqueous RAFT agent can be reduced to a thiol functionality suitable for the grafting of the polymer to the surface of the gold nanoparticles.

Carbohydrate displaying gold nanoparticles have been tailored for bacterial detection by Toyoshima and Miura.[86] Thiol terminated polymers of acrylamide and either *p*-acrylamidophenyl α -mannoside or *p*-acrylamidophenyl *N*-acetyl- β -glucosamine were generated using RAFT polymerisation. The RAFT agent was subsequently cleaved using sodium borohydride to yield the free thiol (Scheme 1.2).

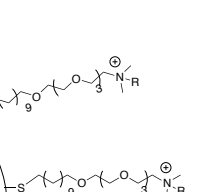
The terminal thiol is advantageous as it reacts readily with the gold nanoparticle surface under mild conditions. The polymers were attached by mixing with gold nanoparticles for 24 hours in water and the functionalised particles purified by centrifugation to yield the pure particles. The attachment of the polymer to the gold nanoparticles was confirmed by measurement of ζ -



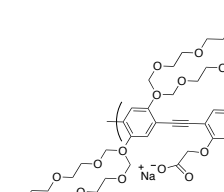
Scheme 1.2: Schematic for generation of thiol terminated mannose-acrylamide-co-acrylamide co-polymer and binding to gold nanoparticles followed by incubation with bacteria.

potential (mV) and measuring the size change of the particles by dynamic light scattering (DLS) and transmission electron microscopy (TEM). The particles were first investigated using ConA, a sugar binding lectin extracted from the Jack beans, whose ability to bind to a variety of sugars e.g. glucose, mannose and fucose, has been utilised to replicate other sugar binding lectins which may be found on organisms such as *E. coli*. The addition of ConA resulted in a visual colour change from red to blue. This same colour change was observed upon addition of *E. coli* (ORN178) which binds to mannose. However when an *E. coli* mutant (ORN208) which does not bind mannose was added, no colour change was observed. The colour change seen in the particle suspension can be attributed to the binding of *E. coli* surface proteins to mannose groups on the particles. Therefore the cationic charge from the amine monomer was not responsible for the bacterial binding. The colour change and thus, aggregation indicated clusters of mannose binding areas on the bacterial surface. This system utilised both the lectins of bacteria combined with the colour change observed when gold nanoparticles aggregate. This system has the advance of enabling the detection of the presence of bacteria by eye.

a)



b)



NP1 R = CCCCCCCC

NP2 R = C1=CC=CC=C1

NP3 R = c1ccc2ccccc2c1

The bacterial sensor consisted of a cationic nanoparticle bound to an anionic conjugated polymer whose fluorescence was inhibited through its binding to the particle. Upon incubation of the sensor with bacteria, which have an innate negative charge, the polymer was displaced from the surface of gold nanoparticle, inducing the conformation change necessary to cause fluorescence (Figure 1.17) in the polymer chain.

Of particular interest in this work was the capability of the sensor to detect reliably different types and also strains of bacteria as a function of the change in fluorescence. The authors speculated that this array system may be of use when rapid differentiation of common pathogens is required but

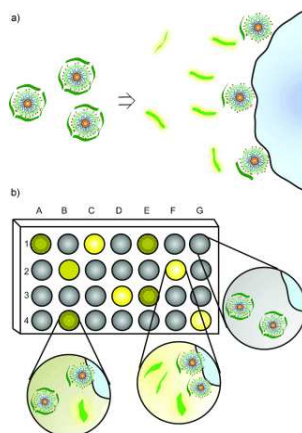


Figure 1.17: Schematic representation of bacterial nano-sensor where a) the bacteria displaces the conjugated polymer from the nanoparticle surface inducing fluorescence and b) the sensor array where varying the bacteria influences the level of fluorescence produced.

question its viability with samples taken from the complicated milieu of infected human specimens.

Conjugated polymer systems

Conjugated polymers, with delocalised π electrons, behave as semi-conductors and can also act as visual transducers in response to the presence of an analyte or a perturbation in their environment.[88] This has allowed these polymers to be applied to the detection of microorganisms such as bacteria.

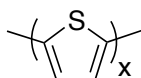


Figure 1.18: General structure of an unsubstituted polythiophene.

Visual recognition is possible using π -conjugated redshift changes in the polymer backbone. Polythiophenes with the general structure shown in Figure 1.18, are an important class of π -conjugated polymeric materials which exhibit optical changes in response to a variety of stimuli due to changes in their planar to non-planar conformation.

The rings may be substituted in order to generate responsive functionalities. Such materials have

been demonstrated to aid visual detection of bacteria (mannose-polythiophene) and viruses (sialic acid-polythiophene) by Baek *et al.*[89]

Polythiophenes were synthesised by co-polymerisation of carbohydrate thiophene monomers and the methyl-ester-protected acid thiophene via polycondensation with iron (III) chloride as a promoter at room temperature under an inert atmosphere. Further to polymerisation and purification the polymers were deprotected using sodium methoxide in methanol and chloroform, followed by sodium hydroxide and dialysis to yield the fully deprotected glycopolymers of the general structure shown in Figure 1.19.

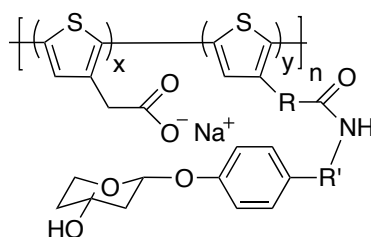


Figure 1.19: General structure of carbohydrate polythiophene. $R = CH_2$ or $CHCH$, R' = various amide spacers.

The polymers were tested initially for their interaction with their respective sugar binding proteins. The sialic acid-polythiophene was tested using *Triticum vulgaris* lectin and the mannose-polythiophene was tested using biotinylated Con A. The sialic acid-polythiophene produced little response to its relevant protein ligand apart from a small blue-shift indicating little effect from the free lectin. The mannose-polythiophene biotin-conA-streptavidin complex demonstrated a small redshift showing the interaction between the lectins and carbohydrates of the polymer. The biochromatic assays between viruses and bacteria with their respective glyco-polythiophenes showed significant red-shifts. The differences between the protein ligands and the biological target were attributed to the polyvalency seen in biomacromolecules. The polymer, upon binding to the biological target, was forced to adopt a planar conformation in order to span the surface

of the target. By contrast in solution, with the ligand, the carboxylic acid and carbohydrate of the glycothiophenes were able to engage in intermolecular hydrogen bonding so the backbone was in a non-planar form. Increasing the length of the spacer increased the shift observed which was attributed to the facilitation of the carbohydrate functionalities to reach across surface ligands on the biological target. The level of colour change was significant to be detected by eye (Figure 1.20).

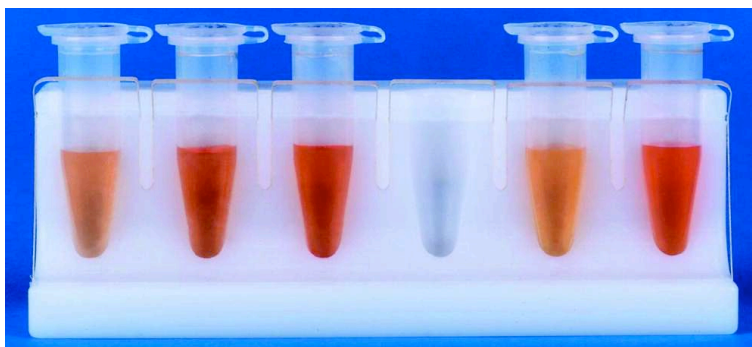


Figure 1.20: Interaction between glyco-polythiophenes and their respective receptor protein. Left-right: Sialic acid polythiophene (SPT), SPT and influenza A virus, SPT and influenza B virus, blank, mannose-polythiophene (MPT), MPT and *E. coli* HB101.[89]

There has been significant work investigating the use of polydiacetylene sensors for bacterial detection. These polymers, like polythiophenes, display the interesting characteristic of exhibiting a colour change in response to a variety of changes that can occur in their environment.

Sun *et al.* generated conjugated polydiacetylene containing liposomes incorporating a mannose displaying lipid and investigated its use as a bacteria detection sensor as well as the influence of inorganic ions upon its sensitivity. The sensors were synthesised from 10,12-Pentacosdiynoic acid (PDA) and a mannose functionalised lipid component. The liposomes were formed using the thin film technique and photopolymerising the liposomes at 254 nm to create covalent, robust, materials which appeared blue when first synthesised. The liposomes have the structure shown in Figure 1.21.

The sensors exhibited a maximal absorbance of 670 nm and so appeared blue to the naked eye,

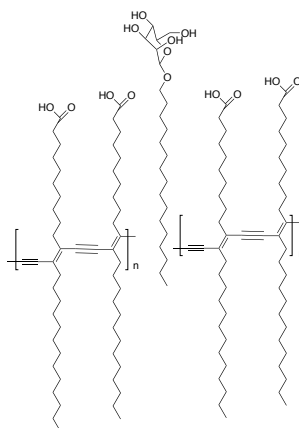


Figure 1.21: Structure of a single layer of photopolymerised glycofunctionalized PDA liposome.

with a small absorbance in the red region at 574 nm. After an incubation time of 2 minutes at 37°C with *E. coli* K12, the liposomes in suspension demonstrated a maximal peak at 574 nm whereas the blue peak decreased. Significantly, the suspension appeared red or purple, depending on the concentration of bacteria used. There was no colour change when no bacteria were added or if the mannose displaying lipid was not included. It was described that ions such as Ca^{2+} increased sensitivity due to increased bacterial binding. Ions which decreased sensitivity such as Cu^{2+} added rigidity to the polymer system, thus preventing the conformation changes necessary to induce the colour change.[90] Although these systems are sensitive and the presence of bacteria can be detected by eye it is somewhat restricted to bacteria displaying the necessary carbohydrate binding lectin. As such these concepts have been extended in a variety of ways to produce other general and specific bacterial detection sensors.

Surface active compounds, biosurfactants or biopolymers are important compounds produced by bacteria and are also found on their surface. They have roles in many essential interfacial processes and can influence biofilm formation and bacterial interactions with surfaces.[12] Examples include glycolipids, peptidolipids and lipopolysaccharides such as that shown in Figure 1.22.

Silbert *et al.* have generated a sensor which can detect the surface-active compounds produced by

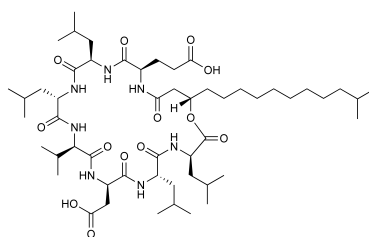


Figure 1.22: Structure of Surfactin, a peptidolipid[3]

proliferating bacteria which are many and varied e.g. lipopolysaccharides from *Escherichia coli* (*E. coli*), and hence the presence of bacterial contamination through colour change and fluorescence. This method can be used for Gram-positive and Gram-negative bacteria. Most interestingly the colour change occurs before bacterial colonies can be seen. The approach used by these authors was unique as it did not include any of the bacterial binding ligands previously reported, instead they took advantage of the release and diffusion of the surface active compounds of bacteria to induce the colour change. As with the work of Sun *et al.* they synthesised polydiacetylene (PDA) vesicles which were in the nanometer range however they included phospholipids. The vesicles visually appeared blue and were incorporated into agar before being polymerised. The growth of bacterial colonies then caused a colour change around the colonies which was detectable by eye and attributed to the diffusion limited release of surface active compounds from the bacteria.[38]

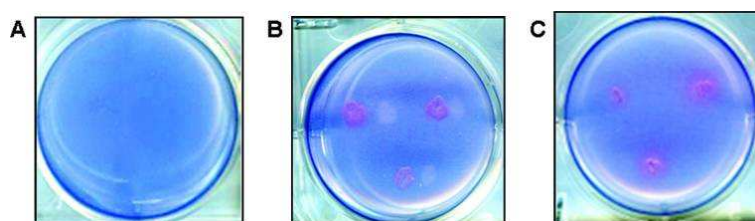


Figure 1.23: Scanned images of (A) Agar plate prior to bacterial inoculation (B) 18 hours after inoculation and incubation at 26°C with 3 colonies of *Bacillus cereus* (C) 18 hours after inoculation and incubation at 26°C with 3 colonies of *E. coli* BL.[38]

These surface active compounds which are used by bacteria to aid in invasion of host tissues and for defence, caused the disruption of the vesicular nanoparticles and induced the colour change and

fluorescence associated with a change in their conformation.

The advantage of this work over that by Sun *et al.* and Baek *et al.* is that it does not require any prior knowledge of the potential bacterium or the presence of very specific carbohydrate recognition sites on the bacteria for it to function. These amphiphilic compounds are utilised by many pathogenic bacteria so this is a more general detection device. The authors also postulate that this work may be particularly pertinent in detection of antibiotic resistance by including them in antibiotic impregnated plates owing to the increase in fluorescence occurring before colonies can be visualised. This will speed up identification of resistance and correct antibiotic selection in the clinic.

1.3.6 Summary of bacterial recognition

Polymers offer many advantages as the materials platform for cell detection and capture. The ability to make polymers in many arrangements e.g. as soluble agents, surface coatings and three-dimensional functional networks, allow a variety of analytic formats. In addition, multi- and polyvalency can be useful in enhancing affinity and avidity for particular strains of micro-organisms. Finally, the ability to couple functionality to allow facile read-out of detection e.g. optical or electronic, means that polymers are a promising class of materials for the future.

1.4 Introduction to materials of cell recognition polymerisation methods

Intelligent polymer systems such as those intended in this project require the use of synthetic techniques which allow great control over the polymer macromolecular features (molecular weight, molecular weight distribution and polymer architecture). This is necessary in order to develop polymers with a high level of specificity. As such, controlled radical polymerisation methods are

particularly suited for material synthesis.

One of the first insights into living polymerisation was published in a groundbreaking paper in Nature by Szwarc.[91] The author described a system where polystyrene chains could be grown due to the presence of anionic reactive intermediates and terminated under the control of the chemist as opposed to the uncontrolled "death" which would otherwise occur.

Conventional radical polymerisation (RP) process continued to be the dominant form of polymerisation. Recently there has been the advent of controlled radical polymerisation (CRP) in which control over radical polymerisation has been attained using a range of mediators spanning from stable organic radicals[92] to transition metals[93, 94] and carbonylthio compounds.[95]

The main difference between CRP and RP is the small proportion of chains that are active in CRP at any one time; this ensures control over the growth of chains and minimises irreversible termination reactions such as chain-chain coupling, disproportionation and transfer to monomer, polymer or solvent which would lead to polydisperse and often ill-defined polymers.[96]

Rather, in CRP the majority of polymer chains are kept in a dormant state thus rates of polymerisation are much slower. CRP has much faster initiation or activation than RP, ensuring all chains are equally active. Its rate of activation is out-matched by its rate of deactivation (Figure 1.24), explaining the short time each chain is active for at any specified moment.[97]

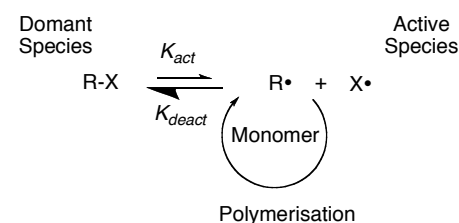


Figure 1.24: General mechanism of CRP.

Discovered in 1995 independently by Sawamoto[94] and Matyjaszewski,[98] ATRP has become one of the most important methods of controlled polymerisation. The mechanism has been detailed at length in the literature.[99, 100, 101]

$$P_n - X + Mt^n / L \xrightleftharpoons[k_{deact}]{k_{act}} P_n^* + X - Mt^{n+1} / L$$

ATRP has been used to produce a wide variety of polymers such as block,[103] random,[104] branched,[105] brushes[106] and star polymers.[107] It is often carried out in homogenous systems of organic solvents or in bulk polymerisations. The polymerisation is affected by a number of factors including the initiator used, the monomer and catalyst (usually consisting of a transition metal and a ligand).

The presence of water can greatly increase the ATRP polymerisation rate of hydrophilic monomers such as hydroxyethyl methacrylate.[108] The presence of water with other solvents increases the

rate of polymerisation however when ATRP is tried with water alone quantitative conversion of monomer into polymer can occur within 2-3 minutes. It has been speculated that this may be due to water-mediated inactivation of Cu^{2+} catalytic quencher, leading to inefficient control over the growth of the forming polymer chains.[109] This was indicative of a loss of control over the polymerisation which can be frequently observed in water based systems.

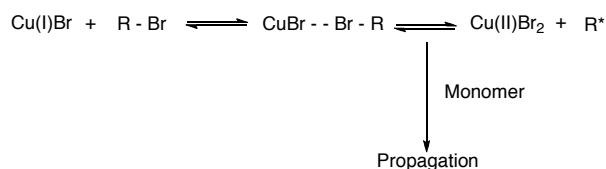
Successful polymerisation of oligo ethylene glycol methacrylate monomers in water has been reported and the characteristics of the system were shown to be well defined.[110] This polymerisation featured fast rates; as low as 15 minutes to 10 hours and polydispersities as low as 1.12. The authors used a mixed halide system to improve the living nature of the reaction.

Bipyridine and 1,1,4,7,10,10-hexamethyltriethylenetetramine (HMTETA) were shown to have comparable rates under these conditions, however slightly better polydispersities were found with bipyridine.

The effect of the ligand to copper salt ratio on the polymerisation kinetics has been studied. When the molar ratios of BiPy:CuCl were 1:1 and 2:1, both conversion and polydispersity were acceptable with values of around 1.2 and linear values found to plots of molecular weight to conversion. The authors noted the dramatic effect of the ligand concentration upon rates. With the ratio of 2:1, the rate was approximately three times faster than with the 1:1 molar ratio. A molar ratio of 3:1 was also investigated which showed a similar increase in polymerisation rates however it had a deteriorative effect upon polydispersity and linearity of molecular weight to conversion. As such a ratio of 2:1 was selected as optimum for the catalyst complex. Catalyst complex concentrations used in aqueous ATRP differ from those of conventional ATRP. This is because catalytic activity is greater in water and each catalyst complex can sustain livingness of approximately ten chains

The reduction in the amount of Cu (I) present is one method of controlling an otherwise rapid polymerisation. The addition of copper (II) can also aid control of the aqueous polymerisation.[111] The ratios of Cu (I):Cu (II), can vary but often 1:9 is selected to obtain polymers of narrow poly-

dispersities. Perrier *et al.* also used a low total quantity of catalyst during their work (initiator:Cu of 1000:1). The rationale behind this technique is due to the equilibrium established between the various oxidation states of copper when involved in ATRP (Scheme 1.4).



Scheme 1.4: Scheme of copper mediated ATRP highlighting the various redox conditions.[111]

Briefly, in water copper (II) will be more coordinated than copper (I) and thus more stable. Water may also compete with ligands for complexation with the metal ion. This prevents the copper (II) from behaving as an effective deactivator and so deactivation will be slower. The deactivation species (Cu(II)X) may undergo hydrolysis to yield the stable yet inactive form of the copper (II) ion chelated with the ligand. This increases the polydispersity of the polymer as described by equation 1.1.

$$\begin{aligned}
 \text{PDI} &= \frac{M_w}{M_n} \\
 &= 1 + \frac{1}{\text{DP}_n} + \left(\frac{[\text{RX}]_0 K_p}{K_{\text{deact}} [\text{MT}^{n+1} \frac{X}{L}]} \right) \left(\frac{2}{\text{conv}} - 1 \right)
 \end{aligned} \tag{1.1}$$

The addition of Cu (II) seeks to circumvent this by moving the ATRP equilibrium towards the dormant species and so increase the number of dormant chains. The excess of Cu (II) salts are introduced in order to regenerate the lost deactivator which is essential component of a controlled polymerisation.[112]

A relatively novel method for over-coming this problem of control has been the introduction of activators generated by electron transfer atom transfer radical polymerisation (AGET ATRP). During this process, the active copper (I) is generated *in situ* from the action of reducing agents upon the more aerobically stable copper (II).[113] In this system all the components are added to a

sealed vessel and then degassed and the polymerisation is initiated by the addition of the reducing species e.g. an aqueous solution of ascorbic acid. Each ascorbic acid molecule in water is capable of reducing two copper atoms.[114]

This method was seen as an improvement on its predecessor of simultaneous reverse and normal initiation (SR & NI) ATRP. This was because SR & NI ATRP required a radical generator that would also initiate chain growth. This would result also in homopolymers of the second monomer when blocks were required.[107]

As discussed the presence of additional oxidised copper salt aids control of the polymerisation so Min *et al.* used substoichiometric quantities of ascorbic acid to ensure the presence of copper (II) in the reaction.[113, 115] This method has also been applied to reduce the concentration of catalyst to levels within the parts per million (ppm) scales as the rate is dependent on the ratio between the different valence states of copper and not concentration.[116] This has the advantage of reducing the levels of the often toxic transition metals catalysts employed and facilitates the development of ATRP as a "green" polymer chemistry process.[117, 118]

1.4.2 ATRP as a route to bacteria binding polymers

Atom transfer radical polymerisation is a useful technique to generate templated bacterial binding polymer ligands. The technique involves slow polymerisation speeds which can enable increased templating as monomer inclusion could be dictated by the spacial position of monomers over time rather than instantaneously at the start. The technique can also allow the polymerisation to be halted before all monomers are included in the polymer chain. In this way the composition of the polymer will still be influenced by the presence of the templates and not the monomer feed. The application of ATRP in water is also biocompatible as the cells do not need exposure to harsh organic solvents and high temperatures.

Chapter 2

Aims of the Thesis

The aim of the project is to examine if bacterial cells have the ability to undergo templating utilising polyvalency and as such produce polymers suitable for their capture. Polymers, templating and the nature of binding shall be assessed. New applications for bacterial controlled chemistries shall be explored.

2.1 Investigation into Functionality

Monomeric candidates shall be selected based upon their potential to bind to bacterial surfaces through rational selection.

Polymers shall be produced using controlled radical polymerisations methods such as ATRP or RAFT to allow for production of polymers of defined architecture.

Binding of polymers shall be assessed and ideal candidates selected for templating.

2.2 Investigation into Toxicity

A selection of polymers displaying functionalities which have been demonstrated as suitable for templating shall have their toxicity against bacteria and human cells investigated.

This will involve well established assays.

2.3 Templating

Templating of bacteria shall be carried out using controlled polymerisation methods to maximise templating effects.

A novel controlled polymerisation method shall be investigated and utilised.

The resultant polymers shall be retrieved from the polymerisation solution and also the bacterial surface.

2.4 Rebinding Studies

Polymers shall be purified and their composition analysed.

Purified polymers shall have their ability to rebind the templated organism investigated and compared to a non-templated bacterium.

2.5 Bacterial mediated chemistry

The use of bacterial mediated chemical processes shall be demonstrated via "click chemistry".

Potential future applications for this shall be discussed.

Chapter 3

Materials and Methods

3.1 Materials

3.1.1 Chemicals

2-(Dimethylamino)ethyl methacrylate (DMAEMA) 97%, 1, 3-propane sultone 99%, 2-bromoethanol 97%, 2-formyl-phenylboronic acid 98% and ethylenediamine 99% were purchased from Alfa Aesar. Copper (I) Bromide 99.999%, α -bromoisobutyryl bromide 98%, 4-(dimethylamino)pyridine 99% and *N*-ethyl-*N'*-(dimethylaminopropyl)carbodiimide hydrochloride (commercial grade) were purchased from the Aldrich Chemical Company.

LB Media, hydrogen chloride 2M in diethyl ether, alizarin red S (AR-S), 3-(Trimethylsilyl)propargyl alcohol (97%), D-glucose, 2,4-dihydroxybenzaldehyde (98%) and *N*-acetylglycine (99%) were obtained from Sigma Aldrich.

Benzyl alcohol 99%, iodomethane 99%, coumarin 343 pure laser grade and oxalyl chloride 98% were purchased from Acros Organics. All the chemicals were used as received without further purification unless otherwise stated.

Further chemicals were obtained from Sigma Aldrich.

Dulbecco's PBS without Ca^{2+} and Mg^{2+} was purchased from Lonza

Other ATRP ligands were synthesised according to methods already published in the literature.[119, 120]

Laboratory communal media was prepared according to university procedures - LB medium: 10 g tryptone, 5 g yeast extract, 10 g NaCl, dissolved in tap water to a final volume of 1 L. LB agar plates also contained 1.5% (w/v) agar.

3.1.2 Bacterial Strains

Escherichia coli (*E. coli*) MG1655 was obtained from stocks held within the university from Dr. Klaus Winzer. Personal stocks were produced of *E. coli* MG1655 according to the following method. Bacteria were spread onto LB agar plates from the university stocks and grown overnight. The next day a streak through several, uniform, representative colonies was carried out. This was used to inoculate 5 mL of LB media which was grown overnight as a primary culture. The next day this was used as 1:1000 dilution to inoculate two sets of sterile LB media (200 mL) in baffled Erlenmeyer flasks. Two batches were grown in parallel at 37°C with agitation (200rpm). One batch was for producing bacteria to monitor the growth curve whilst the other batch was used to produce a bacterial stock for future use. The growth of these bacteria was monitored using measurements of optical density (OD₆₀₀) on a spectrophotometer. Once the bacteria had reached the early exponential phase with an OD₆₀₀ of 0.3 the bacteria were retrieved to use as stock. The stocks were prepared for freezing by centrifuging and washing with 50% glycerol. The samples were then 'shock frozen' by immersing them in liquid nitrogen and then storing in a -80°C freezer.

Numbers of colony forming units were determined with serial dilutions. This was done by diluting the working bacterial suspension in LB medium repeatedly and then adding 100 μ L of the diluted solutions to LB agar plates and growing overnight. The next day the colonies are counted and this figure is multiplied to give the number of viable cells that were in the original suspension. 10^9 colony forming units (CFU) of bacteria were used for the binding experiments.

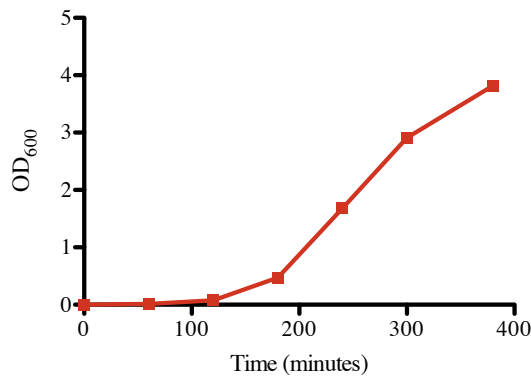


Figure 3.1: Growth curve of *E. coli* MG1655 in LB media at 37°C

Fluorescent *E. coli* MG1655 was generated using a plasmid generated in R. Tsien laboratories [121] and obtained from Dr. Kin Hardie (University of Nottingham).

Streptococcus mutans (*S. mutans*) NCTC 10449 was obtained from GlaxoSmithKline Consumer Healthcare, Weybridge, Surrey. The strain was originally obtained from the National Culture Collection. The *S. mutans* NCTC 10449 were plated from the frozen stocks onto LB agar plates. These bacteria were grown for approximately four days. During this time it was useful to inspect the plates periodically for fast growing contamination.

Colonies appeared small, off-white and round. At the end of the growth period the plate was again thoroughly inspected to ensure there were no signs of contamination and all colonies were homogenous and representative. All the colonies were then removed and transferred to a full 15 mL falcon tube of pre-warmed brain heart infusion broth. This culture was then incubated at 37°C for 24 hours (or 96 hours if LB media was used). Microscopic examination could confirm the culture appears as expected; circular cells linking to form short chains, for example in Figure 3.2. This was used to produce stocks in the same manner as described for *E. coli*.

Pyocyanin negative *Pseudomonas aeruginosa* 223 PAKR76 Δ phzAG1 Δ phzAG2 (Double mutant phzAG1 and phzAG2) was obtained from within Nottingham university from Dr. Stephan

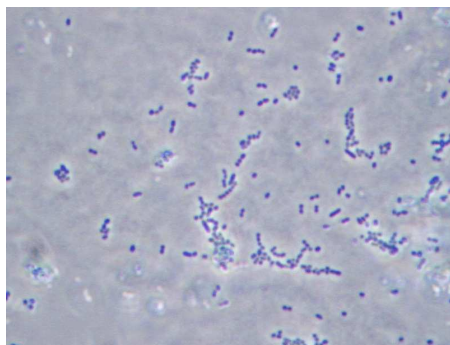


Figure 3.2: Typical phase contrast image of *S. mutans*

Heeb.[122] Personal stocks were produced in the same manner as described for *E. coli*. Green Fluorescent *Pseudomonas aeruginosa* PAO1 pmE6032 GFP was obtained from within Nottingham university from Dr. Stephan Heeb. Stocks were produced of the *Pseudomonas aeruginosa* in the same manner as described for *E. coli*.

3.1.3 Equipment

Mass Spectra (MS) (TOF-ESI) were recorded on a Waters 2795 separation module/Micromass LCT KC453 platform, under positive or negative scan mode where applicable. Purified compounds were directly injected using OpenLynx software.

Nuclear magnetic resonance (NMR) spectroscopy was carried out on the Bruker DPX400 Ultra-ShieldTM. Chemical shifts are reported in ppm (δ units) downfield from internal tetramethylsilane (TMS) or from the -OD signal of deuterated solvents used. Analysis of spectra was done using MestReNova 6.0.2 copyright ©2009 Mestrelab Research S. L.

Aqueous gel permeation chromatography (GPC) was performed on a Polymer Labs GPC50 Plus fitted with differential refractometer (RI), capillary viscometer (DP) and dual angle laser light-scattering (15° and 90°) detectors. The eluent was Dulbecco's PBS without Ca^{2+} and Mg^{2+} , at 30°C and a flow rate of 1 mL/min. The instrument was fitted with a Polymer Labs aquagel-OH

guard column (50×7.5 mm, $8 \mu\text{m}$) followed by a pair of PL aquagel-OH columns (30 and 40, 300×7.5 mm, $8 \mu\text{m}$). Calibration for detector response and inter-detector delays was achieved using a single, narrow PEO standard (Polymer Labs, Mp 128 kDa, $[\eta]$ 1.2968 dL/g) using a dn/dc value of 0.133 g/mL.

Cationic polymer analysis was carried out on the same GPC50 Plus with CatSEC 300 columns. The eluent was 0.1% trifluoroacetic acid, 200 mM sodium chloride at pH 2. The system was calibrated using single, narrow poly(2-vinylpyridine) standards (Polymer Standard Services).

Organic soluble polymer analysis was carried out on the same GPC50 Plus. The columns used were Resipore Mixed-D and they were calibrated with linear polymer standards obtained from Polymer Labs).

Infrared analysis was carried out using Thermo Scientific Nicolet IR 200 FT-IR. Analysis of spectra was done using Omnic 8.0 copyright ©1992-2008 Thermo Fisher Scientific Inc.

Recording fluorescence spectra for chemical compounds was done using the Varian Cary Eclipse fluorescent spectrophotometer.

Samples were lyophilised by first immersing the aqueous samples in liquid nitrogen until frozen. They were then placed in an Edwards Modulyo freeze drier equipped with an Edwards high vacuum pump. The samples were placed under reduced pressure until all water was removed.

Bacterial electroporation was carried out using the BioRad MicroPulser Electroporator.

Bacterial growth curves and measurements of cell density were done at a wavelength of 600 nm on the Biomate 3 spectrophotometer, manufactured by Thermo Scientific.

Bacterial analysis and images were producing using the NIKON EFD3 microscope and the NIKON DXM1200 digital camera. Software used was ACT-1 2.7 copyright ©NIKON. Image analysis was carried out using ImageJ 1.43U.

Redox potentials were recorded using the Hanna ORP redox tester HI-98201 (PHK-072-Y) obtained from Fisher Scientific.

Bacterial aggregation behaviour was measured using the Coulter LS230 particle size analyser (Beckman Coulter, High Wycombe, UK) with suspensions under moderate stirring (pre-set speed level 3 setting). Required bacterial concentration was determined using the in-built software to give an obscuration value between 8-12%.

3.2 Methods

3.2.1 Microscopy binding Experiments

The testing of the produced polymers' binding ability was assessed using a method similar to that already reported in the literature.[51, 55]. Briefly, a 1 mL aliquot of 1 mg/mL aqueous polymer solution was incubated with 10^9 colony forming units (CFU) of bacteria for 30 minutes. After this the bacteria were pelleted and the pellet was washed three times with phosphate buffer solution (PBS) to remove unbound polymer. After washing, the pellet was resuspended in PBS and mounted on microscope slides to be viewed. The same procedure was carried out with a water blank solution to serve as the control. Photographic images were generated using phase contrast and fluorescence microscopy (10,000x) and recorded for comparison.

3.2.2 Aggregation Assay

The aggregation assay was carried out in a way similar to that reported in the literature.[123, 80] Polymer solutions were prepared at a concentration of 1mg/mL in sterile deionised water. Meanwhile bacteria were grown to an OD₆₀₀ such that they were still in the exponential phase of growth (OD₆₀₀ around 0.4). After this they were washed once with PBS and then twice with sterile deionised water. The cells were finally resuspended to a cell density such that when mixed with the polymer solutions they had an OD₆₀₀ \approx 1.9. 0.5 mL of the polymer solution was added to a cuvette followed by 1 mL of the bacteria suspension. The OD₆₀₀ is quickly recorded (T_0) and the change in OD₆₀₀ was followed with time. For boronic containing polymers and its amine control polymer, the pH of the polymer solution was adjusted to pH 9.0.

3.2.3 Fluorescent *E. coli* generation

25 μ L of electrocompetent *E. coli* MG1655 cells were mixed with 1 μ L of plasmid solution in water. They were incubated for several minutes on ice and then added to a 0.2 cm gap electroporation cuvette. The cuvette was then placed into the Bio-Rad MicroPulser Electroporator and exposed to the electronic current pre-programmed for *E. coli* on the device. After the electroporation cells were suspended in 1 mL of LB medium, incubated for 1 hour at 37°C then 10-100 μ L streaked onto 100 μ g/mL ampicillin LB agar plates. Expression of fluorescent protein-encoding gene was induced by growing the bacteria in the presence of 0.2% arabinose.

Chapter 4

Selection of Functionalities A: Charge

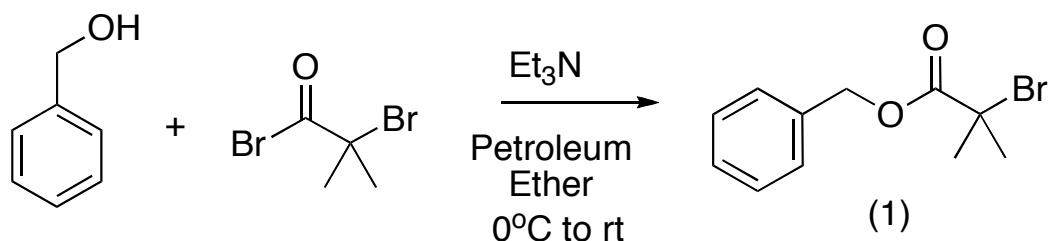
4.1 Introduction

The binding of cationic polymeric materials to negatively charged bacteria has been discussed at length in the literature[51] and in the introductory chapter to this thesis.

There are a variety of cellular components which impart the bacterial cell with a negative surface charge. [11] These are found in both Gram-negative and Gram-positive bacterial cells. Gram-positive cells contain negatively charged acids on the cell surface such as teichoic acid [1] and Gram-negative bacteria contain lipopolysaccharides which are also negatively charged and can be bound by polycations [2, 124]. As well as these two distinct features the membranes of both bacterial classes also contain negatively charged phospholipids which stabilise the cell membrane. All these features contribute to the bacterial cell under normal conditions having an innate negative charge. This presents an ideal target for charged materials to aid in the binding of polymers to bacteria.

4.2 Methods

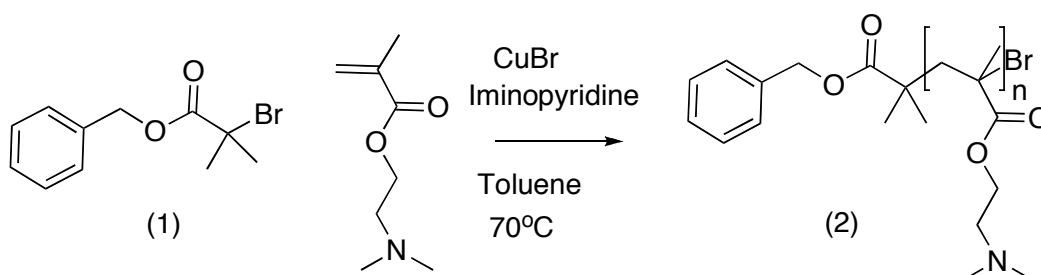
4.2.1 Synthesis of Benzyl-2-bromo-2-methylpropanoate (**1**)



Scheme 4.1: Synthesis of Benzyl-2-bromo-2-methylpropanoate ATRP initiator (**1**).

The ATRP initiator **1** was produced according to Scheme 4.1 by a method previously described in the literature.[125] Benzyl alcohol (15.0 mL, 145 mmol) and triethylamine (16.3 mL, 171 mmol) were dissolved in dichloromethane (150 mL) in a round-bottomed flask and the resulting solution was cooled to 0°C using an ice bath. To this, α -bromoisobutyryl bromide (16.3 mL, 132 mmol) was added dropwise over a period of 30 minutes and then left to stir for two hours. The mixture was washed with water (8 x 50 mL) and then with a saturated sodium bicarbonate aqueous solution (2 x 50 mL). The organic layer was dried over magnesium sulphate, filtered and the volatiles were removed under reduced pressure to yield a yellow oily liquid. This was further purified using vacuum distillation to yield a clear colourless liquid (**1**) (20.98 g, 81.59 mmol, yield: 62%).

IR (neat) ν (cm⁻¹) = 2970 (broad), 1730, 1460, 1390, 1270, 1160, 1100, 735, 696 ¹HNMR (400 MHz, CDCl₃): δ (ppm) = 2.01 (s, 6H, CH₃), 5.26 (s, 2H, CH₂O), 7.51-7.30 (m, 5H, CH_{aryl}). ¹³CNMR (100 MHz, CDCl₃): δ (ppm) = 30.85 (1C, CH₃), 55.86 (1C, CH₃), 67.55 (1C, CH₂), 127.96 (1C, C), 128.40 (1C, C), 128.67 (1C, C), 135.56 (1C, C), 171.32 (1C, C).



Scheme 4.2: Polymerisation of 2-(dimethylamino)ethyl methacrylate by ATRP.

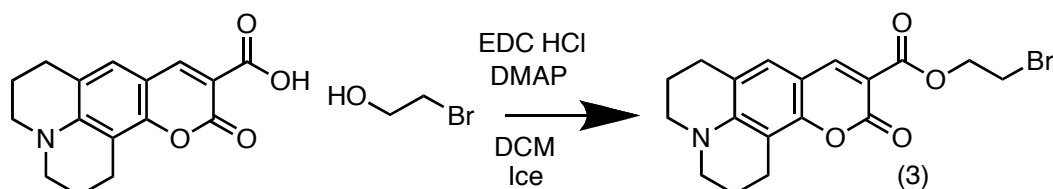
4.2.2 Polymerisation of 2-(dimethylamino)ethyl methacrylate (DMAEMA)

(2)

2-(Dimethylamino)ethyl methacrylate (20.0 g, 127 mmol), (E)-*N*-(pyridine-2-ylmethylene)propan-1-amine (iminopyridine ligand) (397 μ L, 2.54 mmol), benzyl-2-bromo-2-methylpropanoate (**1**) (327 mg, 1.27 mmol) were charged into a large dry Schlenk tube along with toluene (20 mL) as solvent. The tube was sealed with a rubber septum and subjected to five freeze-pump-thaw cycles. At the end the mixture was left frozen and flushed with nitrogen before copper (I) bromide (182 mg, 1.27 mmol) was added. The system was subjected to three nitrogen/vacuum cycles, then the reactor was filled with nitrogen and the temperature adjusted to 70°C with constant stirring ($t = 0$). Aliquots were removed using a degassed syringe at regular time intervals for conversion determination. This was calculated by ^1H NMR spectroscopy by comparing the relative proportion of OCH_2 protons at 4.19 and 4.36 ppm in the polymer and monomer respectively. At the end of the polymerisation the reactor was opened and air was allowed to enter the system, causing the copper catalyst to oxidise to Cu(II) and effectively stopping the polymerisation reaction. During this process the flask was lifted from the bath and the temperature reduced to ambient. The mixture was then passed through two neutral alumina columns in order to remove residual Cu(II) salts present in the reaction mixture. The solution volume was reduced under vacuum and then the polymer obtained through precipitation into petroleum ether. The polymer was analysed by gel permeation chromatography. $\text{DP (GPC)} = 107.1$, $M_n \text{ (GPC)} = 17.1 \text{ kDa}$, $M_n/M_w = (\text{GPC})$

= 1.18 initiating efficiency = 93%; Conversion 93%.

4.2.3 Synthesis of Coumarin 343 alkyl bromide (**3**)



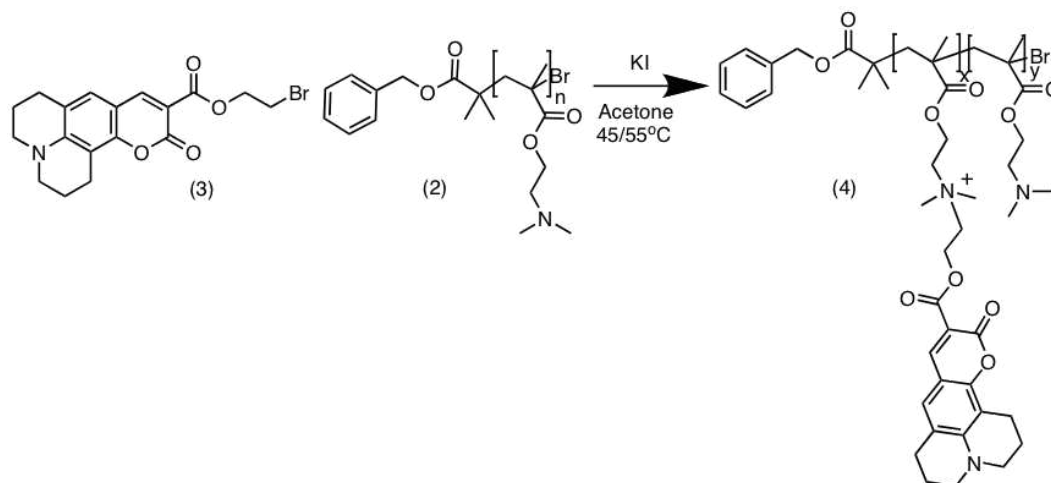
Scheme 4.3: Modification of commercially available Coumarin 343 to produce terminal alkyl bromide.

Coumarin 343 was modified using a method previously described in the literature^[125] for an analogous compound. A solution of coumarin 343 (0.285 g, 1.00 mmol) and bromoethanol (354 μ L, 5.00 mmol) was prepared in dichloromethane (10mL) and cooled to 0°C using an ice bath. To this solution *N*-ethyl-*N*'-3-dimethylaminopropyl)carbodiimide hydrochloride (0.575 g, 3.00 mmol) and 4-(dimethylamino)pyridine (0.006 g, 0.05 mmol) were sequentially added while stirring. This was left to react overnight. The mixture was then washed with water (4 x 50 mL) and dried with magnesium sulfate. After filtration the organic phase was purified further using flash chromatography (CC, SiO₂, dichloromethane/ethylacetate 12:1 vol/vol). The relevant fractions were combined and once the solvent was removed an orange crystalline solid formed (**3**) 0.0972 g, 0.248 mmol, yield: 25%

IR (neat) ν (cm⁻¹) = 2960, 2920, 2852, 2356, 2341, 1725, 1444, 1409, 1257, 1085, 1010, 788, 698 ¹HNMR (400 MHz, CDCl₃): δ (ppm) = 1.89-2.04 (m, 4H, 2CH₂), 2.76 (t, J = 6.0 Hz, 2H, CH₂), 2.87 (t, J = 6.4 Hz, 2H, CH₂), 3.28-3.37 (m, 4H, CH₂N), 3.63 (t, J = 6.3 Hz, 2H, CH₂Br), 4.58 (t, J = 6.3 Hz, 2H, CH₂O), 6.95 (s, 1H, CH_{vinyl}), 8.35 (s, 1H, CH_{aryl}).

4.2.4 Fluorescent labeling of poly(2-(dimethylamino)ethyl methacrylate)

(4)



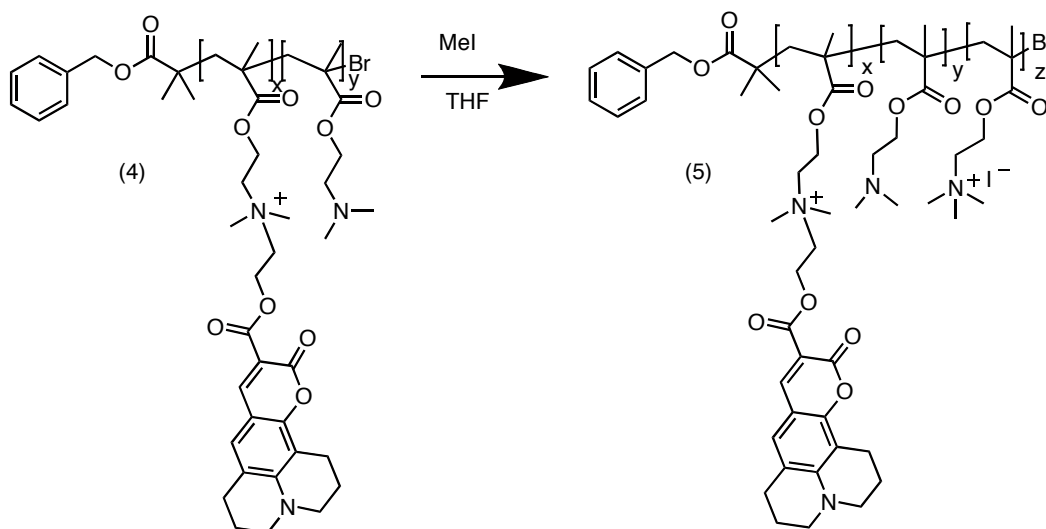
Scheme 4.4: Fluorescent labeling of poly(DMAEMA) scaffold **(2)** using Coumarin 343 alkyl bromide **(3)**. [x][y] = [1][99]

A suspension of pDMAEMA **(2)** (3.19 g, 20.3 mmol of tertiary amine repeating units), coumarin alkyl bromide **(3)** (0.079 g, 0.20 mmol) and potassium iodide (0.337 g, 2.03 mmol) in acetone (70 mL) was sonicated for 30 minutes. This mixture was then allowed to stir at 45°C for 2 days and 55°C for 2 days while monitoring the conversion by thin layer chromatography using chloroform as the solvent. The unreacted coumarin bromide had an $R_f = 0.75$ whilst the fluorescently tagged polymer did not move along the plate ($R_f = 0.00$). The acetone was removed and the mixture redissolved in dichloromethane, filtered to remove the residual salts and the polymer **4** obtained by precipitation into petroleum ether.



Figure 4.1: Fluorescently labelled poly(DMAEMA) (**4**) in aqueous solution (1 mg/mL) illuminated under 365 nm lamp.

4.2.5 Quaternisation of Fluorescent poly(2-(dimethylamino)ethyl methacrylate) (**5**)



Scheme 4.5: Quaternisation of fluorescent pDMAEMA (**4**) using varying amounts of methyl iodide.

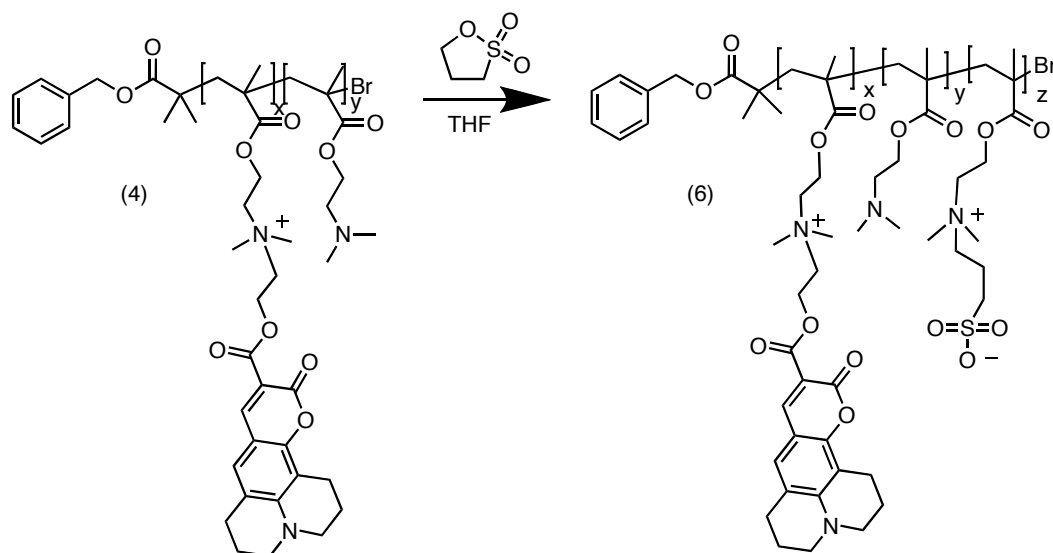
Varying degrees of DMAEMA quaternisation were obtained using a method previously reported in the literature.[51] The method was first perfected on the non-fluorescent polymer (**2**). Then four vessels were prepared containing the fluorescent polymer (**4**) (0.20 g, 1.27 mmol) which were dissolved in tetrahydrofuran (8.2 mL). While stirring, methyl iodide (a. 19.8 μ L, 0.318 mmol; b.

39.6 μL , 0.636 mmol; c. 59.4 μL , 0.954 mmol; d. 79.2 μL , 1.27 mmol) was added. This was stirred for 48 hours giving a precipitate which varied in colour, from yellow to orange, depending on the proportion of methyl iodide added. The solvent was removed under vacuum, the polymers dissolved in deionised water and the resulting yellow solutions freeze-dried to give the desired fluorescent quaternised p(DMAEMA) materials as light yellow solids (**5a**, **5b**, **5c**, **5d**). The experimental degree of quaternisation achieved was calculated by ^1H NMR by observing the decreasing of the signal representing the two protons adjacent to the tertiary amine (2.66 ppm) and the increasing of the signal representing the same two protons in the quaternised amine moieties (3.75 ppm).



Figure 4.2: Quaternised fluorescent poly(DMAEMA) in aqueous solution (1 mg/mL) illuminated with a 365 nm UV lamp. **5a** (left), **5b** (centre left), **5c** (centre right) and **5d** (right).

4.2.6 Sulfobetainisation of Fluorescent poly(2-(dimethylamino)ethyl methacrylate) (6)



Scheme 4.6: Sulfobetainisation of fluorescent pDMAEMA (**4**) using varying amounts of 1,3-propane sultone.

The fluorescent polymer (**4**) was derivatised in varying proportions using a method which had been previously described.[126] The method was first perfected on the non-fluorescent polymer (**2**). Then four vessels were prepared containing the fluorescent polymer (**4**) (0.20 g, 1.27 mmol) dissolved in tetrahydrofuran (8.2 mL). While stirring, 1,3-propane sultone (a. 27.9 μ L, 0.318 mmol; 55.8 μ L, 0.636 mmol; c. 83.7 μ L, 0.954 mmol, 112 μ L, 1.27 mmol) was added. This was stirred for 16 hours at room temperature giving a waxy precipitate. The solvent was removed under reduced pressure and traces of unreacted 1,3-propane sultone were removed by washing the polymers with diethyl ether. Then the excess solvent was removed under vacuum, the polymers dissolved in deionised water and the resulting yellow solutions freeze-dried to give the desired fluorescent sulfobetained p(DMAEMA) as light yellow solids (**6a**, **6b**, **6c**, **6d**).

The experimental degree of sulfobetainisation achieved was calculated by ^1H NMR by observing the decrease of the signal representing the two protons adjacent to the tertiary amine (2.68 ppm)

and the increase of the signal representing the same two protons in the quaternary amine moieties (3.75 ppm).

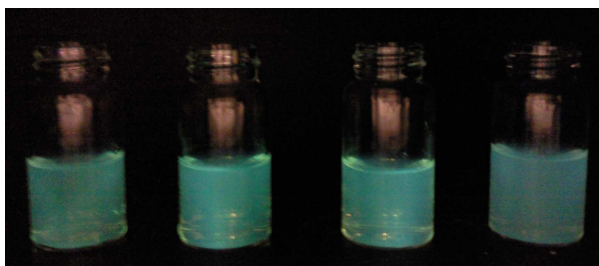


Figure 4.3: Sulfobetained fluorescent poly(DMAEMA) in an aqueous solution of 1 mg/mL illuminated with a 365 nm UV lamp. **6a** (left), **6b** (centre left), **6c** (centre right) and **6d** (right).

4.2.7 Binding experiments and aggregation assay

For the method used in the aggregation assay and the binding experiments, refer to the general methods chapter.

4.3 Results and discussion

Although templating has already been shown to enable the selective binding of microorganisms such as bacteria[61] and their spores[62] these techniques relied upon the production of structures in the size region of 100 μm . and also required incubation times of 2 hours. Both this attributes may be unfavourable within the context of a consumer end-product. As discussed in the introductory chapter, the nature of polyvalency can enable interactions to cumulate to provide a high avidity binder.

It is widely reported in the literature that cationic materials can utilise the innate negative charge of bacterial cells to induce binding and there are also reports of zwitter-ionic materials such as the betaines used here to bind to bacteria.[127] It was therefore decided that a polymer should be

made containing tertiary amines capable of undergoing modifications such as the introduction of charges. 2-(Dimethylamino)ethyl methacrylate is a monomer which is readily available and its use for bacterial aggregation was already reported, thus DMAEMA was an appropriate initial choice.

The effect of charge alone upon polymer binding was investigated. In order for this to be the only characteristic which varied, all other aspects of the polymers were intended to remain constant e.g. polydispersity, DP and M_n . So, from one single polymer a library was created, thus ensuring the other attributes of the polymer would remain unaffected (Figure 1.4).

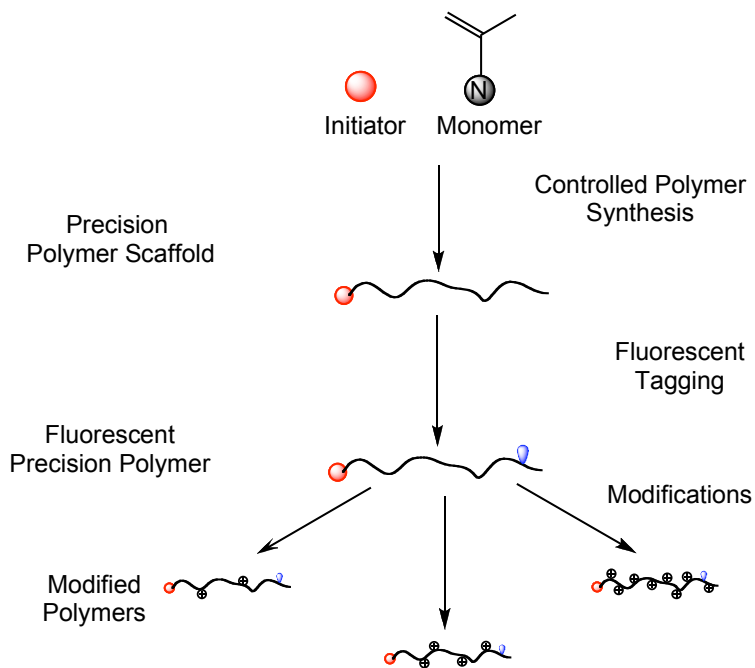


Figure 4.4: Overview of strategy employed. From one single polymer the polymer library was created.

The benzyl ATRP initiator **1** (Scheme 4.1) was synthesised from benzyl alcohol and α -bromo isobutyryl bromide and it was chosen because its benzylic and aromatic protons could be used as ^1H NMR internal standards for the determination of the molecular weight (M_n of the polymers produced in this work, by comparing the signals of the resulting benzyl ester-terminated polymers with relevant signals of the polymer repeating units.

Initiator **1** was then used in conjunction with 2-(dimethylamino)ethyl methacrylate (DMAEMA) as the monomer to yield the well defined polymer scaffold (**2**) $\text{DP (GPC)} = 107.1$, $M_n \text{ (GPC)} = 17.1$ kDa, $M_w/M_n \text{ (GPC)} = 1.18$. The polymerisation of DMAEMA in (Scheme 4.2) exhibited linear pseudo first-order kinetics with respect to monomer concentration (Figure 4.5), which indicated good control over the polymerisation process.

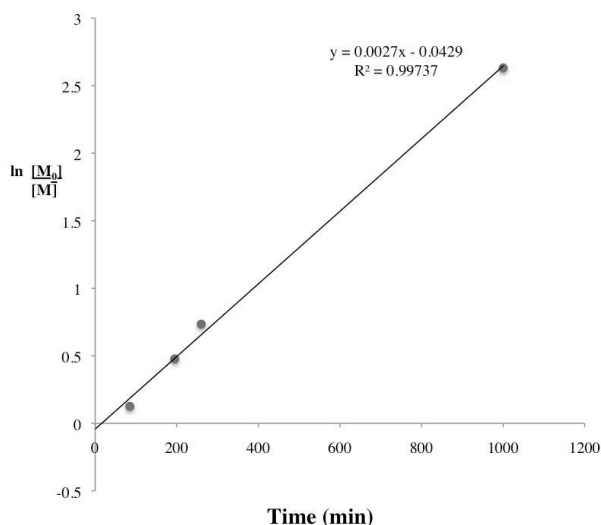


Figure 4.5: Kinetic plot for the polymerisation of DMAEMA in Toluene. Conditions: $[1]:[\text{CuBr}]:[\text{ligand}]:[\text{DMAEMA}] = [1]:[1]:[2]:[100]$

First order kinetics are expected for ATRP systems and are a reflection on how polymerisation is related to monomer concentration. In reality the polymerisation rate is dependent on several parameters (equation 4.1).

$$R_p = k_p[M][P^*] = k_p K_{eq}[M][I]_0 \times [Cu^I] \div [X - Cu^{II}] \quad (4.1)$$

Equation 4.1 defines how the rate of polymerisation in ATRP is dependent on monomer concentration $[M]$, the polymer radical concentration $[P^*]$, the initiator concentration $[I]$ along with the rate constants. However, as the rest of these will stay constant the rate is described a pseudo first order.

In order to assess binding of polymers to the bacteria the former would need to have a functionality attached to the chain which enables visualization of the bacteria-polymer clusters. In this work, the fluorophore coumarin 343 was selected. In order for coumarin 343 to have the necessary functionality to enable its attachment to our p(DMAEMA) polymeric scaffolds it was necessary to convert it first into a corresponding alkyl bromide **3** by reaction with 2-bromoethanol mediated by EDC coupling agent and DMAP as the organocatalyst. Fluorescent tag **3** was then used to tag/quaternise the preformed p(DMAEMA) scaffold **2** in acetone at 45/55°C (**3**:(DMAEMA repeating units) 1:100 mol/mol) using an excess of sodium iodide to convert in situ **3** into its corresponding more reactive alkyl iodide, to give the desired fluorescent p(DMAEMA) **4** (Scheme 4.4). This would ensure that each chain should statistically have only one coumarin group which would minimise the effect the fluorophore would have upon bacterial binding. A three step synthesis of a coumarin 343 ATRP initiator proved to be too uneconomical to justify its use.

This single batch of polymer **4** was then divided in several portions and used to undergo all the subsequent modification reactions. Polymer **4** was used to create a library of polymers with varying degrees of modification. Reaction conditions for the quaternisation and sulfobetainisation steps were optimised first with the non-fluorescent p(DMAEMA) scaffold **2** and only those conditions found successful were carried out on Coumarin 343-fluorescently tagged polymer **4**.

Two different modifications were to be carried out on polymer **4**. These were the introduction

of a permanent positive charge by addition of a methyl group **5** to the p(DMAEMA) tertiary amine repeating unit with CH_3I (Scheme 4.5) and also the creation of a polyzwitterionic material **6** by addition of 1, 3-propane sultone (Scheme 4.6).

For both modifications of polymer **4**, the degree of modification was targeted at 25% (**5a**, **6a**), 50% (**5b**, **6b**), 75% (**5c**, **6c**), 100% (**5d**, **6d**). The experimental level of modification obtained (Table 4.1) was calculated through $^1\text{HNMR}$ by comparing relevant peaks in the modified and unmodified p(DMAEMA) repeating units.

Table 4.1: Degree of modification carried out to fluorescent poly(DMAEMA) **4**

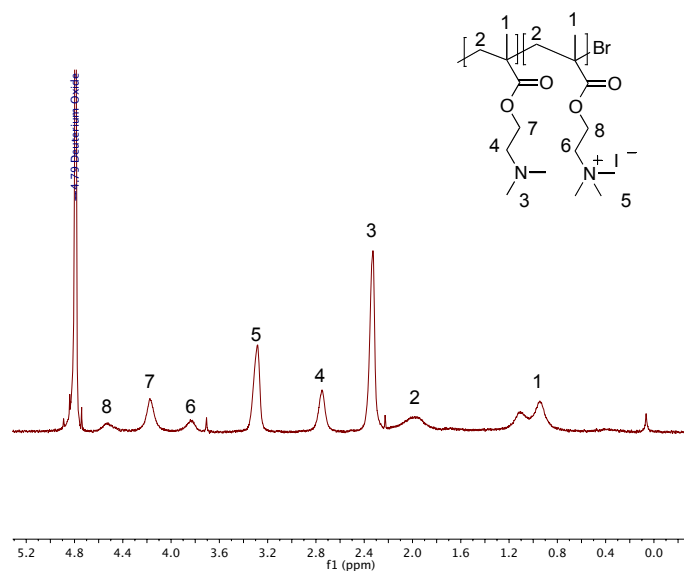
| Targeted Modification (%) | Actual Quaternisation (%) | Actual Sulfobetainisation (%) |
|---------------------------|---------------------------|-------------------------------|
| 25 | 26 (5a) | 30 (6a) |
| 50 | 55 (5b) | 56 (6b) |
| 75 | 80 (5c) | 68 (6c) |
| 100 | 100 (5d) | 100 (6d) |

The protons used for this calculation (peak 4 and 6 in Figure 4.6) were chosen as they were closest geometrically to the amine undergoing the modification therefore were most likely show the greatest difference in their chemical shifts.

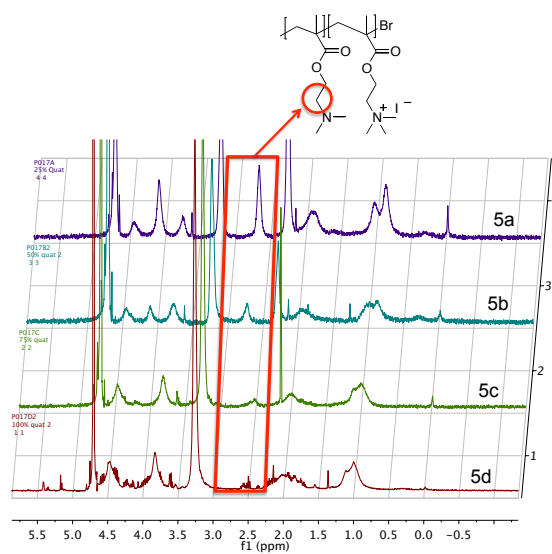
An example of how the $^1\text{HNMR}$ spectra were used is shown in Figure 4.6. The chemical shift for the two protons adjacent to the tertiary amine are highlighted with the red box.

Once purified, the modified polymers were then dissolved in deionised water to create a 1 mg/mL aqueous solution which was used for the subsequent binding experiments.

The 'control' in the binding experiments was the addition of polymer-free water to the bacterial suspension to enable comparison to the appearance of the cells after undergoing the same treatments as those subjected to incubation with the polymers. Photographs were taken and observations



(a)



(b)

Figure 4.6: a) Assigned ^1H NMR spectra of modified polymer **5a** b) ^1H NMR spectra of quaternised poly(DMAEMA) **5** highlighting the decrease in the proportion of protons adjacent to the tertiary amine. Purple (**5a**), turquoise (**5b**), green (**5c**), red (**5d**).

made.

During the incubation period with polymers (**5a - d**) visual observation of aggregation of both *E. coli* (Gram-negative) and *S. mutans* (Gram-positive) bacterial species occurred. In the case of *E. coli* visually the degree of aggregation did not appear to be dependent on the degree of quaternisation of the polymer employed which contrasted with the *S. mutans* where slightly more aggregation was visible between 25% quaternised **5a** compared with 100% **5d**, with the other polymers showing observable intermediate effects. Incubating polymers **6a - d** had similar effects between the species, more aggregation occurred with (**6a**) and less with **6d**. However, during the washing steps the *E. coli* pellets became visually less coloured and the cells returned to their off-white colour. This decrease in colour was inversely proportional to the degree of sulfobetaination i.e. more sulfobetaination, less colour. This was in contrast to the *S. mutans* where the pellets retained their colour irrespective of the level of sulfobetaination.

After washing, the pellets were resuspended and mounted on slides for microscopic viewing.

Microscopically the bacteria incubated with polymers **5a - d** showed a trend to form aggregates with polymers **5a, b, c** however with polymer **5d** there were no visible aggregates but the cells still exhibited fluorescence from the attached polymer. Although no definitive explanation for this phenomenon can be formulated at present, this result suggests that as the level of quaternisation increased the attachment of the polymers to the negatively charged bacteria, increased. The polymers would be expected to saturate the cells surfaces above a threshold concentration, thus generating positively charged bacterial polymer complexes which repelled each other. The microscopic observations between both *E. coli* and *S. mutans* were comparable.

As can be seen in Figure 4.2 of polymers **5a - d** in aqueous solution there was a decrease in the fluorescence of the polymers from **5a** to **5d**. This may have been due to fluorescent quenching from the iodide counterion in the quaternary amine repeating units.[128]

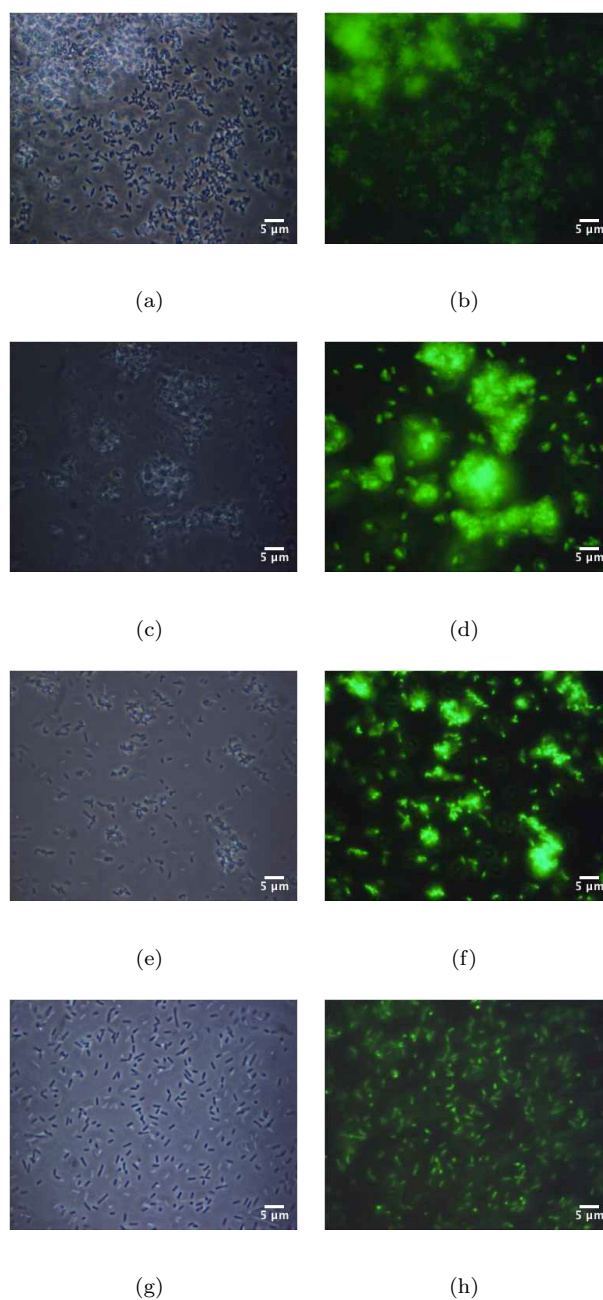


Figure 4.7: Phase contrast and fluorescent microscopy images of polymer **5a** (a & b), **5b** (c & d), **5c** (e & f) and **5d** (g & h) with *E. coli* MG1655 after undergoing procedure described in 3.2.1. The binding of the polymers to the bacteria remains strong however the size of the aggregates decreases.

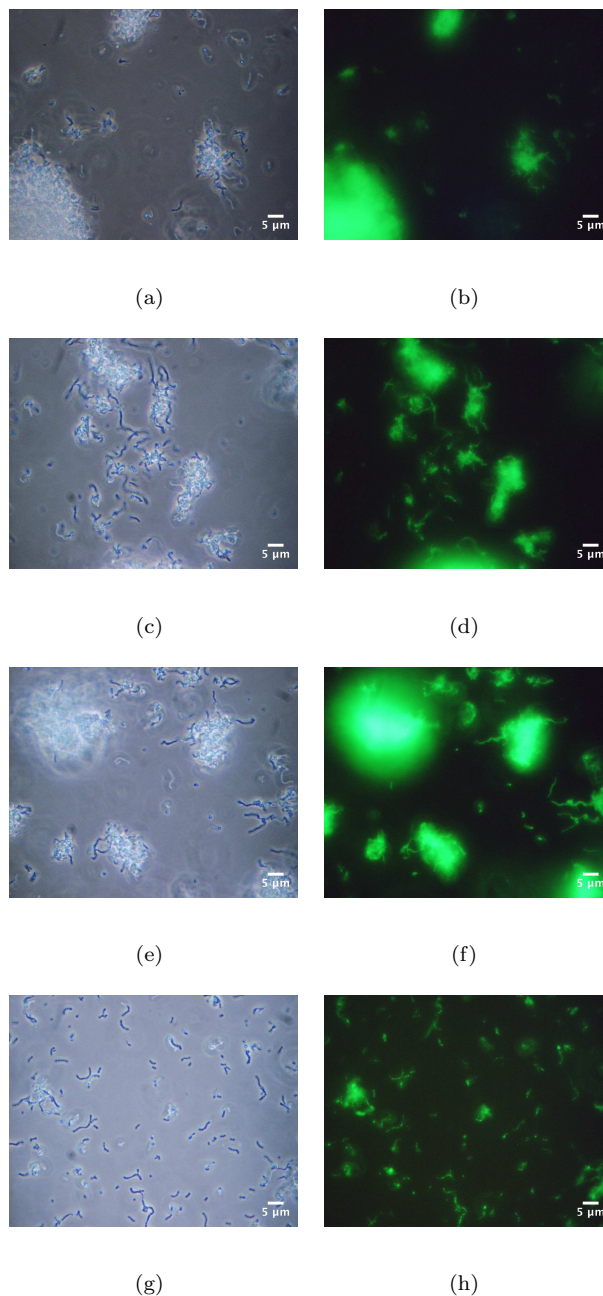


Figure 4.8: Phase contrast and fluorescent microscopy images of polymer **5a** (a & b), **5b** (c & d), **5c** (e & f) and **5d** (g & h) with *S. mutans* NCTC 10449 after undergoing procedure described in 3.2.1. Binding to *S. mutans* remains as the level of quaternisation increases on the polymer chain.

The visualisation of the bacteria incubated with the zwitterionic polymers **6a** - **d** showed more inter-species variation than those of **5a** - **d**.

E. coli populations when observed with phase contrast microscopy were comparable in cell number across images of **6a** - **d**, however, upon switching to fluorescent imaging there was a dramatic decrease in fluorescence as the level of betaine functionality presence in the polymer increased. (Figure 4.9)

This decrease in binding from polymer **6a** to **6d** was not seen during microscopic observation of *S. mutans* (Figure 4.10). However, the decreased binding observed with the zwitter-ionic polymer and *E. coli* is, in part, expected from the literature. Zwitter-ionic polymeric surfaces are promoted for their non-fouling properties and their ability to prevent bacterial adherence. [129, 130] This made the result for *S. mutans* unexpected.

The difference in the binding between polymers **6a** and **6d** with *S. mutans*, if any, was indiscernible through visual examination. When compared to data obtained with the same polymers and *E. coli*, it is highly suggestive that this type of zwitter-ionic betaine polymer exhibited specificity towards *S. mutans*. The difference between the bacteria and polymer binding used is only seen in the betaine polymers. In the case of quaternised polymers similar binding results were seen with *E. coli* and *S. mutans*.

It is interesting to note that as the degree of quaternisation increased, the size of the aggregates decreased. This change was most likely due to the polymer completely encasing the bacteria and as such they then became cationic particles overall and so repelled each other.

The intensity of the fluorescence seen in both of the sets of microscopy images decreased for polymers **5a**, **5b**, **5c** and **5d** respectively but this is not due to decreased polymer binding but, as previously explained, the presence of the iodide counterion which was bound when the polymers were quaternised.

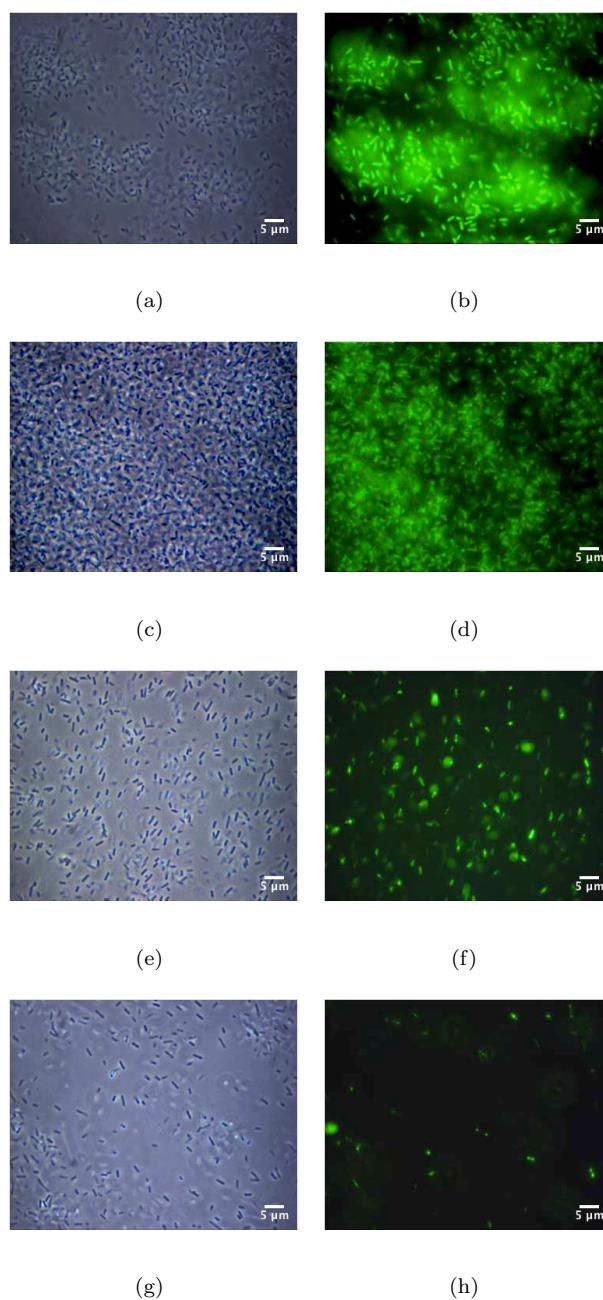


Figure 4.9: Phase contrast and fluorescent microscopy images of polymer **6a** (a & b), **6b** (c & d), **6c** (e & f) and **6d** (g & h) with *E. coli* MG1655 after undergoing procedure described in 3.2.1. It can be seen that as the level of betaine functionality increases the binding of the polymer to the bacteria decreases.

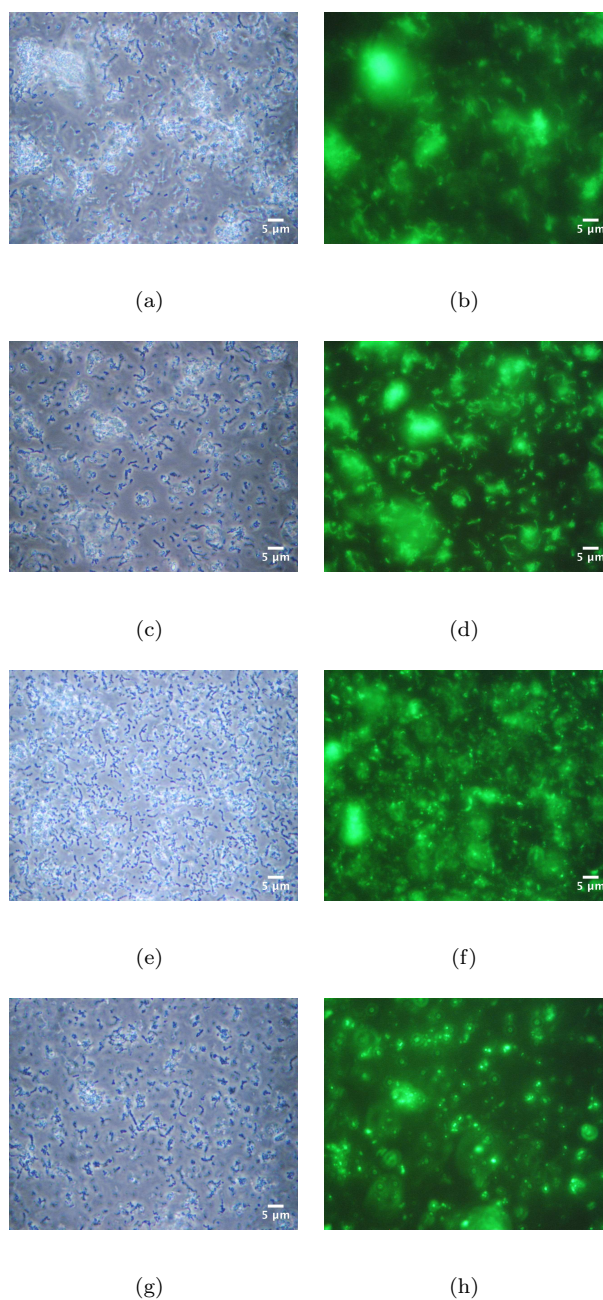


Figure 4.10: Phase contrast and fluorescent microscopy images of polymer **6a** (a & b), **6b** (c & d), **6c** (e & f) and **6d** (g & h) with *S. mutans* NCTC 10449 after undergoing procedure described in 3.2.1. As the levels of betaine functionality is increased the binding to the bacterium remains strong.

In order to assess the validity of the microscopy observations, that the betaine polymers were not binding to *E. coli* and the quaternised polymers were, an aggregation assay was performed. The aggregation assay verified the differences between seen between the two polymers (Figure 4.11).

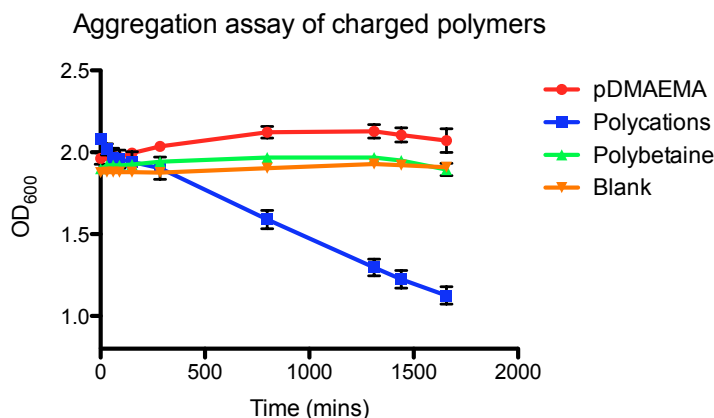


Figure 4.11: Aggregation assay of *E. coli* with the betaine polymer **6d** (green), cationic polymer **5d** (blue), the unmodified polymer backbone (red) and water (orange).

As can be seen in Figure 4.11 the quaternised polymer had a dramatic effect upon the sedimentation behaviour. This result is highly suggestive that the polymer was binding to the bacteria.[131] The duration of the experiment occurred over a longer time scale than for microscopy as the results are a reflection of binding and sedimentation. Although this confirmed what was observed microscopically with *E. coli* it was not possible to perform the aggregation assay using *S. mutans* as it autoaggregated very rapidly most likely due to the presence of its exopolysaccharide.[14] For this reason, whilst considering microscopy images the presence of fluorescence is more important than presence of aggregates. The unmodified polymer had a low binding effect as this aggregation assay was carried out buffered at pH 9 therefore the presence of transient cationic charge at the pDMAEMA secondary amine was minimal.

In order to examine the possible specificity of fully betaine functionalised polymers towards *S. mutans* a dual component binding experiment was devised. This was the same as the normal

binding experiments but rather than using *E. coli* MG1655 wild type, a derivative was used which expresses the fluorescent mCherry protein.[121] This was chosen as it would enable a colour-change test whereby non polymer-bound *E. coli* would fluoresce red, polymer-bound *S. mutans* would fluoresce green and non-specific binding would result in a combination of red and green i.e. amber fluorescence (Figure 4.12)

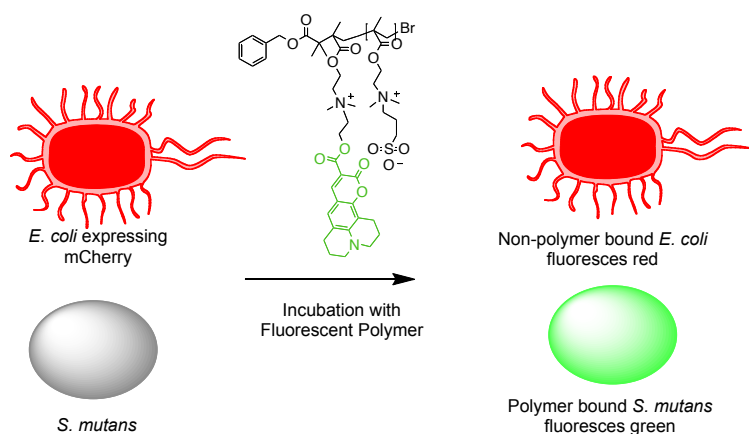
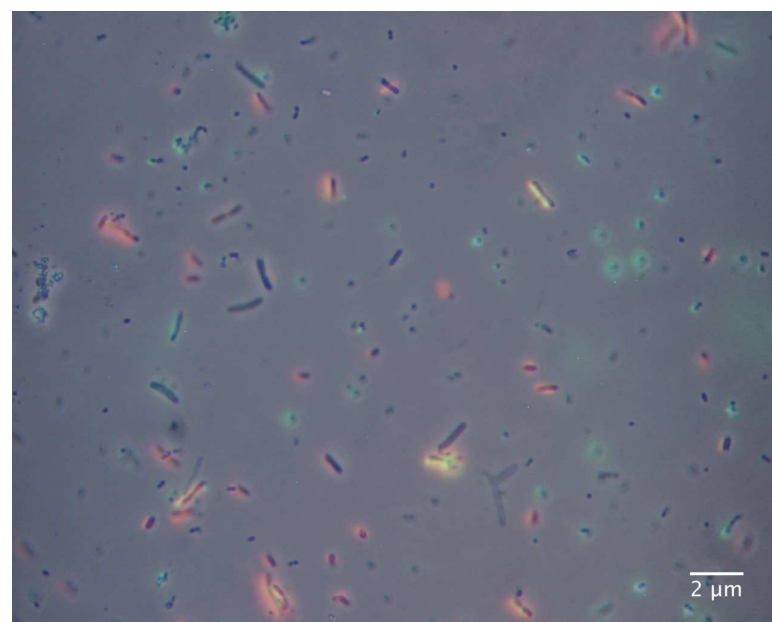
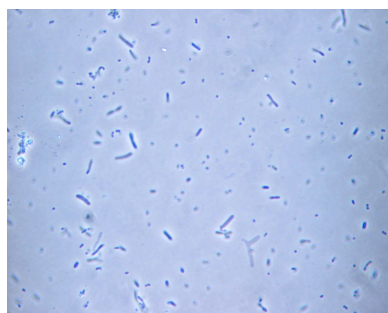


Figure 4.12: General schematic for the mixed culture binding experiment where specific binding can be recognised by comparing fluorescence.

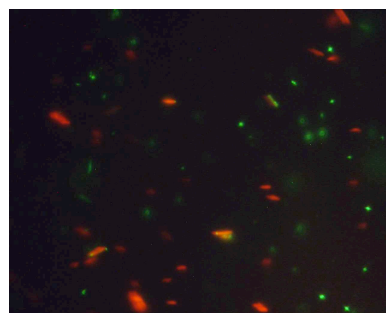
Both cell types were grown to the same cell density before mixing and washing. They were then incubated with the polymer, as before after which the excess was removed in the same washing steps previously described then mounted for microscopy examination. Images were recorded in phase contrast and also fluorescence so that visually the different cell types could be identified not only from their fluorescence, or absence thereof, but also from the cell morphology. The images were then overlaid for comparison and identification of binding behaviour.



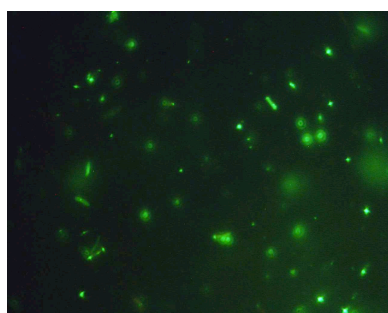
(a)



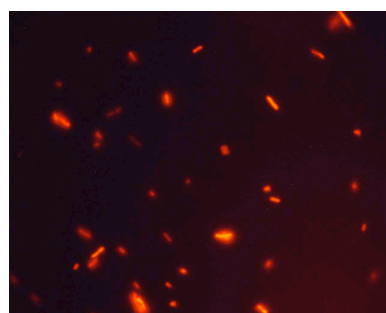
(b)



(c)



(d)



(e)

Figure 4.13: (a) Overlapped images from mixed binding experiment utilising the fluorescent betaine polymer **6d** with *E. coli* MG1655 mCherry and *S. mutans* after undergoing procedure described in 3.2.1. Images were recorded using phase contrast microscopy (b) then separate fluorescent channels (d)-(e) and combined for analysis (c).

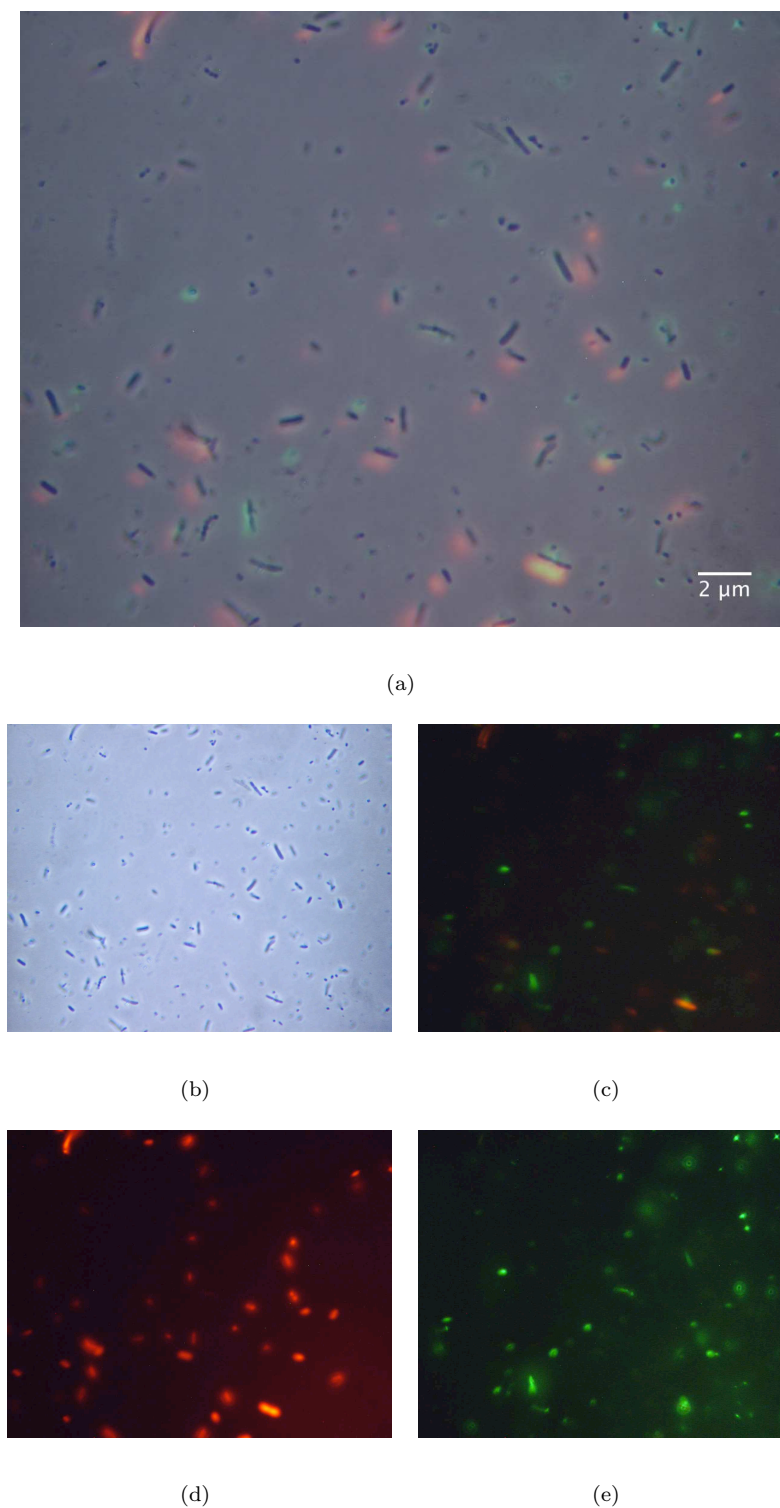


Figure 4.14: (a) Overlapped images from mixed binding experiment utilising the fluorescent betaine polymer **6d** with *E. coli* MG1655 mCherry and *S. mutans* after undergoing procedure described in 3.2.1. Images were recorded using phase contrast microscopy (b) then separate fluorescent channels (d)-(e) and combined for analysis (c).

As can be seen in the images in Figure 4.13 and Figure 4.14 there were only minimal areas of mixed fluorescence (yellow/amber). These areas of mixed fluorescence may be attributed to two processes:

- i)* The polymer may engage in some minimal non-specific binding to *E. coli* which would cause the the green and red fluorescence to overlap resulting in the amber colour.
- ii)* It may also have been due to red *E. coli* positioned adjacent to green fluorescently labelled *S. mutans* so that as a result of the proximity the fluorescence overlaps.

However, on the whole the fluorescence obtained from the polymer and the fluorescence from the red fluorescent protein (mCherry) were largely segregated. This provided further support to the theory that this type of zwitter-ionic functionality afforded from the betaine exhibited preferential binding towards *S. mutans* and was of low binding for *E. coli*.

4.4 Conclusions

A library of polycationic and polyzwitterionic functional polymers has been prepared and their binding to Gram-positive oral *Streptococci mutans* NCTC 10449 and Gram-negative *Escherichia coli* MG1655 was demonstrated.

In summary, a synthetic polymeric 2-(dimethylamino)ethyl methacrylate scaffold $M_n = 17.1$ kDa ($M_n/M_w = 1.18$) was prepared using atom transfer radical polymerisation with the initiator benzyl-2-bromo-2-methylpropanoate. The polymeric scaffold underwent a nucleophilic addition to attach a coumarin 343 fluorescent functionality. The fluorescent polymer was then reacted with methyl iodide and 1,3-propane sultone to create the library of polymers. The degree of this modification was targeted at 25%, 50%, 75% and 100% and the actual level obtained calculated using ^1H NMR spectroscopy to be 26, 55 and 100% for the cationic polymers and 30, 56, 68 and 100% for the betaine polymers.

Polycationic polymers showed indiscriminate binding across the two bacterial species. At 100% quaternised, aggregates were no longer visible but cells were seen as individual polymer bound cells.

In contrast, with the polyzwitterionic polymer, binding could be tuned towards the *Streptococci* strain used in this project by increasing the proportion of zwitterion moieties present on the chain. In the work presented here, preliminary work established the framework of tunable polymers based upon charge to exhibit specificity in bacterial recognition.

Chapter 5

Selection of Functionalities B: Carbohydrates

5.1 Introduction

The presences of sugars on the bacterial surface as well as the ability of bacteria to bind to carbohydrates donates another binding opportunity.

As can be seen in Figure 5.1 carbohydrate presentation and binding is utilised in nature for cell recognition. It is these surface sugars and the bacterial sugar binding lectins we seek to exploit to generate bacterial binding polymers.

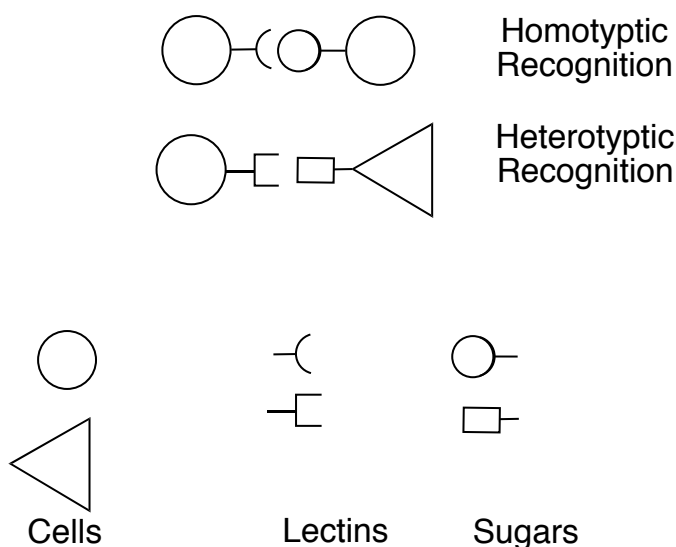


Figure 5.1: Figure showing carbohydrate binding involved in cell recognition. This binding can be either homotypic where it is cells of the same type or heterotypic where it is different types of cells.

5.1.1 Boronic acids to bind bacterial surface sugars

There has been a plethora of work recently on boronic acid residues and their ability to bind diols such as sugars in a potent and specific manner.[132, 133, 134] The influence of this work at the natural-synthetic interface has broad scope.[135] Diols *in vivo* are not restricted to surface sugars and are important bacterial communication molecules however the study of these interactions are outside the scope of this work. The literature for the use of polymeric boronic acids to induce the binding of microorganisms such as bacteria is more restricted and the area less investigated than that of glycopolymers. Boronic acids have however been used to generate bacteria detection systems.[136] Wannapob *et al.* utilised monomeric 3-aminophenylboronic acid attached to a gold electrode for the economical sensitive detection of bacteria. This study, although not using polymers indicates that such bacterial capture may be possible using sugar binding boronic acids moieties.

Polymeric phenylboronic acid systems have been demonstrated by Ivanov *et al.* to cause strong binding of yeast cells.[137] Surfaces were modified with 3-aminophenylboronic acid and polymers of *N,N*-dimethylacrylamide-co-*N*-acryloyl-*m*-aminophenylboronic acid which utilise the strong binding between the boronic acids and the diols found in sugars. The polymers were grafted to glass surfaces and exposed to stained yeast cells. Binding of yeast to the co-polymer (containing boronic acid residues) coated surface was significantly greater than for the polymer without the boronic component or for the bare glass surface. Removal of bacteria by washing the surfaces with buffer was minimal, whilst it was possible to do so by competitive washes with fructose solutions, which has a high affinity for boronic acids.

Such work had demonstrated that boronic acid polymers are capable of binding to microorganisms using their surface sugars and further exploration into its use for binding bacteria is needed.

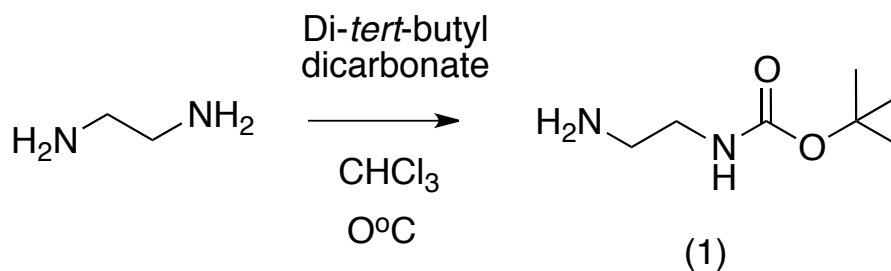
5.1.2 Glycopolymers to bind to bacterial lectins

The presence of carbohydrate recognition sites or lectins are well documented for many bacterial strains. The importance of these molecules for cellular recognition and detection is now being fully explored and understood.[138] Sugars are important binding sites for bacteria and they are also found on the surface of bacteria and so are important to intercellular binding and identification.[40] The sugars both displayed and recognised by cells are known to greatly impact upon pathogenicity and virulence.[46] Many bacteria display specific lectins to aid adherence to the host. For example *E. coli* FimH can bind oligomannose moieties with comparable affinities however the strains of *E. coli* vary in the propensity for their FimH to bind monomannose. This propensity imparts specific colonisation advantages. A high affinity is associated with uropathogenic strains and a low affinity is associated with gut and intestinal strains.[16] Considering this it is unsurprising that carbohydrate displaying polymers enable highly specific systems for bacterial recognition.

5.2 Methods

The complete synthesis of the boronic acid monomer was carried out as previously reported in the literature.[139]

5.2.1 Synthesis of *tert*-butyl (2-aminoethyl)carbamate (**1**)



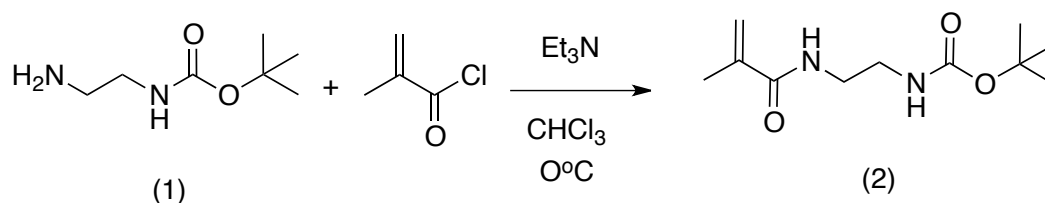
Scheme 5.1: Synthesis of *tert*-butyl (2-aminoethyl)carbamate (**1**).

1,2-Ethylene diamine (14.0 mL, 12.6 g, 209 mmol) was dissolved in chloroform (200 mL) and cooled over ice with stirring. Di-*tert*-butyl dicarbonate (5.00 g, 22.9 mmol) was dissolved in chloroform (50 mL) and added drop-wise to the ethylene diamine solution over 30 minutes. The mixture was left to react for 16 hours. The chloroform was then removed under reduced pressure. To the residue, 100 mL of deionised water were added. The bis-substituted diamine was removed by filtration and the product was extracted from the water into dichloromethane (3×100 mL). The dichloromethane was dried using magnesium sulphate, the magnesium sulphate filtered and then the dichloromethane removed to yield a yellow oily product **1** which was used without further purification. (3.35 g, 20.91 mmol, Yield 91.37%)

IR (KBr) ν (cm^{-1}) = 3359 (broad), 2976, 1691, 1523, 1366, 1252, 1170

^1H NMR (400 MHz, CDCl_3): δ (ppm) = 1.26 (s, 9H, $(\text{CH}_3)_3$), 2.60 (t, $J = 5.9$ Hz, 2H, CH_2NH), 2.97 (dd, $J = 11.2$ Hz, 2H, CH_2NH_2), 5.42 (s, 1H, NH).

Calculated Mass ($\text{C}_7\text{H}_{16}\text{N}_2\text{O}_2$): 160.2149. Mass Found (m/z): 160.4009

5.2.2 Synthesis of *tert*-butyl (2-methacrylamidoethyl)carbamate (**2**)Scheme 5.2: Synthesis of *tert*-butyl (2-methacrylamidoethyl)carbamate (**2**)

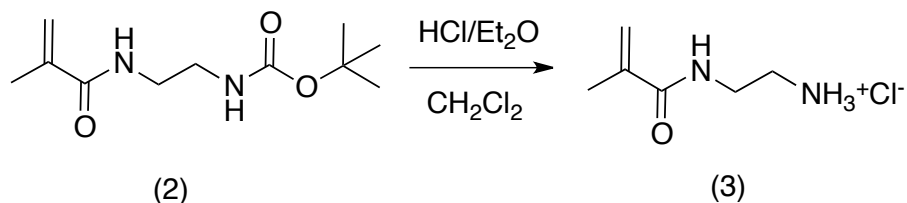
tert-Butyl (2-aminoethyl)carbamate (**1**) (3.31 g, 20.63 mmol) and triethylamine (Et_3N) (8.34 mL, 59.83 mmol) were dissolved in chloroform (30 mL) and stirred over ice. Methacryloyl chloride (2.11 mL, 21.87 mmol) was dissolved in chloroform (20 mL) and added to the reaction mixture with stirring for 30 minutes before being allowed to react for 16 hours. The organic layer was washed with water (5×30 mL) and dried with magnesium sulphate. The magnesium sulphate was filtered and the chloroform was removed under reduced pressure. The product recrystallised using diethyl ether:hexane (3:5) followed by a further recrystallisation with chloroform:diethyl ether:hexane (1:55:55) to yield the product **2** (1.95 g, 8.54 mmol, Yield: 39.0%)

^1H NMR (400 MHz, CDCl_3): δ (ppm) = 1.42 (s, 9H, $(\text{CH}_3)_3$), 1.95 (s, 3H, CH_3), 3.31-3.32 (d, $J = 4.8$ Hz, 2H, CH_2NH), 3.38-3.43 (m, 2H, CH_2NH), 5.02 (s, 1H, NH), 5.31 (s, 1H, CH_2), 5.74 (s, 1H, CH_2), 6.75 (s, 1H, NH)

^{13}C NMR (100 MHz, CDCl_3): δ (ppm) = 18.53 (1C, CH_3), 28.33 (3C, CH_3), 39.92 (1C, CH_2), 41.58 (1C, CH_2), 79.81 (1C, C), 119.93 (1C, CH), 139.49 (1C, C), 157.30 (1C, CO), 168.83 (1C, CO).

Calculated Mass ($\text{C}_{11}\text{H}_{20}\text{N}_2\text{O}_3$): 228.2893. Mass Found (m/z): 228.1441

5.2.3 Synthesis of 2-methacrylamidoethanaminium chloride (**3**)



Scheme 5.3: Synthesis of 2-methacrylamidoethanaminium chloride (**3**)

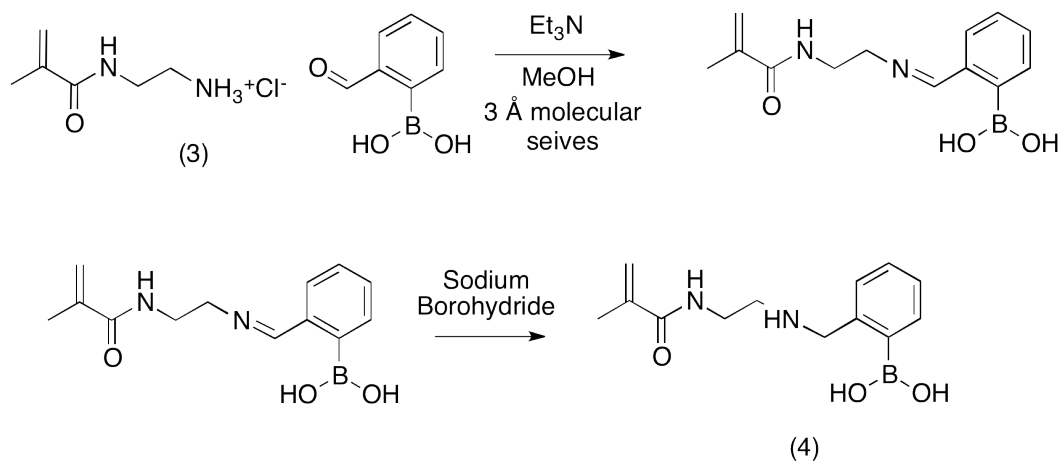
tert-Butyl (2-methacrylamidoethyl)carbamate (**2**) (1.93 g, 8.45 mmol) was dissolved in dichloromethane (20 mL) and 20 mL of hydrogen chloride in diethyl ether (2 M) were added. The reaction mixture was stirred for 24 hours. A hygroscopic precipitate was formed which was filtered and washed with diethyl ether to yield the product **3** (1.17 g, 7.11 mmol, Yield: 84.14%)

¹HNMR (400 MHz, D₂O): δ (ppm) = 1.86 (s, 3H, CH₃), 3.09-3.12 (t, J = 5.9 Hz, 2H, CH₂NH), 3.48-3.51 (t, J = 5.9 Hz, 2H, CH₂NH), 5.43 (s, 1H, CH₂), 5.69 (s, 1H, CH₂).

¹³CNMR (100 MHz, D₂O): δ (ppm) = 17.57 (1C, CH₃), 37.05 (1C, CH₂), 39.28 (1C, CH₂), 121.94 (1C, CH), 138.48 (1C, C), 172.43 (1C, C).

5.2.4 Synthesis of 2-((2-methacrylamidoethylamino)methyl)

phenylboronic acid (4)

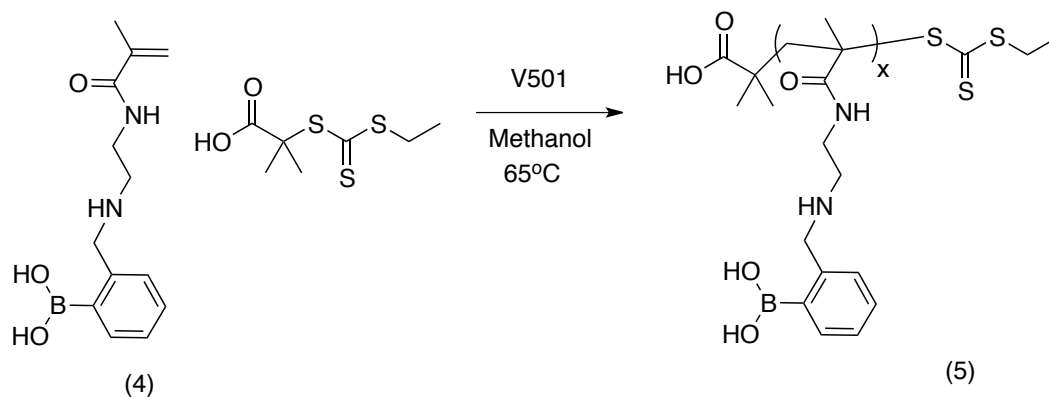
Scheme 5.4: Synthesis of *tert*-butyl (2-aminoethyl)carbamate (4)

2-Aminoethyl methacrylate hydrochloride (**3**) (602 mg, 3.65 mmol), 2-formyl-phenylboronic acid (549 mg, 3.65 mmol), anhydrous triethylamine (3.70 g, 3.65 mmol) and 3 Å molecular sieves (1.00 g) were mixed in anhydrous methanol (5 mL) under nitrogen. The reaction mixture was stirred for two hours with mixing at room temperature before the addition of sodium borohydride (138 mg, 3.65 mmol). This step was followed by further mixing for one hour at room temperature. After this, the mixture was filtered through celite. The filtrate was cooled in an ice bath before being filtered again through celite. The final filtrate had its solvent removed to yield the product **4** (453 mg, 1.73 mmol, Yield = 47.3%).

¹HNMR (400 MHz, MeOD): δ (ppm) = 1.96 (s, 3H, CH₃), 3.03-3.06 (t, J = 6.2 Hz, 2H, CH₂NH), 3.59-3.62 (t, J = 6.2 Hz, 2H, CH₂NH), 3.62 (s, 2H, CH₂C), 5.42 (s, 1H, CH₂), 5.78 (s, 1H, CH₂), 7.15-7.44 (m, 4H, CH_{aryl}).

Calculated mass (C₁₃H₁₉BN₂O₃): 262.1146 Mass found (m/z): 262.0012

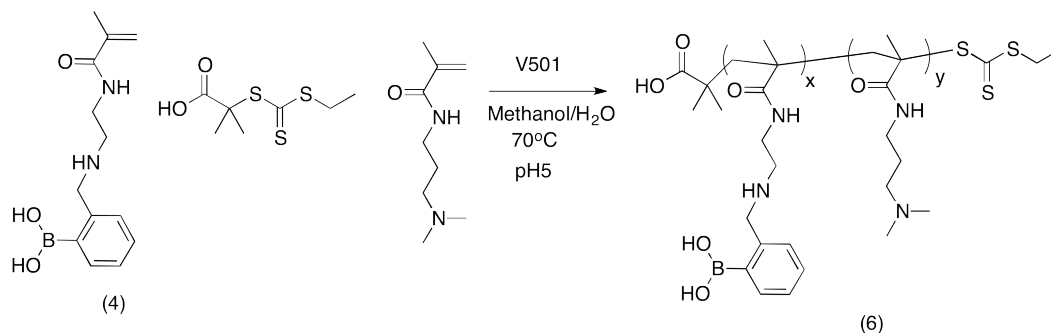
5.2.5 Polymerisation of 2-((2-methacrylamidoethylamino)methyl)phenylboronic acid (5)



Scheme 5.5: Polymerisation of 2-((2-methacrylamidoethylamino)methyl)phenylboronic acid (5)

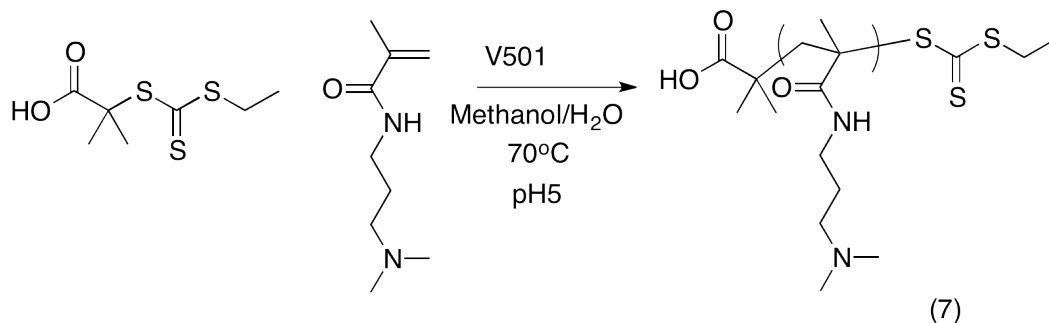
2-((2-methacrylamidoethylamino)methyl)phenylboronic acid (**4**) (200 mg, 0.763 mmol), 2-(((ethylthio)carbonothioyl)thio)-2-methylpropanoic acid (3.43 mg, 0.0153 mmol) and 4,4'-(azobis(4-cyanovaleric acid)) (0.855 mg, 0.00305 mmol) was dissolved in methanol to make a one molar solution relative to monomer concentration. The mixture was degassed with alternating cycles of freezing, vacuum and thawing before heating to 65°C. The polymerisation was monitored using ^1H NMR spectroscopy. At the end of the polymerisation the mixture was cooled and exposed to air before purifying the polymer by precipitation into acetone. Final conversion 32% (Yield = 27.1 mg)

5.2.6 Polymerisation of 2-((2-methacrylamidoethylamino)methyl)phenylboronic acid and *N*-(3-(dimethylamino)propyl) methacrylamide (6)



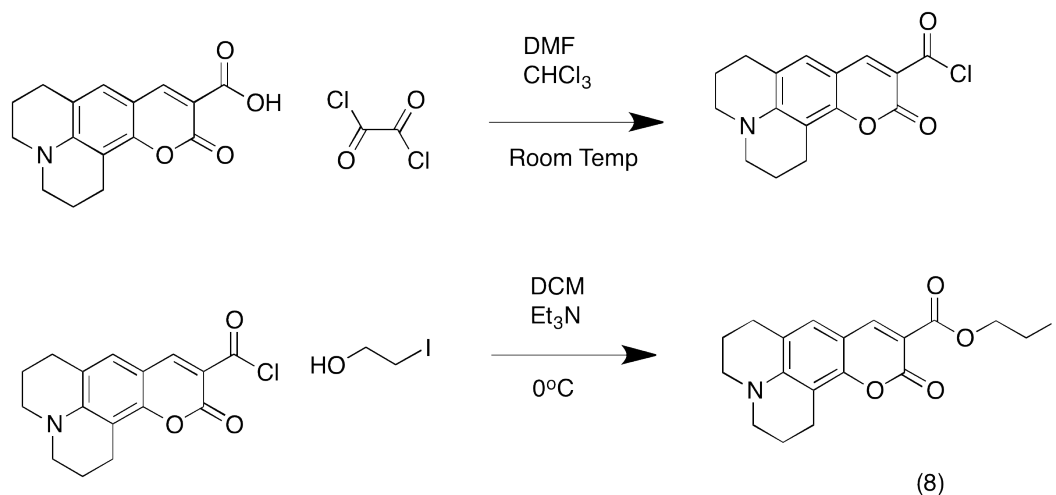
Scheme 5.6: Polymerisation of 2-((2-methacrylamidoethylamino)methyl)phenylboronic acid and *N*-(3-(dimethylamino)propyl)methacrylamide (6)

2-((2-Methacrylamidoethylamino)methyl)phenylboronic acid (4) (51.32 mg, 0.2 mmol) was dissolved in 1 mL of methanol. *N*-(3-(dimethylamino)propyl)methacrylamide (319 μ L, 300 mg, 1.76 mmol) was dissolved in 1 mL of 10 mMol acetate buffer at pH 5. These solutions were then mixed together and 2-(((ethylthio)carbonothioyl)thio)-2-methylpropanoic acid (8.79 mg, 0.039 mmol) and 4,4'-(azobis(4-cyanovaleric acid) (2.2 mg, 0.0079 mmol) were added. The mixture was degassed with alternating cycles of freezing, vacuum and thawing before heating to 70°C. The polymerisation was monitored using ^1H NMR spectroscopy. At the end of the polymerisation the mixture was cooled and exposed to air before purifying the polymer by precipitation into acetone. Final conversion 75% (Yield = 206 mg).

5.2.7 Polymerisation of *N*-(3-(dimethylamino)propyl)methacrylamide (**7**)Scheme 5.7: Polymerisation of *N*-(3-(dimethylamino)propyl)methacrylamide (**7**)

N-(3-(dimethylamino)propyl)methacrylamide (1064 μL , 1000 mg, 5.88 mmol) was dissolved in 3 mL of 10 mMol acetate buffer at pH 5 and 3 mL of methanol. 2-(((Ethylthio)carbonothioyl)thio)-2-methylpropanoic acid (26.7 mg, 0.117 mmol) and 4,4'-(azobis(4-cyanovaleric acid) (6.6 mg, 0.72 mmol) were added. The mixture was degassed with alternating cycles of freezing, vacuum and thawing before heating to 70°C. The polymerisation was monitored using ^1H NMR spectroscopy. At the end of the polymerisation the mixture was cooled and exposed to air before purifying the polymer by precipitation into acetone. Final conversion 64% (Yield = 560 mg).

5.2.8 Synthesis of 2-iodoethyl 11-oxo-2,3,5,6,7,11-hexahydro-1*H*-pyrano[2,3-*f*]pyrido[3,2,1-*ij*]quinoline-10-carboxylate (8)



Scheme 5.8: Synthesis of 2-iodoethyl 11-oxo-2,3,5,6,7,11-hexahydro-1*H*-pyrano[2,3-*f*]pyrido[3,2,1-*ij*]quinoline-10-carboxylate (8)

The conversion of Coumarin 343 to the acid chloride was carried out in a manner previously described in the literature [140] and used without further purification to generate the iodide terminated product **8**.

In brief coumarin 343 (285 mg, 1.00 mmol) was dissolved in anhydrous chloroform (11 mL) in a round bottomed flask. Under a nitrogen atmosphere, oxalyl chloride (881 mg, 6.94 mmol) and dimethylformamide (DMF) (50 μ L) were added to the reaction mixture and stirred for an hour at room temperature. The reaction mixture changed colour from orange to red, gas was evolved and the compound increased in solubility. After one hour the solvent and unreacted acid chloride were removed under reduced pressure to yield a red acid chloride.

A mixture of 2-iodoethanol (304 mg, 138 μ L, 1.00 mmol) and triethylamine (303 mg, 417 μ L, 3.00 mmol) was added to a 50 mL multineck round bottomed flask. To this flask a pressure equalising

addition funnel was connected and the apparatus sealed with a rubber septum. The apparatus was then flushed with nitrogen along with the round bottomed flask containing the coumarin 343 acid chloride for 10 minutes. After this time, anhydrous dichloromethane (5 mL) was added to the multineck round bottomed flask and a further 5 mL added to the round bottomed flask containing the acid chloride. This solid was allowed to dissolve completely before transferring it to the pressure equalising addition funnel. The acid chloride was then added dropwise over ice for 30 minutes. After which it was left to react for 16 hours before diluting with 50 mL of dichloromethane and washing with water (3×30 mL) to remove any unreacted materials. The organic layers were combined and then dried using anhydrous magnesium sulphate before being filtered and the solvent removed under reduced pressure. The mixture was then purified using flash chromatography (CC, SiO₂, dichloromethane/ethylacetate 12:1 vol/vol). The relevant fractions were combined and once the solvent was removed it produced a brown crystalline solid **8** (170 mg, 0.387 mmol, Yield = 38.7%).

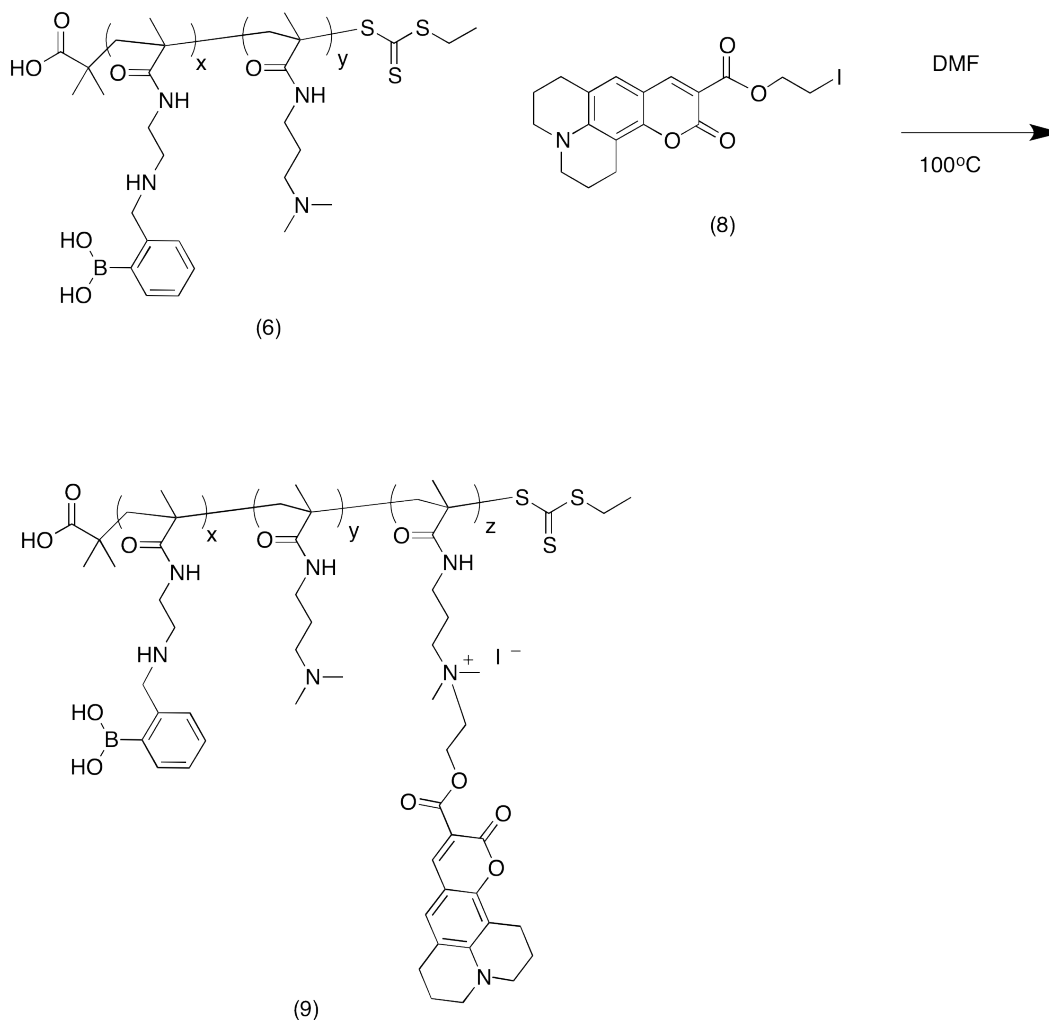
IR (KBr) ν (cm⁻¹) = 3582, 3422, 1750, 1619, 1518, 1442, 1367, 1312, 1239, 1201, 1173, 1111, 665

¹HNMR (400 MHz, CDCl₃): δ (ppm) = 1.92-2.01 (m, 4H, CH₂), 2.87 (t, J = 6.4 Hz, 2H, CH₂), 3.34 (m, J = 6.3 Hz, 4H, CH₂), 3.42 (t, J = 7.0 Hz, 2H, CH₂I), 4.53 (t, J = 7.0 Hz, 2H, CH₂O), 6.95 (s, 1H, CH_{vinyl}), 8.36 (s, 1H, CH_{aryl}).

¹³CNMR (100 MHz, CDCl₃): δ (ppm) = 20.06 (1C, CH₂), 20.14 (1C, CH₂), 21.13 (1C, CH₂), 27.42 (1C, CH₂), 49.92 (1C, CH₂), 50.31 (1C, CH₂), 63.70 (1C, CH₂O), 64.77 (1C, CH₂), 105.76 (1C, C), 106.35 (1C, C), 119.30 (1C, C), 127.14 (1C, C), 148.81 (1C, C), 149.43 (1C, C), 153.59 (1C, C), 158.52 (1C, C), 163.63 (1C, C).

Calculated mass (C₁₈H₁₈INO₄): 439.2460 Mass found (m/z): 440.0467

5.2.9 Fluorescent tagging of poly(2-((2-methacrylamidoethylamino)methyl)phenylboronic acid-co-*N*-(3-(dimethylamino)propyl)methacrylamide) (**9**)



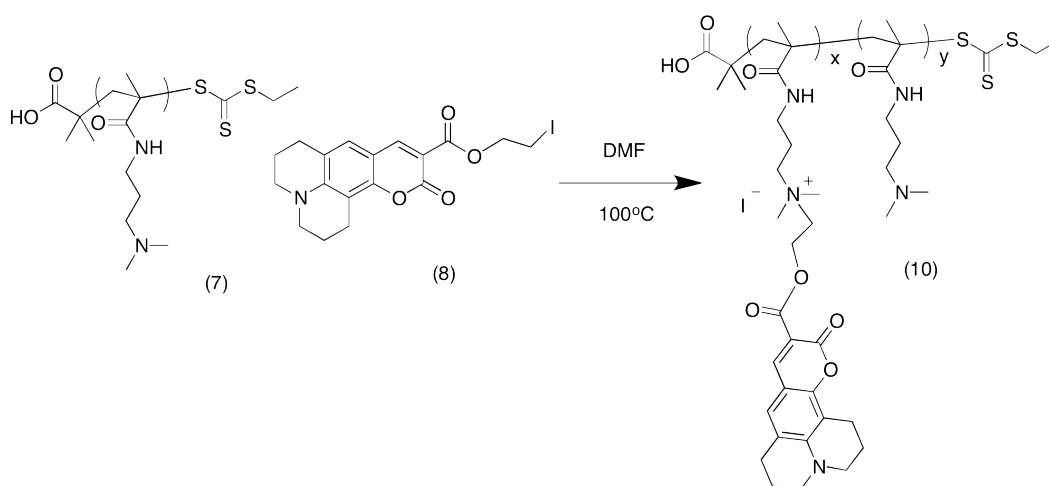
Scheme 5.9: Fluorescent tagging of poly(2-((2-methacrylamidoethylamino)methyl)phenylboronic acid-co-*N*-(3-(dimethylamino)propyl)methacrylamide (**9**). $x = 1$, $y = 13$, $z = 1$.

The boronic co-polymer **6** (50 mg, 0.29 mmol) was dissolved in DMF (5 mL) and transferred to a 50 mL round bottomed flask. To this solution, a solution of coumarin 343 alkyl iodide (**8**) (9 mg, 0.021 mmol) in DMF (5 mL) was added. The resultant mixture was heated with mixing

at 100°C for five days. The reaction was followed regularly using TLC with a mobile phase of DCM:Methanol, 1:1. The unreacted iodo-terminated coumarin **8** gave an R_f of 0.75 whereas the fluorescently tagged polymer **9** stayed at the baseline ($R_f = 0.00$). Once the reaction was completed the product was purified by precipitation into acetone. This precipitation was repeated 3 times and the resultant brown polymer dried in a desiccator for 48 hours to yield a brown powder **9** (5.65 mg, yield: 10.8%).

5.2.10 Fluorescent tagging of

poly(*N*-(3-(dimethylamino)propyl)methacrylamide) (**10**)



Scheme 5.10: Fluorescent tagging of poly(*N*-(3-(dimethylamino)propyl)methacrylamide) (**10**). $x = 1$, $y = 14$.

Following the procedure described for polymer **9**, polymer **10** (15.4 mg, yield: 29.44%) was isolated after precipitation in petroleum ether (3×200 mL) and drying for 48 hours in a desiccator.

5.2.11 Determination of the association constant (K_{eq1}) of Alizarin Red S-2-((2-methacrylamidoethylamino)methyl)phenylboronic acid complex

This method had been previously reported in the literature [141] to determine the binding constant for various diols such as sugars with phenylboronic acid.

100 mL of a 9.0×10^{-6} M solution of alizarin red S (AR-S) in 0.1 M sodium phosphate buffer were made and the pH adjusted to pH 7.4 using 1 M sodium hydroxide. This solution was designated "solution A". 50 mL of solution A were transferred to a 100 mL flask containing 40 mg of 2-((2-methacrylamidoethylamino)methyl)phenylboronic acid (**4**) such that the resultant solution had a concentration of 9.0×10^{-6} M (AR-S) and 2.0×10^{-3} M of 2-((2-methacrylamidoethylamino)methyl)phenylboronic acid (**4**) and this mixture was designated "solution B". These solutions were then mixed to make solutions 1-11 in various ratios as shown in table Table 5.1 and left to homogenise for at least ten minutes before the excitation was recorded at 468 nm and emission recorded at 572 nm in a quartz cuvette.

Table 5.1: Solution composition for determination of the association constant (K_{eq1}) of Alizarin Red S-2-((2-methacrylamidoethylamino)methyl)phenylboronic acid complex. Concentration of AR-S = $9.0 \mu\text{M}$.

| Solution Composition | | | |
|----------------------|------------------------------|------------------------------|--------------------------|
| Solution | Solution A (μL) | Solution B (μL) | Boron Concentration (mM) |
| 1 | 0 | 1000 | 2.0 |
| 2 | 100 | 900 | 1.8 |
| 3 | 200 | 800 | 1.6 |
| 4 | 300 | 700 | 1.4 |
| 5 | 400 | 600 | 1.2 |
| 6 | 500 | 500 | 1.0 |
| 7 | 600 | 400 | 0.8 |
| 8 | 700 | 300 | 0.6 |
| 9 | 800 | 200 | 0.4 |
| 10 | 900 | 100 | 0.2 |
| 11 | 1000 | 0 | 0.0 |

5.2.12 Determination of the association constant (K_{eq}) of glucose-2-((2-methacrylamidoethylamino)methyl)phenylboronic acid complex

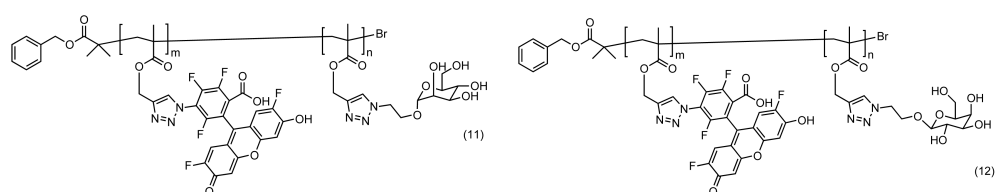
25 mL of *solution B* were transferred to 100 mL flask containing 6 mL of D-glucose solution with a concentration of 542 mg/mL and this was designated "*solution C*". These stock solutions were then mixed to make solutions 1-11 in various ratios as shown in Table 5.2 and left to homogenise for at least ten minutes before the excitation was recorded at 468 nm and emission recorded at 572 nm in a quartz cuvette.

Table 5.2: Solutions for the determination of the association constant (K_{eq}) of glucose-2-((2-methacrylamidoethylamino)methyl)phenylboronic acid complex

| Solution Composition | | | |
|----------------------|-----------------------|-----------------------|------------------------------|
| Solution | Solution B (μ L) | Solution C (μ L) | D-Glucose Concentration (mM) |
| 1 | 0 | 1000 | 582 |
| 2 | 100 | 900 | 524 |
| 3 | 200 | 800 | 466 |
| 4 | 300 | 700 | 407 |
| 5 | 400 | 600 | 349 |
| 6 | 500 | 500 | 291 |
| 7 | 600 | 400 | 233 |
| 8 | 700 | 300 | 175 |
| 9 | 800 | 200 | 116 |
| 10 | 900 | 100 | 58.2 |
| 11 | 1000 | 0 | 0.00 |

5.2.13 Synthesis of fluorescent glycopolymers

The glycopolymers used were synthesised by Giuseppe Stefanetti in the group according to the procedures detailed in the literature [125] and kindly donated for investigation. These were polymers furnished to display either mannose or galactose plus a fluorescent moiety, oregon green.



(a) Structure of Mannose glycopolymer (11)

(b) Structure of Galactose glycopolymer (12)

Figure 5.2: Structure of glycopolymers employed in this study.

Table 5.3: Table of glycopolymer characterisation by different techniques. Where DP = degree of polymerisation, M_n = number average molecular weight, M_w = weight average molecular weight, PDI = poly dispersity index, GPC = gel permeation chromatography.

| Polymer Characterisation | Mannose Polymer (11) | Galactose Polymer (12) |
|--------------------------------|----------------------|------------------------|
| DP (^1NMR) | 73 | 73 |
| M_w (^1NMR) (kDa) | 27 | 27 |
| M_n (GPC)(kDa) | 7.1 | 11 |
| PDI (GPC) | 1.4 | 1.3 |

5.3 Results and Discussion

The surface structure of bacteria is furnished with various organic molecules, many of which are carbohydrate based. For example, lipopolysaccharides found on the surface of Gram-negative bacteria, are made of a lipid (lipid A) and a non-repeating oligosaccharide. These carbohydrate based molecules are key antigenic determinants of bacteria and are highly specific on the strain and species of bacteria.[2] As such, molecules such as these found on the surface of bacteria are highly variable and can offer specific binding epitopes using sugar binding compounds, such as boronic acids. Moreover, the bacterial surface contains sugar binding proteins known as lectins which can facilitate cell recognition and virulence through the bacteria binding to sugars.

5.3.1 Sugar binding polymers

The formation of borate esters with diols such as sugars is highly dependent on pH and also the inclusion of cationic groups afforded by the secondary amines may facilitate the binding and interaction with anionic compounds including diols [139] via Coulomb interactions. Moreover, as has been demonstrated by Shinkai's group an amine at the 1,5-position relative to the boronic acid in particular can lower the pK_a of boronic acid residues, allowing for boron-diol interactions at neutral pH. This is of benefit when considering the application of these moieties in biologically relevant conditions (Figure 5.3).[142]

The binding at neutral pH is attributed to this arrangement facilitating the formation of dative Boron-Nitrogen bonds.[143] Lowering the apparent pK_a of the boronic acid in this way can increase the binding strength of borate bonds formed during interactions with sugars.[141, 78]

Further to the synthesis of 2-((2-methacrylamidoethylamino)methyl)phenylboronic acid (**4**) (Scheme 5.1, Scheme 5.2 and Scheme 5.4) the binding affinity of the monomer for a model sugar; glucose was characterised using the Alizarin Red (AR-S) assay in a manner analogous to that reported already in the literature. [80, 141]

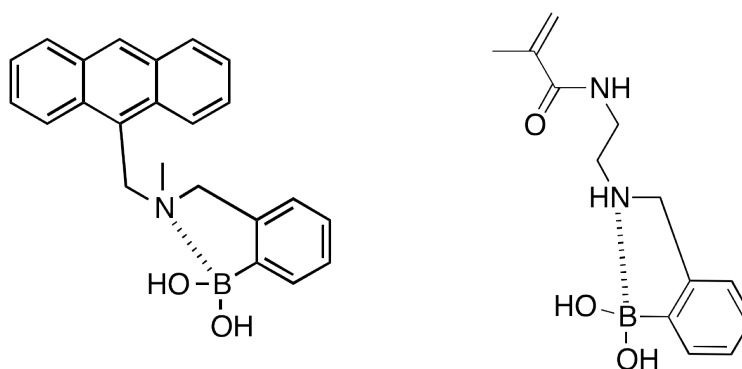


Figure 5.3: Comparison between fluorescent glucose sensor[142] (left) and 2-((2-methacrylamidoethylamino)methyl)phenylboronic acid (**4**) (right) showing dative bond formation between nitrogen and boron.

The Alizarin red (AR-S) assay is a well established fluorescent biological assay whereby binding between sugars and sugar-binding molecules can be understood. The AR-S molecule is utilised to act as a chromophore. Neither the sugar nor the boronic acid are fluorescently active therefore the dye AR-S is employed. This dye becomes fluorescent upon binding to boronic acids and subsequently loses this fluorescence when no longer bound. The fluorescence which is observed is attributed to the binding of the boronic acid monomer to Alizarin Red S as in free AR-S the proton transfer from the phenol groups to the ketone prevents fluorescence in the excited state.

The assay has two steps, the first step involves deriving the binding of AR-S to the boronic acid monomer followed by the competitive displacement of the AR-S by a diol containing compounds such as a sugar (Figure 5.4).

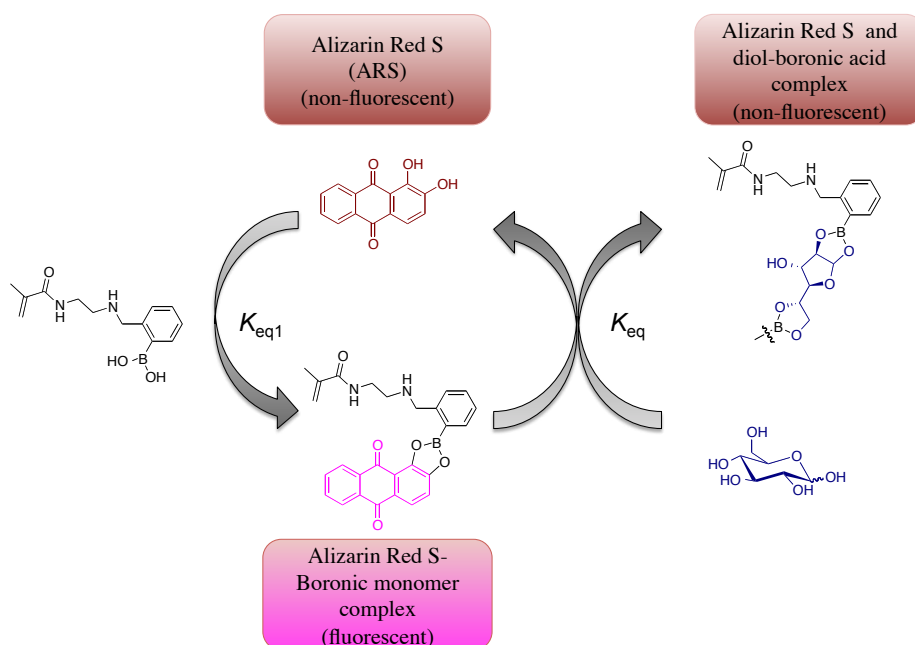


Figure 5.4: Schematic overview of the Alizarin Red assay.

To determine the binding between the boronic acid monomer and the diol it is first necessary to find the binding affinity between **4** and the reporter AR-S (K_{eq1}).

As shown in Table 5.1 solutions of AR-S at pH 7.4 were mixed with solutions of AR-S and the boronic acid monomer in different ratios. This is done such that the concentration of AR-S was constant throughout the experiment whilst the concentration of the boronic acid monomer was varied. Eleven different solutions were used with concentrations ranging from 0 - 2.0 mM of the boronic monomer such that a broad range of concentrations were tested. The solutions were excited at 468 nm the emission spectra were recorded as shown in Figure 5.5.

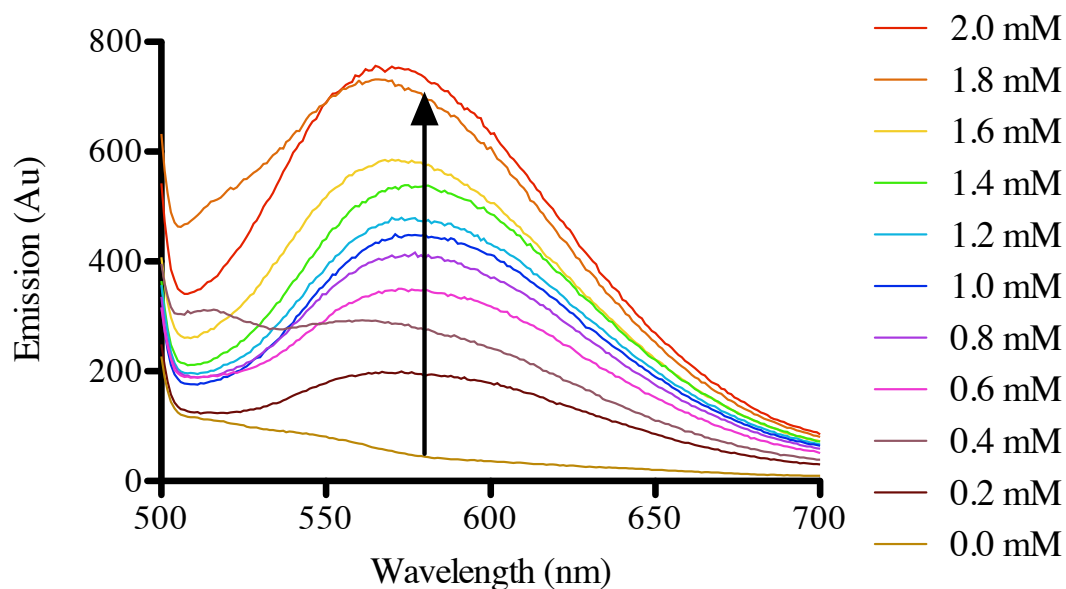


Figure 5.5: Emission spectra of AR-S complex with increasing concentrations of boronic acid **4**

The emission intensity at 572 nm was plotted as a function of boronic monomer **4** and fitted to the Benesi-Hildebrand equation (5.1) to give the affinity constant of AR-S-**4** from the quotient of the intercept and the plot of $\frac{1}{[B]}$ and $\frac{1}{\Delta I_f}$

$$\frac{1}{\Delta I_f} = \frac{1}{\Delta_k \cdot P_0 \cdot K a^1} \cdot \frac{1}{[B]} + \frac{1}{\Delta K \cdot P_0 \cdot [AR-S]_0} \quad (5.1)$$

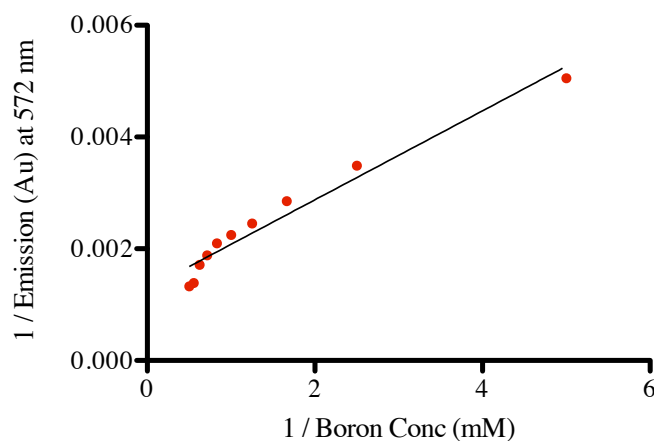


Figure 5.6: Benesi-Hildebrand plot for change in emission at 472 nm as a result of increasing AR-S with increasing concentrations of AR-S-boronic acid complex.

The correlation of the data with the fit as defined by the r^2 value is 0.9584. The Benesi-Hildebrand assumes that the fit of the data is related only to specific binding between the two components, however this is not always the case.

The monomer was synthesised in the solvent methanol. The monomer is capable of binding to the alcohol groups of methanol. The result of this can induce a competitive relationship between the methanol and the Alizarin Red S as opposed to a strictly simple binding relationship. The other issue to consider is the monomer's less than ideal solubility in aqueous media. At the concentrations tested the monomer solutions appeared slightly turbid which would again prevent a typical linear binding relationship taking place. It is also worth consideration that the two molecules used in the study are organic in nature and their solubility in water is limited and through conjugation to each other a less soluble, and so less fluorescent species may be generated.

The data is therefore best fit using a non-linear one sided total fitting using Prism 5 for Mac

OS X version 5.0d and applying the equation 5.2 originally published in the literature.[144]

$$Y = \frac{B_{\max} \cdot X}{K_d} + (NS \cdot X) + \text{Background} \quad (5.2)$$

The equation has a number of assumptions which are:

- i) Binding is a sum of both specific and non-specific binding.
- ii) Non-specific binding is concentration dependent.
- iii) Not all of the reporter engages in binding events.

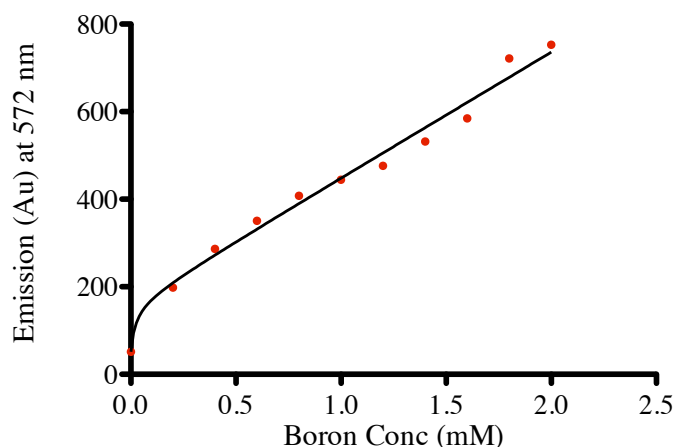


Figure 5.7: Change in emission at 472 nm as a result of increasing AR-S with increasing concentrations of AR-S-boronic acid complex.

This data is fit to a mathematical relationship which defines the relationship between the receptor e.g. the boronic acid to the agonist e.g. the AR-S. The non-linear relationship is best explained using a formulation which assumes the observed binding is as a result of both specific and non-specific binding.

The correlation of the data with the fit as defined by the r^2 value is 0.9859, for the one to one binding with a non-specific component. This would give an association constant of 39.77 mM^{-1} which is less than those values reported for AR-S and phenylboronic acid (1300 M^{-1}).[141]

Next, in order to calculate the binding affinities for the boronic acid monomer and the model sugar diol (glucose), it is then necessary to mix the solutions containing the AR-S-boronic acid monomer complex and a saturated solution of glucose. This will result in solutions which contain different concentrations of the diol. The change in fluorescence is as a result of the sugar displacing the AR-S and thus a decrease in fluorescence as seen in figure Figure 5.8.

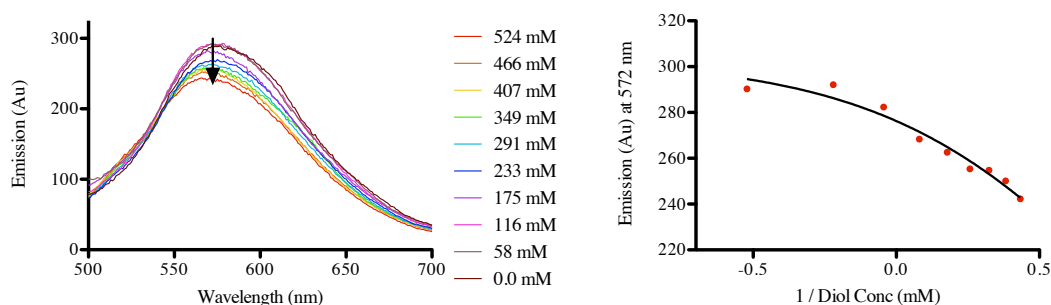


Figure 5.8: Emission spectra of AR-S-boronic acid complex with increasing concentrations of glucose.

Most importantly, from the data it can be confirmed that the monomer binds to diols such as sugars, demonstrated from the decrease in fluorescence as the reporter AR-S is replaced with the model sugar. It is then possible to plot inverse of diol concentration against the emission values. These values are then fit to a competitive one site relationship to obtain the association constant for the model sugar and the boronic acid monomer **4**.

$$\log Curve = \log(10^{\log K_{eq}} \times \frac{1 + [Glucose]}{[Boron]}) \quad (5.3)$$

The correlation of the data with the fit as defined by the r^2 value is 0.9611 and gives a dissociation constant for the AR-S, when competing against the diol, of 6.55 mM ($K_{eq} = 0.15 \text{ mM}^{-1}$). In summary, the assay shows that the monomer species binds to sugar diols and so may be suitable

to use for bacterial binding.

The polymers of the boronic acid monomer were all synthesised by reverse addition- fragmentation chain transfer (RAFT) as opposed to ATRP which had been previously used. This was because of all the controlled radical polymerisation (CRP) techniques, RAFT has proven to be the most versatile for the polymerisation of acrylamides and methacrylamides.[145].

The polymerisation of the boronic monomer as a homopolymer as seen in Scheme 5.5 proceeded to a conversion of 32% however following precipitation the polymer proved to be insoluble in any aqueous solvents suitable for a bacteria culture. Therefore this monomer was re-polymerised again in methanol but with a co-monomer to yield a co-polymer which would have suitable aqueous solubility (Scheme 5.6). The polymerisation of this co-polymer and an amine homopolymer for comparison, proceeded with linear kinetics as can be seen in Figure 5.9.

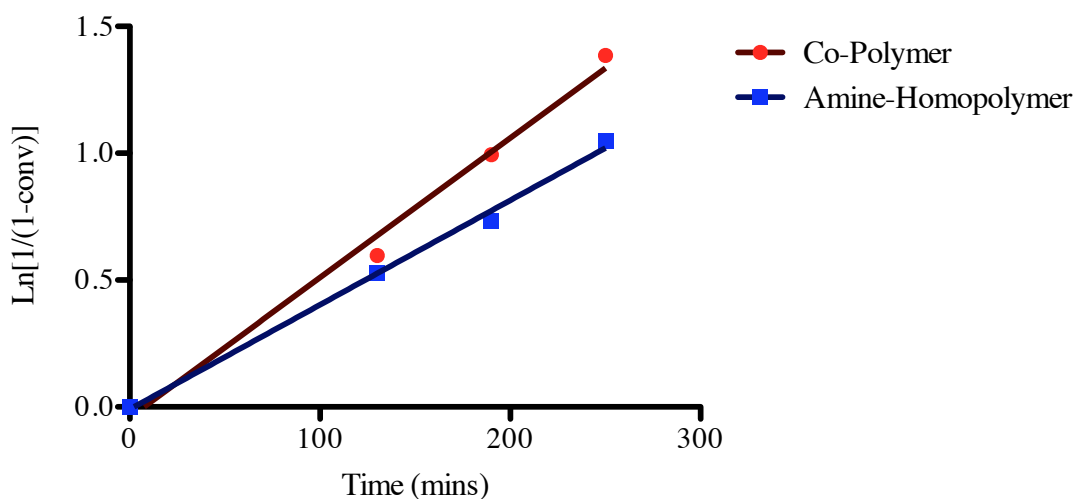


Figure 5.9: Polymerisation of the amine homopolymer and the boronic co-polymer using RAFT.

The linear regression of these points had r^2 values of 0.9901 and 0.9957 for the co-polymer and homopolymer respectively. This result demonstrates the the polymerisation progressed with pseudo-

first order kinetics. The PDIs of the polymers were 1.78 for the boronic co-polymer and 1.52 for the amine homopolymer. These high PDIs can be explained with the high interaction with the columns producing tailing.

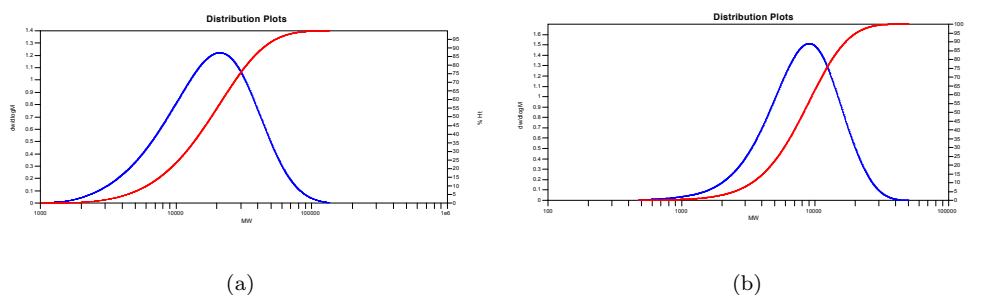


Figure 5.10: GPC traces of a) non-fluorescent boronic co-polymer **6** and b) non-boronic polymer

7

The reason for the production of the amine homopolymer was to act as a suitable control during bacterial binding experiments. From this polymer it is possible to subtract the binding which is attributable to the amine component and so it can be determined what level of binding is as a result of the boronic group *only*.

Once the polymers had been obtained, it was then desirable to convert these into fluorescent polymers to aid fluorescent microscopy and examine the interaction between the polymers and the bacteria. In order to attach the coumarin 343 moiety to polymer it was first modified according to Scheme 5.8 to display a functionality which can conjugate to the tertiary amines on the polymer. This was done by first converting the carboxylic acid into an acid chloride. This was because the acid chloride was much more reactive than the equivalent carboxylic acid and does not require additional coupling agents as demonstrated in the previous chapter to generate the coumarin alkylbromide (Scheme 4.3). The reaction solvent used was chloroform; its boiling point is higher than dichloromethane so that any unreacted oxalyl chloride will be removed while evaporating the solvent in the rotavapor. The coumarin 343 acid chloride was used without further purification

due to the sensitivity of this functionality to hydrolysis. After reaction with the iodoethanol and purification by flash chromatography the pure iodo-terminated product **8** was obtained.

The same conjugation process seen in Scheme 4.4 was then utilised but without the need for halide exchange. The addition of the coumarin functionality to the tertiary amine was utilised to fluorescently tag the polymers to yield the fluorescently labelled boronic co-polymer **9** and the fluorescently labelled amine polymer **10**.

Once labelled, the aqueous solubility of the polymers decreased to the point where they appeared as slightly turbid solutions. Despite this poor solubility, investigation into their binding to *E. coli* and *S. mutans* was carried in a manner similar to but not identical to that of the charged polymers. The difference was that the pH of the solution was adjusted to pH 9.0.

Firstly, each of the polymers (7 mg) was dissolved in sterile deionised water (3 mL) and the pH adjusted to pH 9 using 1M sodium bicarbonate before making the volume up to 7 mL to give a final concentration of 1 mg/mL and a pH of 7 ± 0.2 .

The amine groups found in the polymer would give it a $pK_a \approx 8.0$ based upon similar monomers.[146] Therefore the pH was adjusted to 9.0 to minimise protonation of the polymer's amines. So, binding due to transient protonation is both reduced and is also accounted for with the control amine homopolymer.

The polymers were incubated for 30 minutes with each bacterium, before being washed with phosphate buffered saline once and deionised water twice. After which the cells were mounted onto glass slides for microscopic examination.

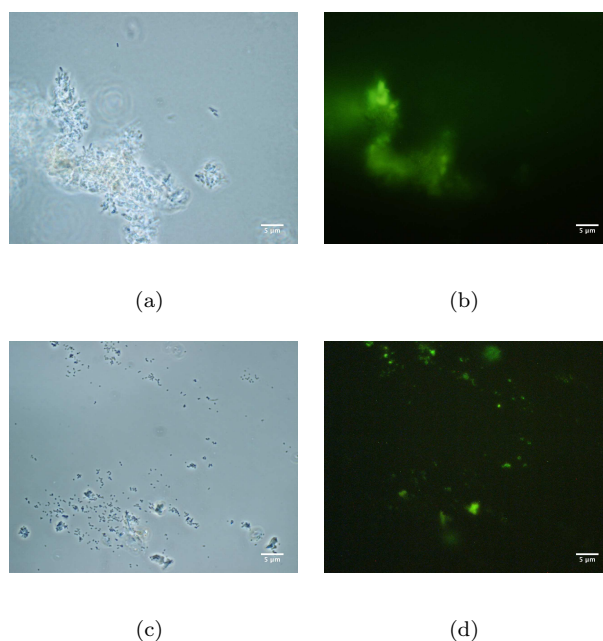


Figure 5.11: Phase contrast and fluorescent microscopy images of polymer **9** with *E. coli* MG1655 (a & b) and *S. mutans* NCTC 10449 (c & d) after undergoing procedure described in 3.2.1

The addition of the fluorescent coumarin group adversely affected the solubility of the polymer as was already apparent upon preparation of the solutions for experimentation. Microscopically it was only possible to view insoluble fluorescent polymer aggregates often surrounded or associated with bacteria (Figure 5.11). For this reason it was wholly impossible to define the effect the boronic acid functionality had upon binding of the polymers to bacteria using the fluorescent microscopy. Moreover, it was seen that the use of the non-fluorescent polymers and phase microscopy indicated a difference in binding between the boronic polymer **6** and non-boronic polymer **7** (Figure 5.12). For this reason, the aggregation assay was again performed on the *E. coli* in order to assess the propensity for these polymers to bind bacterial species with unlabelled polymers **6** and **7**. As with the sample preparation for microscopic imaging, the solutions of the polymers were prepared at a pH of 9 to ensure binding due to the amine group was minimal. The solutions now appeared clear and colourless. There were 5 replicates of each sample. The assay was performed and described in the methods chapter.

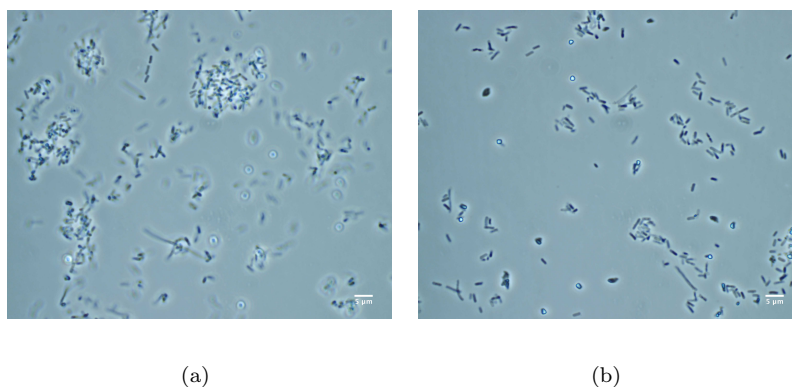


Figure 5.12: Microscopy images of *E. coli* MG1655 with a) Non-fluorescent boronic co-polymer **6** and b) Non-fluorescent, non-boronic polymer **7** after undergoing procedure described in 3.2.1.

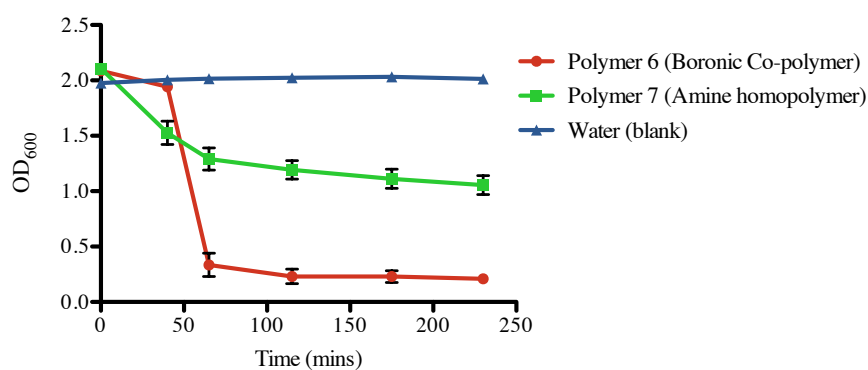


Figure 5.13: Aggregation assay of *E. coli* with boronic and amine polymers.

As can be seen in Figure 5.13 there is a rapid change in the aggregation behaviour of the *E. coli* with time. Not only is this aggregation faster with the boronic polymer than with the amine homopolymer but it is also indeed more significant. This aggregation is further evidence that the binding of boronic containing polymers to bacteria does occur. Adjusting the pH to above the pK_a successfully minimised aggregation caused by the amines found on the polymers.

5.3.2 Sugar displaying polymers

The behaviour of bacteria to bind to different sugars with different propensities has been reported widely in the literature. *E. coli*, whose binding to mannose is facilitated by FimH imparts the bacterium with virulence advantages.[147, 34, 46, 40] It has been reported that *S. mutans* contains sugar binding domains which are preferential for galactose.[148, 13] So, towards the goal of generating specific bacterial targeting ligands through sugar displaying polymers, two polymers were generated. The binding of *S. mutans* by glycopolymers has thus far not been published in the literature.

The glycopolymers were generated from the same polymer backbone using the benzyl initiator described in the chapter on charged polymers (Scheme 4.1). Using the hydrogens of the benzyl ring the molecular weight (M_w) and DP were calculated by ^1H NMR spectroscopy.

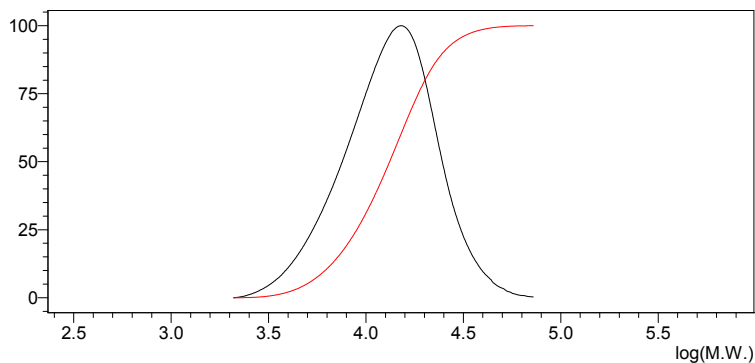


Figure 5.14: Sample GPC trace of Galactose furnished glycopolymer **12**.

The polymers produced had slightly broad PDIs as seen from the GPC traces where tailing was observed (Figure 5.14). Also the M_n differed significantly from that calculated by $^1\text{H NMR}$ and also from each other, is explained by the conventional calibration used on the GPC.

This broadening suggests that there was interaction between the different polymers and the column's stationary phase. The interaction between polymer **11** and **12** with *E. coli* and *S. mutans* was investigated using fluorescent microscopy.

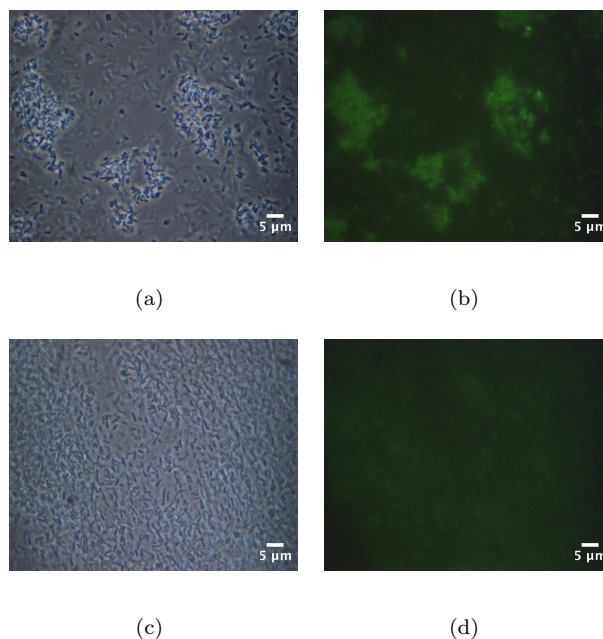


Figure 5.15: Phase contrast and fluorescent microscopy images of *E. coli* MG1655 with mannose glycopolymer **11** (a & b) and galactose glycopolymer **12** (c & d) after undergoing procedure described in 3.2.1

As can be seen in Figure 5.15(a) and (b) the polymer displaying mannose moieties shows significantly greater fluorescence on the *E. coli* when viewed using fluorescence microscopy. This behaviour contrasts with the binding behaviour of the galactose polymers with the *E. coli*.

The galactose polymer showed none or minimal binding to *E. coli* (Figure 5.15(c) and (d)). This result is in agreement with work already in the literature where such comparisons have been carried out between similar polymers by the group of Disney and co-workers.[47] This group also found that mannose displaying polymers bound to *E. coli* and galactose polymers did not. If one considers work by other authors to investigate quantitatively the difference in binding of the monosaccharides, further illumination is given for the differences in binding behaviour.[149]

It can be seen in Table 5.4 that the binding of the FimH found on *E. coli* differs significantly in its ability to bind sugars and that its ability to bind mannose is much greater than its ability to bind galactose.

Table 5.4: Table of K_d for the FimH of *E. coli* for various monosaccharides

| Monosaccharide | K_d |
|----------------|-------------|
| Mannose | 2.3 μ M |
| Glucose | 9.24 mM |
| Galactose | 100 mM |
| Fructose | 31 μ M |

The polymers were also investigated with the bacterium *S. mutans* in the same way as for *E. coli*.

The binding observed by the mannose displaying polymers to the *S. mutans* appears minimal compared to that seen with the *E. coli* whereas binding is greater when the bacteria are incubated with the galactose polymer (Figure 5.16).

This difference in binding behaviour between the mannose and galactose polymers with the *S. mutans* is a behaviour which may be expected when considering the literature. This binding does not appear to be as strong as the binding which *E. coli* has for mannose. However, *S. mutans* has been much less widely investigated than *E. coli* and exact comparable figures quantifying this difference is difficult to ascertain through the literature.

So it can be seen that the choice of the saccharide employed in the polymer system can have a significant effect upon the binding observed in various bacterial strains.

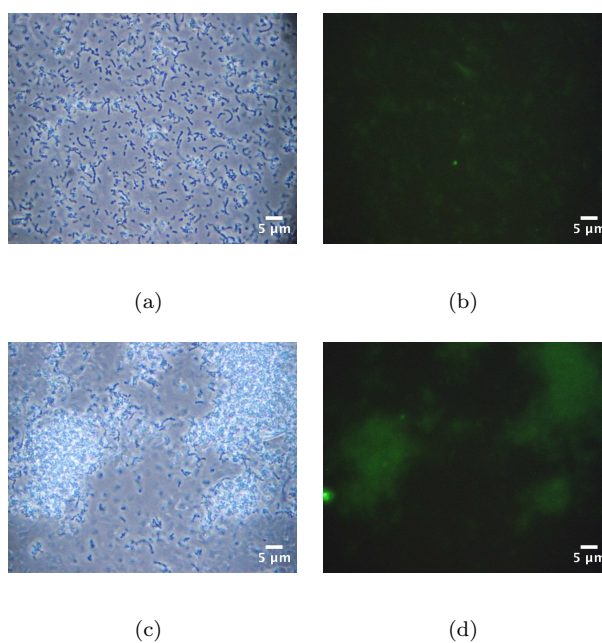


Figure 5.16: Phase contrast and fluorescent microscopy images of *S. mutans* NCTC 10449 with mannose glycopolymer **11** (a & b) and galactose glycopolymer **12** (c & d) after undergoing procedure described in 3.2.1

5.4 Conclusions

These results show that utilising both the sugars found on the bacterial surface as well as the ability of the bacteria to bind to various sugars, specific bacterial-binding polymeric ligands can be designed.

This binding can be tuned according to the desired bacterial strain through judicious examination of the literature and consideration of the bacterial structural features.

Boronic containing polymers represent an under investigated area of research which have now been demonstrated to bind to bacteria. This lack of investigation may be attributable to their poor solubility in the aqueous conditions required for bacterial-polymer interaction studies as well as low affinity and low selectivity.

Glycopolymers are a useful functional material to control bacterial binding in a highly specific and avid manner. These materials show large differences in their interaction with bacteria depending on their composition and are highly water soluble. The monomers can prove problematic due to self polymerisation when working with methacrylate esters.

A novel *S. mutans* binding polymer scaffold has been presented. With judicious comparison using a structurally analogous backbone differences between the biology of *E. coli* and *S. mutans* has been demonstrably proven.

Chapter 6

Polymer Toxicity Testing

6.1 Introduction

Charged polymers have been widely investigated for their antimicrobial action. Polycations in particular are known to act as potent antibacterial agents and their applications have been discussed at length in the literature.[150, 37, 51, 76]

The use of charged polymers such as those prepared in this work have been utilised for DNA and siRNA delivery [151, 152, 146] as well as to promote drug delivery.[153, 154]

As such the actions of the polymers produced in this work, against bacteria and human cells needs to be understood. The benefits yielded can guide the practical usage of the polymers i.e. whether they can be used to retrieve live bacteria or if they are so toxic that they will kill their target. The effects of the polymers on eukaryotic cells needs to be evaluated to indicate if any toxicity could limit their applications *in vivo*.

6.1.1 Actions against bacteria

Cationic polymer materials exhibit highly potent binding and also cytotoxic action against their bacterial target.[155, 156, 54] Much of the early work defining the mechanism by which polycations exert their cytotoxic actions was carried out by Broxton *et al.*[157, 158] Further to binding, the polymers insert themselves within the membranes of the bacteria and disrupt them. The ability of the bacteria to maintain adequate homeostasis and functionality is lost as shown in Figure 6.1

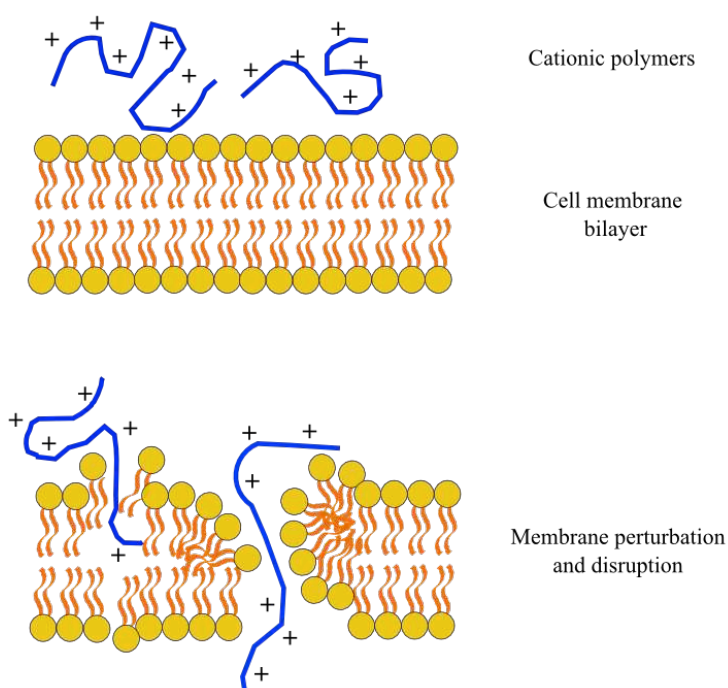


Figure 6.1: Schematic representation of the potential mechanism for cytotoxic action of cationic polymers at membranes. Electrostatic attraction of polycations to anionic phospholipid headgroups is followed by insertion into the membrane and disruption of bilayers.

As can be seen in Figure 6.1 the cationic polymers' strong electrostatic adsorption to membrane surface can alter membrane stability and permeability. When membrane functionality is completely lost there is a bactericidal effect as a result of the precipitation of intracellular components.[159] Matyjaszewski's group generated surfaces based upon poly[2-(dimethylamino)ethyl methacrylate]

(pDMAEMA) which were reacted with iodoethane to introduce a permanent positive charge.[39] These surfaces were extremely effective at killing bacteria and the effectiveness was related to the charge density as extrapolated from initiator density and polymer thickness, both of which had a directly proportional link to killing efficiency of the surface.[51]

Poly[2-(dimethylamino)ethyl methacrylate] has also been modified with iodomethane to create soluble polycations. These polycations exhibited antimicrobial action with minimum inhibitory concentrations (MIC) ranging between 0.1-1 mg/mL for gram-negative bacteria and 0.1- >18mg/mL for Gram-positive bacteria. The polymers, which were not internalised by the bacteria, when used in concentrations four to ten times below their MIC caused a decrease in the MIC of erythromycin against the Gram-negative bacteria used in the study and had a similar effect against the Gram-positive bacteria used. This was attributed to increasing cell permeability given the site of action for erythromycin was within the cell.[52] Similar effects have been reported also by other groups.[53] The killing effect of these polymers has also been shown to be increased when combined with a hydrophobic component.[37] Lenoir *et al.* reported that polycationic surfactants can kill all *E. coli* detectable using a counting method with concentrations as low as 150 μ g/mL with a contact time of two hours. This is a higher concentration than for a comparator; benzalkonium chloride, but the authors note that their relative concentration of quaternary ammonium component is lower in the polymer compared with the monomeric antimicrobial.

6.1.2 Actions against human cells

Polycations have diverse uses which include, but are not restricted to, microbial capture and detection. Other uses within the biomedical field include gene therapy but an understanding of how these polymer materials may interact with eukaryotic cells is needed and what structural properties enhance or decrease toxicity.[160] The use of antimicrobials to prevent or treat infection often involves a careful balance between human and bacterial cell toxicity whereby differences in cell

machinery are utilised to effect an efficient action against bacteria.[161] Bacteria and human cells vary in their susceptibility to cytotoxic agents. Work has already demonstrated that polycations have the ability to enhance susceptibility of bacteria to antibiotics,[53] so through synergistic action it may be possible to minimise human toxicity by both antibiotics and polycations if the boundaries of toxicity are understood.

6.2 Methods

Standard methods have been used to ensure coherence with other work in this field.[162, 163] Concentrations tested were up to and above those concentrations which would be anticipated to be used in any future applications, such as for the removal of oral or tissue pathogens.

6.2.1 Antibacterial Activity - Minimum inhibitory concentration

The investigation into the toxicity of the most binding and least binding polymers against *E. coli* was carried out according to methods described in the literature,[162] with only slight modifications. For example, the minimum inhibitory concentration (MIC) can be described as the concentration of polymer required to inhibit bacterial growth, this has been determined by others using visual inspection; using a patterned background to increase contrast. In this work however these inhibitory concentrations were determined spectroscopically by recording the change in optical density at 600 nm using a plate reader. These were the polymers which were either completely modified to display a permanent positive charge (Cat-P1) or to contain a betaine functionality (Bet-P1) (Figure 6.2).

First a 0.5 McFarland Standard was prepared[162] by creating a 1% w/v solution of anhydrous barium chloride (BaCl_2) and also a 1% w/v (0.18 M) solution of sulphuric acid (H_2SO_4). These solutions were mixed in the appropriate ratios to give the desired McFarland standard. These standards are important to standardise the numbers of cells used for sensitivity testing. In order to obtain the 0.5 standard, 0.5 mL of the barium chloride solution was added to 99.5 mL of the

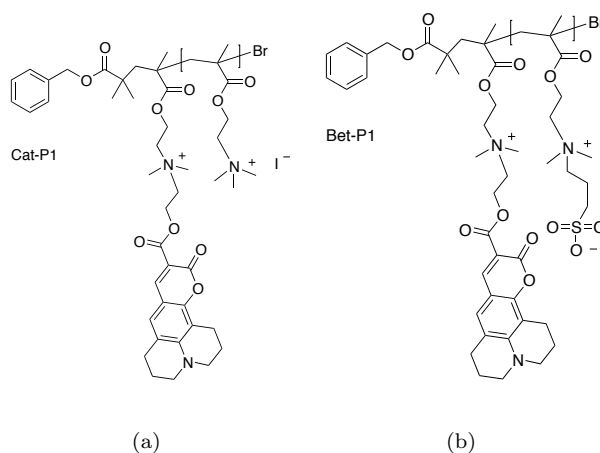


Figure 6.2: Modified a) Cationic pDMAEMA polymer (Cat-P1) and b) Betaine pDMAEMA polymer (Bet-P1) tested against *E. coli* MG1655

sulphuric acid solution followed by mixing vigorously. Further to mixing, the turbidity of the suspension was measured by absorbance at 600 nm (OD_{600}) which is designed to correspond to 107-108 colony forming units (CFU) per millilitre depending on the bacterial strain.

Next, stock solutions were prepared with concentrations of 10,000 mg/L (*A*), 1000 mg/L (*B*) and 100 mg/L (*C*) according to the formula 6.1:

$$\frac{1000}{P} \times (V) \times (C) = W \quad (6.1)$$

Where P = potency (if absent or unknown, assume 1000), V = the desired volume in millilitres, C = final concentration and W = weight of antimicrobial to be dissolved in the volume V of sterile deionised water.

The suspensions were sterile filtered using chemically inert, polyethersulfone filters before being used to aseptically inoculate freshly autoclaved LB media to give the desired concentrations. They were finally vortexed before use to ensure homogeneity.

Bacteria were freshly inoculated onto LB agar plates and left to grow overnight. From the plates a

single, representative and phenotypically homogeneous colony was transferred to 25 mL of freshly autoclaved LB medium in a 250 mL conical flask. This was grown until its turbidity equalled the McFarland standard and was used within 30 minutes of preparation. The experiments were carried out in a 96 well plate with 5 experimental replicates. Each well was inoculated with 100 μL of the correct antimicrobial impregnated media, however the outermost wells were left empty to prevent water loss by evaporation (as these wells are particularly susceptible) during incubation as shown in Figure 6.3.

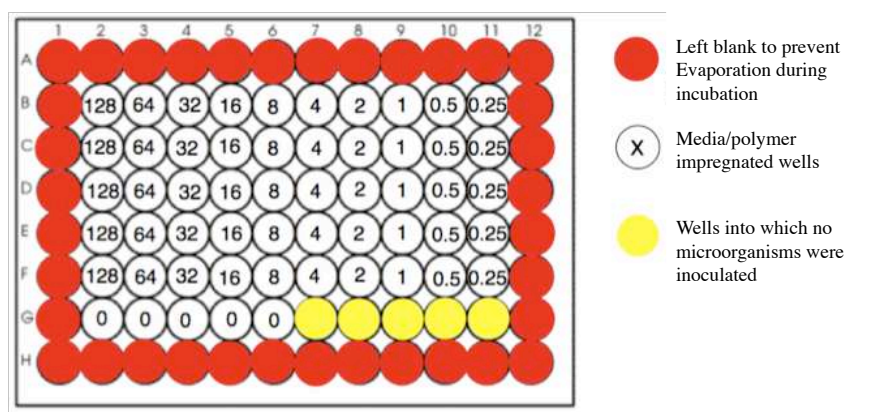


Figure 6.3: Innoculation plan for the testing of the minimum inhibitory concentration of the charged polymers. Those wells numbered describe the concentration of polymer in media in the final preparation. Yellow wells contain media but no bacteria nor polymer.

The plate plan in Figure 6.3 ensured that there were sufficient replicates for reliability and also positive and negative controls, i.e. those wells containing media only and those containing media only and no bacteria inoculated.

To each well, 1 μL of the adjusted bacterial suspension was added (except for the negative controls). The absorbance at 600 nm (OD_{600}) then recorded with four readings per well and the mean calculated (T_0). The plates were then sealed and incubated for 18 hours without agitation. Absorbance values of each well were measured again (T_{18}) and from this the change in optical density recorded according to equation 6.2

$$\text{Change in } (\text{OD}_{600}) = T_{18} - T_0 \quad (6.2)$$

All the values from each well were added together and the mean and standard deviation calculated. These values were plotted on the Y axis and the concentration of polymer plotted along the X axis. From the graph the minimum inhibitory concentration was determined at where the line crossed the X axis corresponding where there was no change in cell density (OD_{600}).

6.2.2 Cytotoxicity testing: 3-(4,5-Dimethylthiazol-2-yl)-

2,5-diphenyltetrazolium bromide (MTT) assay

In the testing of polymer toxicity against human cells, all of the functionalised polymers displaying a permanent positive charge and a permanent betaine functionality (Figure 6.4) were evaluated. Many thanks to Martin Redhead for his assistance by carrying out the cell work.

A 96 well plate was seeded with 0.1 mL of a Caco-2 cell suspension into each well so that each well contained $\approx 15,000$ cells. These were left for 20-24 hours for the cells to attach. Once the cells were plated, serial dilutions of the polymers to obtain concentrations of: 10, 5, 1, 0.5, 0.1, 0.05, 0.01, 0.005 mg/mL in media.

The medium used was Dulbecco's Modified Eagle Medium supplemented with 2 mM L-glutamine, 1000 IU/mL insulin, 10 $\mu\text{g/mL}$ streptomycin and 10% foetal bovine serum (FBS). This was prepared and then left overnight in an incubator to ensure sterility. Once the cells had attached and

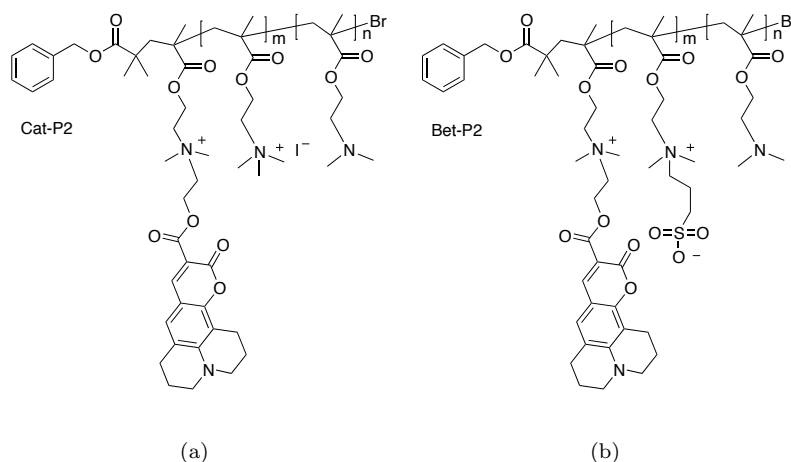


Figure 6.4: Modified a) Cationic pDMAEMA polymer (Cat-P2) and b) Betaine pDMAEMA polymer (Bet-P2) tested against Caco-2 cells. The percentage of 'm' to 'n' were 25% (polymer A), 50% (polymer B), 75% (polymer C) and 100% (polymer D)

the polymer solutions had been confirmed as sterile and suitable for use, the media presently on the cells was removed.

0.1 mL of each of the polymer/media solutions was added to the cells. Controls included one lane of untreated cells and one lane of cells treated with 2% Triton X-100 in media followed by incubation for 24 hours.

After incubation the supernatant was removed and cells washed once with phosphate buffered saline (PBS). Then 0.1 mL of 1 mg/mL MTT reagent in polymer-free medium was added to each well. The plates were then incubated for 2 hours whilst protecting from light by wrapping in foil. After this time has elapsed the MTT/media was removed and 0.2 mL of isopropanol was added to each well. The plate was then placed on an orbital shaker for 5 mins then absorbance at 570 nm using the plate reader is recorded. The data normalised according to equation 6.3:

$$\% \text{ MTT Metabolised} = \frac{\text{Treatment group average} - \text{Triton group average}}{\text{Untreated group average} - \text{Triton group average}} \times 100 \quad (6.3)$$

These data obtained from equation 6.3 were plotted with polymer concentration on the X axis and percentage of MTT metabolised on the Y axis for each polymer.

6.3 Results and Discussion

6.3.1 Minimum inhibitory concentration

In the literature it has been suggested that determination of minimum inhibitory concentration (MIC) can be satisfactorily achieved "*by eye*".[162, 164, 165] This can be carried out using the naked eye but may be aided by holding the bacterial suspension to a piece of lined paper to add contrast. From comparison between all the bacterial suspensions containing the different dilutions of the putative anti-microbial agent one can judge the *break-point*, where no bacterial growth is apparent. This can be both difficult and highly subjective. For these reasons it was decided to utilise a more experimentally robust method where the change in optical density and thus cell growth is measured by absorbance at 600 nm. This ensured the process was free from user bias and gives a more accurate reflection of the true minimum inhibitory concentration.

After incubation for 18 hours over the concentration ranges tested it was apparent that the betaine polymers had no discernable effects upon bacterial growth (Figure 6.5)

This result shown in Figure 6.5 corresponded with both the previous binding experiments in this study and also the literature. When considering the mechanism of action for charged polymers, the first step towards their bactericidal or bacteriostatic action required an initial electrostatic attraction of the polymer towards the bacterial membrane. However, with betaine polymers unable to carry out this first step effectively their actions were minimal. In the literature such surfaces are utilised for their non-fouling and non-adsorbing properties as they prevent bacteria binding to them.[130] However, it has also been reported that the positive charge contained within the zwitter-ionic functionality may be available to engage in binding events with bacteria.[166] The work by

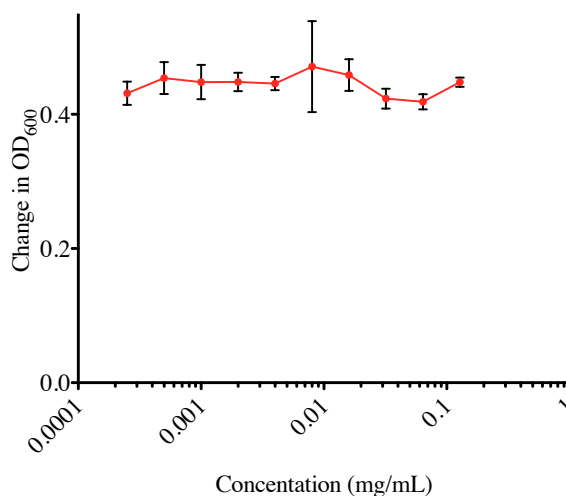


Figure 6.5: Results of MIC assay for the 100% betaine functionalised pDMAEMA Bet-P1 against *E. coli*

Ward *et. al* into the use of similar zwitter-ionic polymers to act as cytotoxic agents suggested that the cationic nitrogen may be able to bind to the bacteria, and the hydrophobic component obtained from the polymer back-bone and the alkylmethacrylate co-monomer allowed for permeation into the cell membrane. The MIC values for their zwitter-ionic polymers were 1125-2000 $\mu\text{g/mL}$ whereas the concentration ranges tested in this work were lower and had a smaller hydrophobic component.

The quaternised polymer differed from the betaine polymer in its cytotoxic behaviour. Over the concentration range tested, a significant decrease in the change of optical density could be observed. This produced a corresponding minimum inhibitory concentration (MIC) for this polymer of 512 mg/L which can be seen in Figure 6.6.

These results show the relatively high bacteriostatic/cytotoxic action of cationic polymers such as those prepared in this work compared with polymers displaying a betaine functionality. The concentrations had initially been tested over the same concentration range as the betaine polymer; from 0 - 128 mg/L, however the early results showed their inhibitory action. As such, higher

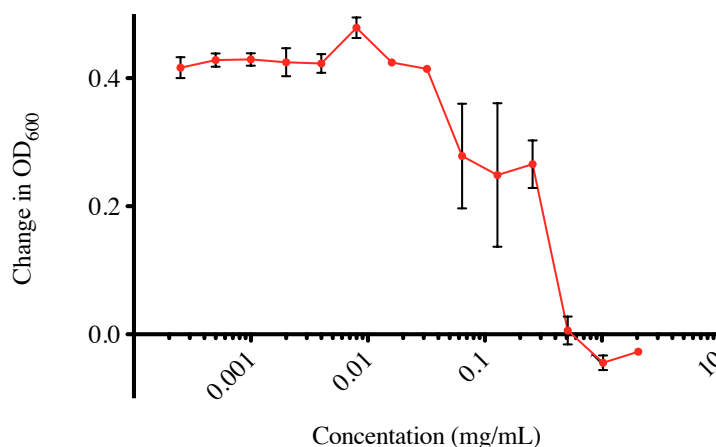


Figure 6.6: Results of MIC assay for the 100% quaternary functionalised pDMAEMA Cat-P1 against *E. coli*.

concentrations were tested of up to 2048 mg/L. Over the concentration range of 8 - 512 mg/L the polymer decreased the growth in bacteria in each well. Variations in the effect of this polymer were low, as indicated by the small standard deviation bars.

At the higher concentrations tested of 512 - 2048 mg/L there was a decrease in the cell density of the sample compared to the starting density (T_0). This may be explained by considering the mechanism of action of cationic polymers. Various groups have explored using similar cationic materials for their cytotoxic action.[51, 39, 127, 167] The postulated mechanism involves an initial electrostatic attraction towards the negatively charged bacterial cell. Once attachment occurs the polymers chains insert into the membranes and disrupt cellular homeostasis. This may have resulted in the production of much smaller particles of bacterial components which diffracted light less and so caused less absorbance at 600nm.

The reason for the difference between the cytotoxicity these two polymers may be explained by the influence the different structures of each polymer (Figure 6.2) and the charge functionalities

they display had upon cell binding. The overall charge for the betaine polymer was neutral as it contained both a positive and negative charge. This may explain the differences in their action as the betaine polymer's cationic functionality at the quaternary nitrogen is neutralised by the negative charge at the oxygen present very close to it in the side-chain structure.

Knowledge of the toxicity of the materials produced is useful to guide future applications. For example, it can be determined that for binding experiments lower concentrations (e.g. < 0.5 mg/mL) are more suitable as this could enable recovery of living cells with minimal damage to their growth or metabolism. However, if it were desirable to kill the bacteria, rather than bind them, it may be more useful to have higher concentrations (e.g. > 1 mg/mL). The differences between the toxicity of the two polymers is also particularly useful given the different binding behaviours the polymers exhibit. This suggests that the zwitter-ionic polymer may be more toxic towards *S. mutans* as it has a greater ability to bind to this bacterium compared to its relatively low binding ability towards *E. coli*. As such selective bacterial killing may be possible.

6.3.2 MTT Assay

The MTT assay was selected to evaluate the toxicity of the polymers as it is a widely used and robust assay. It measures metabolism of the yellow dye 3-(4,5-Dimethylthiazol-2-yl)-2,5-diphenyltetrazolium bromide into formazan, which is purple (Figure 6.7). The cell line chosen was Caco-2 as this is a human epithelial cell line and so will most represent the cell types which would come into contact with the polymer solutions in a real application should any be inadvertently swallowed for example.

This relatively simply assay can provide an indication as to the proportion of cells which are alive or metabolically active. The incubation time of the polymers with the cells was selected to be 24 hours to replicate the maximum length of time which epithelial cells would be in contact with the polymers if they were used. After 24 hours most biological processes would have cleared the

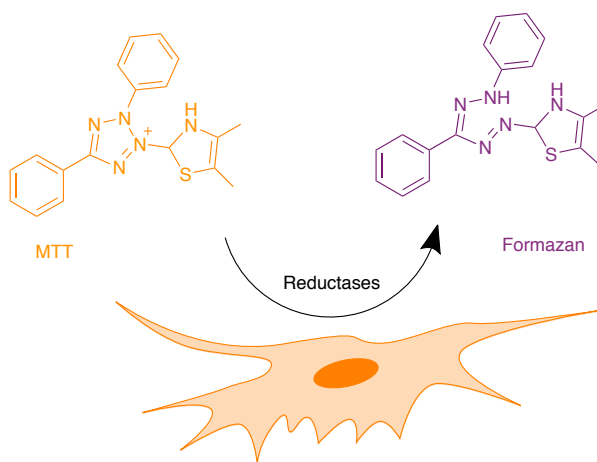


Figure 6.7: The metabolism of the dye MTT from yellow to the purple formazan requires the action of intracellular reductases.

substance from the gastrointestinal tract if some were to be ingested, for example.

The mechanism of action by which cationic and zwitter-ionic polymers exert their effects upon human cells are similar to those seen in bacterial cells.[160] There is an initial binding step followed by membrane disruption and eventual toxicity if the concentration should be high enough or the incubation time long enough. Despite this they have been tested as DNA binding agents and gene delivery vehicles,[146, 152] as well as to facilitate the absorption of protein drugs.[154] Although the mechanisms by which they exert their cytotoxic actions are similar to those with bacteria the results seen with the human cells were different.[163, 160] The results for the cationic polymers are shown in Figure 6.8.

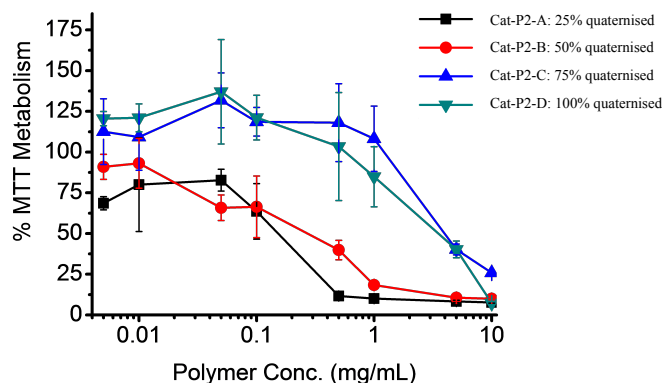


Figure 6.8: Results of MTT assay for polymers modified to contain a permanent cationic charge where Cat-P2-A contains 25% modification, Cat-P2-B contains 50% modification, Cat-P2-C contains 75% modification and Cat-P2-D is 100% modified to display a permanent cationic charge. Cell viability is expressed as a percentage of MTT metabolised compared to the control group.

The results showed that the polymers which were modified the least possessed the greatest toxicity towards the Caco-2 cells. For example at a concentration of 1 mg/mL polymers with 75-100% modification (Cat-P2-C and Cat-P2-D) have a biological activity 100-110% that of the control cells whereas polymers with 25-50% modification (Cat-P2-A and Cat-P2-B) had a biological activity of less than 25% of the cell in the control wells. This suggests that increasing the surface charge on these polymers may not only increase binding to bacteria but will also decrease toxicity to human cells.

This may have been due to the increased proportion of hydrophobic groups found within the polymer chain in the less modified groups. Adding the methyl group to the amine and making it permanently quaternised would have increased its hydrophilicity. So, despite the probable increased binding imparted by the increased positive charge there would have been decreased membrane disruption and the polymer chains were less able to insert themselves within the membranes

of the Caco-2 cells. This is extremely advantageous if one is looking for a highly binding yet low toxicity material. This result is in line with prior work on cationic polymer surfactants where the hydrophobic component played a key role in increasing the toxicity of the polymer.[37]

This compares with the zwitter-ionic polymers in Figure 6.9 where much lower toxicity was observed in the treatment groups apart from those which have only been 25% modified to display the betaine functionality.

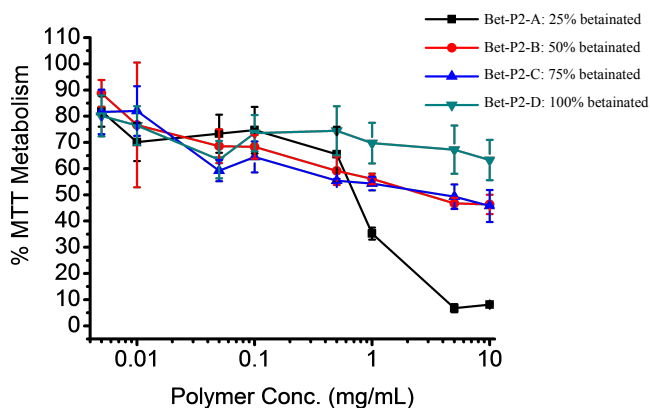


Figure 6.9: Results of MTT assay for polymers modified to contain a permanent betaine functionality where Bet-P2-A contains 25% modification, Bet-P2-B contains 50% modification, Bet-P2-C contains 75% modification and Bet-P2-D is 100% modified to display a permanent betaine functionality. Cell viability is expressed as a percentage of MTT metabolised compared to the control group.

The results of the MTT assay for the zwitter-ionic polymers suggest that the latter functionality was less toxic than the quaternised polymers apart from in the 25% modified group (Bet-P2-A). The lack of the toxicity from the other groups however was most likely as a result of the same reason for which this betaine group had low toxicity towards bacteria. This was because the group has an over-all neutral charge and so its propensity to bind is low. The higher toxicity in the 25% group can be explained in two ways; firstly the decreased level of modification, as with the quaternised polymers results in decreased hydrophilicity which aided the polymer to insert into the cell membranes. Secondly, the increased proportion of unmodified nitrogens meant that there were an increased number able to form temporary cationic charges through the equilibrium established as a function of the pH of the cell media. As the pH of the media was adjusted below the pK_a of DMAEMA this caused a small proportion of the free tertiary nitrogens to be temporarily and dynamically positively charged. Therefore as the polymers became increasingly modified to express the hydrophilic betaine functionality the number of hydrophobic and transiently cationic groups decreased. This contrasts with the 100% modified polymer (Bet-P2-D) which even at the highest concentration tested of 10 mg/mL, the cells retained over 60% viability as determined by MTT metabolism. This means that the polymers which are avid binding and killing agents of bacteria have relatively low toxicity to human cells over similar concentrations and those which can bind *S. mutans* selectively have also low toxicity to human cells.

6.4 Conclusions

The choice of application or usage of a material is often dictated by a balance between concentrations needed for use versus the concentrations which can cause toxicity.

The MTT assay is an important component of any toxicity study and can help guide the choice of future applications for various materials. Knowledge that both the completely modified quaternised and zwitter-ionic polymers have low toxicity could help determine their suitability over those polymers which have been incompletely modified.

For the quaternised polymers, working concentrations for binding and killing bacteria have been determined as well as the toxicity of these polymers towards human Caco-2 cells. It has been demonstrated that the polymers with increased modification and have greater hydrophilicity have lower toxicity for human cells than those with lower levels of modification. This is true also for the zwitter-ionic polymers. However these polymers expressed low toxicity against the bacteria tested. The results suggest that possible uses for these materials could include binding to microbes but yet limit toxicity to the human.

Chapter 7

Auto-nemesis

7.1 Introduction

The recognition and inactivation of pathogenic microorganisms remains a great scientific challenge and a practical problem of enormous significance. Conventional antibiotics have been extremely successful in combating microbial infections, but the emergence of resistant strains of many pathogens is an increasing concern. New approaches to prevent bacterial infections are required that do not invoke the selection of resistant populations. Non-lethal means for targeting bacteria include inactivating their invasive pathways, for example by disrupting cell-cell signalling mechanisms known as Quorum Sensing within microbial populations [73, 72, 81, 76, 79, 75, 82], or, more simply, by sequestering bacteria away from an infective site.

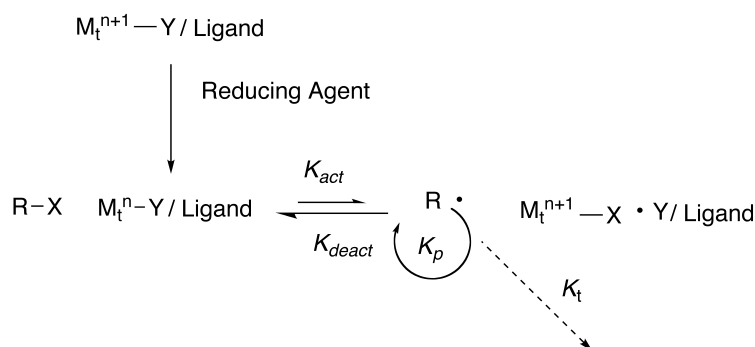
The latter route is attractive also from a diagnostic perspective, as the binding of a specific organism may facilitate detection of pathogens within a large population of non-pathogens and also aid in choice of therapeutic. However, the selective binding of specific bacterial species and/or sub-strains is challenging and currently requires expensive 'cold-chain' reagents such as antibodies and aptamers which precludes their use in non-hospital environments or in developing nations.

Accordingly, there has been interest in developing a route to cell-binding agents that does not require delicate and expensive biological affinity agents, and which can be tailored to produce sequestrants for a wide range of biological targets. Approaches to address this issue have included soft-lithography, molecular imprinting, and multi-valent carbohydrate-receptor mediated cell capture such as those explored earlier in this work.

Of particular usefulness would be enhanced methods for generating polymeric agents which are hydrophilic, soluble and derived from accessible precursors. Such materials are already widely used in diagnostic assays. Hydrophilic polymers are of note too since nearly all bacteria produce complex macromolecules in the form of an Extra-Cellular Matrix (ECM).

One such method to generate hydrophilic molecules and limit cross-linking and so prevent formation of insoluble polymers is controlled radical polymerisation methods. Controlled radical polymerisation (CRP) methods such as atom-transfer radical polymerisation (ATRP) have been the focus of a significant volume of research.[97] The methods enable meticulous control over the polymer architecture and polydispersities approaching unity.[96] Polymerisation directly in pure water as an environmentally friendly solvent and together with lowering the concentration of transition metal catalyst is compatible with the concept of "green chemistry" and also increases biocompatibility due to the toxicity of transition metals.[112, 117, 118]

Activators generated by electron transfer (AGET) ATRP[168] and activators regenerated by electron transfer (ARGET) ATRP[115] are methods employed for ATRP which enable polymerisations in water and significantly reduced transition metal concentrations respectively. AGET involves the *in situ* reduction of copper (II) ions to copper (I) using a reducing agent, for example ascorbic acid (Scheme 7.1) and biological enzymes.[169]



Scheme 7.1: Mechanism of AGET ATRP. The active copper catalyst is obtained through the reduction of copper (II) by a suitable reducing agent. M_t = transition metal, Y = halogen/pseudohalogen, X = halogen, K_{act} = activation rate constant, K_{deact} = deactivation rate constant, K_t = termination rate constant.

Microorganisms have a number of metabolic processes to handle transition metals such as copper used in the ATRP polymerisations.[170] Copper has two important functions in microbiological systems; electron transfer and oxygen handling. For this reason many enzymes, proteins and processes exist to maintain copper homeostasis. These enzymes have been shown to be involved in not only the reduction of copper[171, 172] but also other transition metals.[173]

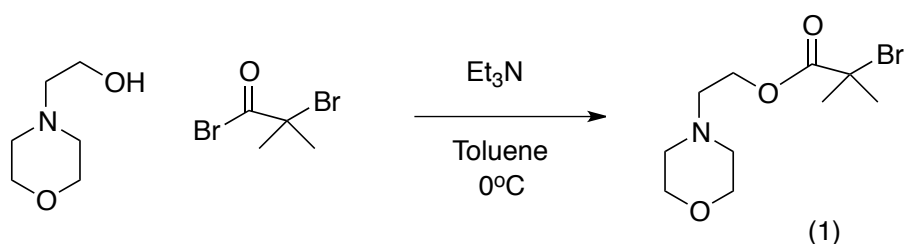
The reduction of transition metals are used in the two aforementioned chemical and biological processes. It is proposed that the two may be combined to generate polymeric materials from vinyl starting monomers. As the polymerisation processes will occur at the bacterial surface it is anticipated that the process will replicate templating and generate materials selective for the bacterium unlike those produced randomly in the absence of bacteria.

As discussed in the introductory chapter, templating involves carrying out a polymerisation in the presence of a target and during polymerisation functional monomers align around the target and results in the production of a more avid binder for the target than if produced in the absence

of the target. As such, the term: "*Auto-nemesis*" is used to describe this process as the bacteria generate the materials to facilitate their demise.

7.2 Methods

7.2.1 Synthesis of 2-(N-Morpholino)ethyl-2-bromobutyrate (1)



Scheme 7.2: Synthesis of 2-(N-Morpholino)ethyl-2-bromobutyrate (**1**).

To a round bottomed flask 8.6 mL (71 mmol) of 4-(2-hydroxyethyl) morpholine and 15.3 mL (107 mmol) of triethylamine were added along with 300 mL of toluene. Over ice, and under nitrogen, 13.2 mL (107 mmol) of α -bromoisobutyryl bromide were added dropwise via a pressure equalising addition apparatus over 3 hours. This mixture was left to react overnight before filtering. The solid was disregarded and the filtrate was washed with 0.1 M sodium carbonate (3×100 mL) and then with water (3×100 mL) before being dried over magnesium sulphate. The toluene was removed under reduced pressure and the brown liquid was purified using flash chromatography (dichloromethane:ethylacetate 4:1) to yield a yellow oil **1** (13.3 g, 47.8 mmol, Yield 67.3%)

^1H NMR (400 MHz, CDCl_3): δ (ppm) = 1.87 (s, 6H, CH_3)₂, 2.47-2.50 (m, 4H, $(\text{CH}_2)_2\text{N}$), 2.63 (t, $J = 5.75$ Hz, 2H, NCH_2CH_2), 3.62-3.65 (m, 4H, $(\text{CH}_2)_2\text{O}$), 4.26 (t, $J = 5.75$ Hz, 2H, $\text{CH}_2\text{CH}_2\text{O}$).
 ^{13}C NMR (100 MHz, CDCl_3): δ (ppm) = 30.72 (CH_3), 53.56 (CBr), 55.63 (NCH_2), 56.52 ($\text{N}(\text{CH}_2)_2$), 63.06 (CH_2O), 66.67 ($\text{O}(\text{CH}_2)_2$), 171.34 (CO).

Calculated Mass (m/z) ($\text{C}_{10}\text{H}_{18}\text{BrNO}_3$): 279.0470 (100%), 281.0450 (97.3%). Mass Found (m/z):

279.0674.

7.2.2 Bacterial Growth

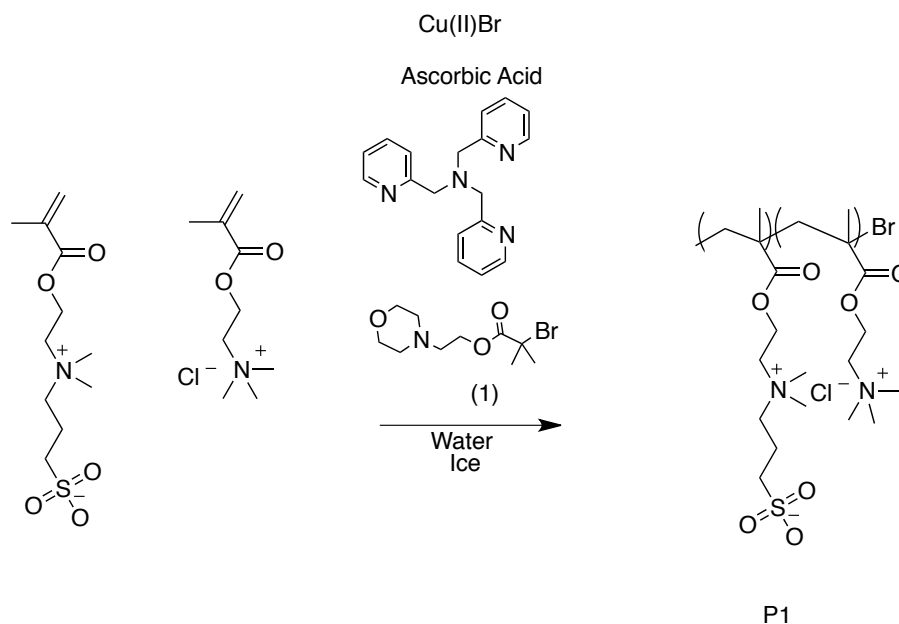
Bacteria were first plated from bacterial stocks stored at -80°C onto freshly poured LB agar plates. The plates were placed in an incubator at 37°C overnight to allow the colonies to grow. The next day a single representative colony was selected and used to inoculate 5 mL of pre-warmed autoclaved LB media. This primary culture was placed in the incubator at 37°C overnight. Meanwhile 500 mL of LB media were prepared and autoclaved before being placed in the incubator. The next day the 500 mL of LB media were inspected for signs of contamination before the 5 mL of primary culture were used to inoculate the larger media volume.

The secondary culture was incubated at 37°C for 24 hours with constant agitation at 190-200 revolutions per minute to a cell density of 3.2 (OD_{600}). After this, the cells were transferred into 250 mL centrifugation buckets and pelleted at a speed of 6,000 g (relative centrifugal force). Each pellet was washed with phosphate buffered saline (PBS) (1×100 mL) then with sterile deionised water (2×100 mL). Finally the pellet was agitated to suspend it in its own residual fluid combined with another pellet and made to 7 mL with sterile deionised water to an OD_{600} of 93.6 (obtained by serial dilutions).

7.2.3 Measurement of redox potential

Bacteria were grown as before and periodically 20 mL of the growth media were withdrawn aseptically and the redox tester was immersed in this medium for 5-10 minutes until the value had stabilised. The sample was then disregarded and probe washed for the next measurement.

7.2.4 Polymerisation of [2-(methacryloyloxy)ethyl]trimethylammonium chloride and [2-(methacryloyloxy)ethyl]dimethyl-(3-sulfopropyl) ammonium hydroxide via. ATRP in water (P1)

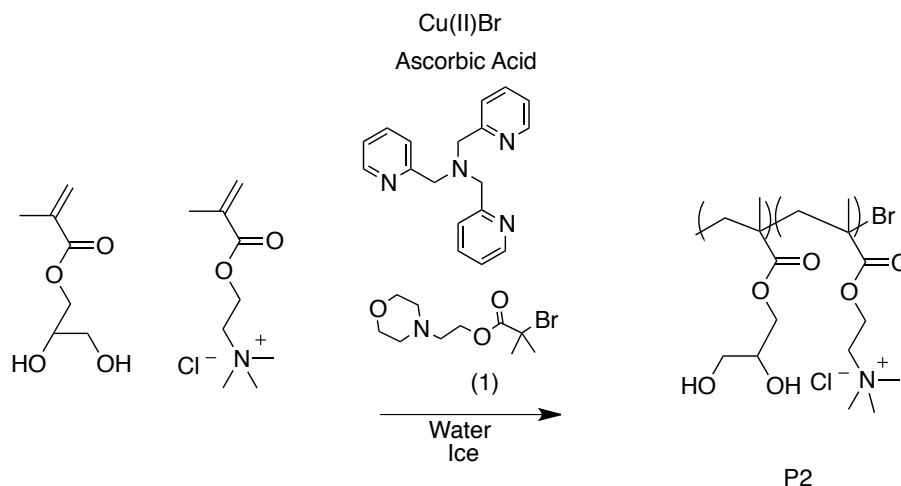


Scheme 7.3: Polymerisation of MEDSA and METAC by AGET ATRP in water (**P1**).

To a reaction tube 194 mg (0.695 mmol) of [2-(methacryloyloxy)ethyl]dimethyl-(3-sulfopropyl)ammonium hydroxide (MEDSA), 144 mg (0.695 mmol) of [2-(methacryloyloxy)ethyl]trimethylammonium chloride (METAC), 1.554 mg (5.6×10^{-3} mmol) of the morpholine initiator (**1**), 200 μ L of a 0.069 M solution of the catalyst (Copper(II) Bromide and tris(2-pyridylmethyl)amine) and 50 μ L of DMSO were added. This mixture was degassed for 30 minutes over ice after which 270 μ L of a degassed 1 mg/mL solution of ascorbic acid was added to begin the polymerisation. The polymerisation was monitored with ^1H NMR spectroscopy over time and when the desired conversion was reached the polymerisation was terminated by exposing to air. The polymers were obtained by dialysis against water for 3 days followed by freeze drying to yield a white amorphous solid. Polymer **P1**. Conversion: 35%

^1H NMR (400 MHz, D_2O): δ (ppm) = 0.99-2.00 (m, 6H, CH_3) (METAC and MEDSA), 2.28 (m, 2H, CH_2SO_3) (MEDSA), 2.98 (m, 2H, $\text{CH}_2\text{CH}_2\text{CH}_2$) (MEDSA), 3.2 (m, 15H, $\text{N}(\text{CH}_3)$) (both), 3.60 (m, 2H, $\text{N}(\text{CH}_3)_2\text{CH}_2$) (MEDSA),, 3.78 (m, 4H, NCH_2) (METAC and MEDSA), 4.49 (m, 4H, COCH_2) (METAC and MEDSA).

7.2.5 Polymerisation of [2-(methacryloyloxy)ethyl]trimethylammonium chloride and 2,3-dihydroxypropyl methacrylate by ATRP in water (P2)



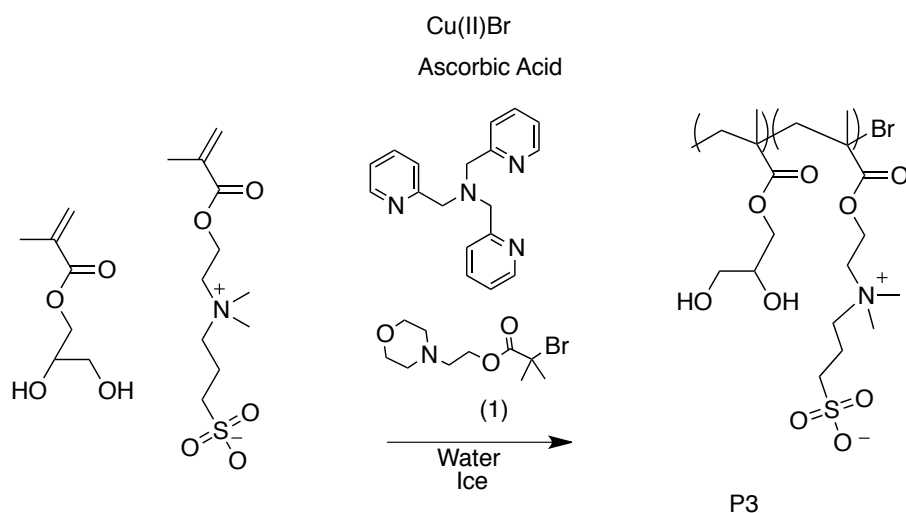
Scheme 7.4: Polymerisation of DHPMA and METAC by ATRP in water (**P2**).

To a reaction tube 111 mg (0.693 mmol) of 2,3-dihydroxypropyl methacrylate (DHPMA), 143 mg (0.693 mmol) of METAC, 1.554 mg (5.6×10^{-3} mmol) of the morpholine initiator (**1**), 200 μL of a 0.069 M solution of the catalyst (Copper(II) Bromide and tris(2-pyridylmethyl)amine) and 50 μL of DMSO were added. This mixture was degassed for 30 minutes over ice after which 270 μL of a degassed 1 mg/mL solution of ascorbic acid was added to begin the polymerisation. The polymerisation was monitored with ^1H NMR spectroscopy over time and when the desired conversion was reached the polymerisation was terminated by exposing to air. The polymers were obtained by dialysis against water for 3 days followed by freeze drying to yield a white amorphous solid.

Polymer **P2**. Conversion: 37%

^1H NMR (400 MHz, D_2O): δ (ppm) = 0.94-2.01 (m, 6H, CH_3) (METAC and DHPMA), 3.26-3.31 (m, 9H, $\text{N}(\text{CH}_3)_3$) (METAC), 3.68 ((m, 2H, CH_2O), 3.71 (m, 2H, $\text{N}(\text{CH}_3)_3\text{CH}_2$), 4.02 (m, 2H, COCH_2CH) (DHPMA), 4.13 (m, 1H, CH_2CO), 4.52 (m, 4H, COCH_2) (METAC).

7.2.6 Polymerisation of [2-(methacryloyloxy)ethyl]dimethyl-(3-sulfopropyl)ammonium hydroxide and 2,3-dihydroxypropyl methacrylate by ATRP in water (**P3**)



Scheme 7.5: Polymerisation of DHPMA and MEDSA by ATRP in water (**P3**).

To a reaction tube 111 mg (0.693 mmol) of DHPMA, 194 mg (0.0693 mmol) of MEDSA, 1.554 mg (5.6×10^{-3} mmol) of the morpholine initiator (**1**), 200 μL of a 0.069 M solution of the catalyst (Copper(II) Bromide and tris(2-pyridylmethyl)amine) and 50 μL of DMSO were added. This mixture was degassed for 30 minutes over ice after which 270 μL of a degassed 1 mg/mL solution of ascorbic acid was added to begin the polymerisation. The polymerisation was monitored with ^1H NMR spectroscopy over time and when the desired conversion was reached the polymerisation was terminated by exposing to air. The polymers were obtained by dialysis against water for 3

days followed by freeze drying to yield a white amorphous solid. Polymer **P3**. Conversion: 30%

^1H NMR (400 MHz, D_2O): δ (ppm) = 0.93-2.03 (m, 6H, CH_3) (DHPMA and MEDSA), 2.23 (m, 2H, CH_2SO_3), 3.03 (m, 2H, $\text{CH}_2\text{CH}_2\text{CH}_2$) (MEDSA), 3.2 (m, 6H, $\text{N}(\text{CH}_3)$), 3.63 (m, 2H, $\text{N}(\text{CH}_3)_2\text{CH}_2$) (MEDSA), 3.68 ((m, 2H, CH_2O), 3.85 (m, 2H, $\text{N}(\text{CH}_3)_3\text{CH}_2$), 4.02 (m, 2H, COCH_2CH) (DHPMA), 4.14 (m, 1H, COCH_2 , 4.55 (m, 4H, COCH_2) (MEDSA).

7.2.7 Optimisation of bacterial ATRP (b-ATRP)

The concentration of catalyst used (Copper(II) Bromide and tris(2-pyridylmethyl)amine) was varied in order to achieve better control over polymerisations. These variations involved not only differences in equimolar copper (II) bromide to tris(2-pyridylmethyl)amine catalytic complex but also the addition of further copper (II) bromide. System 'A' was the system equivalent to those ratios used for conventional AGET ATRP. In system 'B' the concentration of copper (II) bromide was double that of the ligand tris(2-pyridylmethyl)amine. System 'C' was double of both ligand and copper (II) bromide of that found in system 'B'. System 'D' was the same ratio of copper (II) bromide and tris(2-pyridylmethyl)amine as system 'A' but diluted by a factor of 100.

System A: Ratio of initiator to copper to ligand: 1.0 : 2.5 : 2.5 (P4)

To a reaction tube 194 mg (0.695 mmol) of MEDSA, 144 mg (0.695 mmol) of METAC, 1.554 mg (5.6×10^{-3} mmol) of the morpholine initiator (**1**) and 50 μL of DMSO were added. This solution was mixed with bacteria (*E. coli* MG1655) as a 7 mL suspension with an optical density (OD_{600}) of 93.6 and degassed for 30 minutes over ice after which 200 μL of a degassed 0.069 M solution of the catalyst (Copper(II) Bromide and tris(2-pyridylmethyl)amine) were added to begin the polymerisation. The polymerisation was monitored with ^1H NMR spectroscopy over time and when the desired conversion was reached the polymerisation was terminated by exposing to air. Polymers were obtained from the reaction by first washing the cells with deionised water (3×5

mL) followed by washing with a saturated solution of sodium chloride (5 M aq) (3×5 mL). These two separated solutions were then dialysed against water for 3 days followed by freeze drying to obtain the polymers as a white amorphous solids. Polymer **P4-W** (water washes) and Polymer **P4-S** (salt washes). Conversion 70% PDI GPC: 2.33

System B: Ratio of initiator to copper to ligand: 1.0 : 5.0 : 2.5 (P5)

To a reaction tube 194 mg (0.695 mmol) of MEDSA, 144 mg (0.695 mmol) of METAC, 3 mg (0.0139 mmol) of copper (II) bromide, 1.554 mg (5.6×10^{-3} mmol) of the morpholine initiator (**1**) and 50 μ L of DMSO were added. This solution was mixed with bacteria (*E. coli* MG1655) as a 7 mL suspension with an optical density (OD_{600}) of 93.6 and degassed for 30 minutes over ice after which 200 μ L of a degassed 0.069 M solution of the catalyst (Copper(II) Bromide and tris(2-pyridylmethyl)amine) were added to begin the polymerisation. The polymerisation was monitored with $^1\text{HNMR}$ spectroscopy over time and when the desired conversion was reached the polymerisation was terminated by exposing to air. Polymers were obtained from the reaction by first washing the cells with deionised water (3×5 mL) followed by washing with a saturated solution of sodium chloride (5 M aq) (3×5 mL). These two separated solutions were then dialysed against water for 3 days followed by freeze drying to obtain the polymers as a white amorphous solids. Polymer **P5-W** (water washes) and Polymer **P5-S** (salt washes). Conversion: 46% PDI: 2.31.

Reducing catalyst concentration - System C: Ratio of initiator to copper to ligand: 1.0 : 10 : 5.0 (P6)

To a reaction tube 194 mg (0.695 mmol) of MEDSA, 144 mg (0.695 mmol) of METAC, 6 mg (0.0278 mmol) of copper (II) bromide, 1.554 mg (5.6×10^{-3} mmol) of the morpholine initiator (**1**) and 50 μ L of DMSO were added. This solution was mixed with bacteria (*E. coli* MG1655) as a 7 mL suspension with an optical density (OD_{600}) of 93.6 and degassed for 30 minutes over ice after which 400 μ L of a degassed 0.069 M solution of the catalyst (Copper(II) Bromide and

tris(2-pyridylmethyl)amine) were added to begin the polymerisation. The polymerisation was monitored with ^1H NMR spectroscopy over time and when the desired conversion was reached the polymerisation was terminated by exposing to air. Polymers were obtained from the reaction by first washing the cells with deionised water (3×5 mL) followed by washing with a saturated solution of sodium chloride (5 M aq) (3×5 mL). These two separated solutions were then dialysed against water for 3 days followed by freeze drying to obtain the polymers as a white amorphous solids. Polymer **P6-W** (water washes) and Polymer **P6-S** (salt washes). Conversion 41%

**Reducing catalyst concentration - System D: Ratio of initiator to copper to ligand:
1.0 : 0.025 : 0.025 (P7)**

To a reaction tube 194 mg (0.695 mmol) of MEDSA, 144 mg (0.695 mmol) of METAC, 1.554 mg (5.6×10^{-3} mmol) of the morpholine initiator (**1**) and 50 μL of DMSO were added. This solution was mixed with bacteria (*E. coli* MG1655 or *P. aeruginosa* 223 PAKR76) as a 7 mL suspension with an optical density (OD_{600}) of 93.6 and degassed for 30 minutes over ice after which 200 μL of a degassed 0.69 mM solution of the catalyst (Copper(II) Bromide and tris(2-pyridylmethyl)amine) were added to begin the polymerisation. The polymerisation was monitored with ^1H NMR spectroscopy over time and when the desired conversion was reached the polymerisation was terminated by exposing to air. Polymers were obtained from the reaction by first washing the cells with deionised water (3×5 mL) followed by washing with a saturated solution of sodium chloride (5 M aq) (3×5 mL). These two separated solutions were then dialysed against water for 3 days followed by freeze drying to obtain the polymers as a white amorphous solids.

Polymer **P7-WE** (water washes from *E. coli* polymerisations)

Conversion: 32% PDI (GPC): 1.67

^1H NMR (400 MHz, D_2O): δ (ppm) = 0.88-2.03 (m, 6H, CH_3) (METAC and MEDSA), 2.27 (m, 2H, CH_2SO_3) (MEDSA), 2.94 (m, 2H, $\text{CH}_2\text{CH}_2\text{CH}_2$) (MEDSA), 3.25 (m, 15H, $\text{N}(\text{CH}_3)_3$) (both), 3.59 (m, 2H, $\text{N}(\text{CH}_3)_2\text{CH}_2$) (MEDSA), 3.80 (m, 4H, NCH_2) (METAC and MEDSA), 4.49 (m, 4H,

COCH₂) (METAC and MEDSA).

Polymer **P7-SE** (salt washes from *E. coli* polymerisations)

Conversion: 32%

¹HNMR (400 MHz, D₂O): δ (ppm) = 0.99-1.98 (m, 6H, CH₃) (METAC and MEDSA), 2.27 (m, 2H, CH₂SO₃) (MEDSA), 2.97 (m, 2H, CH₂CH₂CH₂) (MEDSA), 3.23 (m, 15H, N(CH₃)₃) (both), 3.59 (m, 2H, N(CH₃)₂CH₂) (MEDSA), 3.79 (m, 4H, NCH₂) (METAC and MEDSA), 4.49 (m, 4H, COCH₂) (METAC and MEDSA).

Polymer **P7-WP** (water washes from *P. aeruginosa* polymerisations)

Conversion: 45%

¹HNMR (400 MHz, D₂O): δ (ppm) = 0.90-2.03 (m, 6H, CH₃) (METAC and MEDSA), 2.27 (m, 2H, CH₂SO₃) (MEDSA), 2.97 (m, 2H, CH₂CH₂CH₂) (MEDSA), 3.23 (m, 15H, N(CH₃)₃) (both), 3.58 (m, 2H, N(CH₃)₂CH₂) (MEDSA), 3.79 (m, 4H, NCH₂) (METAC and MEDSA), 4.48 (m, 4H, COCH₂) (METAC and MEDSA).

Polymer **P7-SP** (salt washes from *P. aeruginosa* polymerisations)

Conversion: 45%

¹HNMR (400 MHz, D₂O): δ (ppm) = 0.91-1.95 (m, 6H, CH₃) (METAC and MEDSA), 2.27 (m, 2H, CH₂SO₃) (MEDSA), 2.97 (m, 2H, CH₂CH₂CH₂) (MEDSA), 3.23 (m, 15H, N(CH₃)₃) (both), 3.59 (m, 2H, N(CH₃)₂CH₂) (MEDSA), 3.79 (m, 4H, NCH₂) (METAC and MEDSA), 4.49 (m, 4H, COCH₂) (METAC and MEDSA).

7.2.8 Investigation into system components

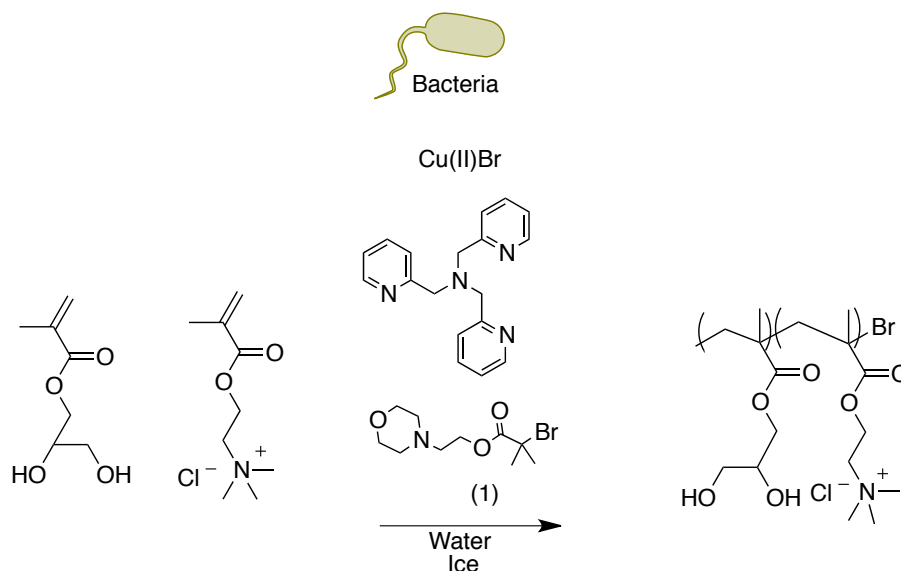
To a reaction tube 310 mg (1.11 mmol) of MEDSA, 57.6 mg (0.278 mmol) of METAC, 1.554 mg (5.6×10^{-3} mmol) of the morpholine initiator (**1**), 50 μ L of DMSO and 200 μ L of 0.069 M solution of the catalyst (Copper(II) Bromide and tris(2-pyridylmethyl)amine) were added. This solution was then mixed with the bacteria (*E. coli* MG1655) as a 7 mL suspension with an optical density (OD₆₀₀) of 93.6 in the presence of air and polymerisation observed by ¹HNMR spectroscopy. The

conditions were modified according to Table 7.1.

Table 7.1: Modifications to polymerisation conditions

| Component | Alteration Type |
|----------------|------------------------------------|
| Catalyst | Omitted |
| Ligand | Omitted |
| Initiator | Omitted |
| <i>E. coli</i> | Omitted |
| <i>E. coli</i> | Washed with PBS only |
| <i>E. coli</i> | Substitued for growth media (5 mL) |
| <i>E. coli</i> | Half quantity used after lysis |

7.2.9 Polymerisation of [2-(methacryloyloxy)ethyl]trimethylammonium chloride and 2,3-dihydroxypropyl methacrylate using bacterial activated ATRP (b-ATRP) (**P8**)



Scheme 7.6: Polymerisation of METAC and 2,3-dihydroxypropyl methacrylate by bacterial activated ATRP (b-ATRP) (**P8**).

To a reaction tube 111 mg (0.693 mmol) of DHPMA, 143 mg (0.0693 mmol) of METAC, 1.554 mg (5.6×10^{-3} mmol) of the morpholine initiator (**1**) and 50 μL of DMSO were added. This solution was mixed with bacteria (*E. coli* MG1655 or *P. aeruginosa* 223 PAKR76) as a 7 mL suspension with an optical density (OD_{600}) of 93.6. and degassed for 30 minutes over ice after which 200 μL of a degassed 0.69 mM solution of the catalyst (Copper(II) Bromide and tris(2-pyridylmethyl)amine) were added to begin the polymerisation. The polymerisation was monitored with ^1H NMR spectroscopy over time and when the desired conversion was reached the polymerisation was terminated by exposing to air. Polymers were obtained from the reaction by first washing the cells with deionised water (5 M aq) (3×5 mL) followed by washing with a saturated solution of sodium chloride (3×5 mL). These two separated solutions were then dialysed against water for

3 days followed by freeze drying to obtain the polymers as a white amorphous solids.

Polymer **P8-WE** (water washes from *E. coli* polymerisations)

Conversion: 38% PDI (GPC): 3.87

$^1\text{HNMR}$ (400 MHz, D_2O): δ (ppm) = 0.95-2.03 (m, 6H, CH_3) (METAC and DHPMA), 3.27 (m, 9H, $\text{N}(\text{CH}_3)_3$) (METAC), 3.67 ((m, 2H, CH_2O), 3.80 (m, 2H, $\text{N}(\text{CH}_3)_3\text{CH}_2$), 4.02 (m, 2H, COCH_2CH) (DHPMA), 4.14 (m, 1H, CH_2CO), 4.53 (m, 2H, COCH_2) (METAC).

Polymer **P8-SE** (salt washes from *E. coli* polymerisations)

Conversion: 38% PDI (GPC): 5.32

$^1\text{HNMR}$ (400 MHz, D_2O): δ (ppm) = 0.94-2.03 (m, 6H, CH_3) (METAC and DHPMA), 3.27 (m, 9H, $\text{N}(\text{CH}_3)_3$) (METAC), 3.67 ((m, 2H, CH_2O), 3.81 (m, 2H, $\text{N}(\text{CH}_3)_3\text{CH}_2$), 4.02 (m, 2H, COCH_2CH) (DHPMA), 4.13 (m, 1H, CH_2CO), 4.54 (m, 2H, COCH_2) (METAC).

Polymer **P8-WP** (water washes from *P. aeruginosa* polymerisations)

Conversion: 29%

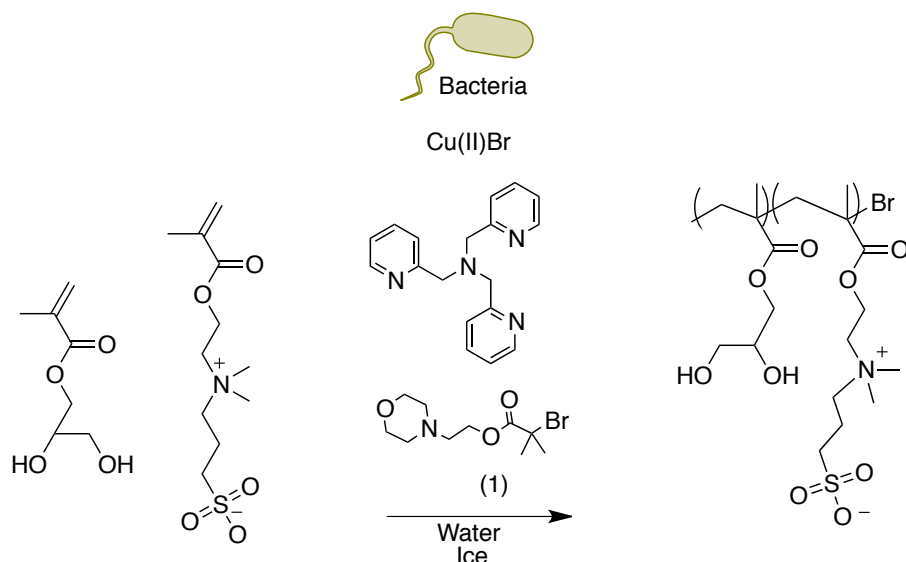
$^1\text{HNMR}$ (400 MHz, D_2O): δ (ppm) = 0.94-2.04 (m, 6H, CH_3) (METAC and DHPMA), 3.26 (m, 9H, $\text{N}(\text{CH}_3)_3$) (METAC), 3.67 ((m, 2H, CH_2O), 3.80 (m, 2H, $\text{N}(\text{CH}_3)_3\text{CH}_2$), 4.01 (m, 2H, COCH_2CH) (DHPMA), 4.11 (m, 1H, CH_2CO), 4.53 (m, 2H, COCH_2) (METAC).

Polymer **P8-SP** (salt washes from *P. aeruginosa* polymerisations)

Conversion: 29%

$^1\text{HNMR}$ (400 MHz, D_2O): δ (ppm) = 0.93-2.01 (m, 6H, CH_3) (METAC and DHPMA), 3.26 (m, 9H, $\text{N}(\text{CH}_3)_3$) (METAC), 3.67 ((m, 2H, CH_2O), 3.80 (m, 2H, $\text{N}(\text{CH}_3)_3\text{CH}_2$), 4.01 (m, 2H, COCH_2CH) (DHPMA), 4.15 (m, 1H, CH_2CO), 4.55 (m, 2H, COCH_2) (METAC).

7.2.10 Polymerisation of [2-(methacryloyloxy)ethyl]dimethyl-(3-sulfopropyl) ammonium hydroxide and 2,3-dihydroxypropyl methacrylate using bacterial activated ATRP (b-ATRP) (P9)



Scheme 7.7: Polymerisation of MESDA and DHPMA by bacterial activated ATRP (b-ATRP) (**P9**).

To a reaction tube 111 mg (0.693 mmol) of DHPMA, 194 mg (0.0693 mmol) of MESDA, 1.554 mg (5.6×10^{-3} mmol) of the morpholine initiator **(1)** and 50 μL of DMSO were added. This solution was mixed with bacteria (*E. coli* MG1655 or *P. aeruginosa* 223 PAKR76) as a 7 mL suspension with an optical density (OD_{600}) of 93.6. and degassed for 30 minutes over ice after which 200 μL of a degassed 0.69 mM solution of the catalyst (Copper(II) Bromide and tris(2-pyridylmethyl)amine) were added to begin the polymerisation. The polymerisation was monitored with ^1H NMR spectroscopy over time and when the desired conversion was reached the polymerisation was terminated by exposing to air. Polymers were obtained from the reaction by first washing the cells with deionised water (5 M aq) (3×5 mL) followed by washing with a saturated solution of sodium chloride (3×5 mL). These two separated solutions were then dialysed against water for

3 days followed by freeze drying to obtain the polymers as a white amorphous solids.

Polymer **P9-WE** (water washes from *E. coli* polymerisations)

Conversion: 35% PDI (GPC): 4.45

^1H NMR (400 MHz, D_2O): δ (ppm) = 0.96-2.03 (m, 6H, CH_3) (DHPMA and MEDSA), 2.23 (m, 2H, CH_2SO_3), 3.03 (m, 2H, $\text{CH}_2\text{CH}_2\text{CH}_2$) (MEDSA), 3.28 (m, 6H, $\text{N}(\text{CH}_3)$), 3.62 (m, 2H, $\text{N}(\text{CH}_3)_2\text{CH}_2$) (MEDSA), 3.68 ((m, 2H, CH_2O), 3.82 (m, 2H, $\text{N}(\text{CH}_3)_3\text{CH}_2$), 4.02 (m, 2H, COCH_2) (DHPMA), 4.15 (m, 1H, CHCOH , 4.53 (m, 2H, COCH_2) (MEDSA).

Polymer **P9-SE** (salt washes from *E. coli* polymerisations)

Conversion: 35% PDI (GPC): 7.25

^1H NMR (400 MHz, D_2O): δ (ppm) = 1.06-1.92 (m, 6H, CH_3) (DHPMA and MEDSA), 2.33 (m, 2H, CH_2SO_3), 3.03 (m, 2H, $\text{CH}_2\text{CH}_2\text{CH}_2$) (MEDSA), 3.28 (m, 6H, $\text{N}(\text{CH}_3)$), 3.62 (m, 2H, $\text{N}(\text{CH}_3)_2\text{CH}_2$) (MEDSA), 3.67 ((m, 2H, CH_2O), 3.82 (m, 2H, $\text{N}(\text{CH}_3)_3\text{CH}_2$), 4.02 (m, 2H, COCH_2) (DHPMA), 4.11 (m, 1H, CHCOH , 4.53 (m, 2H, COCH_2) (MEDSA).

Polymer **P9-WP** (water washes from *P. aeruginosa* polymerisations)

Conversion: 31%

^1H NMR (400 MHz, D_2O): δ (ppm) = 0.93-2.00 (m, 6H, CH_3) (DHPMA and MEDSA), 2.30 (m, 2H, CH_2SO_3), 3.03 (m, 2H, $\text{CH}_2\text{CH}_2\text{CH}_2$) (MEDSA), 3.27 (m, 6H, $\text{N}(\text{CH}_3)$), 3.64 (m, 2H, $\text{N}(\text{CH}_3)_2\text{CH}_2$) (MEDSA), 3.68 ((m, 2H, CH_2O), 3.85 (m, 2H, $\text{N}(\text{CH}_3)_3\text{CH}_2$), 4.02 (m, 2H, COCH_2) (DHPMA), 4.15 (m, 1H, CHCOH , 4.52 (m, 2H, COCH_2) (MEDSA).

Polymer **P9-SP** (salt washes from *P. aeruginosa* polymerisations)

Conversion: 31%

^1H NMR (400 MHz, D_2O): δ (ppm) = 1.04-2.08 (m, 6H, CH_3) (DHPMA and MEDSA), 2.30 (m, 2H, CH_2SO_3), 3.03 (m, 2H, $\text{CH}_2\text{CH}_2\text{CH}_2$) (MEDSA), 3.27 (m, 6H, $\text{N}(\text{CH}_3)$), 3.64 (m, 2H, $\text{N}(\text{CH}_3)_2\text{CH}_2$) (MEDSA), 3.71 ((m, 2H, CH_2O), 3.85 (m, 2H, $\text{N}(\text{CH}_3)_3\text{CH}_2$), 4.02 (m, 2H, COCH_2) (DHPMA), 4.14 (m, 1H, CHCOH , 4.56 (m, 2H, COCH_2) (MEDSA).

7.2.11 Bacterial aggregation measured using the Coulter counter

The machine was set-up as per the manufacturer's requirements. 200 μL of a bacterial suspension with an OD_{600} of 1.9 were added to the flow cell to obtain an obscuration of 8-12% (the machines optimum particle density). At this point the t_0 population distribution was recorded with constant mixing. Then 100 μL of a 1 mg/mL polymer solution was added. The mixture was allowed to equalibriate and the population distribution was recorded after a 15 minute and 30 minute interval.

7.2.12 Bacterial aggregation measured using changes in optical density (OD_{600})

The templated polymers were incubated with each of their bacterium to compare binding behaviour afforded by the templating process. For details of the aggregation assay please refer to the materials and methods chapter.

7.3 Results and Discussion

The presences of various bacterial enzymes on the cell surface enable microbes to carry out different metabolic processes. Some of the enzymes have been demonstrated to reduce transition metals such as copper. This can enable bacterial cells to substitute for ascorbic acid in copper mediated polymerisations. Bacterial cells can reduce the air stable copper (II) into the catalytically useful copper (I).

The growth of the bacteria used progressed in the expected manner; an initial lag phase followed by an exponential and finally a stationary phase of reduced or minimal growth. During these phases the redox potential also changed (Figure 7.1).

Red Zone (0-500 minutes): The media changed during the early growth of the bacteria from an oxidative environment to a reductive one. The reduction potential was at its highest while the cells

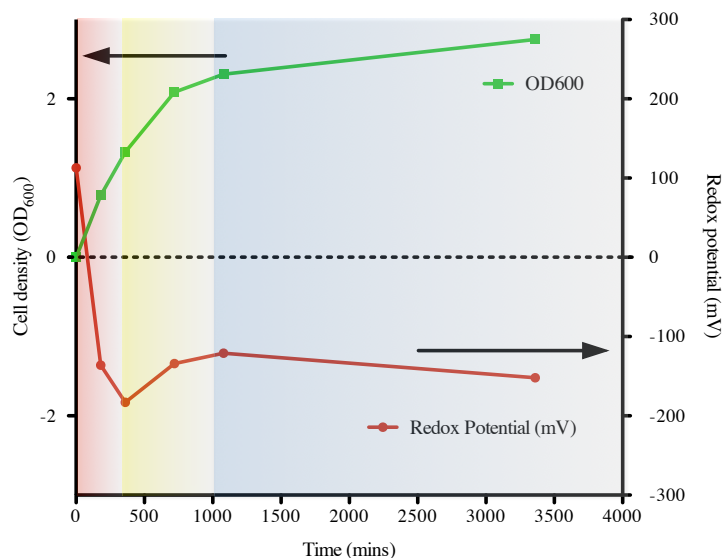


Figure 7.1: Plot of change in OD_{600} and change in redox potential against time.

were in exponential phase. This is explained by the large numbers of highly metabolically active cells during this portion of the growth.

Yellow Zone (500-1000 minutes): Cell numbers were increasing more slowly as nutrients were beginning to be depleted. Some cells die and others prepare to enter dormancy. The reduction potential decreases as the cells here were less active than whilst in the exponential phase. This is the transition to stationary phase.

Blue Zone (1000-4000 minutes): The numbers of cells appear to be increasing more slowly here which is attributable to changes in cell shape and size as the media is deprived of nutrients. Most of the cells are dormant or dead so the residual reduction potential of each cell was low. However as the redox potential is still high as there as a large number of cells carrying out maintenance metabolism.

At the end of this blue zone the cells were harvested. The harvesting was done here as at this stage a large homogenous cell yield can be obtained. After carrying out all the washing steps and

then degassing for polymerisations, all cells will be either dormant with some dead therefore the *number* of cells would be the limiting factor, rather than how metabolically active they were when harvesting began. It can be otherwise difficult to have reproducible batches if they have variations in their growth rate.

Once washed and concentrated the final cell optical density (OD_{600}) was 93.6 and the reduction potential is -244 mV which is ample for synthetic chemistry. The reduction potential was so high further to concentrating the cells, therefore demonstrating that the redox potential was even lower due to concentrating the cells which were responsible for the reduction potential.

A number of ATRP polymerisation conditions were tried using the quaternised and betaine monomers to obtain close to linear polymerisation conditions and improve control over the polymerisation. *System A* (ratio of initiator to copper to ligand: 1.0 : 2.5 : 2.5) yielded rapid polymerisation followed by no further growth, however with the other systems a change in the polymerisation kinetics was readily apparent (Figure 7.2).

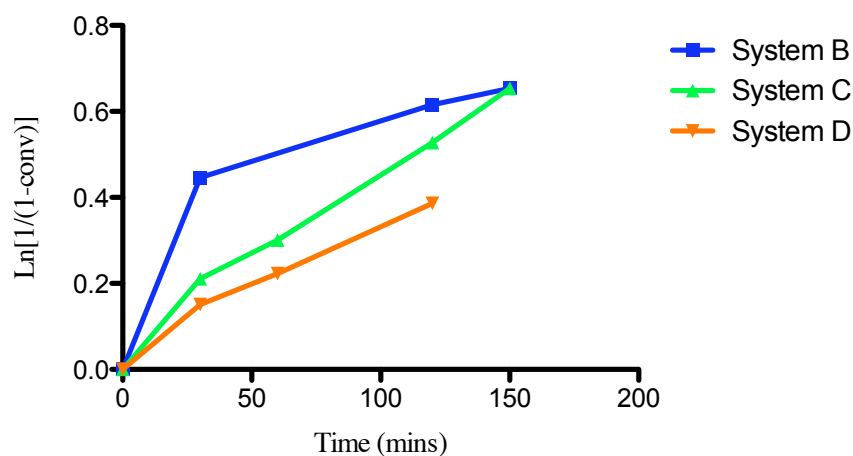


Figure 7.2: Polymerisation kinetics of the different b-ATRP systems.

It was found that system D (initiator : copper : ligand = 1.0 : 0.025 : 0.025) produced the slowest kinetics and also the best control based upon the effect it had upon polydispersity index (PDI)

(Table 7.2). Although the PDI values remained high, this is characteristic of the aqueous CatSec polymer analysis system used.

Table 7.2: Comparison between polymerisation systems

| System | Ratio [initiator][Cu ^{II}][ligand] | Conversion (120 mins) | PDI (water washed polymers) |
|--------|--|-----------------------|-----------------------------|
| A | [1][2.5][2.5] | n/a | 2.33 |
| B | [1][5.0][2.5] | 46% | 2.31 |
| C | [1][10][5.0] | 41% | Trace not found |
| D | [1][0.025][0.025] | 32% | 1.67 |

System D was therefore used for further bacterial activated polymerisations. This system gave a working concentration of copper (II) bromide of 4.42 ng/mL. A series of polymerisations of various functional and non-functional monomers was then carried out in the presence of bacteria using bacterial activated ATRP and their composition compared to that of the non-templated polymerisations produced by standard AGET ATRP.

Pseudomonas aeruginosa PAO1 produces a phenazine chemical called pyocyanin.[174] This molecule is an oxidising virulence factor and its production by *P. aeruginosa* PAO1 had prevented early attempts at b-ATRP using this bacterium. In order to generate the polymers with *Pseudomonas aeruginosa* it was necessary to use a pyocyanin negative *Pseudomonas aeruginosa* PAO1 mutant: strain PAKR76 Δ phzAG1 Δ phzAG2 (Double mutant phzAG1 and phzAG2).[122]

The first *templated* polymers produced were those of the quaternary (METAC) and betaine (MEDSA) monomers. The results of these are summarised in Table 7.3. The final composition was obtained by comparing the ratio between the protons adjacent to the quaternary nitrogen on each monomer (Figure 7.3).

This composition was obtained by comparing the integrals of the CH_2 adjacent to the quaternary nitrogen only seen on MEDSA at 3.58 ppm to those found on both monomers at 3.79 ppm. The value of the integral for the CH_2 in MEDSA at 3.58 ppm was subtracted from the integral at 3.79 ppm to give the proportion of the total polymer constituted of METAC.

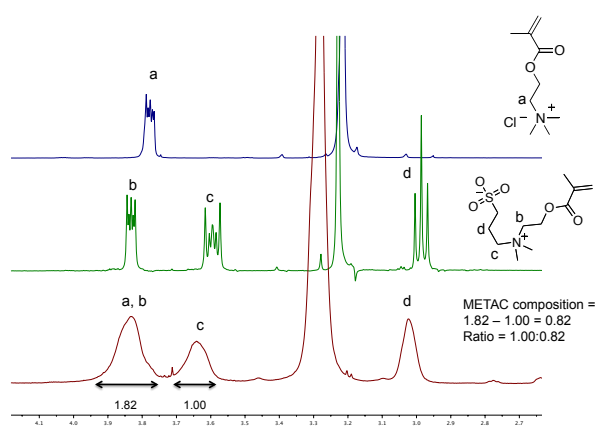


Figure 7.3: Representative example of co-polymer composition calculation of METAC and MEDSA for polymer **P1**.

As can be seen in Table 7.3 there are significant differences in composition between polymers produced by standard AGET ATRP and those produced using b-ATRP. As expected from estimations of monomer reactivity ratios (chapter E) the composition of the standard polymer had very similar composition of both monomers with only slightly greater inclusion of MEDSA. The washing steps employed whereby cells were washed initially with sterile deionised water followed by a saturated salt solution produced two distinct polymer populations. Those polymers which were weakly bound and less positivity charged were removed easily whilst those which were stronger bound required the use of the high ionic solution in order to disrupt the electrostatic interactions with the bacterial cell. The polymers removed from the bacterial surface were also more polydisperse (e.g. P7-WE

Table 7.3: Analysis of polymer composition for METAC and MEDSA. Ratios are expressed as (MEDSA:METAC)

| Polymer | Monomer feed (MEDSA:METAC) | Conversion (%) | Composition (MEDSA:METAC) |
|--------------|-------------------------------|-------------------|------------------------------|
| P1 | 1.00 : 1.00 | 35 | 1.00 : 0.82 |
| P7-WE | 1.00 : 1.00 | 32 | 1.00 : 0.44 |
| P7-SE | 1.00 : 1.00 | 32 | 1.00 : 0.95 |
| P7-WP | 1.00 : 1.00 | 45 | 1.00 : 0.28 |
| P7-SP | 1.00 : 1.00 | 45 | 1.00 : 1.54 |

PDI = 1.67) than those found in solution (P7-SE PDI = 2.01) which may be attributed to the complex topography of the bacterial surface.

The same polymerisation process was carried out the with each of the functional monomers, co-polymerised with a non-charged hydrophilic monomer to act as a molecular spacer. In this way, differences in the selection for each of the functionalities by the templating process could be compared better due to the putative binding of the betaine monomer.[166]

First, the cationic monomer was polymerised with a hydrophilic monomer (DHPMA). Initially they were polymerised using standard AGET ATRP to yield polymer **P2** this was then compared to the b-ATRP polymers **P8-WE**, **P8-SE**, **P8-WP** and **P8-SP**. This comparison was used by comparing the integrals of 2 protons of the glycerol adjacent to the hydroxyl to the protons of adjacent to the ester in the quaternary monomer METAC (Figure 7.4).

This was done for all the polymers and the results of which are shown in Table 7.4. When the non-binding DHPMA monomer was included in the polymerisations the templating effects seen are still present, especially in the case of *E. coli*.

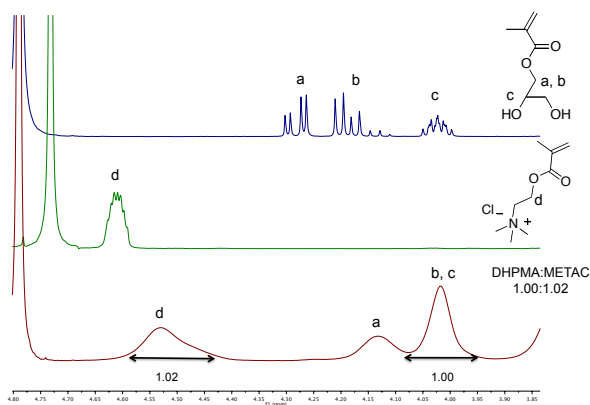


Figure 7.4: Representative example of co-polymer composition calculation of METAC and DHPMA for polymer **P2**.

Table 7.4: Analysis of polymer composition for METAC and DHPMA. Ratios are expressed as (DHPMA:METAC)

| Polymer | Monomer feed (DHPMA:METAC) | Conversion (%) | Composition (DHPMA:METAC) |
|--------------|-------------------------------|-------------------|------------------------------|
| P2 | 1.00 : 1.49 | 37 | 1.00 : 1.02 |
| P8-WE | 1.00 : 1.49 | 38 | 1.00 : 0.96 |
| P8-SE | 1.00 : 1.49 | 38 | 1.00 : 1.24 |
| P8-WP | 1.00 : 1.49 | 29 | 1.00 : 0.86 |
| P8-SP | 1.00 : 1.49 | 29 | 1.00 : 0.98 |

These data demonstrate further that the inclusion of the cationic monomer can be increased during the polymerisations with the bacteria. The increase is observed in the salt washed polymers which are those purported to be obtained from the bacterial surface. The reason for its increase is explained, as before, due to its electrostatic interaction with the bacterial cell. The effects viewed, are most dramatic with the *E. coli* suggesting its surface has a greater negative charge.[175, 176] Again it can be seen that the polymers removed from the bacterial surface were also more poly-disperse (e.g. P8-WE PDI = 3.87) than those found in solution (e.g. P8-SE PDI = 5.32).

The interaction between bacteria such as *E. coli* and monomers such as MEDSA has been discussed in the literature although it has been reported to prevent bacteria adhering to polymer coated surfaces[177, 130] whilst at the same time this same monomer has also been implicated in binding to other bacteria.[166] This information may explain a reduction in the inclusion of the binding, cationic monomer during the MEDSA and METAC polymerisations. The betaine monomer, whilst not binding strongly to bacteria may facilitate the weak attraction of the growing polymer chain towards the bacteria. However when this monomer is substituted for the hydrophilic bystander monomer, such transient interactions become less favourable. For this reason it can be demonstrated that templating with the quaternary monomer is observed. In order to assess if MEDSA can be templated the monomer was also polymerised with b-ATRP as a co-polymer with the monomer DHPMA to investigate if it does interact with bacteria as is suspected. Further to polymerisation the composition was analysed in the same way as for the DHPMA/METAC polymer as shown in Figure 7.5.

The differences between the polymer compositions shown in Table 7.5 shows that with *E. coli* and to a lesser extent *P. aeruginosa*, the presence of the betaine charge helps facilitate templating. This is supported by the data shown in Table 7.3. In the analysis of the polymers of both betaine and cationic functionalities the *P. aeruginosa* templated polymers showed greater inclusion of the cationic monomer versus the betaine monomer. This suggested that the betaine monomer had a

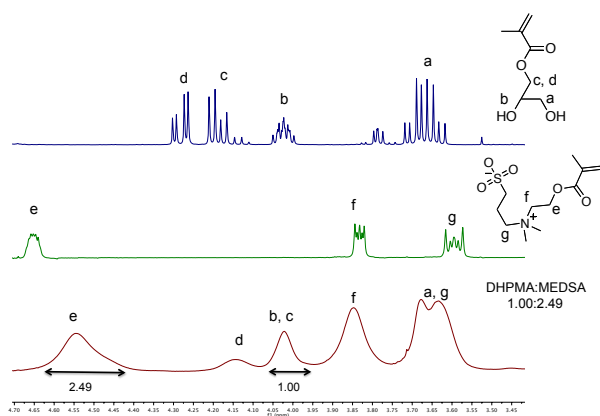


Figure 7.5: Representative example of co-polymer composition calculation of MEDSA and DHPMA for polymer **P3**.

Table 7.5: Analysis of polymer composition for METAC and DHPMA. Ratios are expressed as (DHPMA:MEDSA)

| Polymer | Monomer feed (DHPMA:MEDSA) | Conversion (%) | Composition (DHPMA:MEDSA) |
|--------------|-------------------------------|-------------------|------------------------------|
| P3 | 1.00 : 2.75 | 38 | 1.00 : 2.49 |
| P9-WE | 1.00 : 2.75 | 35 | 1.00 : 2.32 |
| P9-SE | 1.00 : 2.75 | 35 | 1.00 : 3.01 |
| P9-WP | 1.00 : 2.75 | 31 | 1.00 : 2.26 |
| P9-SP | 1.00 : 2.75 | 31 | 1.00 : 2.68 |

greater level of interaction with the *E. coli* cell. When the templating polymerisation was carried out with the betaine monomer (MEDSA) and the non-binding DHPMA what is observed is that the salt washed polymer had a greater inclusion of MEDSA compared to the water washed polymer. This is particularly the case with *E. coli*. These results suggest that the *E. coli* cell would have a greater negative charge on the surface as it interacts stronger with METAC, which is supported by various reports in the literature relating to the subject.[175, 176] As said, this also explains the apparent decrease in the proportion of METAC found in the *E. coli* templated polymers when both METAC and MEDSA were polymerised with both bacteria. The polymers again removed from the bacterial surface were more polydisperse (e.g. P9-WE PDI = 4.45) than those found in solution (e.g P9-SE PDI = 7.25).

Once templated polymers were produced (whose composition varied), it was then necessary to investigate how this difference in composition, could translate into differences in binding behaviour. Using the Coulter Counter it was possible to observe not only the presence of aggregates but the size of the aggregates could be quantified. The investigations using the Coulter Counter was supported by microscopy.

As can be seen Figure 7.6 the bacteria when suspended in deionised water were found in populations of few bacteria aggregated together as each bacterium has an approximate diameter of 1 μm . This may be larger or smaller for a single bacterium as the coulter counter assumes spherical particles and both bacterial strains are rod shaped. It can also be seen that *P. aeruginosa* PAO1 pmE6032 GFP auto-aggregates to a greater extent than *E. coli* MG1655 mCherry.

As can be seen in Figure 7.7 the non-templated polymer produces a general broad aggregation behaviour where cell clusters range from single cells to multiple. This result indicates that the binding of **P1** is moderate although very general. It can be explained by the presence of binding groups distributed randomly throughout the chain; large clusters are formed where the cationic group is concentrated and where there are few of them, smaller clusters are formed.

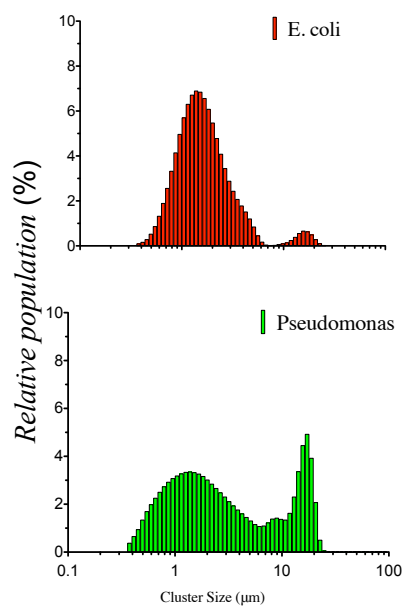
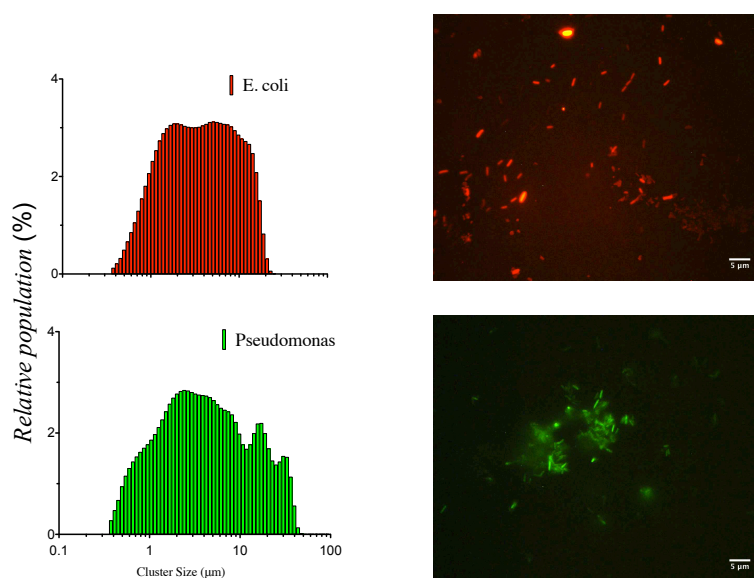


Figure 7.6: Bacteria population sizes with no polymer.

Figure 7.7: Aggregation behaviours of *E. coli* MG1655 mCherry and *P. aeruginosa* PAO1 pmE6032 GFP with P1

The aggregation behaviour of the templated polymers were then analysed in the same way.

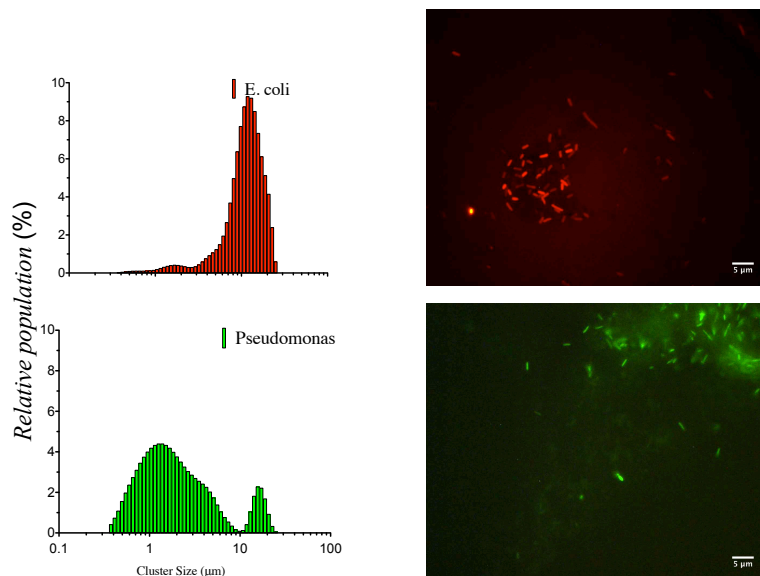


Figure 7.8: Aggregation behaviours of *E. coli* MG1655 mCherry and *P. aeruginosa* PAO1 pmE6032 GFP with **P7-WE**

With polymer **P7-WE** which should be poorly templated however a difference in aggregation behaviour between *E. coli* MG1655 mCherry and *P. aeruginosa* PAO1 GFP can be observed. This data suggests that templating has occurred even with the polymer which was removed during the water washing steps after templating for *E. coli*. This contrasts where it appears that to aggregation profile for *P. aeruginosa* is the same as the cells only in water. It would be expected that the polymer only removed during the salt washes i.e. those polymers which are most strongly bound should exhibit templating.

The unusual aggregation behaviour with **P7-SE** indicates that with increased inclusion of the cationic monomer (METAC) there is increased binding across both bacteria strains. The templating process which occurred produced an avid bacterial binding polymer but lacks discrete microbial differentiation. It should be noted however that more of the *E. coli* cells were shifted into an aggregated state and also into larger clusters than those for *P. aeruginosa*, which as explained previously

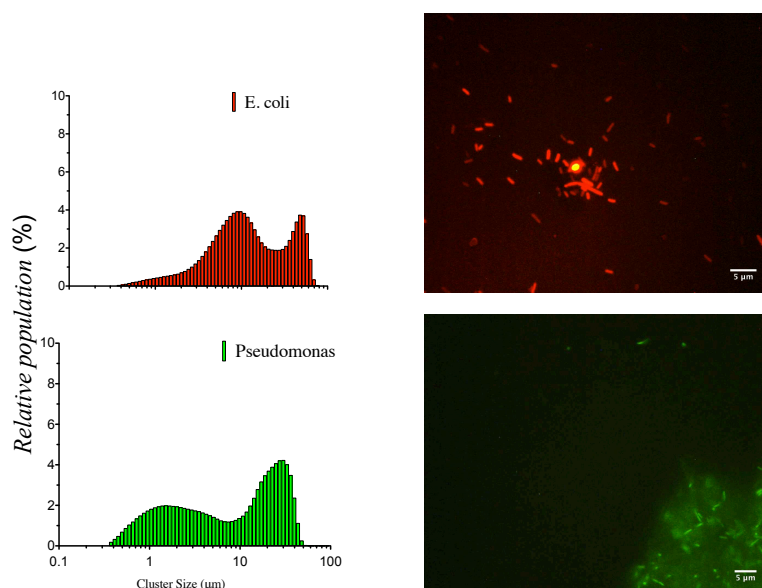


Figure 7.9: Aggregation behaviours of *E. coli* MG1655 mCherry and *P. aeruginosa* PAO1 pmE6032 GFP with **P7-SE**

is due to the increased betaine content, which although a poor binding monomer still binds *E. coli* more than *P. aeruginosa*. And so templating with both monomers is demonstrable.

The *P. aeruginosa* templated polymers **P7-WP** and **P7-SP** were also investigated for their ability to bind both their templated bacterium and *E. coli*.

When incubated with **P7-WP** we find that the interaction between the *E. coli* and the polymer is lowest and moderate for *P. aeruginosa* (Figure 7.10). If the composition of the polymer is analysed as shown in Table 7.3 the content of METAC is lower than for other templated polymers. Despite this, the result suggests that templating for *P. aeruginosa* was moderate perhaps there may be a degree of sequencing. Sequencing in this case may be where pockets of high binding monomers are clustered together during templating which compares with the random monomer sequence in the non-templated polymer **P1** and also most likely polymer **P7-WP**.

In the case of polymer **P7-SP**, the most avid bound polymer removed from the *P. aeruginosa* surface during successive salt washes, it can be seen that it induces greater aggregation in its

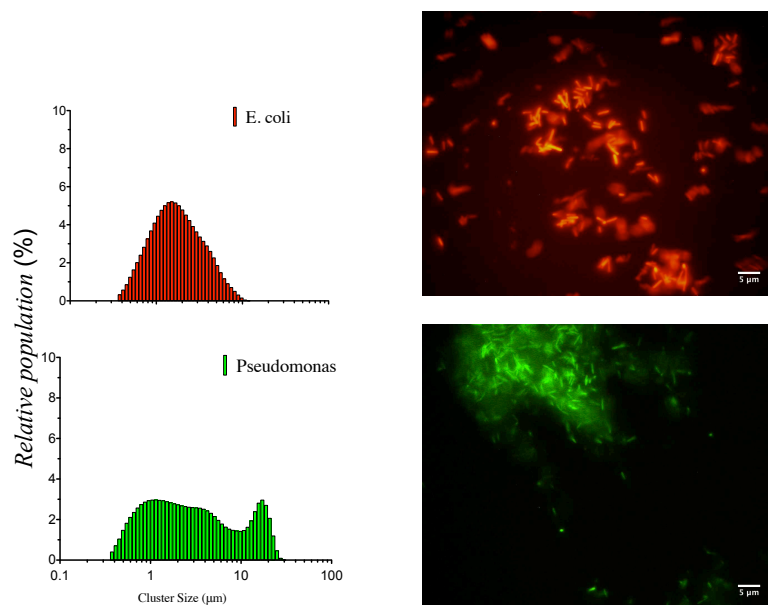


Figure 7.10: Aggregation behaviours of *E. coli* MG1655 mCherry and *P. aeruginosa* PAO1 pmE6032 GFP with **P7-WP**

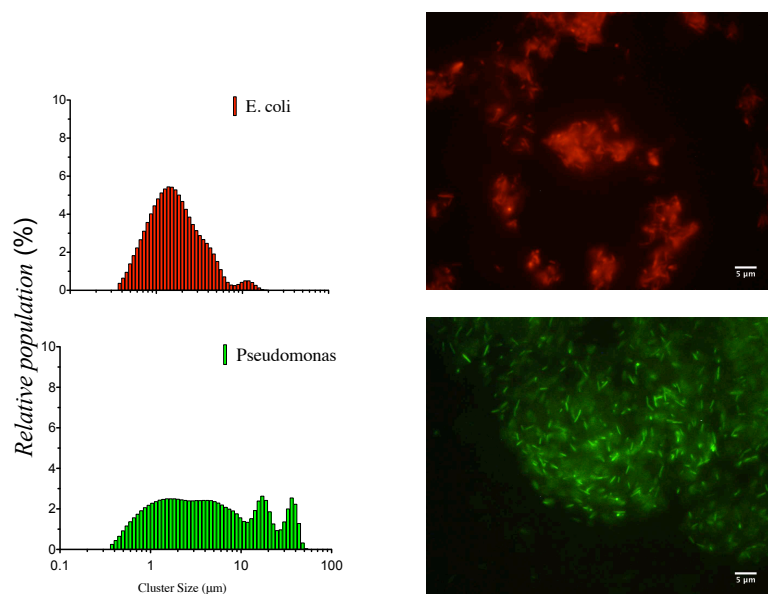


Figure 7.11: Aggregation behaviours of *E. coli* MG1655 mCherry and *P. aeruginosa* PAO1 pmE6032 GFP with **P7-SP**

template compared to with **P7-WP**, yet less with the *E. coli* according to the coulter counter (Figure 7.11). However, by microscopy we see that it is capable of forming distinct aggregates with both bacterium. This binding is greater than with **P7-WP** which may be attributed to the larger proportion of cationic charge found in this polymer (Table 7.3).

The polymer may also be utilising subtle differences in cell surface chemistries. *P. aeruginosa* and *E. coli* are both Gram-negative bacteria whose outer membrane contains features such as phospholipids to give them a negative charge. The polymer inserting into the cell wall of *P. aeruginosa* may facilitate network formation and increase aggregate size. This binding may be further facilitated by the *P. aeruginosa* inherently existing as small clumps of biofilm in suspension.[178] The *E. coli* may also require more betaine functionality in the polymer to enable strong binding as opposed to the smaller clustering viewed microscopically during the first experimental chapter, where highly cationic polymers did not result in large aggregates. The *E. coli* is constituted of structures such as lipopolysaccharides, phospholipids and lipoproteins for example[2] and these structure may interact better with the inclusion of betaine functionality. Various organic betaines have already been shown to be taken up by *E. coli*[179] which is supportive of this. Further analysis of the effects of the templated polymers upon bacterial cluster sizes can be found in the appendix.

When comparison is drawn between this data and that obtained from the aggregation assay we see a similar pattern. The *E. coli* templated polymers are bound more by their templates (Figure 7.12). This result provides further support to the success of the templating process. In this assay binding, and cross-linking of bacteria leads to the formation of bacterial aggregates which then sink under gravity. The faster they sediment the greater the binding. As seen during this assay the templated polymers induce much greater binding than the non-templated polymer and also the native sedimentation of the bacteria in water.

This result compares with the data found when the assay is repeated with *P. aeruginosa* and their templates (Figure 7.13)

In this case we see that although the templated polymer obtained during the salt wash causes

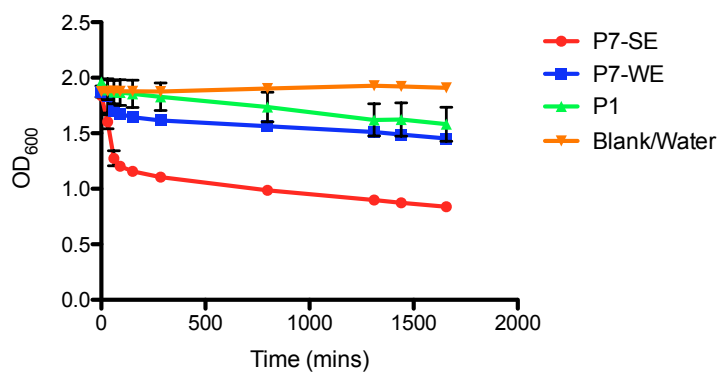


Figure 7.12: Plot of change in OD₆₀₀ against time for *E. coli* bacteria with its templated polymers, non-templated polymers and water.

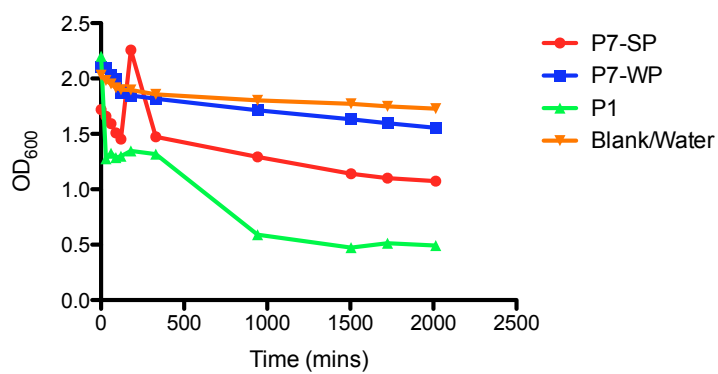


Figure 7.13: Plot of change in OD₆₀₀ against time for *P. aeruginosa* bacteria with its templated polymers, non-templated polymers and water.

indeed more aggregation than the polymer obtained from the water wash, this aggregation is not exceeded by the control polymer **P1**. It should be noted that during this experiment there was the formation of very large aggregates in sample **P7-SP** which caused the spike in the OD₆₀₀. The large aggregates sank in the cuvette and their periphery remained within the range of the laser of the spectrophotometer.

The data obtained from the aggregation assay provides further evidence that the templating of the bacteria produces polymers which differ not only in the composition but also their rebinding behaviour.

7.4 Conclusions

A novel method of activating ATRP using bacterial enzymatic reduction has been found (b-ATRP) and utilised to generate polymers. The polymerisation system was capable of using levels of copper (II) bromide as low as 4.42 ng/mL. Such systems generated polymers according to linear kinetics.

These polymers varied in their composition compared with those produced by AGET ATRP according to ¹HNMR analysis. The differences in composition reflected differences in the cell used to generate the polymer.

These differences in composition translate into differences in binding to and aggregation with bacteria. The subtle differences in composition and the large variation in binding behaviour is suggestive of differences of the sequences of monomers within the polymers chain.

Chapter 8

”Click” Chemistry applications

8.1 Introduction

The term ”*click*” chemistry was first employed by Sharpless *et al.* to define a series of spring-loaded reactions.[180] These reactions have a thermodynamic favourability such that the formation of a single product is often quantitatively produced. The reactions now known as ”click” chemistry were already previously in use, however the criteria for these reactions to be called click are now clearly defined as:

...modular, wide in scope, give very high yields, generate only inoffensive byproducts that can be removed by nonchromatographic methods, stereospecific...simple reaction conditions...”[180]

There are a number of various reactions known as ”click” chemistry including ring opening and protecting group, however the most commonly used type is that of the Huisgen 1,3-dipolar cycloaddition[181] catalysed by copper (I).[182]

The most common method by which the copper catalysed reaction takes place is by mixing the

components together along with copper (II) followed by the addition of a reducing agent like ascorbic acid to generate the copper (I) *in situ*.^[183] This method is similar to that used for AGET ATRP. The reactions are synthetically simple and thus extremely useful.

8.1.1 Applications of "click" chemistry

Industrial and pharmaceutical chemistry ideally should be simple and with high yields. The ability of "click" chemistry to generate products with selectivity and quantitatively has led to its increasing utilisation within these industries.^[184, 185, 186] It enables the rapid production of pharmaceutical libraries from analogous starting compounds to increase specificity of the lead drug core.^[187, 188] The products produced are not only chemically useful for their ease of formation but are also biologically relevant.^[189]

The ability to produce cytotoxic antimicrobials from innocuous starting compounds is of particular interest. It can be seen in the literature, where a series of antimicrobial agents whose structure is based upon the 1,2,3-triazole ring structure, that such opportunities may be possible e.g. tazobactam and cefatrizine. "Click" chemistry has already been utilised to generate novel compounds based upon a bis β -lactam and found them to have antifungal and antibacterial properties.^[190] Other groups have chosen to focus on using click chemistry for bioconjugation and tagging.^[191] This application of "click" chemistry enabled the production of specific tagging negating issues from bulky fluorescent moieties.

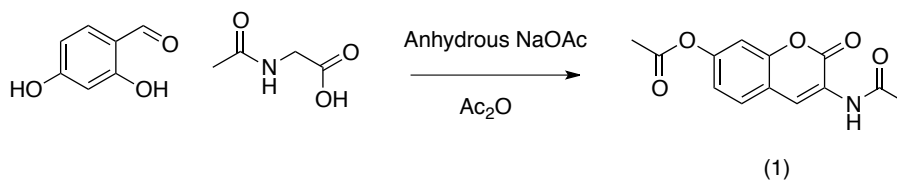
Herein, it is demonstrated how "click" chemistry can be applied to tag microorganisms in a general way. The reporter fluoresces to indicate the successful completion of the bacterial activated "click" reaction. The process demonstrates the potentially useful nature of the bacterial mediated process to engage in "click" chemistry.

Bacterial reduction potential derived from its surfaces enzymes shall be utilised as before in the activation of synthetic chemistry through reduction in transition metals. This is the first time such processes have been used in this way.

8.2 Methods

3-Azo-7-hydroxycoumarin was synthesised according to the method first described by Sivakumar *et al.* with only a slight modification of the procedure for safety purposes.[192]

8.2.1 Synthesis of 3-acetamido-2-oxo-2*H*-chromen-7-yl acetate (**1**)



Scheme 8.1: Synthesis of 3-acetamido-2-oxo-2*H*-chromen-7-yl acetate (**1**).

A mixture of 2,4-dihydroxy benzaldehyde (2.8 g, 20 mmol), *N*-acetylglycine (2.3 g, 20 mmol) and anhydrous sodium acetate (4.9 g, 60 mmol) were added to 100 mL of acetic anhydride in a round bottomed flask. To the flask a reflux apparatus was attached and the mixture heated with stirring until reflux occurred. The mixture was then left to reflux for 4 hours until the reaction had completed and a colour change was observed from light yellow to red. After cooling ice was added to the mixture and it was left overnight to produce a highly crystalline yellow solid **1** (2.70 g, 10.4 mmol Yield 51%).

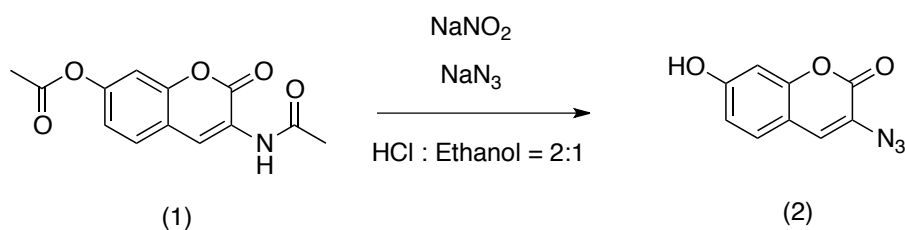
IR (KBr) ν (cm⁻¹) = 3342, 1760, 1720, 1682, 1536, 1373, 1252, 1209, 1157, 916

¹HNMR (400 MHz, CDCl₃): δ (ppm) = 2.25 (s, 3H, (NHCO), 2.34 (s, 3H, (OCOCH₃), 7.06-7.09 (dd, J = 2.23 Hz, 1H, CHCN), 7.13 (d, J = 2.27 Hz, 1H, CHCO), 7.50-7.52 (d, J = 8.47 Hz, 1H, COCH), 8.02 (s, 1H, (NH), 8.67 (s, 1H, (CHC).

^{13}C NMR (100 MHz, CDCl_3): δ (ppm) = 21.11 (1C, CH_3), 24.74 (1C, CH_3), 110.08 (1C, CH), 117.63 (1C, C), 119.63 (1C, CH), 122.72 (1C, CH), 123.56 (1C, CH), 128.37 (1C, C), 150.12 (1C, C), 151.35 (1C, C), 158.48 (1C, CO), 168.86 (1C, CO), 169.35 (1C, CO).

Calculated Mass ($\text{C}_{13}\text{H}_{11}\text{NO}_5$) $[\text{M}-\text{H}^+]$: 261.2314 Mass Found (m/z): 260.9206

8.2.2 Synthesis of 3-azo-7-hydroxycoumarin (**2**)



Scheme 8.2: Synthesis of 3-azo-7-hydroxycoumarin (**2**).

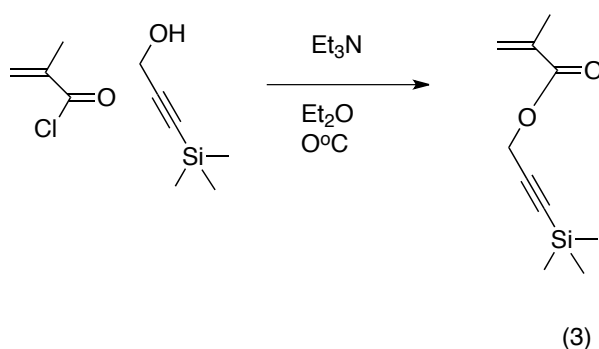
The protected coumarin **1** (2.65 g, 10.1 mmol) was dissolved in a mixture of concentrated hydrochloric acid and absolute ethanol (30 mL) in a ratio of 2:1. To the flask, reflux apparatus was attached. The mixture was heated with stirring until reflux occurred and the mixture was left to reflux for 60 minutes. After this time had elapsed ice water (40 mL) was added and then sodium nitrite (2.76 g, 40.0 mmol). This mixture was left to react for 20 minutes before the pH was adjusted to 6.7 in an ice bath with the frequent addition of ice to the bath. This pH adjustment was done to prevent the evolution of hydrazoic acid (HN_3) gas which is both toxic and explosive. Once the pH had reached a safe value of 6.7, sodium azide (3.90 g, 60.0 mmol) was added very slowly in small portions before the mixture was then left to react for a further 15 minutes. The crude product was extracted into ethylacetate (200 mL x 6) before being purified by flash chromatography (CC, SiO_2) using a solvent gradient of ethyl acetate to petroleum ether to yield the product **2** (180 mg, 0.886 mmol, Yield: 8.73%)

IR (KBr) ν (cm^{-1}) = 3425 (broad), 2922, 2120, 1680, 1623, 1319, 1343, 1259, 1224

^1H NMR (400 MHz, CDCl_3): δ (ppm) = 6.71 (d, J = 2.1 Hz, 1H, CHCOH), 6.78 (dd, J = 8.5 Hz, 2.3, 1H, CH), 7.35 (d, J = 3.4 Hz, 1H, CH), 7.37 (s, 1H, CHN_3)

^{13}C NMR (100 MHz, CDCl_3): δ (ppm) = 102.50 (1C, CH), 111.80 (1C, CH), 114.25 (1C, C), 121.61 (1C, CN_3), 128.32 (1C, C), 129.56 (1C, CH), 153.22 (1C, CO), 157.77 (1C, C), 160.73 (1C, COH).

8.2.3 Synthesis of 3-(trimethylsilyl)prop-2-yn-1-yl methacrylate (**3**)



Scheme 8.3: Synthesis of 3-(trimethylsilyl)prop-2-yn-1-yl methacrylate (**3**)

The synthesis of 3-(trimethylsilyl)prop-2-yn-1-yl methacrylate was done in a manner previously reported in the literature.[125] To a flask, 3-(trimethylsilyl)propargyl alcohol (11.6 mL, 78.0 mmol) and anhydrous triethylamine (14.2 mL, 101 mmol) was added with diethyl ether (50 mL). A pressure equalising addition funnel was fitted containing methacryloyl chloride (8.80 mL, 93.0 mmol). The round bottomed flask was cooled over ice before the methacryloyl chloride was added drop-wise under nitrogen. When all of the methacryloyl chloride had been added the mixture was lifted from the ice and left to react for 24 hours. After this time the precipitate was filtered and disregarded, then the solvent was removed under vacuum. The crude product was purified further using flask chromatography (CC, SiO_2 , petroleum ether then petroleum ether : diethyl ether = 50 : 1) to give monomer **3** (8.34 g 42.5 mmol Yield: 54%)

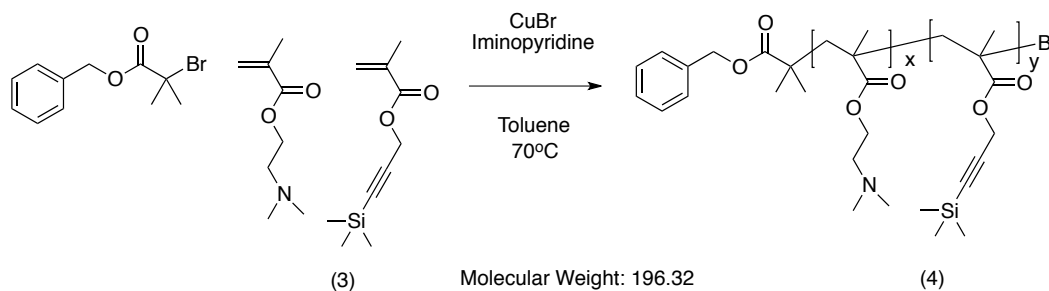
IR (neat) ν (cm^{-1}) = 2960, 2832, 2185, 1717, 1678, 1451, 1366, 1315, 1293, 1251, 969, 944,

881, 761, 700, 645

^1H NMR (400 MHz, CDCl_3): δ (ppm) = 0.17 (s, 9H, $\text{Si}(\text{CH}_3)_3$), 1.95 (s, 3H, CH_3), 4.75 (s, 2H, CH_2), 5.6 (s, 1H, CH), 6.1 (s, 1H, CH).

^{13}C NMR (100 MHz, CDCl_3): δ (ppm) = 0.48 (3C, $(\text{CH}_3)_3$), 18.07 (1C, CH_3), 52.69 (1C, CH_2), 91.48 (1C, CH), 99.18 (1C, CH), 125.98 (1C, CH), 135.63 (1C, C), 166.06 (1C, C)

8.2.4 Polymerisation of 2-(dimethylamino)ethyl methacrylate (DMAEMA) and 3-(trimethylsilyl)prop-2-yn-1-yl methacrylate (4)

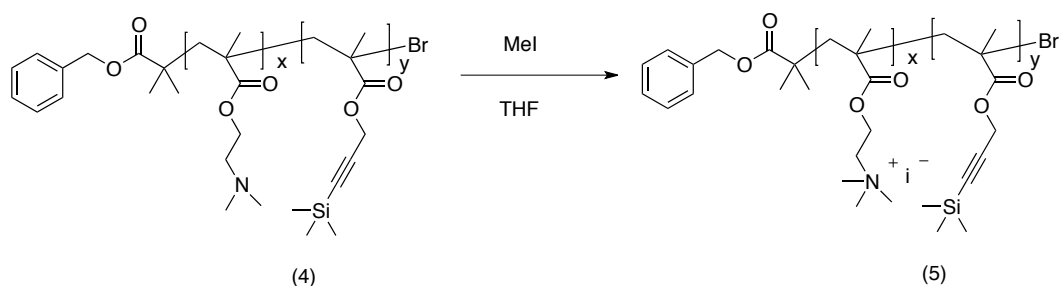


Scheme 8.4: Polymerisation of 2-(dimethylamino)ethyl methacrylate and 3-(trimethylsilyl)prop-2-yn-1-yl methacrylate (TMSPMA) (**3**) by ATRP. Theoretical ratio: $x = 10.59$, $y = 1$, ratio by ^1H NMR $x = 13.85$, $y = 1$

2-(Dimethylamino)ethyl methacrylate (9.33 g, 59.3 mmol), 3-(trimethylsilyl)prop-2-yn-1-yl methacrylate (**3**) (1.1 g, 5.6 mmol), (E)-N-(pyridine-2-ylmethylene)octan-1-amine (iminopyridine ligand) (546 μL , 2.37 mmol), benzyl-2-bromo-2-methylpropanoate (305 mg, 1.19 mmol) were charged into a large dry Schlenck tube along with toluene (10 mL) as solvent. The tube was sealed with a rubber septum and subjected to five freeze-pump-thaw cycles. At the end of the degassing the mixture was left frozen, flushed with nitrogen and copper (I) bromide (170 mg, 1.19 mmol) was added. The system was then subjected to three nitrogen/vacuum cycles with freezing and thawing, then the reactor was filled with nitrogen and the temperature adjusted to 70°C with constant stirring ($t = 0$). At the end of the polymerisation the reactor was opened and air was allowed to enter the

system, causing the copper catalyst to oxidise to Cu(II) and effectively stopping the polymerisation reaction. During this process the flask was lifted from the bath and the temperature reduced to ambient. The mixture was then passed through two neutral alumina columns in order to remove residual Cu(II) salts present in the reaction mixture. The volume was reduced under vacuum and then the polymer obtained through precipitation into petroleum ether. The polymer was analysed by gel permeation chromatography. M_n (GPC) = 9.2 kDa, PDI (GPC) = 1.28, Conversion 21%

8.2.5 Quaternisation of poly((DMAEMA)-co-(TMSPMA)) (5)

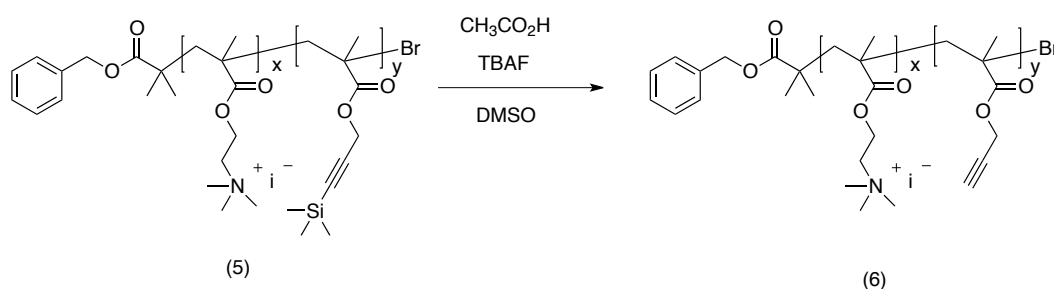


Scheme 8.5: Quaternisation of polymer (4) using methyl iodide. Ratio by $^1\text{HNMR}$ $x = 13.85$, $y = 1$

Polymer **4** (1.8g) was dissolved in tetrahydrofuran (50 mL) with a magnetic stirring bar. The flask was sealed with a rubber septum and methyl iodide (914 μL , 14.69 mmol) was added. The mixture was left to react for 48 hours. After this time the flask was opened and the solvent removed under reduced pressure to yield a yellow solid **5** (poly((TMAEMA)-co-(TMSPMA))). The quaternisation of the polymer was confirmed using $^1\text{HNMR}$ spectroscopy.

8.2.6 Deprotection of poly((TMAEMA)-co-(TMSPMA)) (6)

Polymer **5** (1.3 g) was dissolved in water (20 mL) with a magnetic stirring bar. To this mixture 500 μL (8.73 mmol) of glacial acetic acid were added followed by 8 mL of a 1 M solution of tetra-*n*-butylammonium fluoride. The reaction mixture was stirred with continual monitoring by $^1\text{HNMR}$



Scheme 8.6: Removal of trimethylsilyl (TMS) protecting group from poly((TMAEMA)-co-(TMSPMA))

for the disappearance of the TMS protecting group. After 16 hours the polymer was completely deprotected. To the mixture, water (10 mL) was added and the solution dialysed against sodium chloride for 3 days followed by 3 days of deionised water before freeze drying.

8.2.7 Bacterial mediated "click" reaction

The bacteria for the reaction were grown in a manner similar to that used for the templating polymerisations.

Fresh *E. coli* were streaked from the bacterial stocks stored at -80°C onto LB agar plates. These were allowed to grow overnight at 37°C until colonies were visible. A single representative colony was removed and used to inoculate 5 mL of pre-warmed autoclaved LB media. This was incubated for 8 hours at 37°C and this primary culture was used to inoculate 500 mL of pre-warmed autoclaved media. This was incubated with agitation for 20-24 hours.

The cells were washed of media and then washed once with PBS and twice with sterile deionised water before resuspending them to a volume of 5 mL using sterile deionised water to produce the bacterial experimental stock.

The 3-azo-7-hydroxycoumarin (**2**) (5 mg, 0.0246 mmol) was dissolved in 200 μL of DMSO and the alkyne co-polymer (**6**) (50 mg) was dissolved in deionised water (2 mL) before mixing to

produce a slightly turbid, non-fluorescent mixture.

20 μL of the non-fluorescent azide-polymer mixture were added to 20 μL of the bacterial stock and used for *macroscopic* fluorescent imaging. The macroscopic imaging was done using a black, clear bottomed 96 well plate and an ultraviolet transilluminator. Comparison was drawn between the bacteria and the azide-polymer mixture singly.

The remaining stock was mixed with bacteria for *microscopic* imaging along with the components of the stock separately. The resultant polymer was obtained by washing the cells with water once and brine once.

8.3 Results and Discussion

The confirmation of a "click" reaction using the evolution of fluorescence into the system is an incredibly powerful and precise diagnostic tool. It affords the user a simple "yes" or "no" result on whether the reaction was successful or not.

The 3-azo-7-hydroxycoumarin (**2**) has a useful and relatively unique property of changing from a non-fluorescent molecule into a fluorescent moiety after "click" has been successful. To utilise this, a system was devised whereby electrostatic attraction and copper mediated click chemistry could fluorescently tag bacteria. This process would be mediated by the bacterial biochemical machinery. As such an experimental plan was designed to utilise a difunctional polymer and the non-fluorescent coumarin azide derivative according to Figure 8.1.

The difunctional polymer synthesised in Scheme 8.4, Scheme 8.5 and Scheme 8.6 contains two useful moieties towards the desired fluorescent tagging shown in Figure 8.1. The polymer contains a nitrogen which has been permanently modified to have a cationic charge which is suitable for binding to the bacteria in a highly avid manner. It also contains an alkyne to which 3-azo-7-hydroxycoumarin (**20**) can react and induce fluorescence on the bacterial surface.

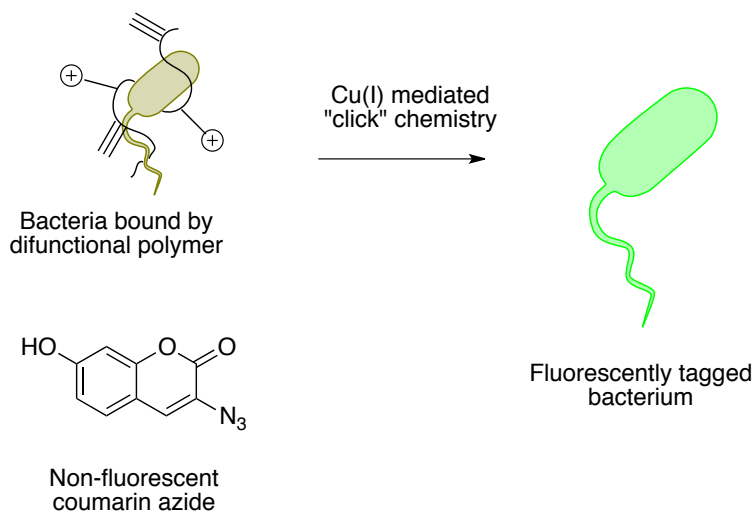


Figure 8.1: Schematic overview for bacterial mediated fluorescent bacterial tagging.

The synthesis of the azide was carried out in a manner analogous to that used by Sivakumar *et al.*[192]. The first step whereby the protected coumarin was formed required the reaction mixture to be poured over ice however yields were increased when the product was allowed to crystallise over time after the addition of ice to the reaction mixture.

The next notable deviation from the procedure outlined in the literature was the adjustment of the pH in the second step. The deprotection was carried out using concentrated hydrochloric acid before the addition of sodium nitrite to form the diazonium salt. This transformation occurs at acidic pH as it is essential in order to generate the nitrous acid *in situ*. However if the pH were to be kept so acidic the risk of an explosive reaction with sodium azide would be too high as well as the production of volatile, toxic HN_3 to justify using this reaction.

For this reaction the pH was raised to 6.7 which would undoubtedly decrease the yield as the diazonium would be less stable, moreover local increases in temperature would also decrease the yield further as substitution with water and formation of the alcohol would be facilitated by higher temperatures. However, the substitution of the diazonium with the azide was still possible and the product 3-azo-7-hydroxycoumarin (**2**) was obtained.

The azide functionality in 3-azo-7-hydroxycoumarin is extremely electron rich and as such is a potent quencher of the fluorescence of the molecule. The quenching of fluorescence using electron rich groups has been utilised by a number of groups to act as a molecular probe.[193] [194] However, further to the successful "click" reaction, the azide and alkyne are converted into triazole ring (Figure 8.2)



Figure 8.2: Schematic overview for bacterial mediated fluorescent bacterial tagging. R = methacrylate based polymer.

This conjugated ring formation greatly enhances the fluorescence of the molecule. And so the confirmation of "click" occurring can be easily identified using fluorescence.

The difunctional polymer polymer was produced using the TMS-protected alkyne monomer and DMAEMA. The TMS-protected monomer prevents any cross-linking reactions which can occur during polymer synthesis if the unprotected alkyne monomer was used instead.

The polymer was reacted with methyl iodide to attach a permanent cationic charge to the polymer and increase water solubility. Such polycations has been previously demonstrated in this thesis to induce highly avid binding to bacteria. So, this polymer will not only bind bacteria but will, further to removal of the TMS protecting group, be capable of forming the triazole ring with the azide, mediated by copper (I).

The removal of the TMS protecting group from the polymer was monitored using ^1H NMR tracking the removal of the methyls. The gradual decrease in size of the peaks corresponding to the $\text{Si}(\text{CH}_3)_3$ can be seen in Figure 8.3.

Once removed, the alkynes are then available for reaction with the azide dye. As described in the subsection on the method for bacterial mediated click, the polymer and azide when mixed were slightly turbid. This turbidity was due to the suboptimal solubility of the azide in the aqueous

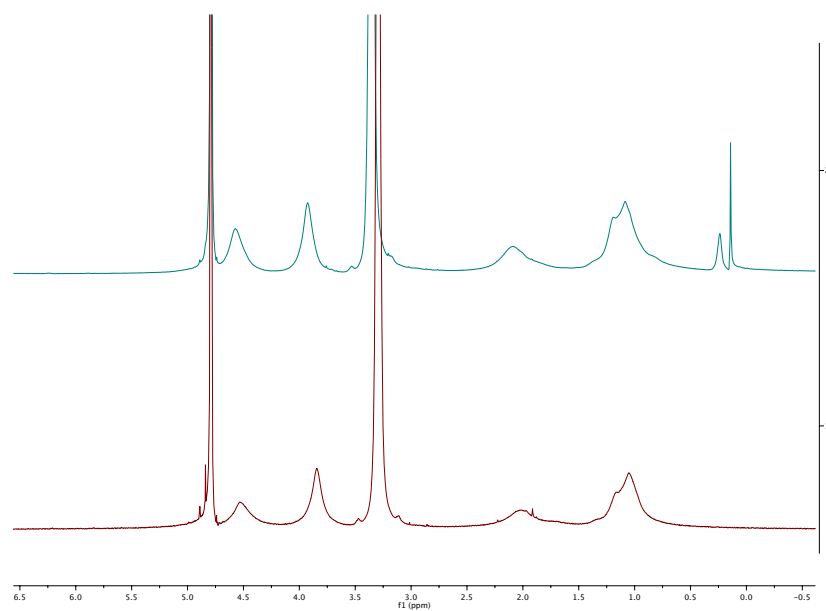


Figure 8.3: removal of the TMS protecting group from the polymer was monitored using ^1H NMR tracking the removal of the methyls.

media. It was however not possible to increase the organic solvent component of the mixture above 10%. This solvent restriction is because of the adverse effects this would have upon the stability of the *E. coli* membrane.[195]

Once the bacteria were mixed with the polymer-azide mixture the evolution of fluorescence was readily apparent as seen in Figure 8.4.

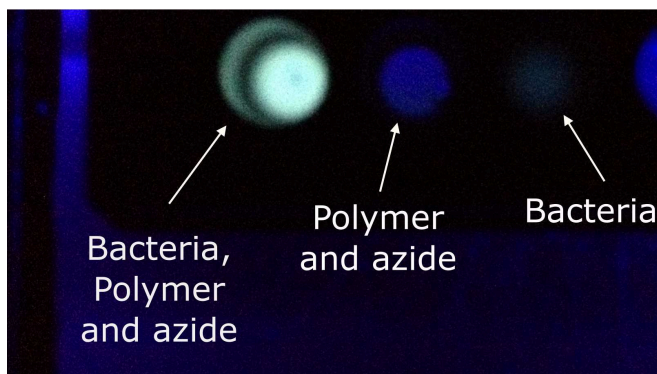


Figure 8.4: Macroscopic image of bacterial mediated "click" fluorescence using a ultraviolet transilluminator.

The production of the fluorescence as a result of the successful click was apparent within 3 minutes.

It was also possible to observe the change in fluorescence microscopically.

Microscopy was first carried out on the bacteria alone to compensate for any auto-fluorescence which may occur.[196]

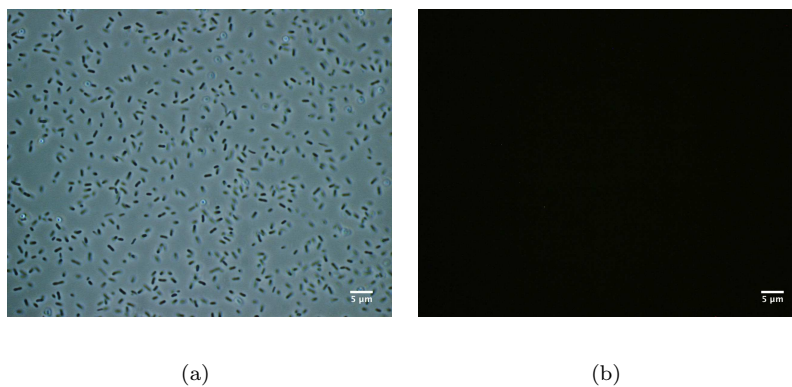


Figure 8.5: Phase contrast (a) and fluorescent (b) microscopy images of *E. coli* MG1655 with no polymer or azide present.

As can be seen in Figure 8.5 the auto-fluorescence observed using fluorescent microscopy was minimal to zero. The bacteria can also be observed as well distributed with few aggregates. Next it was necessary to ensure no fluorescence was due to any one of the chemical components added to the bacteria separately, particularly the coumarin azide.

When the bacteria were incubated with the alkyne displaying polymer no fluorescence was observed (Figure 8.6 a& b). However the formation of large bacterial aggregates made up of hundreds of bacteria demonstrates that the bacteria were bound and cross-linked by the cationic polymer due to electrostatic attraction. The final control was with the coumarin azide with the bacteria.

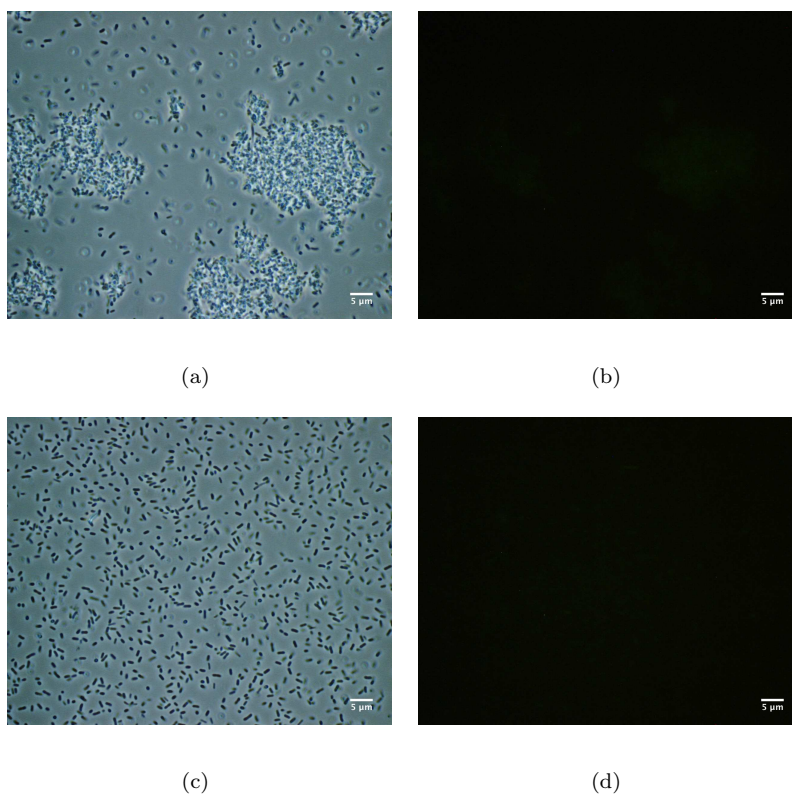


Figure 8.6: Phase contrast and fluorescent microscopy images of *E. coli* MG1655 with either alkyne polymer (6) (a & b) or 3-azo-7-hydroxycoumarin (2) (c & d).

No fluorescent bacteria were observed in the presence of the azide on its own (Figure 8.6 c & d).

All controls were thus established for each of the components for the bacterial-click system.

It was possible to state that observed fluorescence which occurs when all the components are mixed with the bacteria was therefore due to the clicking of the alkyne and azide together. As such, the microscopy was carried out with the two components together and the resulting bacterial suspension observed microscopically (Figure 8.7).

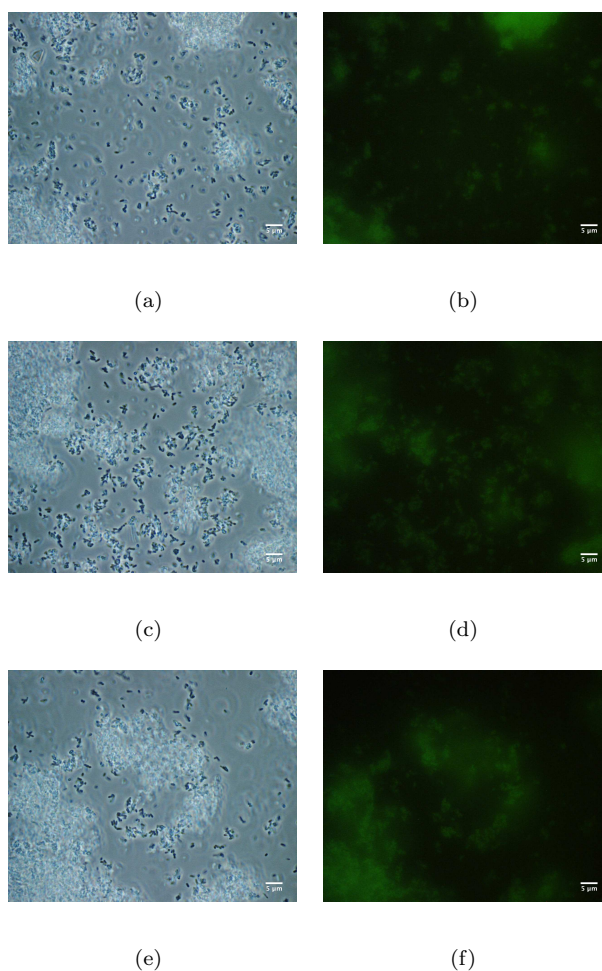


Figure 8.7: Microscopy images of *E. coli* MG1655 mixed with 3-azo-7-hydroxycoumarin (**2**) and alkyne polymer **6**.

As can be seen in all three sets of microscopic images there was a marked increase in the observed

fluorescence when both components were used. The fluorescence was also focused on the bacterial surface. This contrasts to when a non-binding fluorescent molecule is used; what is observed is a diffuse fluorescence resulting in a green hue to the whole image.

Most interestingly the click mediated fluorescence occurred *before* the addition of the copper-ligand complex. This rapid clicking may be due to several factors. Copper in trace amounts is utilised by growing bacteria as part of their respiratory cycle and so it is released and absorbed by bacterial cells.[170] There may also be the presences of low levels of copper in the de-ionised water which can participate in the click reaction. However, the most likely source of the copper was from the original synthesis of polymer **4** (Scheme 8.4) which was carried out by copper mediated ATRP. In the literature there are a number of papers by various authors which aim to reduce the remaining copper levels after the production of polymers by ATRP.[197, 198] If comparison is drawn between the polymer and typical ATRP ligands [99] which are generally organic molecules containing a nitrogen heteroatom, it can be seen they are similar. Such ligands form tight complexes with transition metals and so from this perspective it can be understood how residual copper content from the polymerisation would be difficult to remove and levels sufficient for click chemistry may remain.

So, although the addition of copper was not required, the "click" reaction was successful indicated by the presence of fluorescence. This fluorescence was attributed to the azide reacting with the alkyne on the polymer. Thin layer chromatography with ethyl acetate as the solvent showed that after the click-reaction fluorescence remained at the baseline which is indicative of a large molecule, such as a polymer, unable to move through the silica plate with the solvent.

The low levels of copper required for the "click" chemistry indicates further uses for this bacterial-mediated process. There has been reports in the literature of synthetic antibiotics produced using "click" chemistry.[199][200] In these reports the synthesis of the antibiotic molecule is carried out using a click chemistry triazole formation, similar to the cycloaddition used here.

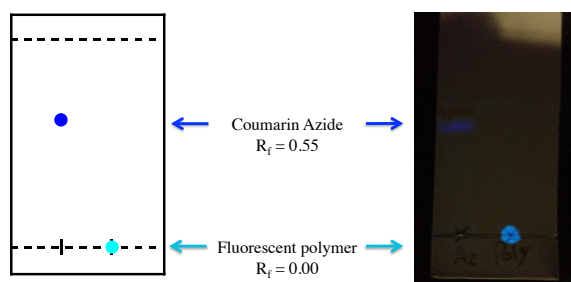


Figure 8.8: Ultraviolet image of TLC plate of the polymer after "click" and coumarin azide with the solvent of ethylacetate.

Herein, it is proposed that the cationic functionality draws the polymer towards the reductive zone on the bacterial surface and this favours the click-chemistry reaction to occur under environments with low copper concentrations and in the presence of air. The process could be adapted to generate antimicrobial compounds such as those already reported in the literature except but from benign starting materials which, once exposed to copper (I) would be clicked into a cytotoxic molecule. Such a micro-synthetic process could have the benefits of creating zones of high concentrations of the antimicrobial around the bacteria whilst sparing the neighbouring cells from the cytotoxic effects.

Further uses for this experimental design could be to develop a microbial assay whereby large numbers of strains of bacteria can be tested for their ability to reduce transition metals as a mechanism to further understand bacterial physiology and identify those bacteria susceptible to an auto-nemesis approach.

8.4 Conclusions

Bacterial reduction of transition metals has been applied to label bacteria by means of click-chemistry.

It has been demonstrated using a simple "yes" or "no" click-fluorescent molecule that bacteria can engage in this synthetic chemistry.

These experiments have given insights into other possible uses for this behaviour of bacteria to not only facilitate the production of their own binding polymers but also molecules which will cause their demise.

Chapter 9

Discussion and Conclusions

Bacteria are the cause of a significant disease burden in society as well as significant contributors to industrial and biotechnological applications. It is hard to envisage a world where a person's life is not impacted upon by the microscopic world out of human sight. During the 20th Century the introduction of cytotoxic antibiotics came into the forefront in the battle against the hidden world. However with increased and uncontrolled use in both humans and animals, the decrease in effectiveness of the chemical agents is now adversely affecting patient outcomes.[201, 202] Twenty years ago Harold Neu reported to Science there was a crisis in antibiotic resistance.[203] He predicted that as resistance grew new antibacterial agents would be required in addition to hygiene measures.

Bacterial resistance to chemical antibacterial agents is facilitated by chromosomal and plasmid modifications and horizontal gene transfer to alter bacterial enzymes and structures.[204] Such resistance mechanisms may be overcome by hijacking the bacterial enzymes which are essential to life as well as those surface features which are unable to be altered. It was therefore planned to generate bacteriospecific ligands through templating the bacterial cell.

Initial investigations during this work sought to investigate which functionalities could offer spe-

cific binding ligands in a facile manner. From the lead ligands would be selected based upon now only binding affinities but also ease of use, production and manipulation. These monomers once templated with bacteria would generate more targeted macromolecular scaffolds compared to those polymerised in a random way. This way the composition of the polymer would be dictated by the bacteria rather than chemical process characteristics such as monomer reactivity ratios. As seen in Figure 1.4 in chapter 1 there are numerous bacterial features the polymer chemist can target. A *focused design* approach was used whereby the influence of charge and carbohydrates were investigated in detail. Using the example of *E. coli* in Figure 9.1, various functionalities were identified as existing upon the bacterial binding spectrum.

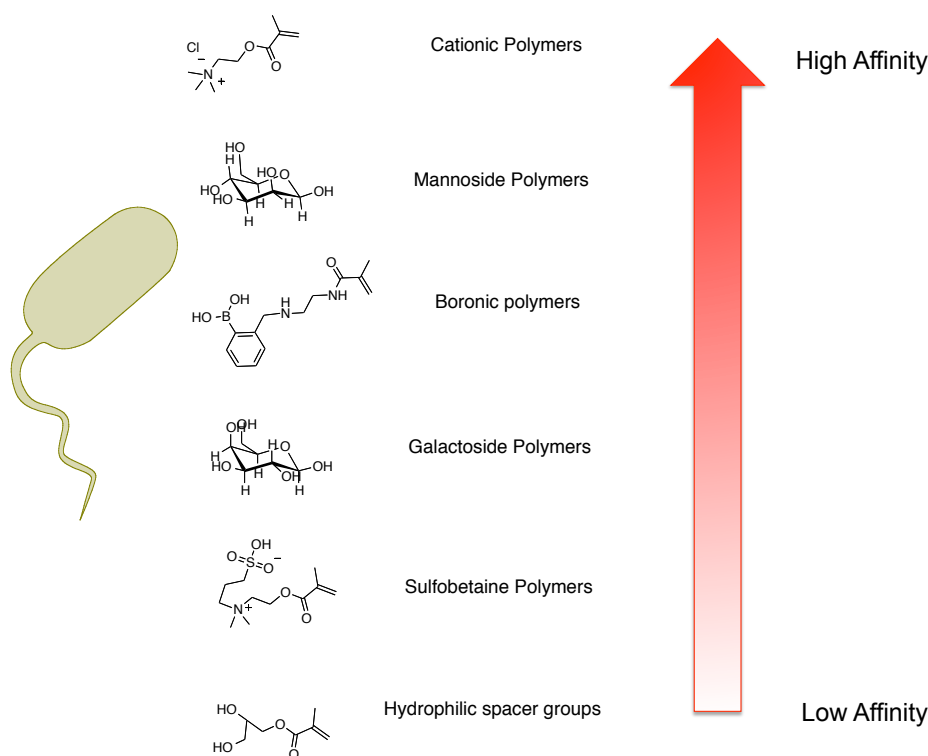


Figure 9.1: Chemical bacterial binding spectrum.

The contribution of the functionalities has been thoroughly investigated within the literature however the application of these towards generating templated linear polymers had yet to be

investigated. Other groups who have sought to template bacterial cells have focused upon generating structural templates with further enhancement of the templating through electrostatic interactions.[205, 62] Research using soft-lithography has used cells to generate surfaces where the topography is dictated by the cells.[63] This is different from the work presented here, whereby the polymer composition is dictated by cell template rather than simply the feed ratio and reactivity ratio. Within this work the principles of bacterial auto-nemesis were demonstrated through both the generation of bacterial ligands and bacterial mediated cell labelling (Figure 9.2).

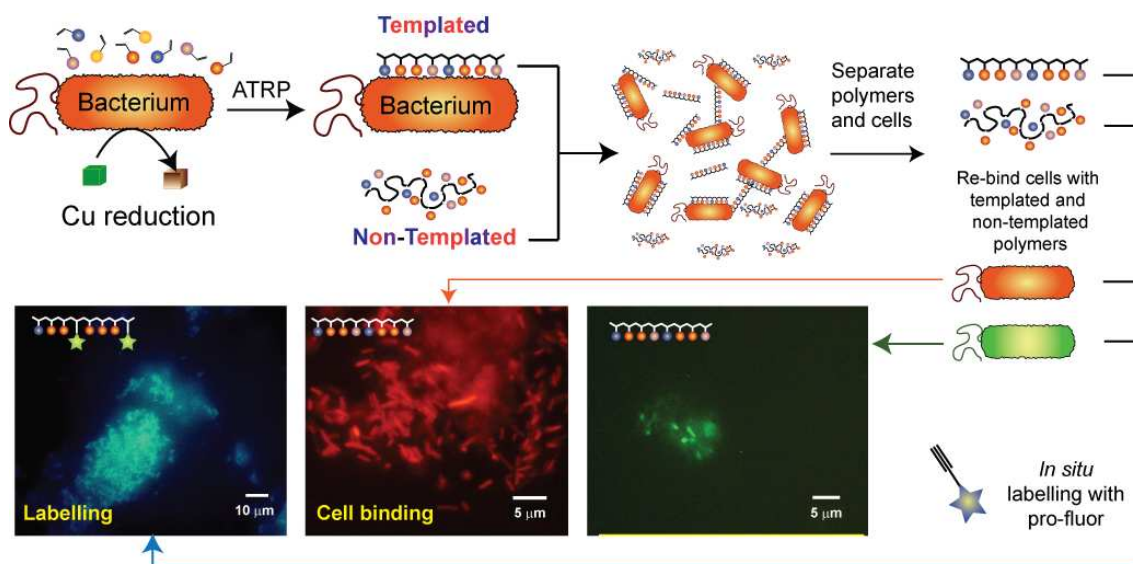


Figure 9.2: Bacterial auto-nemesis.

The templating process is required to occur at the bacterial surface. Use of bacterial enzymes in synthetic chemistry has been known for many years.[206] The principle involvement of NADH/NADH-Linked Cupric Reductase has been commonly implicated in the reduction of copper[172, 170] and other transition metals[173] by the bacterial cell.

Atom transfer radical polymerisation (ATRP), namely activator generated by electron transfer ATRP requires the reduction of the air-stable copper (II) bromide to the catalytically active Cu^{1+} species. Whilst the utilisation of biological enzymes to facilitate this process is not en-

tirely novel[169] the use of whole bacteria cells to carry it out is. The change in bacterial growth conditions was followed with time and it was noted that increasing cells numbers increased the reduction potential of the growth media. Concentrating the cells enabled polymerisations which followed linear growth kinetics whilst only requiring concentrations of copper (II) bromide as low as 4.42 ng/mL in a reaction vessel of 7-8 mL and generated templated polymers (Figure 9.3).

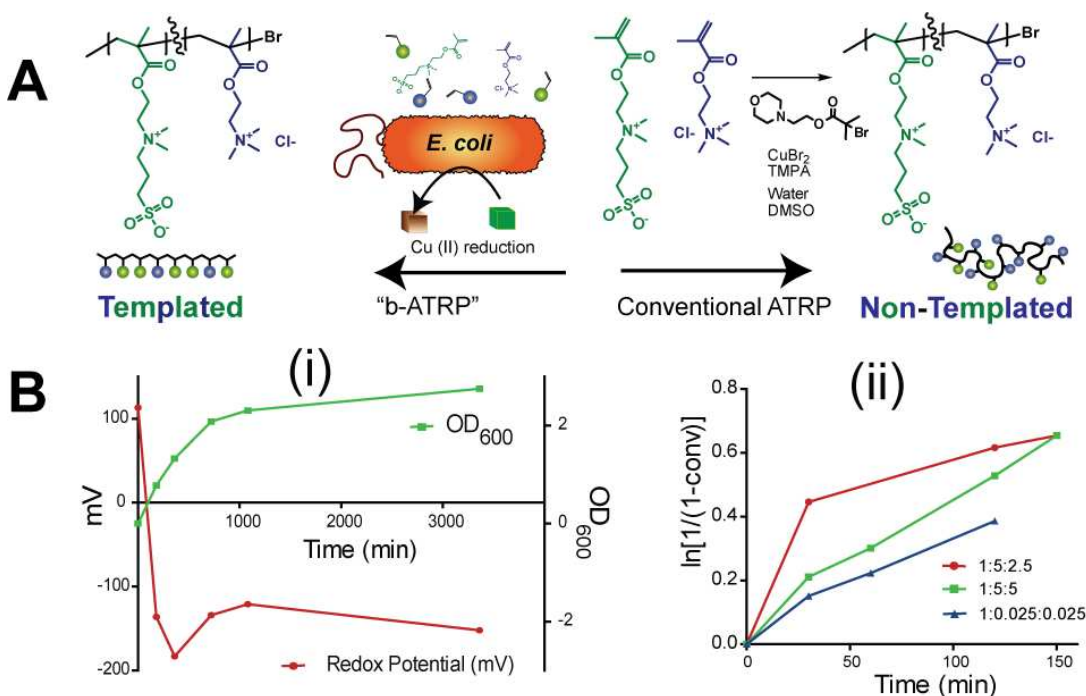


Figure 9.3: A) Bacterial ATRP to generate templated ligands versus conventional AGET ATRP to generate random non-templated polymers. B) i) Change in growth media redox potential (red) and cell numbers (OD₆₀₀) (green) against time. ii) Optimisation of b-ATRP polymerisation kinetics through alteration of initiator and catalyst ratio (Initiator : Ligand : Copper (II) bromide).

This process was possible with *E. coli* and *P. aeruginosa* cells to generate materials which were specific for their bacterial template. The specificity was determined using microscopy and particle size counting. This data is summarised in Figure 9.4. The cell and their respective templated were matched.

The benefits to generating such specific bacterial ligands could aid in both the removal and detec-

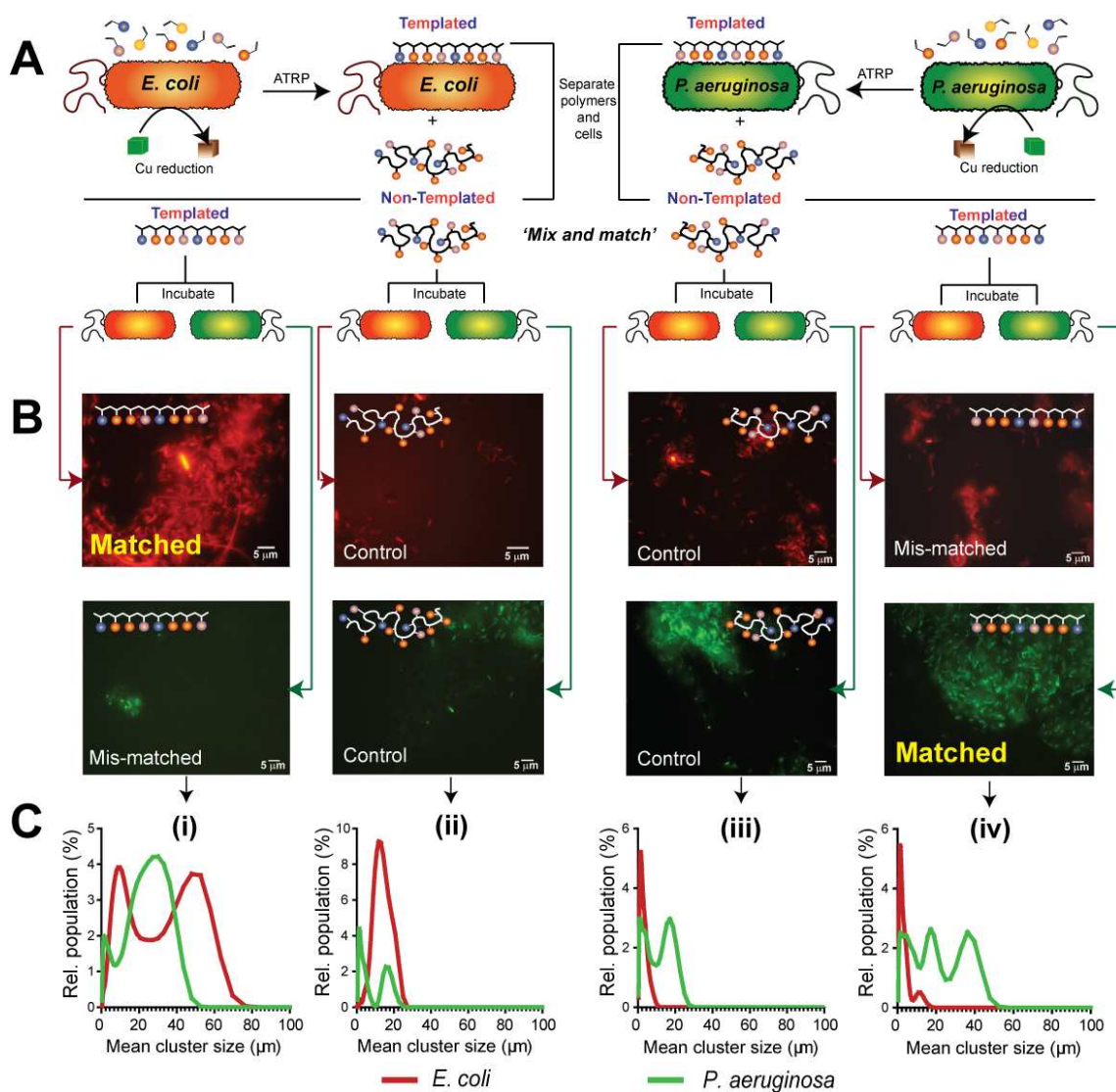


Figure 9.4: A) *E. coli* and *P. aeruginosa* cells were templated using the same bacterial ATRP process. B) *E. coli* MG1655 mCherry and *P. aeruginosa* PAO1 pmE6032 GFP fluorescent cells were used to demonstrate the aggregation behaviour due to the templated and non-templated polymers. C) Particle size analysis of the bacterial clusters were quantified to demonstrate the effect of templating upon bacterial aggregation.

tion of microbes. These have far reaching benefits towards the ongoing challenges facing clinicians and the public world wide. The same biochemical process can also be hijacked to enable cell labelling as was done so using click chemistry.

More exciting is the concept of local pro-drug activation. This could be another direction whereby the project can benefit the struggle against the bacterial resistance. It is recognised that often a limiting factor in a novel chemical entity coming to clinical use as an antibiotic is its toxicity towards non-targets cells.[207, 208] In Science, Michael Fischbach and Christopher Walsh reported on the virtual innovation void, whereby novel entities were developed only through generational advancements of old scaffolds.[209] What is needed are "new scaffolds for old targets" and also novel methods to generate cytotoxicity. Ideally these would be uninhibited by toxicity towards the human host. Bacterial transition-metal reduction and so, *click* chemistry may offer a unique method.

Compounds with antibiotic activity currently exist which contain triazole rings.[200] The development of such starting compounds shown in Figure 9.5 which display low toxicity to human cells yet, once combined yield highly cytotoxic compounds would be ideal for a novel approach towards antibiotic development. Moreover, this approach could negate the problem of peak-trough pharmacokinetics, whereby sub-therapeutic concentrations are found, promoting further bacterial resistance. This is overcome by *local* high concentrations of the compound found at the surface continually regenerated from the circulating non-toxic pool.

This method may yield in an alternative approach to the continuing problem of antibiotic resistance.

In conclusion a series of functionalities were assessed for their ability to bind a variety of pathogenic bacteria. The binding observed was found to be highly dependent on the chemical functionalities employed. Polycations offered the strongest binding but poorly specific. Boronic acid containing polymers were assessed for their ability to bind to the sugars displayed on the bacterial surface.

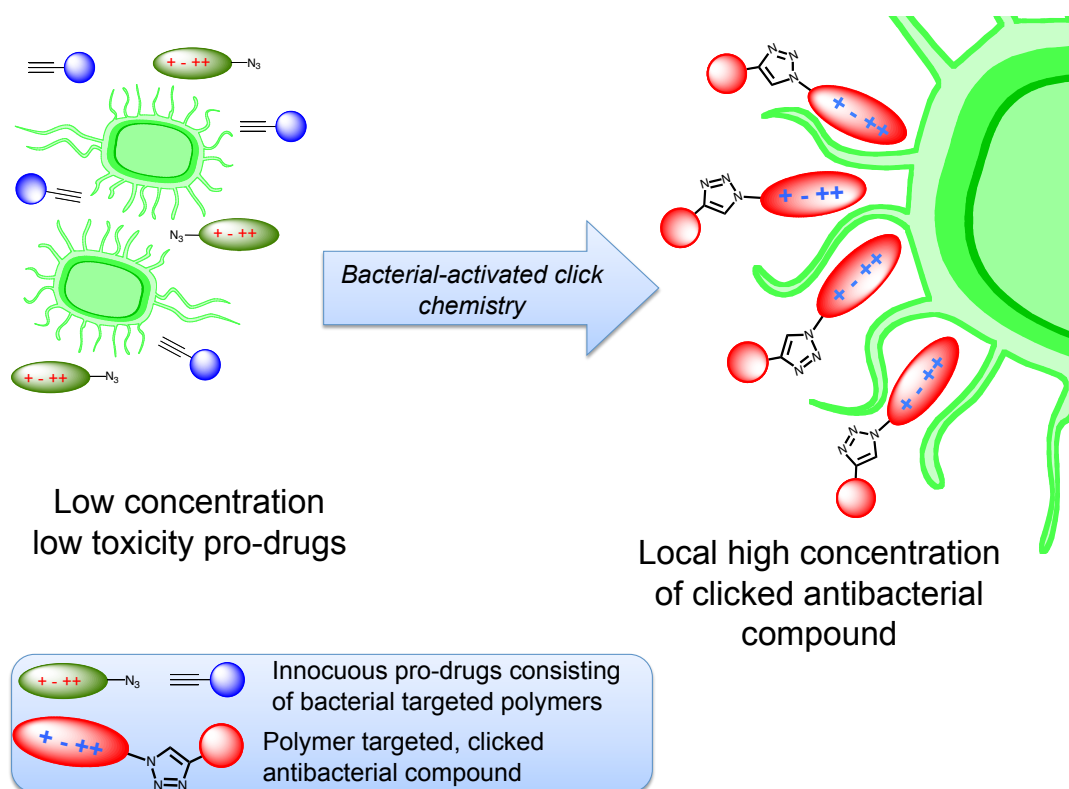


Figure 9.5: Bacterial activated of non-toxic antibiotic prodrugs into a triazole-containing antibiotic compound.

Using the enzymes found on the bacterial surface, atom transfer polymerisation was utilised to generate polymers whose composition and binding behaviour differed from those produced by conventional activator generated by electron transfer atom transfer radical polymerisation.

The same biological process were manipulated to activate click chemistry through copper reduction. This was used to fluorescently tag bacteria using dual functionality polymeric materials. This localised chemical synthetic approach could offer a novel pathway to generate cytotoxic compounds at the bacterial surface and thereby overcome bacterial resistance.

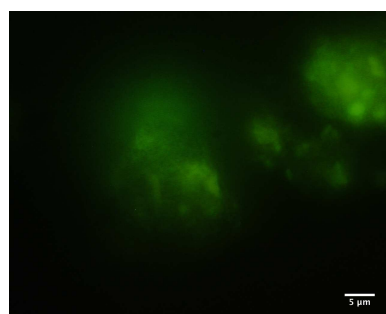
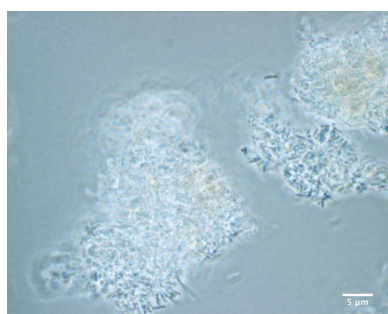
The bacterial generated polymeric ligands and bacterial activated "click" chemistry demonstrates true auto-nemesis.

Appendix A

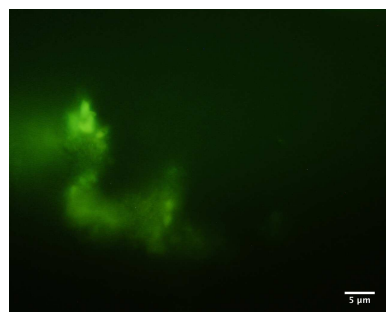
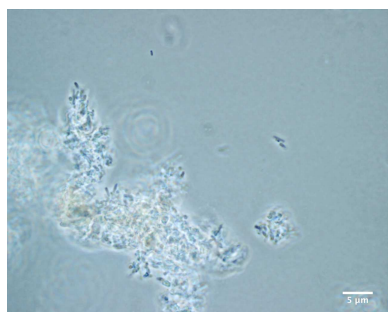
Supporting Microscopy Images

A.1 Microscopy images - Boronic investigations

A.1.1 Boronic co-polymer and controls

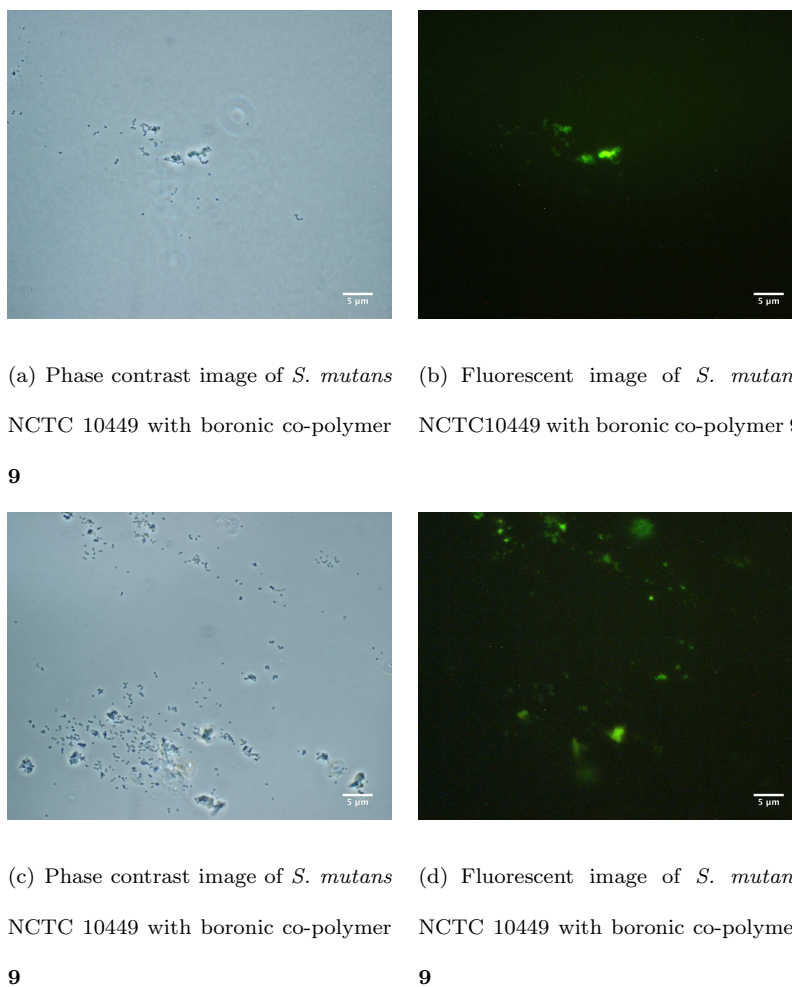


(a) Phase contrast image of *E. coli* MG1655 with boronic co-polymer **9** (b) Fluorescent image of *E. coli* MG1655 with boronic co-polymer **9**

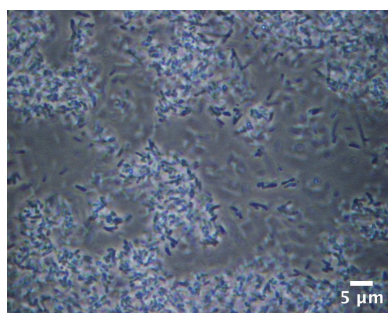


(c) Phase contrast image of *E. coli* MG1655 with boronic co-polymer **9** (d) Fluorescent image of *E. coli* MG1655 with boronic co-polymer **9**

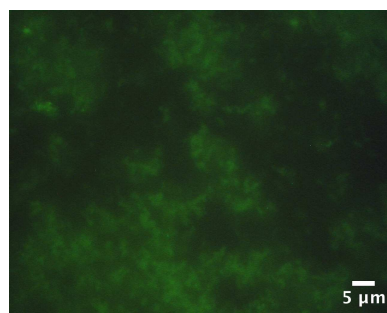
Figure A.1: Microscopy images of boronic co-polymer **9** with *E. coli* MG1655

Figure A.2: Microscopy images of boronic co-polymer **9** with *S. mutans* NCTC10449

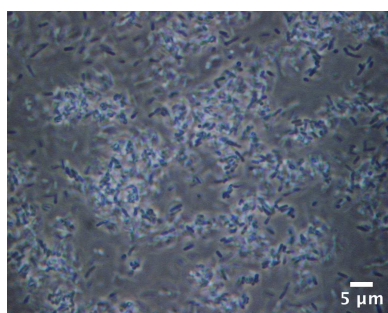
A.1.2 Microscopy image - Glycopolymers



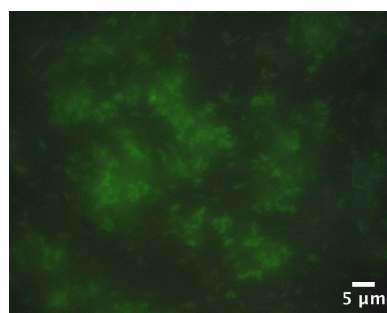
(a) Phase contrast image of *E. coli* MG1655 with mannose polymer **11**



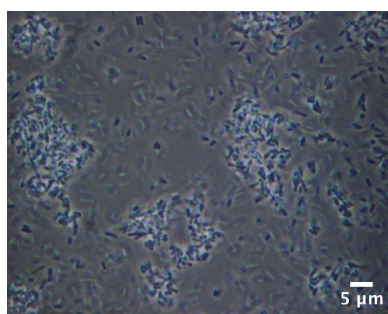
(b) Fluorescent image of *E. coli* MG1655 with mannose polymer **11**



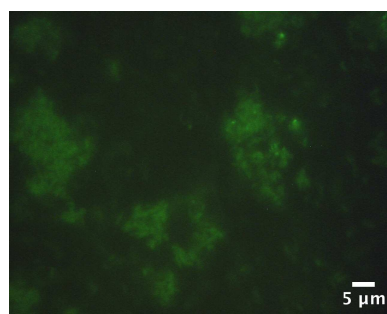
(c) Phase contrast image of *E. coli* MG1655 with mannose polymer **11**



(d) Fluorescent image of *E. coli* MG1655 with mannose polymer **11**



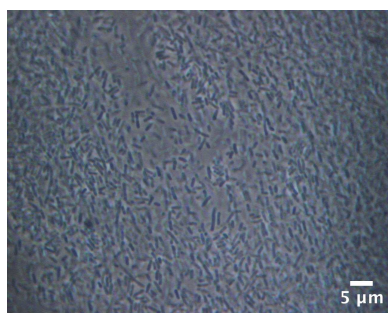
(e) Phase contrast image of *E. coli* MG1655 with mannose polymer **11**



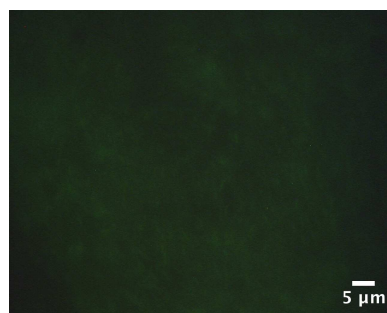
(f) Fluorescent image of *E. coli* MG1655 with mannose polymer **11**

Figure A.3: Microscopy images of mannose displaying glycopolymer **11** with *E. coli* MG1655

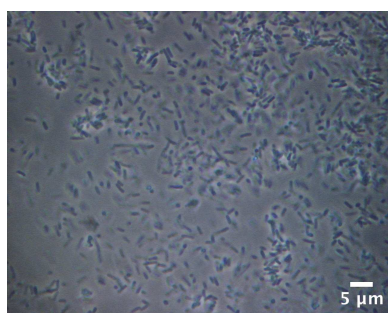
A.2 Click chemistry supporting images



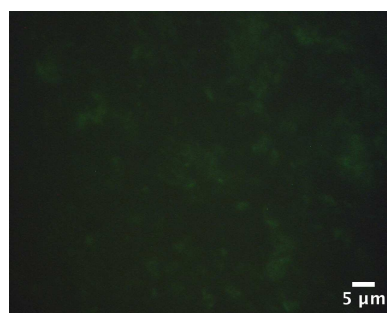
(a) Phase contrast image of *E. coli*
MG1655 with galactose polymer **12**



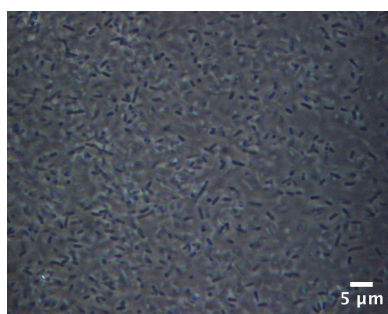
(b) Fluorescent image of *E. coli*
MG1655 with galactose polymer **12**



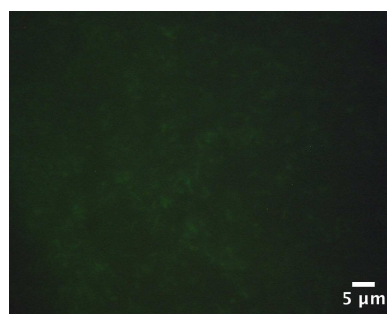
(c) Phase contrast image of *E. coli*
MG1655 with galactose polymer **12**



(d) Fluorescent image of *E. coli*
MG1655 with galactose polymer **12**

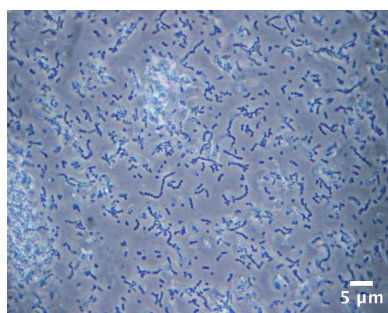


(e) Phase contrast image of *E. coli*
MG1655 with galactose polymer **12**

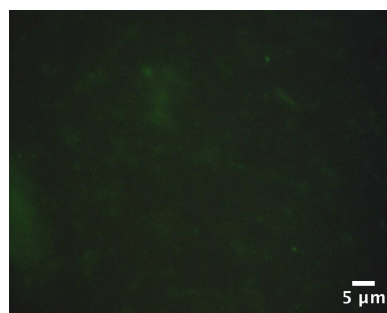


(f) Fluorescent image of *E. coli*
MG1655 with galactose polymer **12**

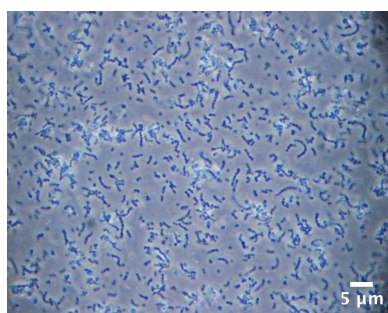
Figure A.4: Microscopy images of mannose displaying glycopolymer **12** with *E. coli* MG1655



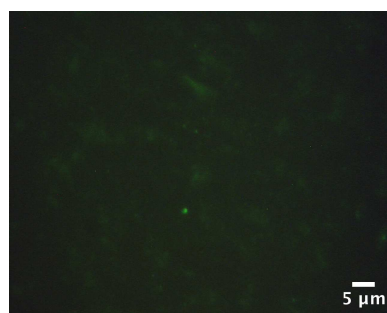
(a) Phase contrast image of *S. mutans*
NCTC 10449 with mannose polymer **11**



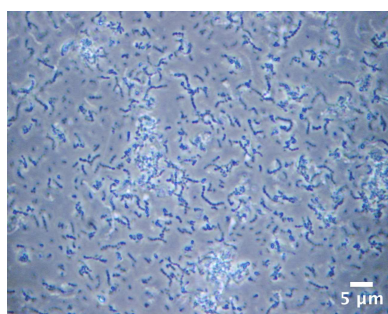
(b) Fluorescent image of *S. mutans*
NCTC 10449 with mannose polymer **11**



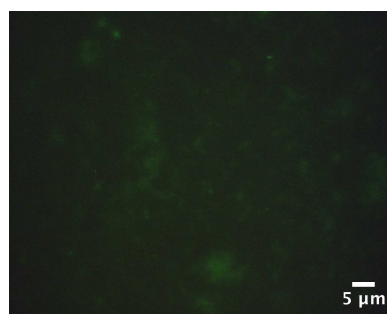
(c) Phase contrast image of *S. mutans*
NCTC 10449 with mannose polymer **11**



(d) Fluorescent image of *S. mutans*
NCTC 10449 with mannose polymer **11**

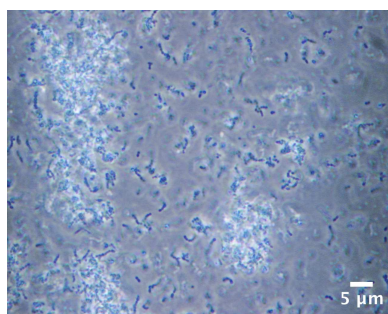


(e) Phase contrast image of *S. mutans*
NCTC 10449 with mannose polymer **11**



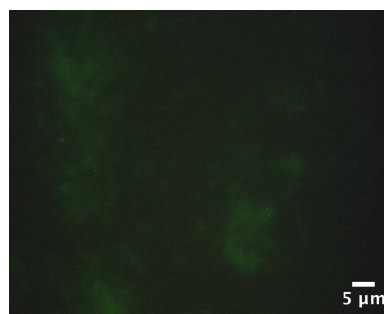
(f) Fluorescent image of *S. mutans*
NCTC 10449 with mannose polymer **11**

Figure A.5: Microscopy images of mannose displaying glycopolymer with *S. mutans* NCTC 10449



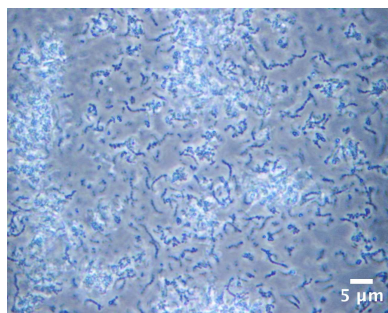
(a) Phase contrast image of *S. mutans*
NCTC 10449 with galactose polymer

12



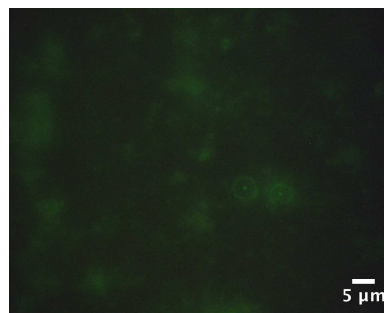
(b) Fluorescent image of *S. mutans*
NCTC 10449 with galactose polymer

12



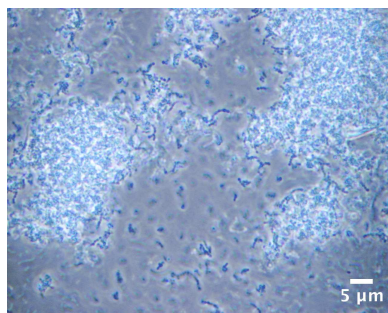
(c) Phase contrast image of *S. mutans*
NCTC 10449 with galactose polymer

12



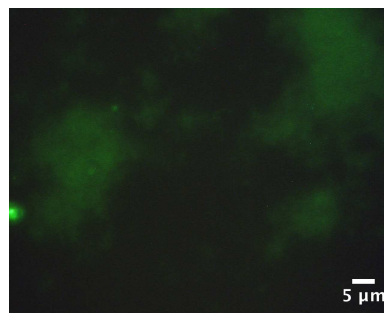
(d) Fluorescent image of *S. mutans*
NCTC 10449 with galactose polymer

12



(e) Phase contrast image of *S. mutans*
NCTC 10449 with galactose polymer

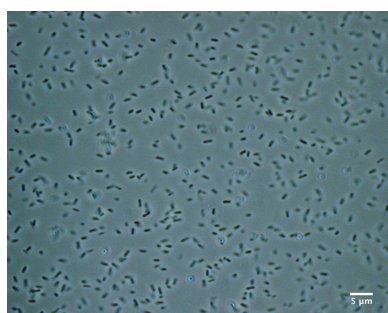
12



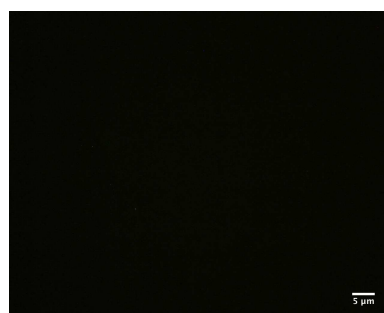
(f) Fluorescent image of *S. mutans*
NCTC 10449 with galactose polymer

12

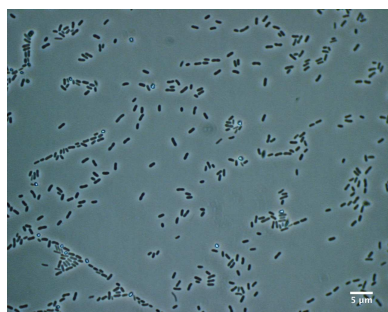
Figure A.6: Microscopy images of galactose displaying glycopolymer **12** with *S. mutans* NCTC 10449



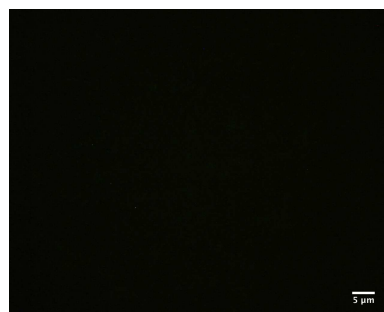
(a) Phase contrast image of *E. coli*
MG1655



(b) Fluorescent image of *E. coli*
MG1655

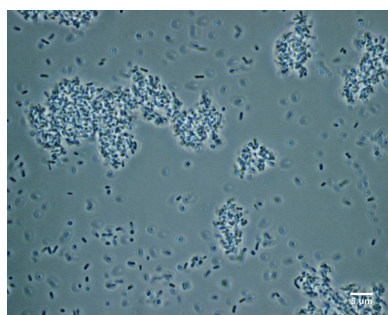


(c) Phase contrast image of *E. coli*
MG1655

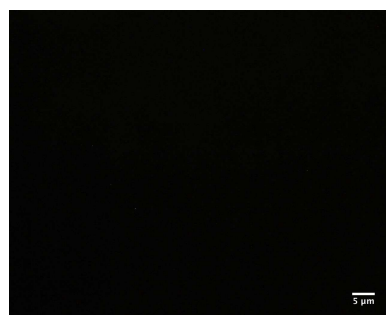


(d) Fluorescent image of *E. coli*
MG1655

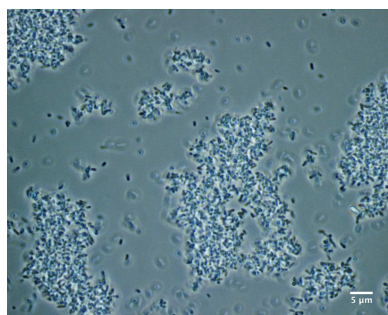
Figure A.7: Microscopy images of *E. coli* MG1655 with no polymer or azide present.



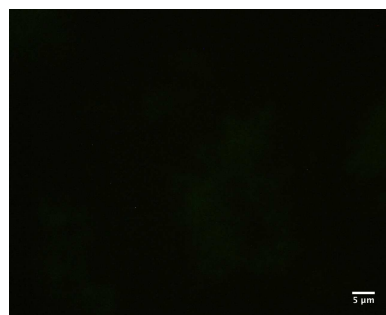
(a) Phase contrast image of *E. coli*
MG1655 with polymer **6**



(b) Fluorescent image of *E. coli*
MG1655 with polymer **6**

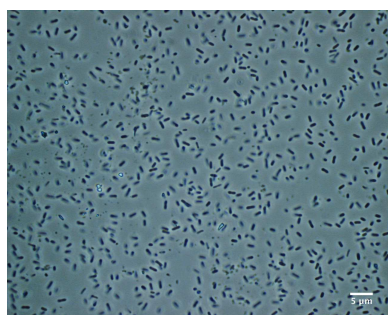


(c) Phase contrast image of *E. coli*
MG1655 with polymer **6**

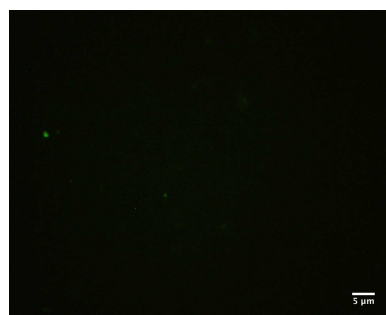


(d) Fluorescent image of *E. coli*
MG1655 with polymer **6**

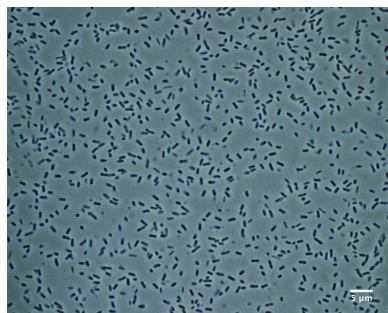
Figure A.8: Microscopy images of *E. coli* MG1655 with polymer **6** but no azide.



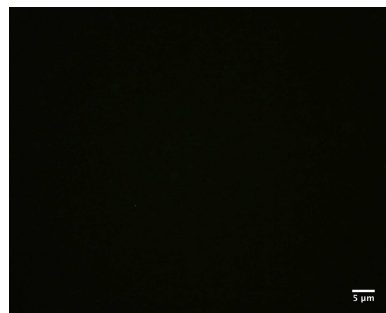
(a) Phase contrast image of *E. coli*
MG1655 with coumarin azide **2**



(b) Fluorescent image of *E. coli*
MG1655 with coumarin azide **2**



(c) Phase contrast image of *E. coli*
MG1655 with coumarin azide **2**



(d) Fluorescent image of *E. coli*
MG1655 with coumarin azide **2**

Figure A.9: Microscopy images of *E. coli* MG1655 with 3-azo-7-hydroxycoumarin (**2**) but no alkyne polymer.

Appendix B

Supporting Spectra

B.1 Benzyl-2-bromo-2-methylpropanoate

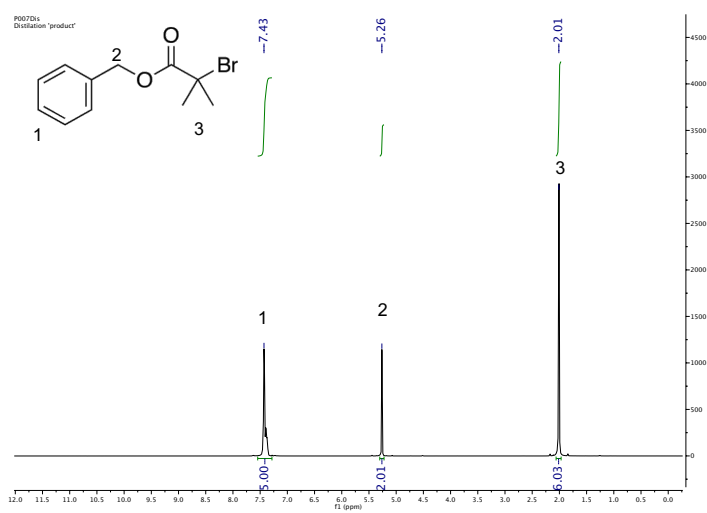


Figure B.1: ¹H NMR spectra of Benzyl-2-bromo-2-methylpropanoate.

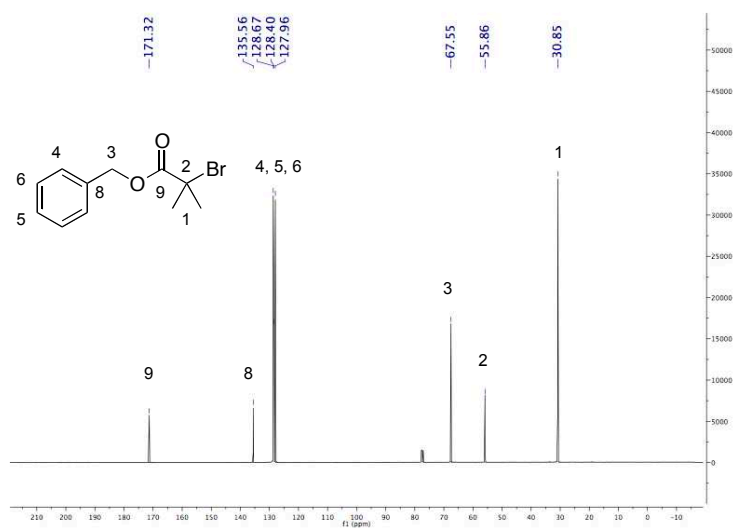
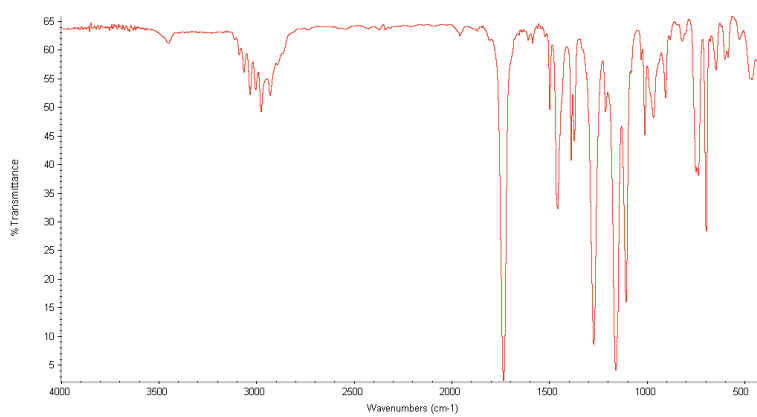
Figure B.2: ^{13}C NMR spectra of Benzyl-2-bromo-2-methylpropanoate.

Figure B.3: FT-IR spectra of Benzyl-2-bromo-2-methylpropanoate.

B.2 Coumarin 343 alkyl bromide

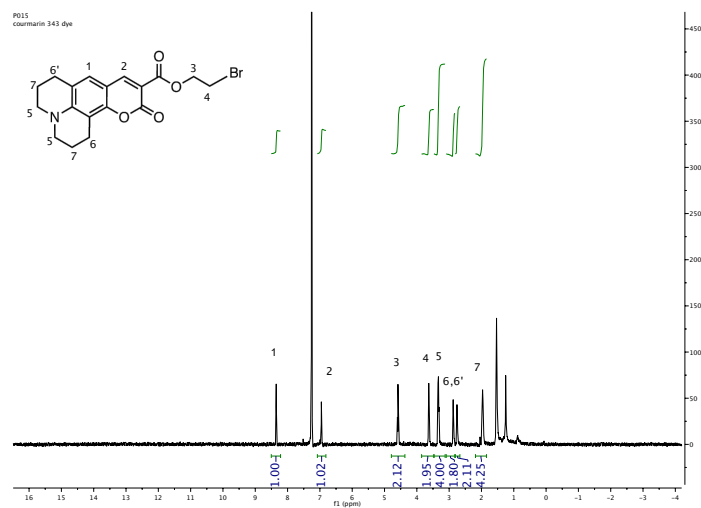


Figure B.4: ^1H NMR spectra of Coumarin 343 alkyl bromide.

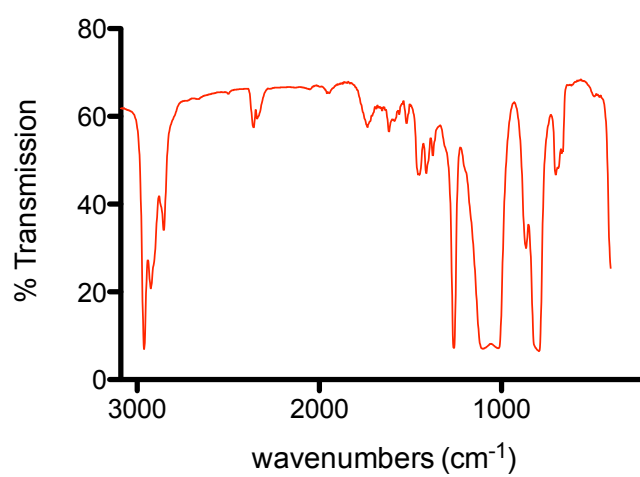
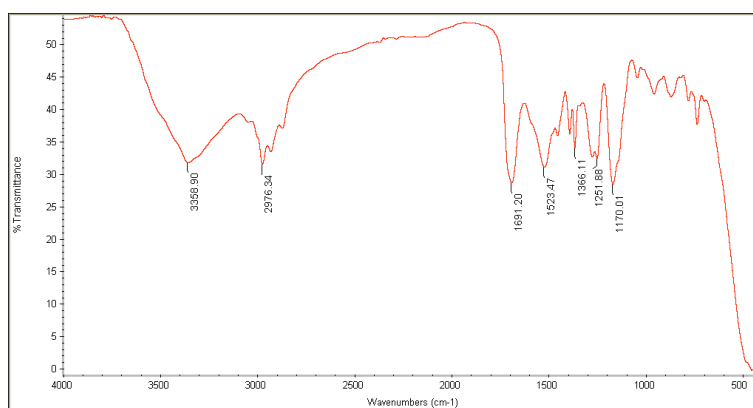
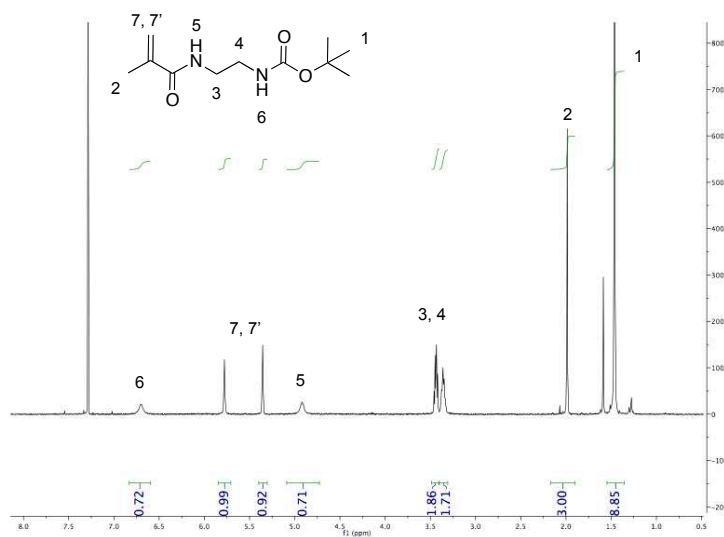
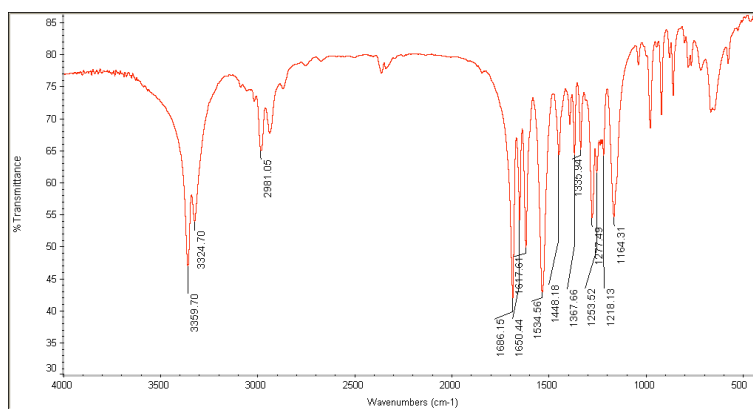
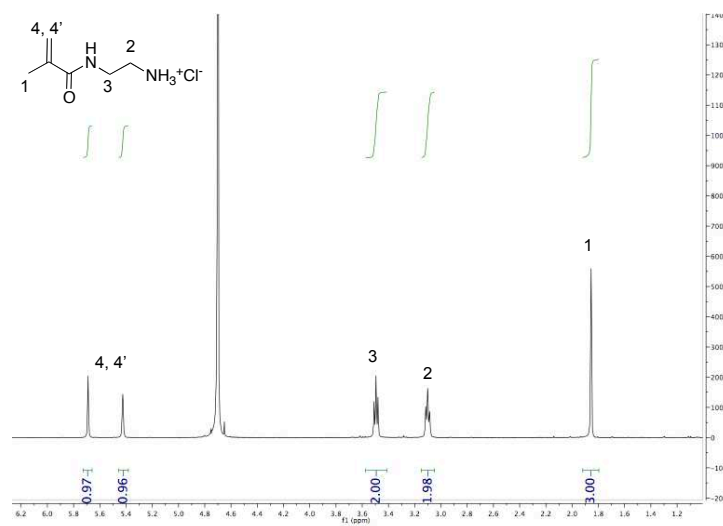
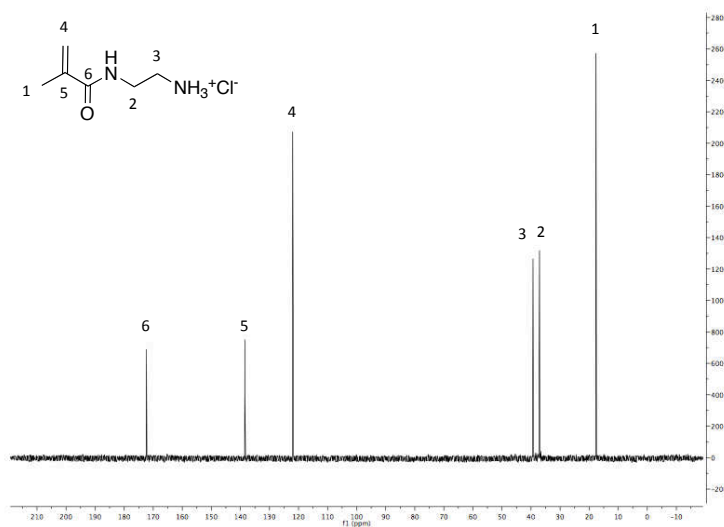


Figure B.5: FT-IR spectra of Coumarin 343 alkyl bromide.

B.3 *tert*-butyl (2-aminoethyl)carbamateFigure B.6: FT-IR spectra of *tert*-butyl (2-aminoethyl)carbamate

B.4 *tert*-butyl (2-methacrylamidoethyl)carbamateFigure B.7: ¹H NMR spectra of *tert*-butyl (2-methacrylamidoethyl)carbamateFigure B.8: FT-IR spectra of *tert*-butyl (2-methacrylamidoethyl)carbamate.

B.5 2-methacrylamidoethanaminium chlorideFigure B.9: ^1H NMR spectra of 2-methacrylamidoethanaminium chloride.

Figure B.10: ^{13}C NMR spectra of 2-methacrylamidoethanaminium chloride.

B.6 2-((2-methacrylamidoethylamino)methyl)phenylboronic acid

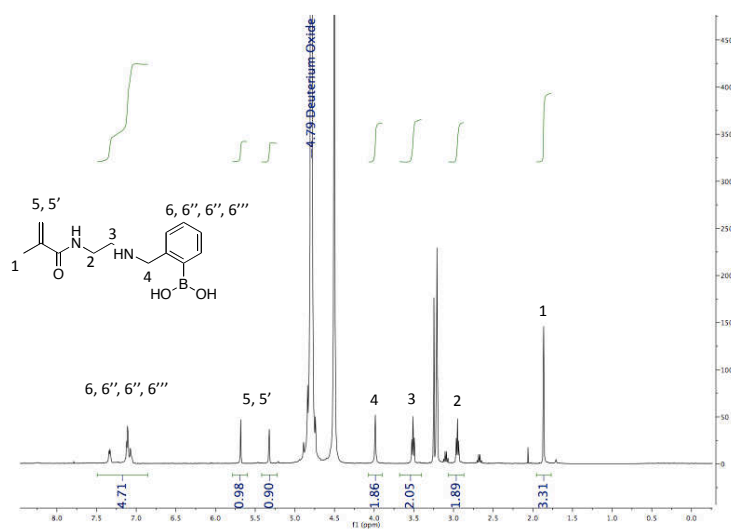


Figure B.11: ¹H NMR spectra of 2-((2-methacrylamidoethylamino)methyl)phenylboronic acid.

B.7 Coumarin 343 iodide

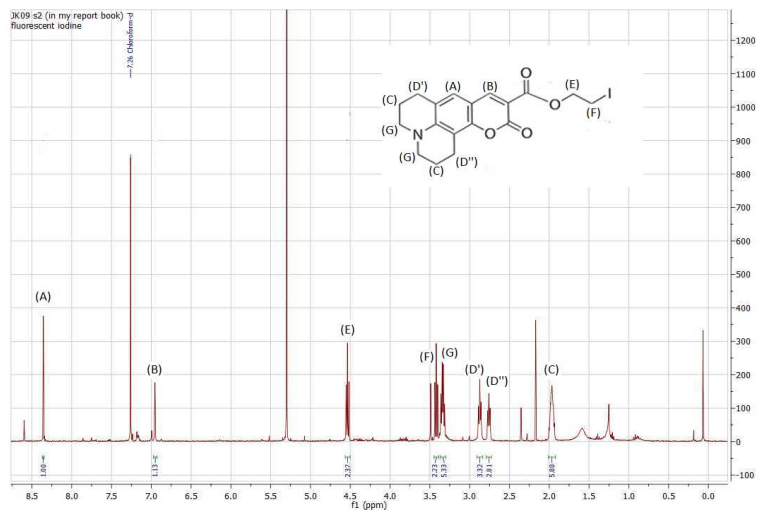
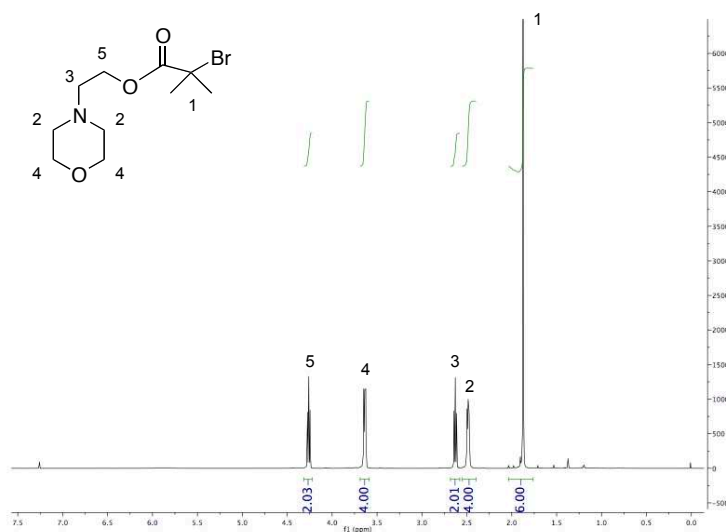


Figure B.12: ^1H NMR spectra of iodide terminated coumarin dye.

B.8 2-(N-Morpholino)ethyl-2-bromobutyrateFigure B.13: ^1H NMR spectra of 2-(N-Morpholino)ethyl-2-bromobutyrate.

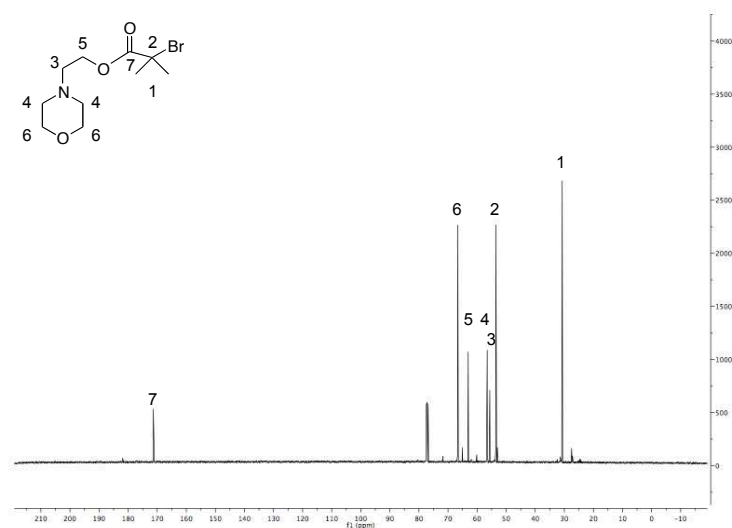
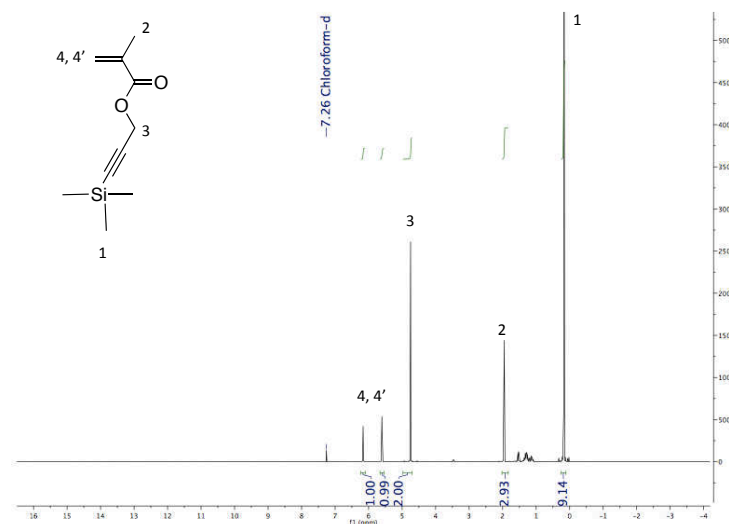


Figure B.14: ^{13}C NMR spectra of 2-(N-Morpholino)ethyl-2-bromobutyrate.

B.9 3-(trimethylsilyl)prop-2-yn-1-yl methacrylateFigure B.15: ^1H NMR spectra of 3-(trimethylsilyl)prop-2-yn-1-yl methacrylate.

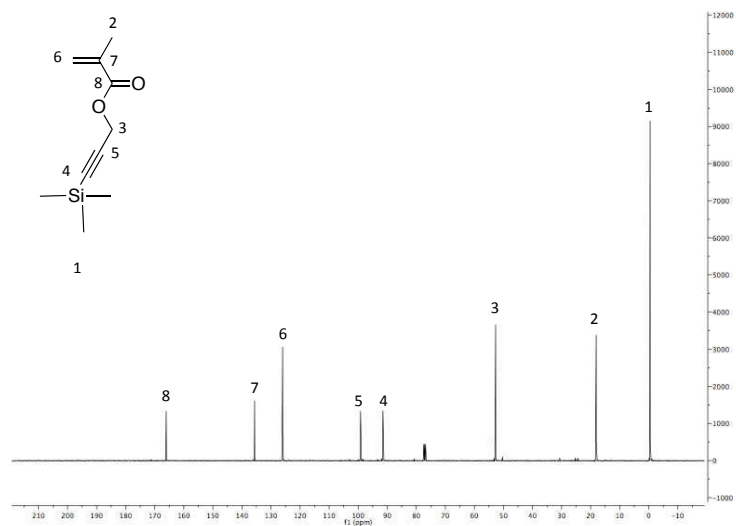
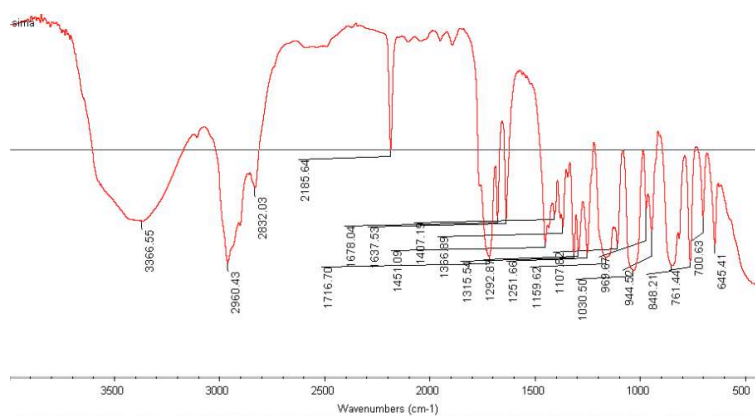
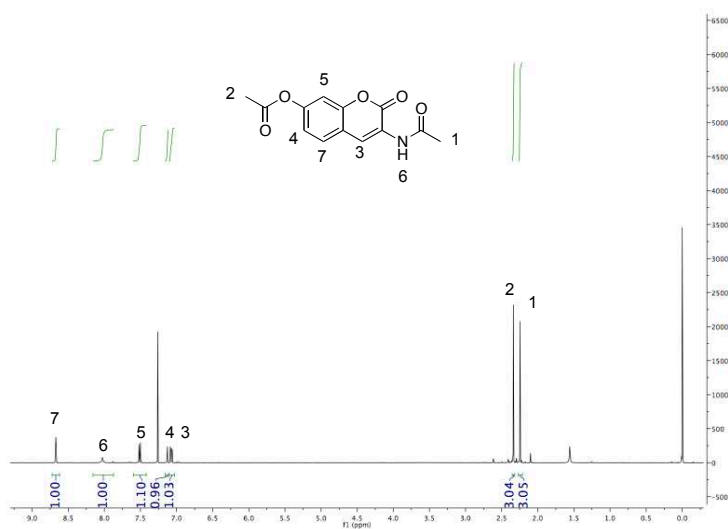
Figure B.16: ¹³CNMR spectra of 3-(trimethylsilyl)prop-2-yn-1-yl methacrylate.

Figure B.17: FT-IR spectra of 3-(trimethylsilyl)prop-2-yn-1-yl methacrylate.

B.10 3-acetamido-2-oxo-2*H*-chromen-7-yl acetateFigure B.18: ^1H NMR spectra of 3-acetamido-2-oxo-2*H*-chromen-7-yl acetate.

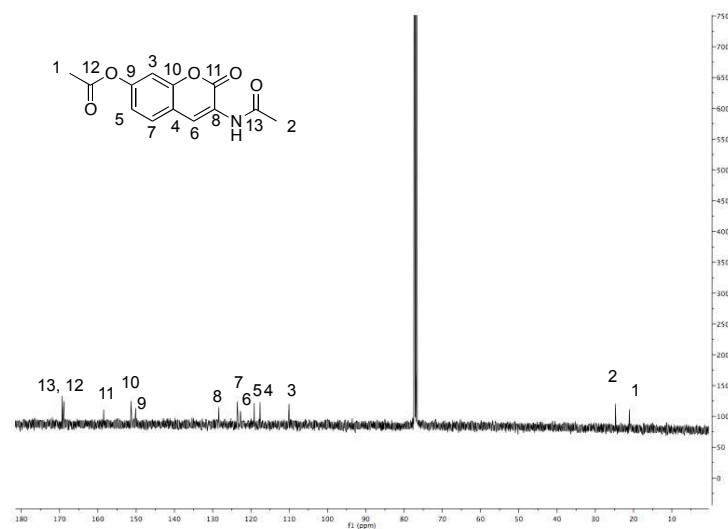
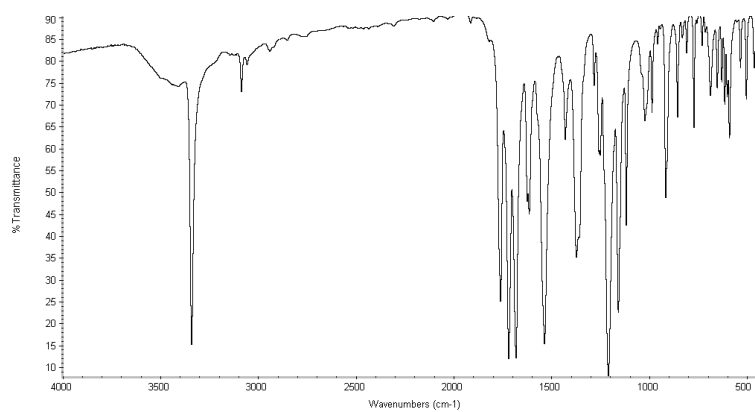
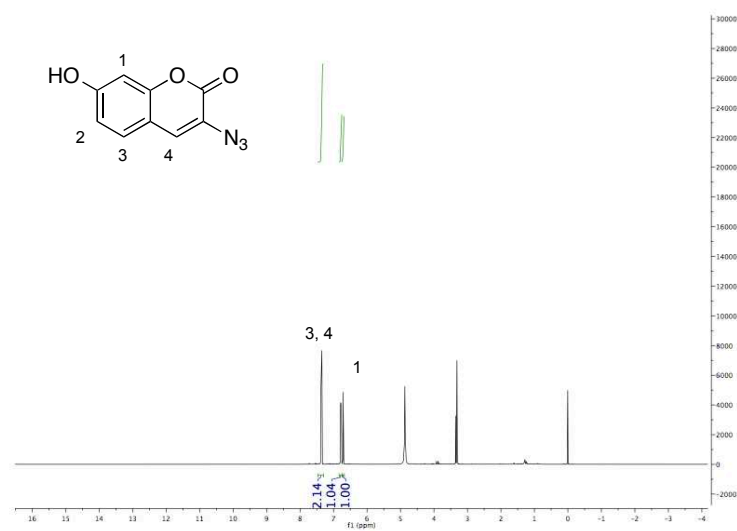
Figure B.19: ^{13}C NMR spectra of 3-acetamido-2-oxo-2H-chromen-7-yl acetate.

Figure B.20: FT-IR spectra of 3-acetamido-2-oxo-2H-chromen-7-yl acetate.

B.11 3-azo-7-hydroxycoumarinFigure B.21: ^1H NMR spectra of 3-azo-7-hydroxycoumarin.

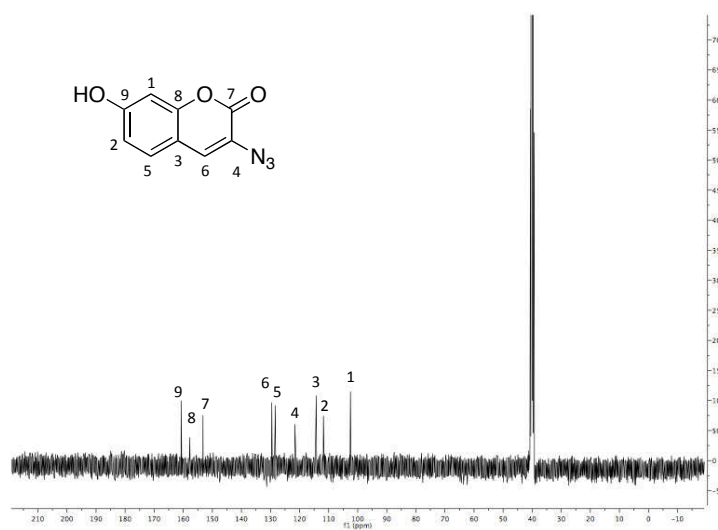
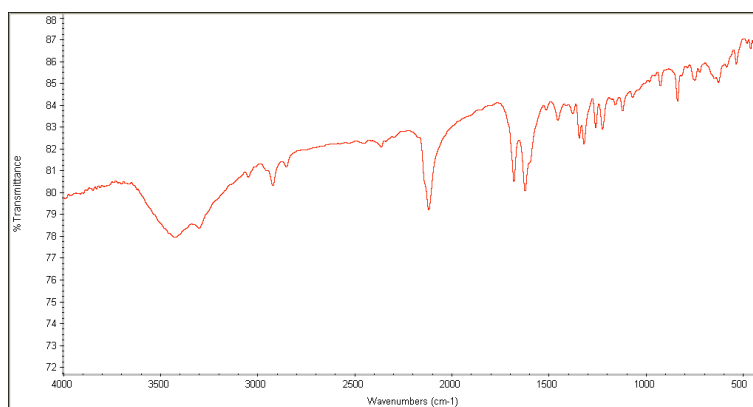
Figure B.22: ^{13}C NMR spectra of 3-azo-7-hydroxycoumarin.

Figure B.23: FT-IR spectra of 3-azo-7-hydroxycoumarin.

B.12 Zwitterionic and Quaternary Templated Polymers

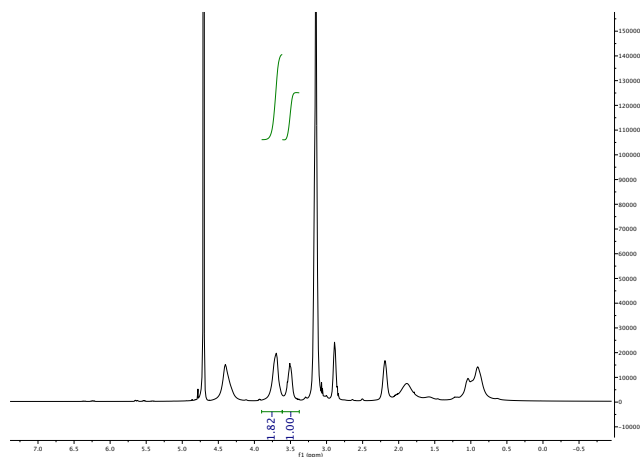


Figure B.24: ^1H NMR spectra of non-templated polymer of MEDSA AND METAC.

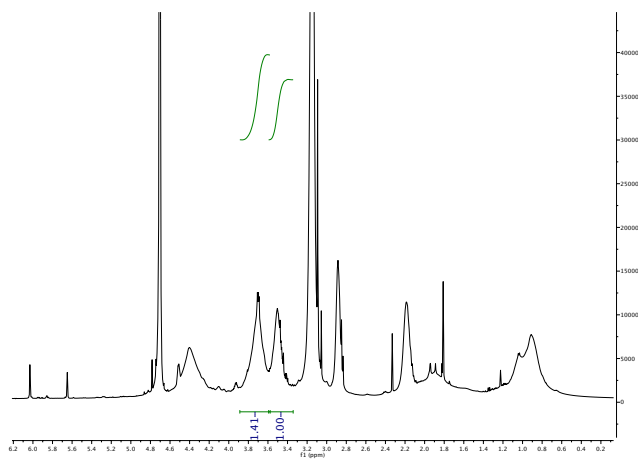


Figure B.25: ^1H NMR spectra of water wash *E. coli* templated polymer of MEDSA AND METAC.

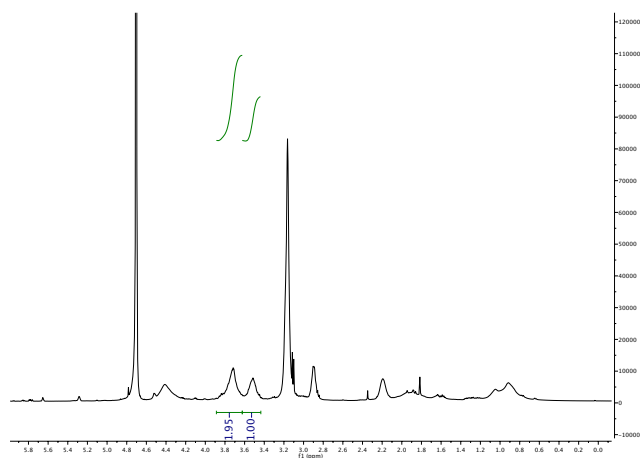


Figure B.26: ^1H NMR spectra of salt wash *E. coli* templated polymer of MEDSA AND METAC.

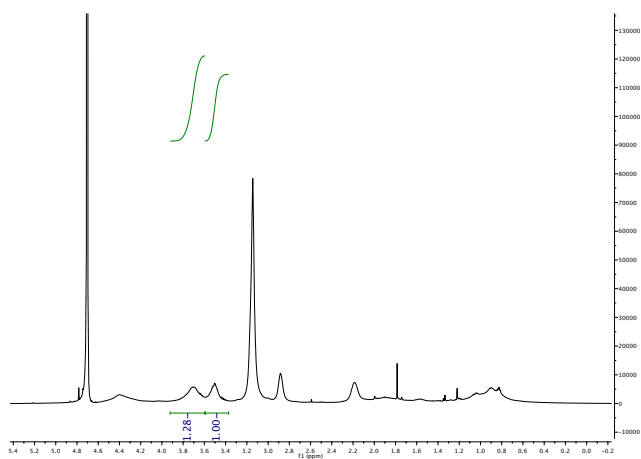


Figure B.27: ^1H NMR spectra of water wash *P. aeruginosa* templated polymer of MEDSA AND METAC.

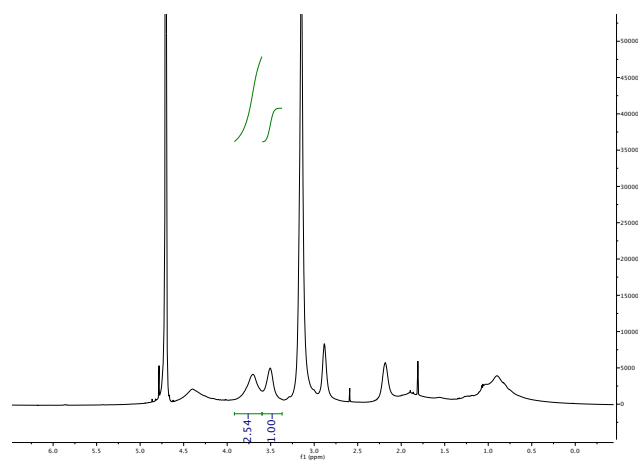


Figure B.28: ^1H NMR spectra of salt wash *P. aeruginosa* templated polymer of MEDSA AND METAC.

B.13 Zwitterionic and Glycerol Templated Polymers

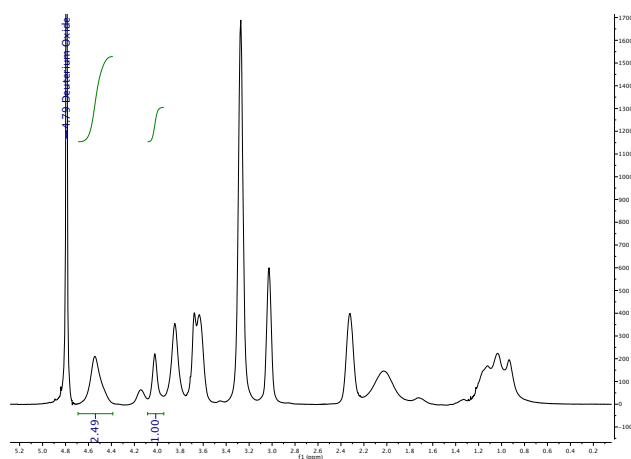


Figure B.29: ^1H NMR spectra of non-templated polymer of MEDSA AND DHPMA.

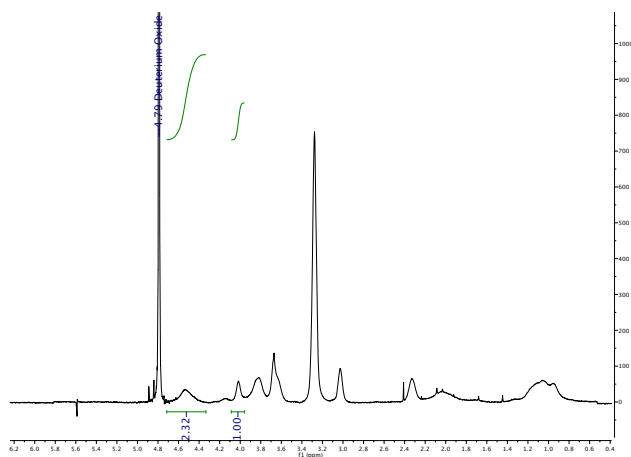


Figure B.30: ^1H NMR spectra of water wash *E. coli* templated polymer of MEDSA AND DHPMA.

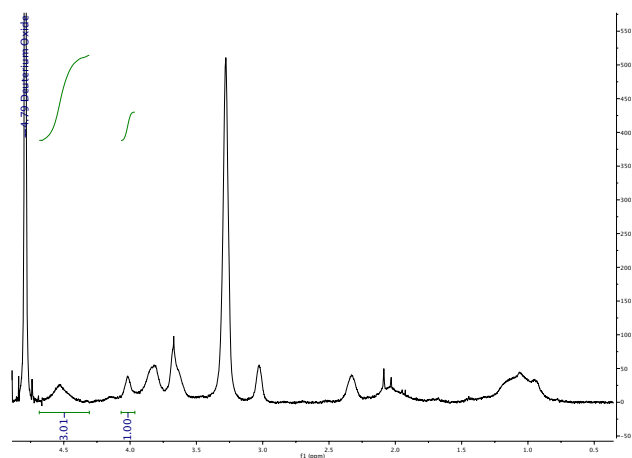


Figure B.31: ^1H NMR spectra of salt wash *E. coli* templated polymer of MEDSA AND DHPMA.

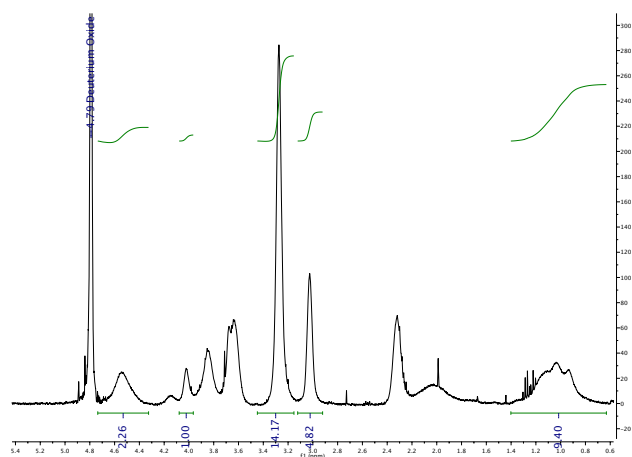


Figure B.32: ^1H NMR spectra of water wash *P. aeruginosa* templated polymer of MEDSA AND DHPMA.

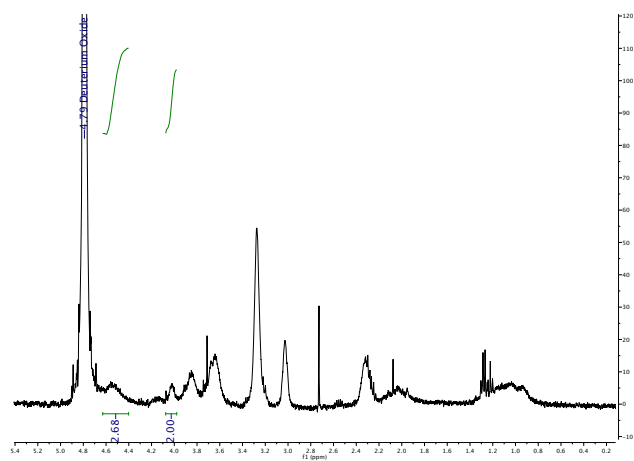


Figure B.33: ^1H NMR spectra of salt wash *P. aeruginosa* templated polymer of MEDSA AND DHPMA.

B.14 Quaternary and Glycerol Templated Polymers

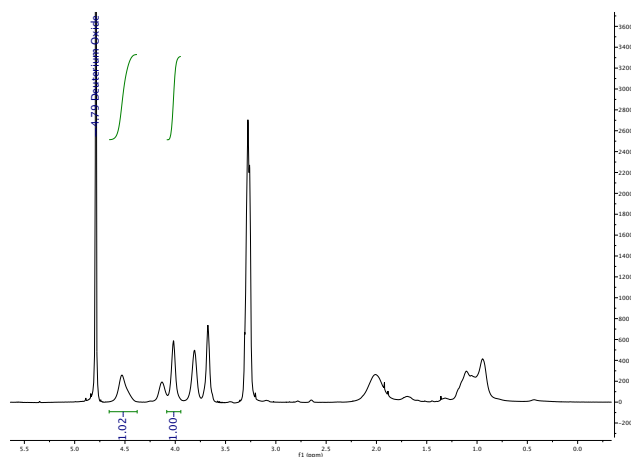


Figure B.34: ^1H NMR spectra of non-templated polymer of METAC AND DHPMA.

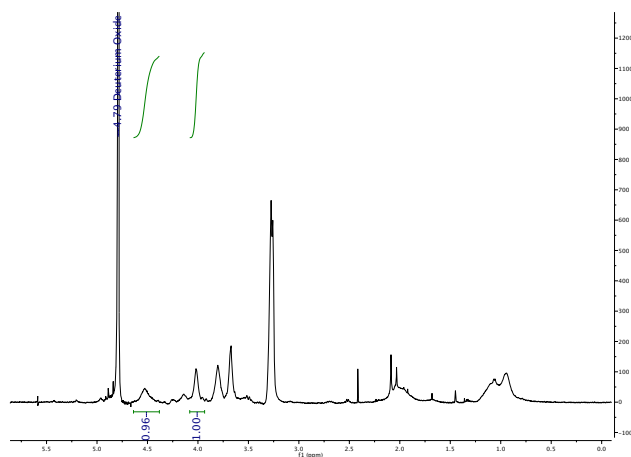


Figure B.35: ^1H NMR spectra of water wash *E. coli* templated polymer of METAC AND DHPMA.

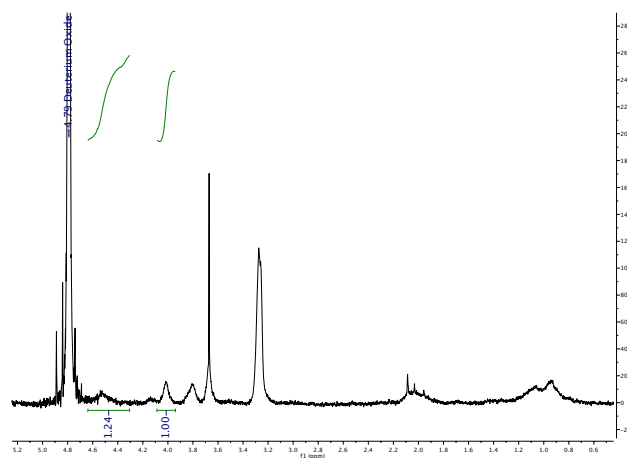
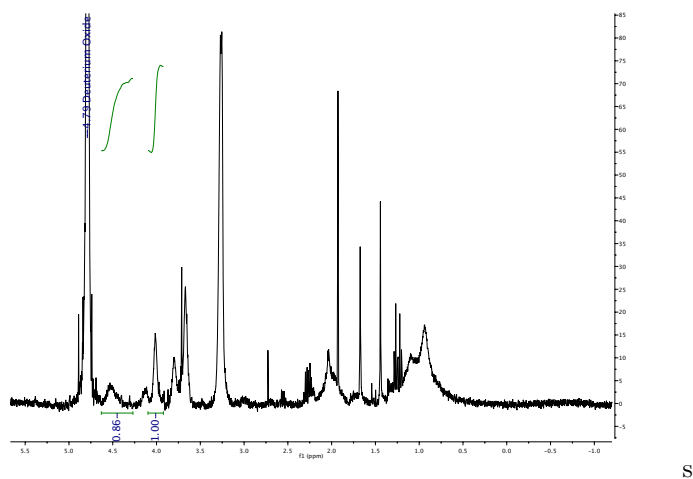


Figure B.36: ^1H NMR spectra of salt wash *E. coli* templated polymer of METAC AND DHPMA.



S

Figure B.37: ^1H NMR spectra of water wash *P. aeruginosa* templated polymer of METAC AND DHPMA.

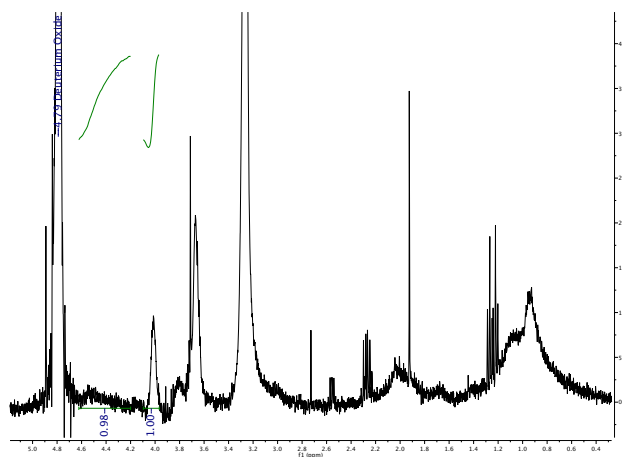


Figure B.38: ^1H NMR spectra of salt wash *P. aeruginosa* templated polymer of METAC AND DHPMA.

Appendix C

Additional Supporting Information

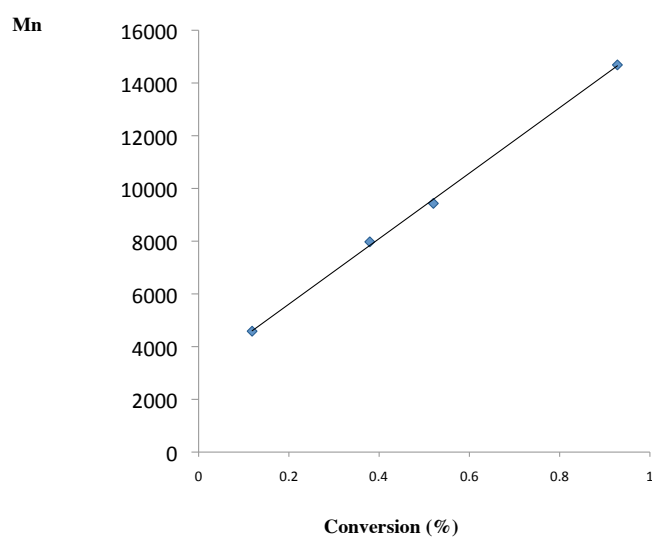


Figure C.1: GPC data for the polymerisation of 2-(dimethylamino)ethyl methacrylate by ATRP in the charge chapter.

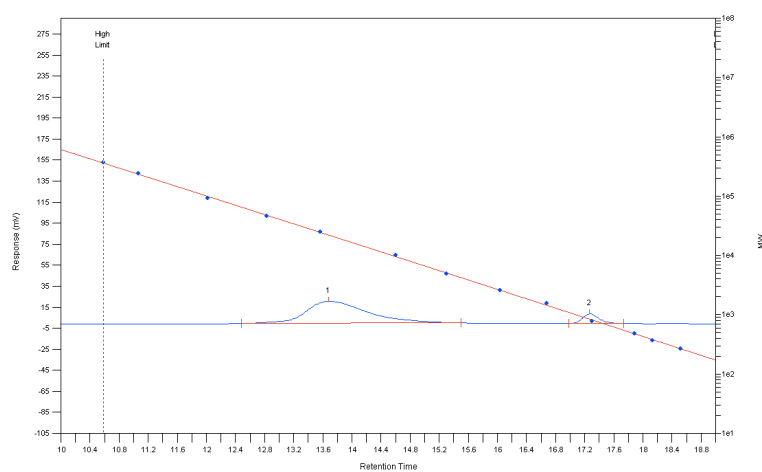


Figure C.2: GPC data for poly(2-(dimethylamino)ethyl methacrylate) by ATRP in the charge chapter.

Appendix D

Analysis of bacterial clustering with templated polymers

D.1 Introduction

The size distributions and patterns of clustering behaviour of the two bacteria with the non-templated and templated polymers were further analysed to extract further information about the binding patterns of the polymers. This analysis is to support the information already presented in the main templating chapter and was carried out by Dr Francisco Fernandez Trillo, MRSC, PostDoctoral Research Fellow, Division of Drug Delivery and Tissue Engineering, Boots Science Building, University of Nottingham, NG7 2RD, UK.

D.2 Method

Size distributions of bacterial clusters was determined under moderate stirring (default speed 5 setting) to the required concentration as indicated by the in-built display software. Particle size ranges were defined using PSS-Duke standards (Polymer Standard Service, Kromatek Ltd, Dunmow, UK).

Particle size distribution was then determined as a function of the particle diffraction using the Coulter software (version 2.11a) and plotted as a function of the percentage of distribution volume.

In a typical experiment, μ 200 L of a bacterial suspension with an OD_{600} of 1.9 were added to the flow cell (~ 14 mL) to obtain an obscuration of 8-12%. At this point the t_0 population distribution was recorded with constant mixing. Then 100 μ L of a 1 mg/mL polymer solution were added, the mixture was allowed to equilibrate and the population distribution was recorded after 15 and 30 minutes.

In order to determine the relative populations of individual bacteria, dimers and clusters, particle size distributions were deconvoluted using the `peakfit.m` command

(<http://terpconnect.umd.edu/toh/spectrum/InteractivePeakFitter.htm#command>) in MATLAB[®] R2012a package. The size of the clusters was then normalised to a single bacteria size (1.5 μ m), so that the relative population of unimers (~ 1.5 μ m), dimers (~ 3 μ m) and clusters (≥ 4.5 μ m) could be plotted as a function of time.

D.3 Results and discussion

The results of the analyses of the data are expressed graphically where the change in the size distribution from the coulter counter is shown on the left and the populations of unimers, dimers and clusters of bacteria are shown in the right.

D.3.1 Control Polymers

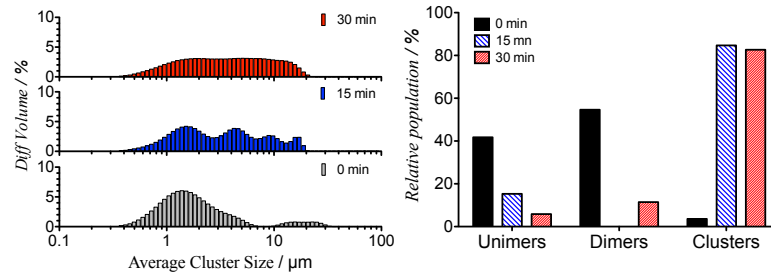


Figure D.1: Change in *E. coli* MG1655 cluster sizes with time in suspension with the non-templated control polymer **P1** (left) and the relative population of unimers, dimers and clusters at each time point (right).

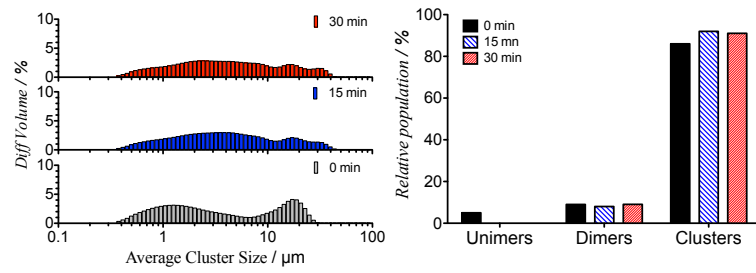


Figure D.2: Change in *P. aeruginosa* PA01 GFP cluster sizes with time in suspension with the non-templated control polymer **P1** (left) and the relative population of unimers, dimers and clusters at each time point (right).

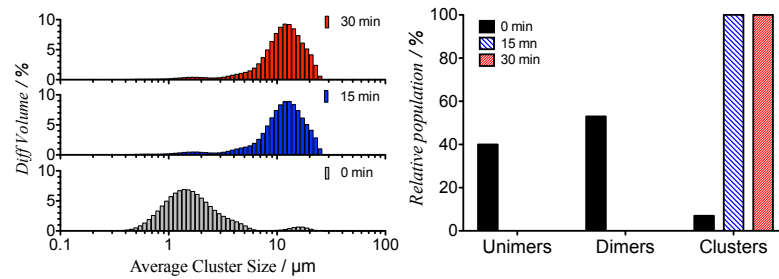
D.3.2 *E. coli* water washed polymers (P7-WE)

Figure D.3: Change in *E. coli* MG1655 cluster sizes with time in suspension with the water washed *E. coli* templated polymer **P7-WE** (left) and the relative population of unimers, dimers and clusters at each time point (right).

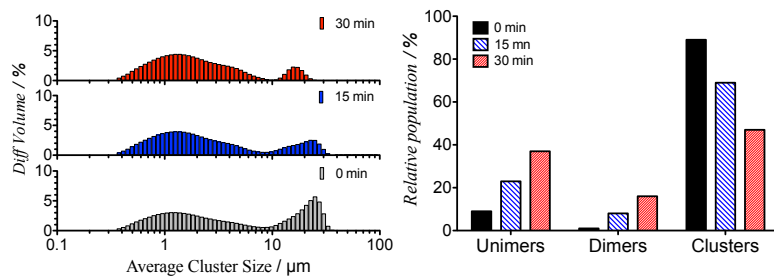


Figure D.4: Change in *P. aeruginosa* PA01 GFP cluster sizes with time in suspension with the water washed *E. coli* templated polymer **P7-WE** (left) and the relative population of unimers, dimers and clusters at each time point (right).

D.3.3 *E. coli* salt washed polymers (P7-SE)

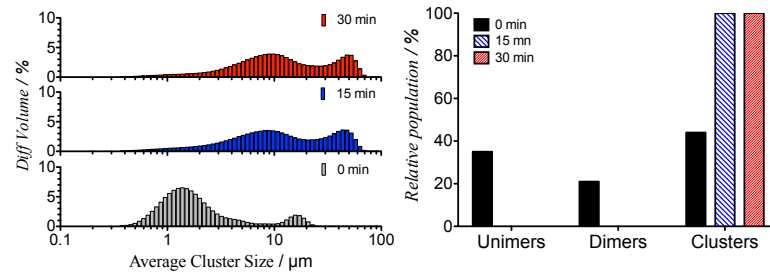


Figure D.5: Change in *E. coli* MG1655 cluster sizes with time in suspension with the salt washed *E. coli* templated polymer **P7-SE** (left) and the relative population of unimers, dimers and clusters at each time point (right).

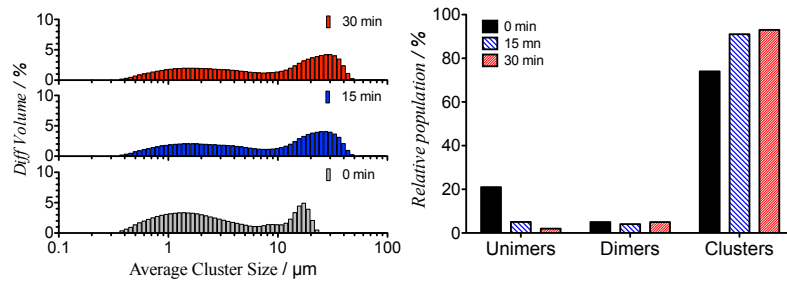


Figure D.6: Change in *P. aeruginosa* PA01 GFP cluster sizes with time in suspension with the salt washed *E. coli* templated polymer **P7-SE** (left) and the relative population of unimers, dimers and clusters at each time point (right).

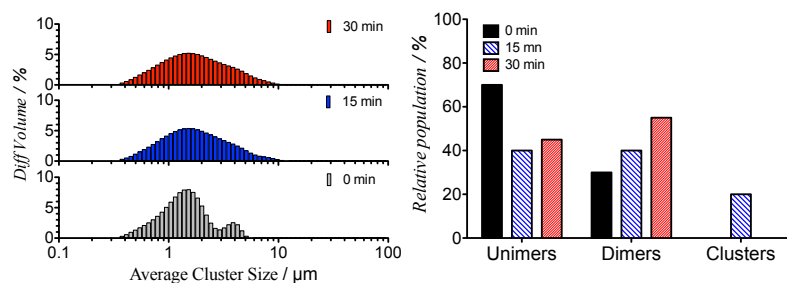
D.3.4 *P. aeruginosa* water washed polymers (P7-WP)

Figure D.7: Change in *E. coli* MG1655 cluster sizes with time in suspension with the water washed *P. aeruginosa* templated polymer **P7-WP** (left) and the relative population of unimers, dimers and clusters at each time point (right).

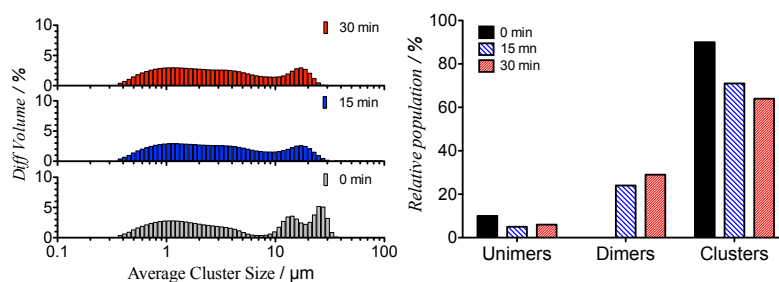


Figure D.8: Change in *P. aeruginosa* PA01 GFP cluster sizes with time in suspension with the water washed *P. aeruginosa* templated polymer **P7-WP** (left) and the relative population of unimers, dimers and clusters at each time point (right).

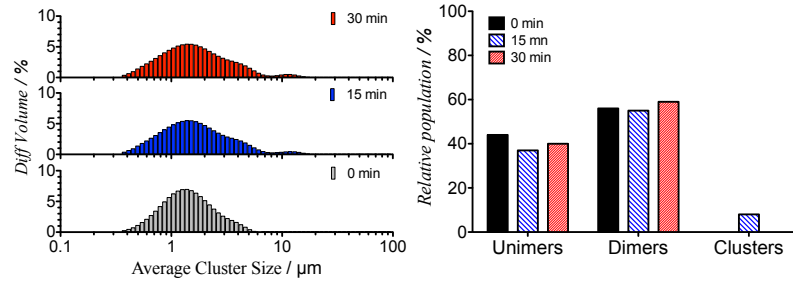
D.3.5 *P. aeruginosa* salt washed polymers (P7-SP)

Figure D.9: Change in *E. coli* MG1655 cluster sizes with time in suspension with the salt washed *P. aeruginosa* templated polymer **P7-SP** (left) and the relative population of unimers, dimers and clusters at each time point (right).

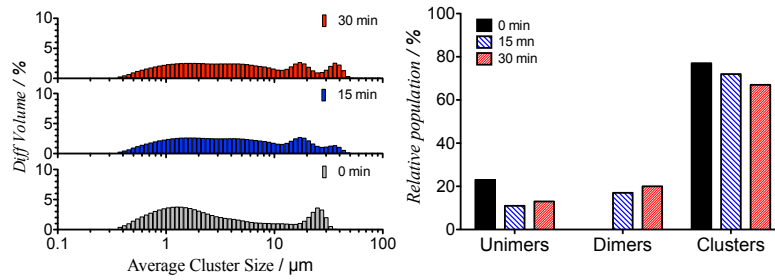


Figure D.10: Change in *P. aeruginosa* PA01 GFP cluster sizes with time in suspension with the salt washed *P. aeruginosa* templated polymer **P7-SP** (left) and the relative population of unimers, dimers and clusters at each time point (right).

Appendix E

Estimation of monomer reactivity ratios

E.1 Introduction

The monomer reactivity ratios were calculated at low conversion ($< 10\%$). This was done to ensure the monomer feed ratio at the start was the same as the monomer feed ratio at the end of the polymerisation period ensuring the composition of the polymer was dictated by the monomers reactivity and not monomer concentration.

E.2 Methods

The polymers of METAC and MEDSA were generated across a range of monomer ratios using AGET ATRP according to the methods described.

E.2.1 METAC:MEDSA ratio of 85:15 R1

To a schlenk tube MEDSA (58 mg, 0.21 mmol), METAC (340 μ L (72% aqueous solution), 245 mg, 1.18 mmol), copper (II) bromide (3.10 mg, 0.0134 mmol), TPMA (8.02, 0.0134 mmol), 2-(*N*-morpholino)ethyl-2-bromobutyrate (1.55 mg, 5.55 μ mol) and sodium *p*-toluenesulfonate (54 mg, 0.278 mmol) as an internal standard were added. The resultant mixture was degassed for 30 minutes over ice. After this time 270 μ L of 1mg/mL solution of ascorbic acid was added to begin the polymerisation. The polymerisation was stopped after 31 minutes by opening the flask to air. The polymer was purified by dialysis for 7 days followed by freeze drying to yield polymer **R1**. The polymer composition was analysed as described in the methods of the templating chapter using ^1H NMR spectroscopy.

E.2.2 METAC:MEDSA ratio of 90:10 R2

To a schlenk tube MEDSA (38.9 mg, 0.139 mmol), METAC (360 μ L, 259 mg, 1.25 mmol), copper (II) bromide (3.10 mg, 0.0134 mmol), TPMA (8.02, 0.0134 mmol), 2-(*N*-morpholino)ethyl-2-bromobutyrate (1.55 mg, 5.55 μ mol) and sodium *p*-toluenesulfonate (54 mg, 0.278 mmol) as an internal standard were added. The resultant mixture was degassed for 30 minutes over ice. After this time 270 μ L of 1mg/mL solution of ascorbic acid was added to begin the polymerisation. The polymerisation was stopped after 31 minutes by opening the flask to air. The polymer was purified by dialysis for 7 days followed by freeze drying to yield polymer **R2**. The polymer composition was analysed as described in the methods of the templating chapter using ^1H NMR spectroscopy.

E.2.3 METAC:MEDSA ratio of 94:6 R3

To a schlenk tube MEDSA (23.2 mg, 0.08 mmol), METAC (375 μ L, 270 mg, 1.30 mmol), copper (II) bromide (3.10 mg, 0.0134 mmol), TPMA (8.02, 0.0134 mmol), 2-(*N*-morpholino)ethyl-2-bromobutyrate (1.55 mg, 5.55 μ mol) and sodium *p*-toluenesulfonate (54 mg, 0.278 mmol) as an internal standard were added. The resultant mixture was degassed for 30 minutes over ice. After

this time 270 μL of 1mg/mL solution of ascorbic acid was added to begin the polymerisation. The polymerisation was stopped after 31 minutes by opening the flask to air. The polymer was purified by dialysis for 7 days followed by freeze drying to yield polymer **R3**. The polymer composition was analysed as described in the methods of the templating chapter using ^1H NMR spectroscopy.

E.2.4 METAC:MEDSA ratio of 94:6 **R4**

To a schlenk tube MEDSA (7.74 mg, 0.028 mmol), METAC (391 μL , 282 mg, 1.36 mmol), copper (II) bromide (3.10 mg, 0.0134 mmol), TPMA (8.02, 0.0134 mmol), 2-(*N*-morpholino)ethyl-2-bromobutyrate (1.55 mg, 0.00555 mmol) and sodium *p*-toluenesulfonate (54 mg, 0.278 mmol) as an internal standard were added. The resultant mixture was degassed for 30 minutes over ice. After this time 270 μL of 1mg/mL solution of ascorbic acid was added to begin the polymerisation. The polymerisation was stopped after 31 minutes by opening the flask to air. The polymer was purified by dialysis for 7 days followed by freeze drying to yield polymer **R4**. The polymer composition was analysed as described in the methods of the templating chapter using ^1H NMR spectroscopy.

E.2.5 Calculation of reactivity ratios

The estimation of the monomer reactivity ratios was calculated using the error in variables model (EVM) method,[210] and the computer programme "*Reactivity ratios error in variable model*" (RREVM).[211]

E.2.6 Results and Discussion

As discussion there was a necessity for the polymerisation of the two monomers to be maintained at low conversion in order to ensure the final polymer composition was dictated by the monomers reactivity ratio and not concentration effects. These concentration effects can become more dominant as the conversion of the monomers increases. A series of preliminary polymerisations were carried out before the conditions used to generate polymers **R1-4** were used. The final conversions

ranged between 3.5-7% conversion.

The compositions of the polymers were carried out in the same manner as that used in the templating chapter; by comparing the integrals of the CH_2 adjacent to the quaternary nitrogen only seen on MEDSA at 3.58 ppm to those found on both monomers at 3.79 ppm. The value of the integral for the CH_2 in MEDSA at 3.58 ppm was subtracted from the integral at 3.79 ppm to give the proportion of the total polymer constituted of METAC. The analyses are summarised in table Table E.1.

Table E.1: Analysis of polymer composition for METAC and MEDSA for the calculation of monomer reactivity ratios. Ratios are expressed as (METAC:MEDSA)

| Polymer | Monomer feed (METAC:MEDSA) | Conversion (%) | Composition (METAC:MEDSA) |
|-----------|-------------------------------|-------------------|------------------------------|
| R1 | 85 : 15 | 7.0 | 87 : 13 |
| R2 | 90 : 10 | 5.5 | 92 : 8.0 |
| R3 | 94 : 6.0 | 3.5 | 96.2 : 3.8 |
| R4 | 98 : 2.0 | 6.0 | 99 : 1.0 |

The reactivity ratios were calculated using the Mayo-Lewis instantaneous copolymer composition equation (E.1).

$$\frac{F_1}{F_2} = \frac{r_1 \cdot [M_1]^2 + [M_2][M_1]}{r_2 \cdot [M_2]^2 + [M_1][M_2]} \quad (\text{E.1})$$

This is where F_x were the experimental mole fractions of the monomers (METAC and MEDSA) that were incorporated into the copolymer after conversion. The value of r_x represents the reactivity ratio values and $[M_x]$ was the molar feed ratios of the monomers. The starting values of the reactivity ratios were input as 1, the experimental error was placed as 5%.

The estimation of the reactivity ratio values calculated by the RREVM programme were:

$$r_{\text{METAC}} = 0.9988$$

$$r_{\text{MEDSA}} = 1.0012$$

The programme also produces a graphical display of the 95% confidence intervals for the estimation of reactivity ratio which is shown in Figure E.1.

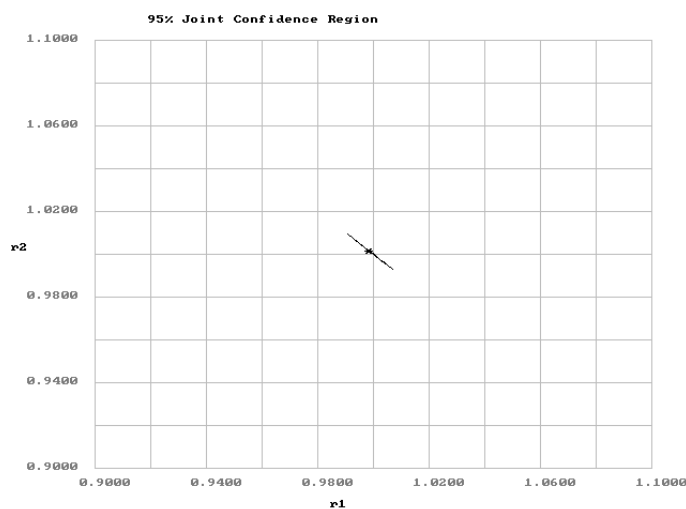


Figure E.1: Graph of the 95% confidence intervals for the estimation of METAC AND DHPMA reactivity ratios. The reactivity ratio value for METAC is given by r_1 on the x axis and MEDSA is given by r_2 on the y axis.

These values are in agreement with the value obtained from the blank polymerisation in the tempating chapter. Where polymer **P1** had a feed ratio of 1.00 : 1.00 (METAC:MEDSA) and a final polymer composition ratio of 0.82 : 1.00 (METAC:MEDSA) and 35% conversion.

Bibliography

- [1] C. Weidenmaier and A. Peschel, “Teichoic acids and related cell-wall glycopolymers in gram-positive physiology and host interactions,” *Nature reviews microbiology*, vol. 6, pp. 276–87, April 2008.
- [2] C. R. H. Raetz and C. Whitfield, “Lipopolysaccharide endotoxins,” *Annual review of biochemistry*, vol. 71, pp. 635–700, November 2002.
- [3] Y.-L. Yang, Y. Xu, P. Straight, and P. C. Dorrestein, “Translating metabolic exchange with imaging mass spectrometry,” *Nature Chemical Biology*, vol. 5, pp. 885–887, Nov 2009.
- [4] I. Patel, T. Seemungal, M. Wilks, S. Lloyd-Owen, G. Donaldson, and J. Wedzicha, “Relationship between bacterial colonisation and the frequency, character, and severity of copd exacerbations,” *Thorax*, vol. 57, no. 9, pp. 759–764, 2002.
- [5] P. B. Lockhart, M. T. Brennan, H. C. Sasser, P. C. Fox, B. J. Paster, and F. K. Bahrani-Mougeot, “Bacteremia associated with toothbrushing and dental extraction,” *Circulation*, vol. 117, pp. 3118–3125, Jun 2008.
- [6] J. Roberts and P. Sockett, “The socio-economic impact of human salmonella enteritidis infection,” *International journal of food microbiology*, vol. 21, no. 1-2, pp. 117–129, 1994.
- [7] G. Pasparakis and C. Alexander, “Synthetic polymers for capture and detection of microorganisms,” *The Analyst*, vol. 132, pp. 1075–1082, Jan 2007.

- [8] M. Kaplan and L. Kaplan, "The gram stain and differential staining," *Journal of Bacteriology*, vol. 25, pp. 309–321, March 1933.
- [9] T. Beveridge and L. Graham, "Surface layers of bacteria.," *Microbiology and Molecular Biology Reviews*, vol. 55, pp. 684–705, December 1991.
- [10] K. H. Schleifer and O. Kandler, "Peptidoglycan types of bacterial cell walls and their taxonomic implications," *Bacteriological reviews*, vol. 36, pp. 407–77, December 1972.
- [11] Y. Shai, "Mode of action of membrane active antimicrobial peptides," *Biopolymers*, vol. 66, no. 4, pp. 236–248, 2002.
- [12] T. Neu, "Significance of bacterial surface-active compounds in interaction of bacteria with interfaces," *Microbiological Reviews*, vol. 60, no. 1, pp. 151–166, 1996.
- [13] H. Mukasa and H. Slade, "Structure and immunological specificity of the streptococcus mutans group b cell wall antigen," *Infection and immunity*, vol. 7, no. 4, pp. 578–585, 1973.
- [14] S. Hamada and H. Slade, "Biology, immunology, and cariogenicity of streptococcus mutans," *Microbiological Reviews*, vol. 44, pp. 331–384, June 1980.
- [15] H. Mukasa and H. Slade, "Mechanism of adherence of streptococcus mutans to smooth surfaces i. roles of insoluble dextran-levan synthetase enzymes and cell wall polysaccharide antigen in plaque formation," *Infection and Immunity*, vol. 8, no. 4, pp. 555–562, 1973.
- [16] C. Bouguénec, "Adhesins and invasins of pathogenic escherichia coli," *International journal of medical microbiology*, vol. 295, no. 6-7, pp. 471–478, 2005.
- [17] P. A. Murray, D. G. Kern, and J. R. Winkler, "Identification of a galactose-binding lectin on fusobacterium nucleatum fn-2," *Infection and Immunity*, vol. 56, pp. 1314–1319, May 1988.
- [18] E. Weiss, B. Shanitzki, M. Dotan, N. Ganeshkumar, P. Kolenbrander, and Z. Metzger, "Attachment of fusobacterium nucleatum pk 1594 to mammalian cells and its coaggregation

- with periodontopathogenic bacteria are mediated by the same galactose-binding adhesin," *Oral microbiology and immunology*, vol. 15, no. 6, pp. 371–377, 2000.
- [19] J. Banas and M. Vickerman, "Glucan-binding proteins of the oral streptococci," *Critical Reviews in Oral Biology & Medicine*, vol. 14, pp. 89–99, Mar 2003.
- [20] D. J. Lynch, T. L. Fountain, J. E. Mazurkiewicz, and J. A. Banas, "Glucan-binding proteins are essential for shaping streptococcus mutans biofilm architecture," *Fems Microbiol Lett*, vol. 268, pp. 158–165, Jan 2007.
- [21] W. Moore, L. Holdeman, R. Smibert, I. Good, J. Burmeister, K. Palcanis, and R. Ranney, "Bacteriology of experimental gingivitis in young adult humans.," *Infection and immunity*, vol. 38, no. 2, pp. 651–667, 1982.
- [22] W. Loesche and S. Syed, "Bacteriology of human experimental gingivitis: effect of plaque and gingivitis score," *Infection and Immunity*, vol. 21, pp. 821–829, Jan 1978.
- [23] L. Li, S. Redding, and A. Dongari-Bagtzoglou, "Candida glabrata, an emerging oral opportunistic pathogen," *Journal of dental research*, vol. 86, pp. 204–215, March 2007.
- [24] A. J. Grau, H. Becher, C. M. Ziegler, C. Lichy, F. Buggle, C. Kaiser, R. Lutz, S. Bültmann, M. Preusch, and C. E. Dörfer, "Periodontal disease as a risk factor for ischemic stroke," *Stroke*, vol. 35, pp. 496–501, January 2004.
- [25] L. Jansson, S. Lavstedt, and L. Frithiof, "Relationship between oral health and mortality rate," *Journal of clinical periodontology*, vol. 29, pp. 1029–1034, November 2002.
- [26] L. Jansson, S. Lavstedt, L. Frithiof, and H. Theobald, "Relationship between oral health and mortality in cardiovascular diseases," *Journal of clinical periodontology*, vol. 28, pp. 762–768, August 2001.
- [27] R. Selwitz, A. Ismail, and N. Pitts, "Dental caries," *The Lancet*, vol. 369, no. 9555, pp. 51–59, 2007.

- [28] W. J. Loesche, "Role of streptococcus mutans in human dental decay," *Microbiological reviews*, vol. 50, pp. 353–380, December 1986.
- [29] W. Loesche, J. Rowan, L. Straffon, and P. Loos, "Association of streptococcus mutans with human dental decay," *Infection and Immunity*, vol. 11, pp. 1252–1260, June 1975.
- [30] R. J. Lamont and H. F. Jenkinson, "Life below the gum line: pathogenic mechanisms of porphyromonas gingivalis," *Microbiology and molecular biology reviews*, vol. 62, pp. 1244–1263, December 1998.
- [31] B. Paster, S. Boches, J. Galvin, R. Ericson, C. Lau, V. Levanos, A. Sahasrabudhe, and F. Dewhirst, "Bacterial diversity in human subgingival plaque," *Journal of Bacteriology*, vol. 183, pp. 3770–3783, June 2001.
- [32] S. S. Socransky, A. D. Haffajee, M. A. Cugini, C. Smith, and R. L. Kent, "Microbial complexes in subgingival plaque," *Journal of clinical periodontology*, vol. 25, pp. 134–144, February 1998.
- [33] D. Ivnitski, I. Abdel-Hamid, P. Atanasov, and E. Wilkins, "Biosensors for detection of pathogenic bacteria," *Biosensors and Bioelectronics*, vol. 14, no. 7, pp. 599–624, 1999.
- [34] M. Mammen, S. Choi, and G. Whitesides, "Polyvalent interactions in biological systems: implications for design and use of multivalent ligands and inhibitors," *Angewandte Chemie International Edition*, vol. 37, no. 20, pp. 2754–2794, 1998.
- [35] G. B. Sigal, M. Mammen, G. Dahmann, and G. M. Whitesides, "Polyacrylamides bearing pendant -sialoside groups strongly inhibit agglutination of erythrocytes by influenza virus: the strong inhibition reflects enhanced binding through cooperative polyvalent interactions," *Journal of the American Chemical Society*, vol. 118, pp. 3789–3800, April 1996.

- [36] K. El-Boubbou, C. Gruden, and X. Huang, "Magnetic glyco-nanoparticles: A unique tool for rapid pathogen detection, decontamination, and strain differentiation," *Journal of the American Chemical Society*, vol. 129, no. 44, pp. 13392–13393, 2007.
- [37] S. Lenoir, C. Pagnouille, C. Detrembleur, M. Galleni, and R. Jérôme, "New antibacterial cationic surfactants prepared by atom transfer radical polymerization," *Journal of Polymer Science Part A: Polymer Chemistry*, vol. 44, no. 3, pp. 1214–1224, 2006.
- [38] L. Silbert, I. B. Shlush, E. Israel, A. Porgador, S. Kolusheva, and R. Jelinek, "Rapid chromatic detection of bacteria by use of a new biomimetic polymer sensor," *Applied and Environmental Microbiology*, vol. 72, pp. 7339–7344, November 2006.
- [39] H. Murata, R. Koepsel, K. Matyjaszewski, and A. Russell, "Permanent, non-leaching antibacterial surfaces-2: How high density cationic surfaces kill bacterial cells," *Biomaterials*, vol. 28, pp. 4870–4879, August 2007.
- [40] N. Sharon and H. Lis, "Lectins as cell recognition molecules," *Science*, vol. 246, no. 4927, pp. 227–234, 1989.
- [41] A. Lamanna, J. Gestwicki, L. Strong, S. Borchardt, R. Owen, and L. Kiessling, "Conserved amplification of chemotactic responses through chemoreceptor interactions.," *Journal of bacteriology*, vol. 184, pp. 4981–4987, September 2002.
- [42] J. Gestwicki, C. Cairo, L. Strong, K. Oetjen, and L. Kiessling, "Influencing receptor-ligand binding mechanisms with multivalent ligand architecture," *Journal of the American Chemical Society*, vol. 124, pp. 14922–14933, Jan 2002.
- [43] K. Mortell, R. Weatherman, and L. Kiessling, "Recognition specificity of neoglycopolymers prepared by ring-opening metathesis polymerization," *Journal of the American Chemical Society*, vol. 118, pp. 2297–2298, Jan 1996.

- [44] M. Kanai, K. Mortell, and L. Kiessling, "Varying the size of multivalent ligands: The dependence of concanavalin a binding on neoglycopolymer length," *Journal of the American Chemical Society*, vol. 119, pp. 9931–9932, Jan 1997.
- [45] R. Owen, J. Gestwicki, T. Young, and L. Kiessling, "Synthesis and applications of end-labeled neoglycopolymers," *Organic letters*, vol. 4, pp. 2293–2296, July 2002.
- [46] N. Sharon, "Bacterial lectins, cell-cell recognition and infectious disease," *FEBS letters*, vol. 217, no. 2, pp. 145–157, 1987.
- [47] M. Disney, J. Zheng, T. Swager, and P. Seeberger, "Detection of bacteria with carbohydrate-functionalized fluorescent polymers," *Journal of the American Chemical Society*, vol. 126, no. 41, pp. 13343–13346, 2004.
- [48] G. Pasparakis, A. Cockayne, and C. Alexander, "Control of bacterial aggregation by thermoresponsive glycopolymers," *Journal of the American Chemical Society*, vol. 129, no. 36, pp. 11014–11015, 2007.
- [49] G. Pasparakis and C. Alexander, "Sweet talking double hydrophilic block copolymer vesicles," *Angewandte Chemie International Edition*, vol. 47, no. 26, pp. 4847–4850, 2008.
- [50] P. Gilbert and L. Moore, "Cationic antiseptics: diversity of action under a common epithet," *Journal of applied microbiology*, vol. 99, pp. 703–715, Oct 2005.
- [51] L. Rawlinson, S. Ryan, G. Mantovani, J. Syrett, D. Haddleton, and D. Brayden, "Antibacterial effects of poly (2-(dimethylamino ethyl) methacrylate) against selected gram-positive and gram-negative bacteria," *Biomacromolecules*, vol. 11, no. 2, pp. 443–453, 2010.
- [52] B. Weisblum, "Insights into erythromycin action from studies of its activity as inducer of resistance," *Antimicrobial agents and chemotherapy*, vol. 39, no. 4, p. 797, 1995.
- [53] M. Vaara and T. Vaara, "Polycations sensitize enteric bacteria to antibiotics," *Antimicrobial agents and chemotherapy*, vol. 24, no. 1, p. 107, 1983.

- [54] J. Tiller, C. Liao, K. Lewis, and A. Klibanov, "Designing surfaces that kill bacteria on contact," *Proceedings of the National Academy of Sciences*, vol. 98, no. 11, p. 5981, 2001.
- [55] V. Krishnamurthy, L. Quinton, L. Estroff, S. Metallo, J. Isaacs, J. Mizgerd, and G. Whitesides, "Promotion of opsonization by antibodies and phagocytosis of gram-positive bacteria by a bifunctional polyacrylamide," *Biomaterials*, vol. 27, no. 19, pp. 3663–3674, 2006.
- [56] S. J. Metallo, R. S. Kane, R. E. Holmlin, and G. M. Whitesides, "Using bifunctional polymers presenting vancomycin and fluorescein groups to direct anti-fluorescein antibodies to self-assembled monolayers presenting d-alanine-d-alanine groups," *Journal of the American Chemical Society*, vol. 125, pp. 4534–40, Apr 2003.
- [57] J. Rao, J. Lahiri, L. Isaacs, R. Weis, and G. Whitesides, "A trivalent system from vancomycin d-ala-d-ala with higher affinity than avidin biotin," *Science*, vol. 280, pp. 708–711, May 1998.
- [58] C. Bertozzi and M. Bednarski, "Antibody targeting to bacterial cells using receptor-specific ligands," *Journal of the American Chemical Society*, vol. 114, no. 6, pp. 2242–2245, 1992.
- [59] J. Shepherd, P. Sarker, K. Swindells, I. Douglas, S. MacNeil, L. Swanson, and S. Rimmer, "Binding bacteria to highly branched poly (n-isopropyl acrylamide) modified with vancomycin induces the coil-to-globule transition," *Journal of the American Chemical Society*, vol. 132, pp. 1736–1737, 2010.
- [60] C. Alexander, H. S. Andersson, L. I. Andersson, R. J. Ansell, N. Kirsch, I. A. Nicholls, J. O'Mahony, and M. J. Whitcombe, "Molecular imprinting science and technology: a survey of the literature for the years up to and including 2003," *Journal of molecular recognition*, vol. 19, pp. 106–180, March 2006.
- [61] A. Aherne, C. Alexander, M. Payne, and N. Perez, "Bacteria-mediated lithography of polymer surfaces," *Journal of the American Chemical Society*, vol. 118, no. 36, pp. 8771–8772, 1996.

- [62] S. D. Harvey, G. M. Mong, R. M. Ozanich, J. S. Mclean, S. M. Goodwin, N. B. Valentine, and J. K. Fredrickson, "Preparation and evaluation of spore-specific affinity-augmented bio-imprinted beads," *Analytical and bioanalytical chemistry*, vol. 386, pp. 211–219, September 2006.
- [63] O. Hayden and F. Dickert, "Selective microorganism detection with cell surface imprinted polymers," *Advanced Materials*, vol. 13, no. 19, pp. 1480–1483, 2001.
- [64] R. Schirhagl, E. W. Hall, I. Fuereder, and R. N. Zare, "Separation of bacteria with imprinted polymeric films," *Analyst*, vol. 137, pp. 1495–1499, March 2012.
- [65] F. Dickert, O. Hayden, R. Bindeus, K. Mann, D. Blaas, and E. Waigmann, "Bioimprinted qcm sensors for virus detection—screening of plant sap," *Anal Bioanal Chem*, vol. 378, no. 8, pp. 1929–1934, 2004.
- [66] M. Jenik, A. Seifner, P. Lieberzeit, and F. L. Dickert, "Pollen-imprinted polyurethanes for qcm allergen sensors," *Analytical and Bioanalytical Chemistry*, vol. 394, pp. 523–528, May 2009.
- [67] F. Dickert, O. Hayden, P. Lieberzeit, C. Haderspoeck, R. Bindeus, C. Palfinger, and B. Wirl, "Nano-and micro-structuring of sensor materials—from molecule to cell detection," *Synthetic Metals*, vol. 138, no. 1-2, pp. 65–69, 2003.
- [68] K. Nealson and J. Hastings, "Bacterial bioluminescence: its control and ecological significance," *Microbiology and Molecular Biology Reviews*, vol. 43, pp. 496–518, December 1979.
- [69] M. Miller and B. Bassler, "Quorum sensing in bacteria," *Annual Reviews in Microbiology*, vol. 55, no. 1, pp. 165–199, 2001.
- [70] C. M. Waters and B. L. Bassler, "Quorum sensing: Cell-to-cell communication in bacteria," *Annual review of cell and developmental biology*, vol. 21, pp. 319–346, Nov 2005.

- [71] T. D. Kievit, R. Gillis, S. Marx, C. Brown, and B. Iglewski, "Quorum-sensing genes in pseudomonas aeruginosa biofilms: their role and expression patterns," *Applied and environmental microbiology*, vol. 67, no. 4, p. 1865, 2001.
- [72] M. Hentzer, H. Wu, J. B. Andersen, K. Riedel, T. BRasmussen, N. Bagge, N. Kumar, M. ASchembri, Z. Song, P. Kristoffersen, M. Maneeld, J. WCosterton, S. Molin, L. Eberl, P. Steinberg, S. Kjelleberg, and N. H. andMichael Givskov, "Attenuation of pseudomonas aeruginosa virulence by quorum sensing inhibitors," *The EMBO Journal*, vol. 22, no. 15, pp. 3803–3815, 2003.
- [73] C. Lowery, J. Park, G. Kaufmann, and K. Janda, "An unexpected switch in the modulation of ai-2-based quorum sensing discovered through synthetic 4, 5-dihydroxy-2, 3-pentanedione analogues," *Journal of the American Chemical Society*, vol. 130, no. 29, pp. 9200–9201, 2008.
- [74] A. Garner, J. Park, J. Zakhari, C. Lowery, A. Struss, D. Sawada, G. Kaufmann, and K. Janda, "A multivalent probe for ai-2 quorum sensing receptors," *Journal of the American Chemical Society*, 2011.
- [75] T. Ikeda, Y. Inoue, A. Suehiro, H. Ikeshoji, T. Ishida, N. Takiguchi, A. Kuroda, J. Kato, and H. Ohtake, "The effects of cyclodextrins on autoinducer activities of quorum sensing in pseudomonas aeruginosa," *Journal of inclusion phenomena and macrocyclic chemistry*, vol. 44, no. 1, pp. 381–382, 2002.
- [76] N. Kato, T. Morohoshi, T. Nozawa, H. Matsumoto, and T. Ikeda, "Control of gram-negative bacterial quorum sensing with cyclodextrin immobilized cellulose ether gel," *Journal of inclusion phenomena and macrocyclic chemistry*, vol. 56, pp. 55–59, October 2006.
- [77] N. Kato, T. Tanaka, S. Nakagawa, T. Morohoshi, K. Hiratani, and T. Ikeda, "Control of virulence factor expression in opportunistic pathogens using cyclodextrin immobilized gel," *Journal of inclusion phenomena and macrocyclic chemistry*, vol. 57, pp. 419–423, Mar 2007.

- [78] J. Lorand and J. Edwards, "Polyol complexes and structure of the benzenboronate ion," *The Journal of Organic Chemistry*, vol. 24, pp. 769–774, June 1959.
- [79] N. Ni, G. Choudhary, H. Peng, M. Li, H. Chou, C. Lu, E. Gilbert, and B. Wang, "Inhibition of quorum sensing in *vibrio harveyi* by boronic acids," *Chemical biology & drug design*, vol. 74, no. 1, pp. 51–56, 2009.
- [80] X. Xue, G. Pasparakis, N. Halliday, K. Winzer, S. M. Howdle, C. J. Cramphorn, N. R. Cameron, P. M. Gardner, B. G. Davis, F. Fernandez-Trillo, and C. Alexander, "Synthetic polymers for simultaneous bacterial sequestration and quorum sense interference," *Angewandte Chemie International Edition*, vol. 50, pp. 9852–9856, Sep 2011.
- [81] E. V. Piletska, G. Stavroulakis, K. Karim, M. J. Whitcombe, I. Chianella, A. Sharma, K. E. Eboigbodin, G. K. Robinson, and S. A. Piletsky, "Attenuation of *vibrio fischeri* quorum sensing using rationally designed polymers," *Biomacromolecules*, vol. 11, pp. 975–980, 2010.
- [82] E. V. Piletska, G. Stavroulakis, L. D. Larcombe, M. J. Whitcombe, A. Sharma, S. Primrose, G. K. Robinson, and S. A. Piletsky, "Passive control of quorum sensing: Prevention of *pseudomonas aeruginosa* biofilm formation by imprinted polymers," *Biomacromolecules*, vol. 12, pp. 1067–1071, 2011.
- [83] K. Xavier and B. Bassler, "Luxs quorum sensing: more than just a numbers game," *Current opinion in microbiology*, vol. 6, no. 2, pp. 191–197, 2003.
- [84] H. Donabedian, "Quorum sensing and its relevance to infectious diseases," *Journal of Infection*, vol. 46, pp. 207–214, May 2003.
- [85] S. G. Spain, L. Albertin, and N. R. Cameron, "Facile in situ preparation of biologically active multivalent glyconanoparticles," *Chem. Commun.*, p. 4198, Jan 2006.

- [86] M. Toyoshima and Y. Miura, "Preparation of glycopolymer-substituted gold nanoparticles and their molecular recognition," *Journal of Polymer Science Part A: Polymer Chemistry*, vol. 47, pp. 1412–1421, Mar 2009.
- [87] R. Phillips, O. Miranda, C.-C. You, V. Rotello, and U. Bunz, "Rapid and efficient identification of bacteria using gold-nanoparticle–poly(para-phenyleneethynylene) constructs," *Angewandte Chemie International Edition*, vol. 47, pp. 2590–2594, Mar 2008.
- [88] D. McQuade, A. Pullen, and T. Swager, "Conjugated polymer-based chemical sensors," *Chemical Reviews*, vol. 100, no. 7, pp. 2537–2574, 2000.
- [89] M. Baek, R. Stevens, and D. Charych, "Design and synthesis of novel glycopolythiophene assemblies for colorimetric detection of influenza virus and e. coli," *Bioconjugate Chem*, vol. 11, no. 6, pp. 777–788, 2000.
- [90] C. Sun, Y. Zhang, Y. Fan, Y. Li, and J. Li, "Mannose-escherichia coli interaction in the presence of metal cations studied in vitro by colorimetric polydiacetylene/glycolipid liposomes," *Journal of inorganic biochemistry*, vol. 98, no. 6, pp. 925–930, 2004.
- [91] M. Szwarc, "'living' polymers," *Nature*, vol. 178, pp. 1168–1169, November 1956.
- [92] M. Georges, R. Veregin, P. Kazmaier, and G. Hamer, "Narrow molecular weight resins by a free-radical polymerization process," *Macromolecules*, vol. 26, no. 11, pp. 2987–2988, 1993.
- [93] B. Wayland, G. Poszmik, S. Mukerjee, and M. Fryd, "Living radical polymerization of acrylates by organocobalt porphyrin complexes," *Journal of the American Chemical Society*, vol. 116, no. 17, pp. 7943–7944, 1994.
- [94] M. Kato, M. Kamigaito, M. Sawamoto, and T. Higashimura, "Polymerization of methyl methacrylate with the carbon tetrachloride/dichlorotris-(triphenylphosphine) ruthenium (ii)/methylaluminum bis (2, 6-di-tert-butylphenoxide) initiating system: possibility of living radical polymerization," *Macromolecules*, vol. 28, no. 5, pp. 1721–1723, 1995.

- [95] J. Chiefari, Y. Chong, F. Ercole, and J. Krstina, "Living free-radical polymerization by reversible addition-fragmentation chain transfer: The raft process," *Macromolecules*, vol. 31, no. 16, pp. 5559–5562, 1998.
- [96] T. Patten, J. Xia, T. Abernathy, and K. Matyjaszewski, "Polymers with very low polydispersities from atom transfer radical polymerization," *Science*, vol. 272, no. 5263, p. 866, 1996.
- [97] W. Braunecker and K. Matyjaszewski, "Controlled/living radical polymerization: Features, developments, and perspectives," *Progress in Polymer Science*, vol. 32, no. 1, pp. 93–146, 2007.
- [98] J. Wang and K. Matyjaszewski, "Controlled/" living" radical polymerization. atom transfer radical polymerization in the presence of transition-metal complexes," *Journal of the American Chemical Society*, vol. 117, no. 20, pp. 5614–5615, 1995.
- [99] W. Tang, Y. Kwak, and W. Braunecker, "Understanding atom transfer radical polymerization: Effect of ligand and initiator structures on the equilibrium constants," *Journal of the American Chemical Society*, vol. 130, pp. 10702–10713, Jan 2008.
- [100] K. Matyjaszewski and J. Xia, "Atom transfer radical polymerization," *Chemical Reviews*, vol. 101, no. 9, pp. 2921–2990, 2001.
- [101] M. Kamigaito, T. Ando, and M. Sawamoto, "Metal-catalyzed living radical polymerization," *Chemical Reviews*, vol. 101, no. 12, pp. 3689–3746, 2001.
- [102] M. Krzysztow, *Controlled Radical Polymerization: State of the Art in 2008*, ch. 2, pp. 3–13. American Chemical Society, 2009.
- [103] Z. Zhang, G. Liu, and S. Bell, "Synthesis of poly (solketal methacrylate)-block-poly (2-(dimethylamino) ethyl methacrylate) and preparation of nanospheres with cross-linked shells," *Macromolecules*, vol. 33, no. 21, pp. 7877–7883, 2000.

- [104] R. Teoh, K. Guice, and Y. Loo, "Atom transfer radical copolymerization of hydroxyethyl methacrylate and dimethylaminoethyl methacrylate in polar solvents," *Macromolecules*, vol. 39, no. 25, pp. 8609–8615, 2006.
- [105] K. Matyjaszewski, P. Miller, J. Pyun, G. Kickelbick, and S. Diamanti, "Synthesis and characterization of star polymers with varying arm number, length, and composition from organic and hybrid inorganic/organic multifunctional initiators," *Macromolecules*, vol. 32, no. 20, pp. 6526–6535, 1999.
- [106] J. Pyun, T. Kowalewski, and K. Matyjaszewski, "Synthesis of polymer brushes using atom transfer radical polymerization," *Macromolecular rapid communications*, vol. 24, no. 18, pp. 1043–1059, 2003.
- [107] M. Li, N. Jahed, K. Min, and K. Matyjaszewski, "Preparation of linear and star-shaped block copolymers by atp using simultaneous reverse and normal initiation process in bulk and miniemulsion," *Macromolecules*, vol. 37, no. 7, pp. 2434–2441, 2004.
- [108] W. Huang, J. Kim, M. Bruening, and G. Baker, "Functionalization of surfaces by water-accelerated atom-transfer radical polymerization of hydroxyethyl methacrylate and subsequent derivatization," *Macromolecules*, vol. 35, no. 4, pp. 1175–1179, 2002.
- [109] K. Robinson, M. Khan, M. de Paz Banez, X. Wang, and S. Armes, "Controlled polymerization of 2-hydroxyethyl methacrylate by atp at ambient temperature," *Macromolecules*, vol. 34, no. 10, pp. 3155–3158, 2001.
- [110] X.-S. Wang and S. P. Arnes, "Facile atom transfer radical polymerization of methoxy-capped oligo(ethylene glycol) methacrylate in aqueous media at ambient temperature," *Macromolecules*, vol. 33, pp. 6640–6647, 2000.

- [111] S. Perrier, S. Armes, X. Wang, F. Malet, D. Haddleton, and E. FM, "Copper (i)-mediated radical polymerization of methacrylates in aqueous solution," *Journal of Polymer Science Part A Polymer Chemistry*, vol. 39, no. 10, pp. 1696–1707, 2001.
- [112] N. Tsarevsky, T. Pintauer, and K. Matyjaszewski, "Deactivation efficiency and degree of control over polymerization in atp in protic solvents," *Macromolecules*, vol. 37, no. 26, pp. 9768–9778, 2004.
- [113] K. Min, H. Gao, and K. Matyjaszewski, "Preparation of homopolymers and block copolymers in miniemulsion by atp using activators generated by electron transfer (aget)," *Journal of the American Chemical Society*, vol. 127, no. 11, pp. 3825–3830, 2005.
- [114] J. Oh, K. Min, and K. Matyjaszewski, "Preparation of poly (oligo (ethylene glycol) monomethyl ether methacrylate) by homogeneous aqueous aget atp," *Macromolecules*, vol. 39, no. 9, pp. 3161–3167, 2006.
- [115] K. Min, H. Gao, and K. Matyjaszewski, "Use of ascorbic acid as reducing agent for synthesis of well-defined polymers by arget atp," *Macromolecules*, vol. 40, no. 6, pp. 1789–1791, 2007.
- [116] K. Matyjaszewski, W. Jakubowski, K. Min, W. Tang, J. Huang, W. Braunecker, and N. Tsarevsky, "Diminishing catalyst concentration in atom transfer radical polymerization with reducing agents," *Proceedings of the National Academy of Sciences*, vol. 103, no. 42, pp. 15309–15314, 2006.
- [117] N. V. Tsarevsky and K. Matyjaszewski, "Environmentally benign atom transfer radical polymerization: Towards "green" processes and materials," *Journal of Polymer Science Part A: Polymer Chemistry*, vol. 44, pp. 5098–5112, Sep 2006.
- [118] N. Tsarevsky and K. Matyjaszewski, "'green" atom transfer radical polymerization: From process design to preparation of well-defined environmentally friendly polymeric materials," *Chemical Reviews*, vol. 107, no. 6, pp. 2270–2299, 2007.

- [119] D. Haddleton, C. Jasieczek, M. Hannon, and A. Shooter, "Atom transfer radical polymerization of methyl methacrylate initiated by alkyl bromide and 2-pyridinecarbaldehyde imine copper(i) complexes," *Macromolecules*, vol. 30, pp. 2190–2193, Jan 1997.
- [120] K. Matyjaszewski and J. Xia, "Controlled/'living' radical polymerization. atom transfer radical polymerization catalyzed by copper (i) and picolylamine complexes," *Macromolecules*, vol. 32, no. 8, pp. 2434–2438, 1999.
- [121] N. Shaner, R. Campbell, P. Steinbach, B. Giepmans, A. Palmer, and R. Tsien, "Improved monomeric red, orange and yellow fluorescent proteins derived from *discosoma* sp. red fluorescent protein," *Nature biotechnology*, vol. 22, no. 12, pp. 1567–1572, 2004.
- [122] A. Zaborin, K. Romanowski, S. Gerdes, C. Holbrook, F. Lepine, J. Long, V. Poroyko, S. Diggle, A. Wilke, and K. Righetti, "Red death in *caenorhabditis elegans* caused by *pseudomonas aeruginosa* pao1," *Proceedings of the National Academy of Sciences*, vol. 106, no. 15, pp. 6327–6332, 2009.
- [123] K. Eboigbodin, J. Newton, A. Routh, and C. Biggs, "Role of nonadsorbing polymers in bacterial aggregation," *Langmuir*, vol. 21, no. 26, pp. 12315–12319, 2005.
- [124] W. Rocque, S. Fesik, A. Haug, and E. McGroarty, "Polycation binding to isolated lipopolysaccharide from antibiotic-hypersusceptible mutant strains of *escherichia coli*," *Antimicrobial agents and chemotherapy*, vol. 32, no. 3, p. 308, 1988.
- [125] V. Ladmiral, G. Mantovani, and G. Clarkson, "Synthesis of neoglycopolymers by a combination of "click chemistry" and living radical polymerization," *Journal of the American Chemical Society*, vol. 128, pp. 4823–4830, April 2006.
- [126] P. Ravi, S. Dai, and K. C. Tam, "Synthesis and self-assembly of [60]fullerene containing sulfobetaine polymer in aqueous solution," *Journal of Physical Chemistry B*, vol. 109, pp. 22791–8, Dec 2005.

- [127] S. Roy and P. K. Das, "Antibacterial hydrogels of amino acid-based cationic amphiphiles," *Biotechnology and bioengineering*, vol. 100, pp. 756–764, Jul 2008.
- [128] C. Geddes, "Optical halide sensing using fluorescence quenching," *Measurement Science and Technology*, vol. 12, pp. R53–R88, 2001.
- [129] G. Cheng, Z. Zhang, S. Chen, J. Bryers, and S. Jiang, "Inhibition of bacterial adhesion and biofilm formation on zwitterionic surfaces," *Biomaterials*, vol. 28, no. 29, pp. 4192–4199, 2007.
- [130] G. Li, G. Cheng, H. Xue, S. Chen, F. Zhang, and S. Jiang, "Ultra low fouling zwitterionic polymers with a biomimetic adhesive group," *Biomaterials*, vol. 29, no. 35, pp. 4592–4597, 2008.
- [131] H. Liu, Y. Yang, X. Shen, Z. Zhang, P. Shen, and Z. Xie, "Role of dna in bacterial aggregation," *Current Microbiology*, vol. 57, no. 2, pp. 139–144, 2008.
- [132] T. James, K. Sandanayake, and S. Shinkai, "Saccharide sensing with molecular receptors based on boronic acid," *Angewandte Chemie International Edition in English*, vol. 35, no. 17, pp. 1910–1922, 1996.
- [133] T. James, H. Shinmori, M. Takeuchi, and S. Shinkai, "A saccharide 'sponge'. synthesis and properties of a dendritic boronic acid," *Chemical Communications*, no. 6, pp. 705–706, 1996.
- [134] T. James, K. Sandanayake, and S. Shinkai, "Chiral discrimination of monosaccharides using a fluorescent molecular sensor," *Nature*, vol. 374, pp. 345–347, March 1994.
- [135] B. S. J Cambre, "Biomedical applications of boronic acid polymers," *Polymer*, vol. 52, pp. 4631–4643, Jan 2011.
- [136] R. Wannapoba, P. Kanatharanaa, W. Limbuta, A. Numnuama, P. Asawatreratanakula, C. Thammakheta, and P. Thavarungkula, "Affinity sensor using 3-aminophenylboronic acid for bacteria detection," *Biosensors and Bioelectronics*, vol. 26, pp. 357–364, Oct 2010.

- [137] A. Ivanov, H. Panahi, M. Kuzimenkova, L. Nilsson, B. Bergenståhl, H. Waqif, M. Jahanshahi, I. Galaev, and B. Mattiasson, "Affinity adhesion of carbohydrate particles and yeast cells to boronate-containing polymer brushes grafted onto siliceous supports," *Chemistry : a European journal*, vol. 12, no. 27, pp. 7204–7214, 2006.
- [138] M. Ambrosi, N. Cameron, and B. Davis, "Lectins: tools for the molecular understanding of the glycode," *Organic & biomolecular chemistry*, vol. 3, pp. 1593–1608, May 2005.
- [139] W. Sun, H. Bandmann, and T. Schrader, "A fluorescent polymeric heparin sensor," *Chemistry : a European journal*, vol. 13, no. 27, pp. 7701–7707, 2007.
- [140] J. V. Gompel and G. Schuster, "Chemiluminescence of organic peroxides: intramolecular electron-exchange luminescence from a secondary perester," *Journal of Organic Chemistry*, vol. 52, no. 8, pp. 1465–1468, 1987.
- [141] G. Springsteen and B. Wang, "A detailed examination of boronic acid-diol complexation," *Tetrahedron*, vol. 58, pp. 5291–5300, June 2002.
- [142] K. S. T James and S. Shinkai, "Novel photoinduced electron-transfer sensor for saccharides based on the interaction of boronic acid and amine," *Journal of the Chemical Society, Chemical Communications*, pp. 477–478, Jan 1994.
- [143] G. Wulff, "Selective binding to polymers via covalent bonds. the construction of chiral cavities as specific receptor sites," *Pure and Applied Chemistry*, vol. 54, pp. 2093–2102, Jan 1982.
- [144] S. Swillens, "Interpretation of binding curves obtained with high receptor concentrations: practical aid for computer analysis.," *Molecular pharmacology*, vol. 47, pp. 1197–1203, June 1995.
- [145] G. Moad, J. Chiefari, Y. Chong, J. Krstina, R. Mayadunne, A. Postma, E. Rizzardo, and S. Thang, "Living free radical polymerization with reversible addition: fragmentation chain transfer(the life of raft)," *Polymer International*, vol. 49, no. 9, pp. 993–1001, 2000.

- [146] P. V. de Wetering, J. Cherng, H. Talsma, D. Crommelin, and W. Hennink, “2-(dimethylamino) ethyl methacrylate based (co) polymers as gene transfer agents,” *Journal of controlled release*, vol. 53, no. 1, pp. 145–153, 1998.
- [147] I. Ofek and E. Beachey, “Mannose binding and epithelial cell adherence of escherichia coli,” *Infection and Immunity*, vol. 22, pp. 247–254, October 1978.
- [148] V. Schöler, A. Lussi, A. Kage, and R. Seemann, “Glycan-binding specificities of streptococcus mutans and streptococcus sobrinus lectin-like adhesins,” *Clinical oral investigations*, vol. 16, pp. 789–796, June 2012.
- [149] J. Bouckaert, J. Berglund, M. Schembri, E. D. Genst, L. Cools, M. Wührer, C. Hung, J. Pinkner, R. Slättegård, and A. Zavialov, “Receptor binding studies disclose a novel class of highaffinity inhibitors of the escherichia coli fimh adhesin,” *Molecular Microbiology*, vol. 55, no. 2, pp. 441–455, 2005.
- [150] L. Timofeeva and N. Kleshcheva, “Antimicrobial polymers: mechanism of action, factors of activity, and applications,” *Applied microbiology and biotechnology*, vol. 89, pp. 475–492, Feb 2011.
- [151] C. Ornelas-Megiatto, P. Wich, and J. Frechet, “Polyphosphonium polymers for sirna delivery: An efficient and non-toxic alternative to polyammonium carriers,” *Journal of the American Chemical Society*, 2012.
- [152] W. Hinrichs, N. Schuurmans-Nieuwenbroek, P. VanDeWetering, and W. Hennink, “Thermosensitive polymers as carriers for dna delivery,” *Journal of controlled release*, vol. 60, no. 2, pp. 249–259, 1999.
- [153] G. Borchard, H. Lueen, A. de Boer, J. Verhoef, C. Lehr, and H. Junginger, “The potential of mucoadhesive polymers in enhancing intestinal peptide drug absorption. iii: Effects of

- chitosan-glutamate and carbomer on epithelial tight junctions in vitro,” *Journal of controlled release*, vol. 39, no. 2, pp. 131–138, 1996.
- [154] G. McEwan, M. Jepson, B. Hirst, and N. L. Simmons, “Polycation-induced enhancement of epithelial paracellular permeability is independent of tight junctional characteristics,” *Biochimica et biophysica acta*, vol. 1148, pp. 51–60, May 1993.
- [155] Y. Huang, Y. Wang, and X. Yan, “Amine-functionalized magnetic nanoparticles for rapid capture and removal of bacterial pathogens,” *Environmental science & technology*, vol. 44, pp. 7908–7913, September 2010.
- [156] J. Huang, H. Murata, R. Koepsel, A. Russell, and K. Matyjaszewski, “Antibacterial polypropylene via surface-initiated atom transfer radical polymerization,” *Biomacromolecules*, vol. 8, no. 5, pp. 1396–1399, 2007.
- [157] P. Broxton, P. Woodcock, and P. Gilbert, “A study of the antibacterial activity of some polyhexamethylene biguanides towards escherichia coli atcc 8739,” *Journal of applied microbiology*, vol. 54, pp. 345–353, June 1983.
- [158] P. Broxton, P. Woodcock, K. Heatley, and P. Gilbert, “Interaction of some polyhexamethylene biguanides and membrane phospholipids in escherichia coli,” *The Journal of applied bacteriology*, vol. 57, pp. 115–124, August 1984.
- [159] Y. Wang, Z. Zhou, J. Zhu, Y. Tang, T. D. Canady, E. Y. Chi, K. S. Schanze, and D. G. Whitten, “Dark antimicrobial mechanisms of cationic phenylene ethynylene polymers and oligomers against escherichia coli,” *Polymers*, vol. 3, pp. 1199–1214, Jul 2011.
- [160] D. Fischer, Y. Li, B. Ahlemeyer, J. Kriegelstein, and T. Kissel, “In vitro cytotoxicity testing of polycations: influence of polymer structure on cell viability and hemolysis,” *Biomaterials*, vol. 24, no. 7, pp. 1121–1131, 2003.

- [161] E. Böttger, B. Springer, T. Prammananan, Y. Kidan, and P. Sander, "Structural basis for selectivity and toxicity of ribosomal antibiotics," *EMBO reports*, vol. 2, no. 4, pp. 318–323, 2001.
- [162] J. Andrews, "Determination of minimum inhibitory concentrations," *Journal of Antimicrobial Chemotherapy*, vol. 48, no. Supplement 1, pp. 5–16, 2001.
- [163] M. J. Bruining, H. G. Blaauwgeers, R. Kuijter, E. Pels, R. M. Nuijts, and L. H. Koole, "Biodegradable three-dimensional networks of poly(dimethylamino ethyl methacrylate). synthesis, characterization and in vitro studies of structural degradation and cytotoxicity," *Biomaterials*, vol. 21, pp. 595–604, Mar 2000.
- [164] J. Williams, "Bac guidelines on sensitivity testing," *Journal of Antimicrobial Chemotherapy*, vol. 31, no. 6, pp. 1001–1003, 1993.
- [165] I. Wiegand, K. Hilpert, and R. E. Hancock, "Agar and broth dilution methods to determine the minimal inhibitory concentration (mic) of antimicrobial substances," *Nature protocols*, vol. 3, no. 2, pp. 163–175, 2008.
- [166] M. Ward, M. Sanchez, M. Elasmri, and A. Lowe, "Antimicrobial activity of statistical poly-methacrylic sulfopropylbetaines against grampositive and gramnegative bacteria," *Journal of applied polymer science*, vol. 101, no. 2, pp. 1036–1041, 2006.
- [167] E. Kenawy, F. Abdel-Hay, A. El-Shanshoury, and M. El-Newehy, "Biologically active polymers: synthesis and antimicrobial activity of modified glycidyl methacrylate polymers having a quaternary ammonium and phosphonium groups," *Journal of controlled release*, vol. 50, no. 1-3, pp. 145–152, 1998.
- [168] W. Jakubowski and K. Matyjaszewski, "Activator generated by electron transfer for atom transfer radical polymerization," *Macromolecules*, vol. 38, pp. 4139–4146, April 2005.

- [169] S. J. Sigg, F. Seidi, K. Renggli, T. B. Silva, G. Kali, and N. Bruns, "Horseradish peroxidase as a catalyst for atom transfer radical polymerization," *Macromolecular Rapid Communications*, vol. 32, pp. 1710–1715, November 2011.
- [170] C. Rensing and G. Grass, "Escherichia coli mechanisms of copper homeostasis in a changing environment," *FEMS Microbiology Reviews*, vol. 27, no. 23, pp. 197–213, 2003.
- [171] L. Rodriguez-Montelongo, L. C. DeLaCruz-Rodriguez, R. N. Farías, and E. M. Massa, "Membrane-associated redox cycling of copper mediates hydroperoxide toxicity in escherichia coli," *Biochimica et Biophysica Acta (BBA) - Bioenergetics*, vol. 1144, pp. 77–84, Aug 1993.
- [172] V. Rapisarda, L. Montelongo, R. Farías, and E. Massa, "Characterization of an nadh-linked cupric reductase activity from the escherichia coli respiratory chain," *Archives of biochemistry and biophysics*, vol. 370, no. 2, pp. 143–150, 1999.
- [173] Y. Wang and H. Shen, "Bacterial reduction of hexavalent chromium," *Journal of Industrial Microbiology & Biotechnology*, vol. 14, no. 2, pp. 159–163, 1995.
- [174] H. Hassan and I. Fridovich, "Mechanism of the antibiotic action pyocyanine.," *Journal of bacteriology*, vol. 141, no. 1, pp. 156–163, 1980.
- [175] N. Mitik-Dineva, J. Wang, V. K. Truong, P. Stoddart, F. Malherbe, R. J. Crawford, and E. P. Ivanova, "Escherichia coli, pseudomonas aeruginosa, and staphylococcus aureus attachment patterns on glass surfaces with nanoscale roughness," *Current microbiology*, vol. 58, pp. 268–273, Mar 2009.
- [176] M. V. Loosdrecht, J. Lyklema, W. Norde, G. Schraa, and A. Zehnder, "Electrophoretic mobility and hydrophobicity as a measured to predict the initial steps of bacterial adhesion.," *Applied and Environmental Microbiology*, vol. 53, no. 8, pp. 1898–1901, 1987.

- [177] G. Cheng, Z. Zhang, S. Chen, J. Bryers, and S. Jiang, "Inhibition of bacterial adhesion and biofilm formation on zwitterionic surfaces," *Biomaterials*, vol. 28, no. 29, pp. 4192–4199, 2007.
- [178] D. Schleheck, N. Barraud, J. Klebensberger, J. S. Webb, D. McDougald, S. A. Rice, and S. Kjelleberg, "Pseudomonas aeruginosa pao1 preferentially grows as aggregates in liquid batch cultures and disperses upon starvation," *PLoS ONE*, vol. 4, p. e5513, May 2009.
- [179] P. Larsen, L. Sydnès, B. Landfald, and A. Strøm, "Osmoregulation in escherichia coli by accumulation of organic osmolytes: betaines, glutamic acid, and trehalose," *Archives of microbiology*, vol. 147, no. 1, pp. 1–7, 1987.
- [180] H. Kolb, M. Finn, and K. Sharpless, "Click chemistry: diverse chemical function from a few good reactions," *Angewandte Chemie International Edition*, vol. 40, no. 11, pp. 2004–2021, 2001.
- [181] R. Huisgen, "1, 3dipolar cycloadditions. past and future," *Angewandte Chemie International Edition*, vol. 2, pp. 565–598, Jan 1963.
- [182] V. Rostovtsev, L. Green, V. Fokin, and K. Sharpless, "A stepwise huisgen cycloaddition process: copper (i)catalyzed regioselective "ligation" of azides and terminal alkynes," *Angewandte Chemie International Edition*, vol. 114, no. 14, pp. 2708–2711, 2002.
- [183] J. Geng, G. Mantovani, L. Tao, J. Nicolas, G. Chen, R. Wallis, D. Mitchell, B. Johnson, S. Evans, and D. Haddleton, "Site-directed conjugation of "clicked" glycopolymers to form glycoprotein mimics: binding to mammalian lectin and induction of immunological function," *Journal of the American Chemical Society*, vol. 129, no. 49, pp. 15156–15163, 2007.
- [184] C. D. Hein, X.-M. Liu, and D. Wang, "Click chemistry, a powerful tool for pharmaceutical sciences," *Pharmaceutical research*, vol. 25, pp. 2216–2230, Oct 2008.

- [185] H. Kolb and K. Sharpless, "The growing impact of click chemistry on drug discovery," *Drug discovery today*, vol. 8, no. 24, pp. 1128–1137, 2003.
- [186] J. Moses and A. Moorhouse, "The growing applications of click chemistry," *Chem. Soc. Rev.*, vol. 36, pp. 1249–1262, May 2007.
- [187] A. Brik, J. Muldoon, Y.-C. Lin, J. H. Elder, D. S. Goodsell, A. J. Olson, V. V. Fokin, K. B. Sharpless, and C.-H. Wong, "Rapid diversity-oriented synthesis in microtiter plates for in situ screening of hiv protease inhibitors," *Chembiochem : a European journal of chemical biology*, vol. 4, pp. 1246–1248, November 2003.
- [188] M. Giffin, H. Heaslet, A. Brik, Y. Lin, G. Cauvi, C. Wong, D. McRee, J. Elder, C. Stout, and B. Torbett, "A copper (i)-catalyzed 1, 2, 3-triazole azide alkyne click compound is a potent inhibitor of a multidrug-resistant hiv-1 protease variant," *Journal of Medicinal Chemistry*, vol. 51, no. 20, pp. 6263–6270, 2008.
- [189] S. G. Agalave, S. R. Maujan, and V. S. Pore, "Click chemistry: 1,2,3-triazoles as pharmacophores," *Chemistry – An Asian Journal*, vol. 6, pp. 2696–2718, Aug 2011.
- [190] N. S. Vatmurge, B. G. Hazra, V. S. Pore, F. Shirazi, M. V. Deshpande, S. Kadreppa, S. Chattopadhyay, and R. G. Gonnade, "Synthesis and biological evaluation of bile acid dimers linked with 1,2,3-triazole and bis--lactam," *Organic & Biomolecular Chemistry*, vol. 6, pp. 3823–3830, October 2008.
- [191] A. Speers and B. Cravatt, "Profiling enzyme activities in vivo using click chemistry methods," *Chemistry & biology*, vol. 11, no. 4, pp. 535–546, 2004.
- [192] K. Sivakumar, F. Xie, B. Cash, S. Long, H. Barnhill, and Q. Wang, "A fluorogenic 1,3-dipolar cycloaddition reaction of 3-azidocoumarins and acetylenes," *Organic letters*, vol. 6, pp. 4603–4606, November 2004.

- [193] G. Lemieux, C. de Graffenried, and C. Bertozzi, "A fluorogenic dye activated by the Staudinger ligation," *Journal of the American Chemical Society*, vol. 125, no. 16, pp. 4708–4709, 2003.
- [194] S. Franzen, W. Ni, and B. Wang, "Study of the mechanism of electron-transfer quenching by boron-nitrogen adducts in fluorescent sensors," *The Journal of Physical Chemistry B*, vol. 107, no. 47, pp. 12942–12948, 2003.
- [195] H. C. Ansel, W. P. Norred, and I. L. Roth, "Antimicrobial activity of dimethyl sulfoxide against *Escherichia coli*, *Pseudomonas aeruginosa*, and *Bacillus megaterium*," *Journal of Pharmaceutical Sciences*, vol. 58, pp. 836–839, July 1969.
- [196] N. Bao, B. Jagadeesan, A. Bhunia, Y. Yao, and C. Lu, "Quantification of bacterial cells based on autofluorescence on a microfluidic platform," *Journal of Chromatography A*, vol. 1181, no. 1, pp. 153–158, 2008.
- [197] L. Mueller and K. Matyjaszewski, "Reducing copper concentration in polymers prepared via atom transfer radical polymerization," *Macromolecular Reaction Engineering*, vol. 4, pp. 180–185, March 2010.
- [198] Y. Shen, S. Zhu, and R. Pelton, "Soluble and recoverable support for copper bromide-mediated living radical polymerization," *Macromolecules*, vol. 34, pp. 3182–3185, April 2001.
- [199] K. Rathwell, J. Sperry, and M. Brimble, "Synthesis of triazole analogues of the nanaomycin antibiotics using 'click chemistry'," *Tetrahedron*, vol. 66, no. 23, pp. 4002–4009, 2010.
- [200] I. Dreier, S. Kumar, H. Søndergaard, M. Rasmussen, L. Hansen, J. Kongsted, B. Vester, and P. Nielsen, "A click chemistry approach to pleuromutilin derivatives, part 2: Conjugates with acyclic nucleosides and their ribosomal binding and antibacterial activity," *Journal of Medicinal Chemistry*, vol. 55, pp. 2067–2077, March 2012.

- [201] M. J. Schwaber and Y. Carmeli, "Antimicrobial resistance and patient outcomes: the hazards of adjustment," *Critical Care*, vol. 10, no. 5, p. 164, 2006.
- [202] D. P. Raymond, S. J. Pelletier, T. D. Crabtree, H. L. Evans, T. L. Pruett, and R. G. Sawyer, "Impact of antibiotic-resistant gram-negative bacilli infections on outcome in hospitalized patients," *Critical care medicine*, vol. 31, no. 4, pp. 1035–1041, 2003.
- [203] H. Neu, "The crisis in antibiotic resistance.," *Science*, vol. 257, no. 5073, pp. 1064–1073, 1992.
- [204] J. Davies and D. Davies, "Origins and evolution of antibiotic resistance," *Microbiology and Molecular Biology Reviews*, vol. 74, pp. 417–433, September 2010.
- [205] C. Alexander and E. Vulfson, "Spatially functionalized polymer surfaces produced via cell-mediated lithography," *Advanced Materials*, vol. 9, pp. 751–755, October 1997.
- [206] G. Whitesides and C. Wong, "Enzymes as catalysts in synthetic organic chemistry," *Angewandte Chemie International Edition in English*, vol. 24, no. 8, pp. 617–638, 1985.
- [207] M. Evans, D. Feola, and R. Rapp, "Polymyxin b sulfate and colistin: old antibiotics for emerging multiresistant gram-negative bacteria," *The Annals of pharmacotherapy*, vol. 33, pp. 960–967, September 1999.
- [208] M. Falagas, A. P. Grammatikos, and A. Michalopoulos, "Potential of old-generation antibiotics to address current need for new antibiotics," *Expert Review of Anti-infective Therapy*, vol. 6, pp. 593–600, Jan 2008.
- [209] M. A. Fischbach and C. T. Walsh, "Antibiotics for emerging pathogens," *Science*, vol. 325, pp. 1089–1093, Aug 2009.
- [210] R. VanDerMeet, H. N. Linssen, and A. L. German, "Improved methods of estimating monomer reactivity ratios in copolymerization by considering experimental errors in both

variables,” *Journal of Polymer Science Part A Polymer Chemistry*, vol. 16, pp. 2915–2930, November 1978.

- [211] A. L. Polic, T. A. Duever, and A. Penlidis, “Case studies and literature review on the estimation of copolymerization reactivity ratios,” *Journal of Polymer Science Part A: Polymer Chemistry Polymer Chemistry*, vol. 36, no. 5, pp. 813–822, 1998.